Characterisation of L-cell secretory mechanisms and colonic enteroendocrine cell subpopulations

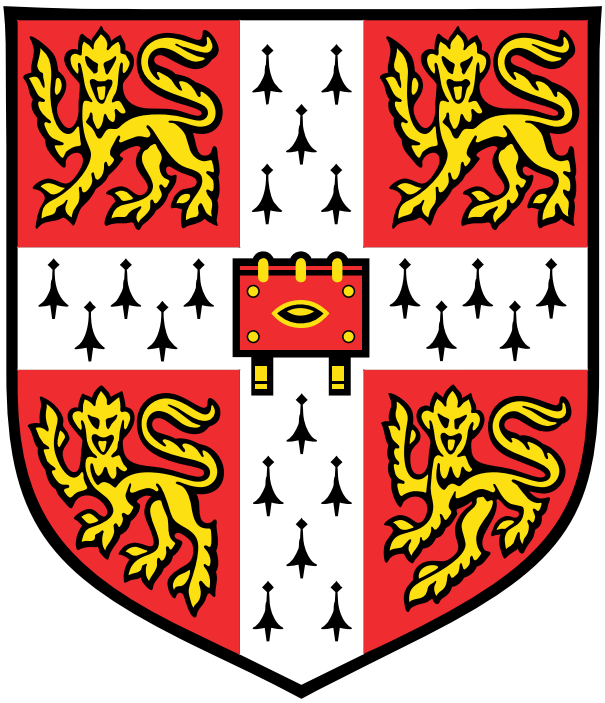

Lawrence Billing
Downing College, Cambridge

This dissertation is submitted for the degree of Doctor of Philosophy

September 2018

Abstract

Enteroendocrine cells (EECs) are chemosensitive cells of the gastrointestinal epithelium that exert a wide range of physiological effects via production and secretion of hormones in response to ingested nutrients, bacterial metabolites and systemic signals. Glucagon-like peptide-1 (GLP-1) is one such hormone secreted from so-called L-cells found in both the small and large intestines. GLP-1 exerts an anorexigenic effect and together with glucose-dependent insulinotropic polypeptide (GIP), restores postprandial normoglycaemia through the incretin effect. These effects are exploited by GLP-1 analogues in the treatment of type 2 diabetes. GLP-1 may also contribute to weight-loss and remission of type 2 diabetes following bariatric surgery which increases postprandial GLP-1 excursions.

Here we investigated stimulus secretion coupling in L-cells. A novel 2D culture system from murine small intestinal organoids was established as an *in vitro* model. This was used to characterise synergistic stimulation of GLP-1 secretion in response to concomitant stimulation by bile acids through the G_s-protein coupled receptor GPBAR1 and free fatty acids through the G_q-coupled receptor FFAR1.

Roughly half of colonic, but not small intestinal, L-cells co-produce the orexigenic peptide insulin-like peptide 5 (INSL5). This hitherto poorly examined subpopulation of L-cells was characterised through transcriptomic analysis, intracellular calcium imaging (using a novel GCaMP6F-based transgenic mouse model), LC/MS peptide quantification and 3D super resolution microscopy (3D-SIM). Based on the observed prevalent co-storage of GLP-1, PYY and INSL5 in secretory vesicles and similar secretory responses of both hormones to a range of different stimuli strengths (including short chain fatty acids, angiotensin II and arginine vasopressin (AVP)) it was concluded that GLP-1, PYY and INSL5 are co-secreted, rather than being selectively recruited by different stimuli.

To further characterise the diversity of colonic EECs, single cell RNA-sequencing (scRNA-seq) was performed on cells isolated from mice with a pan-EEC fluorescent marker (NeuroD1-Cre:Rosa26-EYFP). This illustrated that INSL5-producing L-cells form one of two

transcriptomically distinct subpopulations of L-cells in the murine colon, with the other distinguished by expression of neurotensin (*Nts)*. Another major EEC subpopulation, enterochromaffin (EC) cells could be split into three groups, mechanosensitive and pro-inflammatory EC cells distinguished respectively by *Piezo2* and *Tac1* expression and a third *Sct*-expressing group. Immunofluorescent labelling and RT-qPCR analysis revealed that the *Nts*-expressing and *Insl5*-expressing L-cell subpopulations are proximally and distally enriched in the murine colon, respectively. In primary cultures, angiotensin II and AVP stimulated INSL5, GLP-1 and PYY but not NTS secretion, correlating with selective expression profiles of the cognate receptors in the L-cell subpopulations.

In summary, the work presented suggests that different L-cell subpopulations exist that respond to different stimuli, but that hormones co-expressed in individual L-cells are co-released upon stimulation. Differences in receptor expression between these subpopulations and other EEC-populations might be exploitable for selective hormone recruitment for the therapy of diabetes, obesity and other diseases.

Declaration

This dissertation is the result of my own work and includes nothing which is the outcome of work done in collaboration except as specified here and in the main body of text. Secretion experiments in chapter 3 were carried out in collaboration with Deborah Goldspink. All secretion experiments in chapter 4 were conducted and analysed by Pierre Larraufie. The fitting of 3D Gaussian distributions to 3D-SIM images and subsequent analysis in chapter 4 was carried out by Christopher Smith. For the scRNA-seq analysis in chapter 5, Brian Lam was responsible for the quality control, read alignment and generating quantified raw counts for each cell analysed. The work presented here is not substantially the same as any that I have submitted, or, is being concurrently submitted for a degree or diploma or other qualification at the University of Cambridge or any other University or similar institution than declared here. I further state that no substantial part of my dissertation has already been submitted, or, is being concurrently submitted for any such degree, diploma or other qualification at the University of Cambridge. It does not exceed the prescribed word limit of 60,000 words by the Clinical Medicine and Clinical Veterinary Medicine Degree Committee.

Lawrence Billing

Publications

Co-storage and release of insulin-like peptide-5, glucagon-like peptide-1 and peptideYY from murine and human colonic enteroendocrine cells.

Billing, L.J., Smith, C.A., Larraufie, P., Goldspink, D.A., Galvin, S., Kay, R.G., Howe, J.D., Walker, R, Pruna, M, Glass, L, Pais, R, Gribble, F.M., Reimann, F.

Molecular Metabolism. 2018;16: 65-75. PMID: 30104166.

Mechanistic insights into the detection of free fatty and bile acids by ileal glucagon-like peptide-1 secreting cells.

Goldspink, D.A., Lu, V.B., Billing, L.J., Larraufie, P., Tolhurst, G., Gribble, F.M., Reimann, F.

Molecular Metabolism. 2018; 7:90-101. PMID: 29167062

A Transcriptome-Led Exploration of Molecular Mechanisms Regulating Somatostatin-Producing D-Cells in the Gastric Epithelium.

Adriaenssens, A., Lam, B.Y.H., Billing, L., Skeffington, K., Sewing, S., Reimann, F., Gribble, F.

Endocrinology. 2015; 156(11):3924-36. PMID: 26241122

Table of contents

Abstract I

Declaration III

Publications IV

Table of contents V

Acknowledgements VIII

Abbreviations IX

Chapter 1. Introduction 1

1.1. Obesity and type 2 diabetes 1

1.1.1. Global epidemics 1

1.1.2. Pathophysiology 1

1.2. Pharmacological treatments of obesity: 2

1.2.1. Pancreatic lipase inhibitors - orlistat 2

1.2.2. Amphetamine derivatives 2

1.2.3. Sibutramine 3

1.2.4. CB1 receptor inverse agonists - rimonabant 3

1.2.5. Dual treatment with naltrexone and bupropion 3

1.2.6. Lorcaserin 4

1.2.7. Incretin mimetics 4

1.3. Pharmacological treatments of type 2 diabetes 5

1.3.1. Metformin 5

1.3.2. Insulin 5

1.3.3. K_{ATP} channel inhibitors - sulphonylureas and glinides 6

1.3.4. Incretin mimetics 6

1.3.5. DPP-4 inhibitors 6

1.4. Surgical treatment of obesity and type 2 diabetes – bariatric surgery 8

1.5. Targeting the enteroendocrine system – a novel therapeutic approach 10

1.6. Enteroendocrine cells – chemosensitive epithelial cells 11

1.7. Enteroendocrine cell subtypes 13

1.7.1. Proglucagon derived peptides 14

1.7.2. Peptide YY 16

1.7.3. Insulin-like peptide 5 17

1.7.4. Cholecystokinin 17

1.7.5. Neurotensin 18

1.7.6. Somatostatin 19

1.7.7. Serotonin 20

1.8. Modelling the enteroendocrine system *in vitro* 21

1.8.1. Immortalised cell line models 21

1.8.2. Primary tissue 21

1.8.3. Gastrointestinal organoids 22

1.9. Hypotheses explored in this thesis 25

Chapter 2. Materials and Methods 26

2.1. Solutions and culture media 26

2.2. Animal procedures and ethics 28

2.3. Transgenic mice 28

2.4. Fluorescence activated cell sorting 30
2.4.1. Collagenase Digestion 30
2.4.2. Flow cytometry 30
2.5. Tissue culture methods 31
2.5.1. Primary cultures 31
2.5.2. Small intestinal organoids culture 31
2.6. Secretion assays 35
2.6.1. Measuring GLP-1 secretion from organoid cultures 35
2.6.2. Measuring GLP-1, PYY and INSL5 secretion from colonic crypt cultures 36
2.7. Immunohistochemistry 38
2.7.1. Organoid cultures 38
2.7.2. Primary cultures 38
2.7.3. Tissue sections 39
2.7.4. Colonic Wholemounts 39
2.8. Imaging 41
2.8.1. Confocal microscopy 41
2.8.2. Intracellular calcium imaging 41
2.8.3. 3D-SIM imaging of GLP-1, PYY and INSL5 vesicles 42
2.8.4. Imaging of colonic wholemounts 44
2.9. Transcriptomic techniques 45
2.9.1. Real-time quantitative PCR 45
2.9.2. Single-cell RNA-sequencing 46

Chapter 3. Synergy between FFAR1 and GPBAR-1 signalling in L-cells 49
3.1. Introduction 49
3.2. Aims 49
3.3. Background 50
3.3.1. Lipid digestion and free fatty acid absorption 50
3.3.2. L-cell FFA and bile acid sensing 53
3.3.3. Synergistic effects of coactivation of G_q and G_s signalling pathways on GLP-1 secretion 55
3.4. Results 57
3.4.1. Bile acids and FFAR1 agonists elicit intracellular calcium responses in organoid-derived L-cells 57
3.4.2. GPBAR-A potentiates L-cell intracellular calcium responses to TAK-875 59
3.4.3. GPBAR-A potentiates L-cell intracellular calcium responses to KCl 61
3.4.4. GPBAR-A potentiates GLP-1 secretory responses to TAK-875 63
3.5. Discussion 65
3.5.1. Organoid L-cells replicate native L-cell physiology 65
3.5.2. GPBAR1 and FFAR1 stimulation triggers L-cell intracellular Ca^{2+} and GLP-1 secretory responses 65
3.5.3. Co-activation of GPBAR-1 and FFAR1 potentiates L-cell intracellular Ca^{2+} and GLP-1 responses 66
3.6. Concluding remarks 71

Chapter 4. Characterisation of INSL5-producing cells 72
4.1. Introduction 72
4.2. Aims: 72
4.3. Background 73
4.3.1. Physiological stimuli of colonic L-cells: 73
4.3.2. Vesicular localisation of GLP-1 and PYY 76
4.4. Results 78
4.4.1. Induction of specific GFP/GCaMP6F expression within INSL5-producing cells 78

4.4.2. INSL5 cells express cognate GPCRs of known GLP-1 secretagogues 79
4.4.3. Physiological stimuli trigger intracellular Ca^{2+} transients in cultured INSL5 cells 80
4.4.4. GLP-1 secretagogues induce concomitant PYY and INSL5 secretion 82
4.4.5. The majority of INSL5, GLP-1 and PYY secretory vesicles label for all three peptides 84
4.5. Discussion 92
4.5.1. Verification of the Insl5-rtTA/TET-GCaMP6FΔCMV and Insl5-rTA/TET-GFP mouse models in vivo and ex vivo 92
4.5.2. INSL5 cells display intracellular Ca^{2+} responses to GLP-1 secretagogues 92
4.5.3. GLP-1 secretagogues trigger concomitant PYY and INSL5 secretion 94
4.5.4. Co-storage of INSL5, PYY and GLP-1 likely underlies co-secretion 94
4.5.5. Physiological Implications 96
4.6. Concluding remarks 97

Chapter 5. A single cell RNA-seq based examination of colonic enteroendocrine cells 99
5.1. Introduction 99
5.2. Aims 99
5.3. Background 100
5.3.1. Colonic EEC subtypes: 100
5.3.2. Single cell RNA-seq techniques 102
5.4. Results 104
5.4.1. Cluster analysis of colonic NeuroD1 scRNA-seq 104
5.4.2. Differential expression of GPCRs in colonic EEC subgroups 110
5.4.3. RT-qPCR examination of INSL5 cells 115
5.4.4. Regional expression of EEC markers 116
5.4.5. Regional expression of GPCRs highlighted by scRNA-seq analysis 117
5.4.6. Immunofluorescent labelling of INSL5, PYY and NTS in wholemounted murine colon 119
5.4.7. Secretory responses 121
5.5. Discussion 125
5.5.1. Colonic L-cells split into distinct proximal *Nts*-expressing and distal *Insl5*-expressing subgroups 125
5.5.2. *Insl5*-expressing and *Nts*-expressing L-cells display functional differences in GPCR repertoire 128
5.5.3. Colonic enterochromaffin cells comprise of three subpopulations marked by *Sct*, *Tac1* and *Piezo2* expression 130
5.5.4. D-cells form a transcriptomically distinct group of colonic EECs 133
5.5.5. Unexpected identification of goblet cells in a FACS-purified NeuroD1 cell population 133
5.5.6. Concluding remarks 134

Chapter 6. General discussion 135
6.1. Summary of key findings 135
6.1.1. GPBAR-1 activation potentiates FFAR1-mediated GLP-1 secretion 135
6.1.2. INSL5, PYY and GLP-1 are co-stored and co-released from L-cells 136
6.1.3. Murine colonic L-cells divide into *Insl5*-expressing and *Nts*-expressing cells 138
6.1.4. Colonic enterochromaffin cells split into 3 distinct subpopulations 140
6.1.5. Colonic enteroendocrine cells exhibit distinct GPCR repertoires 141
6.2. Future directions 142
6.2.1. Establishing the physiological roles of INSL5 142
6.2.2. Selective pharmacological targeting of EEC subtypes 143
6.3. Concluding remarks 144

Bibliography 145

Appendices 179

Acknowledgements

I would like to thank my supervisors Fiona Gribble and Frank Reimann for providing guidance and support in my scientific endeavours. Gratitude is also expressed to colleagues in the lab who have aided my scientific development with patience and good humour. I would also like to thank the staff at the Flow Cytometry Core at the Cambridge Institute for Medical Research (CIMR) and the Core Biochemical Assay Laboratory (CBAL). I would like to acknowledge the Wellcome Trust for funding my 4-year PhD studentship. Finally, I would like to thank my friends and family for their continued support and encouragement.

Abbreviations

3D-SIM	3D structured illumination microscopy
5-HT	5-hydroxytryptamine
AC	Adenylate cyclase
ACE	Angiotensin converting enzyme
ADF	Advanced DMEM/F-12
AgoPAM	Agonists also capable of acting as positive allosteric modulators
AMPK	Adenosine monophosphate-activated protein kinase
ASBT	Apical sodium-dependent bile acid transporter
ATP	Adenosine triphosphate
AVP	Arginine vasopressin
BB	Bombesin
BMP	Bone morphogenetic protein
BSA	Bovine serum albumin
CALCRL	Calcitonin receptor-like receptor
cAMP	Cyclic adenosine monophosphate
CART	Cocaine and amphetamine regulated transcript
CB1	Cannabinoid type 1 receptor
CCK	Cholecystokinin
CgA	Chromogranin A
CRH	Corticotropin-releasing hormone
CT	Cycle threshold
DAG	Diacylglycerol
DMEM	Dulbecco's modified Eagle's medium
DMSO	Dimethyl sulfoxide
DPP-4	Dipeptidyl peptidase-4
DREADD	Designer receptors activated by designer drugs
EC cell	Enterochromaffin cell
EEC	Enteroendocrine cell
EGF	Epidermal growth factor
ENS	Enteric nervous system
EPAC	Exchange protein directly activated by cAMP
EYFP	Enhanced yellow fluorescent protein
FACS	Fluorescence activated cell sorting
FBS	Fetal bovine serum
FDA	Food and Drug Administration
FFA	Free fatty acid
Fsk	Forskolin
GCGR	Glucagon receptor
GFP	Green fluorescent protein
GIP	Gastric insulinotropic peptide
GLP-1	Glucagon-like peptide 1

GPBAR-1	G protein-coupled bile acid receptor 1
GPCR	G-protein coupled receptor
GRP	Gastrin releasing peptide
HFD	High fat diet
IBD	Inflammatory bowel disease
IBS	Irritable bowel syndrome
INSL5	Insulin-like peptide 5
IP_3	Inositol triphosphate
K_{ATP}	ATP-sensitive potassium channel
KCl	Potassium Chloride
LC/MS	Liquid chromatography-mass spectrometry
LCFA	Long chain fatty acid
LGR5	Leucine-rich repeat-containing G-protein coupled receptor 5
2-MAG	2-monoacylglycerol
MCFA	Medium chain fatty acid
MSH	Melanocyte-stimulating hormone
MUC2	Mucin 2
NeuroD1	Neuronal differentiation 1
NMB	Neuromedin B
NPY	Neuropeptide Y
NTS	Neurotensin
PBS	Phosphate buffered saline
Pcsk	Prohormone convertase
PFA	Paraformaldehyde
PKA	Protein kinase A
PKC	Protein kinase C
PLC	Phospholipase C
POMC	Pro-opiomelanocortin
PP	Pancreatic polypeptide
PYY	Peptide YY
RT-qPCR	Real-time quantitative reverse transcription PCR
rtTA	Reverse tetracycline transactivator
Rxfp4	Relaxin family peptide receptor 4
RYGB	Roux-en Y gastric bypass
SCFA	Short chain fatty acid
Scg2	Secretogranin 2
scRNA-seq	Single cell RNA-sequencing
SCT	Secretin
SG:T1	Sodium-glucose transport protein 1
SNARE	Soluble N-ethylmaleimide factor attachment protein receptor
SST	Somatostatin
t-SNE	t-distributed stochastic neighbour embedding
TDCA	Taurodeoxycholic acid

UMI	Unique molecular identifier
VGCC	Voltage gated calcium channel

Chapter 1. Introduction

1.1. Obesity and type 2 diabetes

1.1.1. Global epidemics

The global prevalence of both obesity and type 2 diabetes has increased dramatically since the end of the second world war. In large part this has been due to increased food availability and calorie intake combined with an increase in sedentary behaviour (i.e. reduced calorie expenditure). In the UK, 26% of adults were estimated to be obese in 2016, whilst in 2017 an estimated 3.7 million people were living with diagnosed diabetes and 12.3 million were at increased risk of developing type 2 diabetes [1,2]. The estimated annual cost to the NHS was £13.75bn for obesity management in 2012 and £6.1bn for diabetes management in 2014 [3,4]. A large percentage of these costs derive from treatment of complications, highlighting the need for more effective therapeutic interventions for obesity and type 2 diabetes.

1.1.2. Pathophysiology

Obesity is characterised by abnormally high levels of adipose deposition whilst type 2 diabetes is characterised by insulin resistance and pancreatic beta cell dysfunction [5,6]. Under normal physiological conditions, post-prandial insulin secretion from beta-cells counteracts the increase in glycaemia seen following glucose absorption from a meal. This is achieved by a combination of insulin-stimulated glucose uptake by peripheral tissues and glycogen synthesis in the liver [7]. Insulin resistance in type 2 diabetes attenuates the glycaemia-lowering actions of endogenous insulin to insufficient levels to restore normoglycaemia and hence leads to the pathological state of hyperglycaemia.

Obesity and type 2 diabetes are strongly associated. In fact, obesity is a predictive risk factor of developing insulin resistance and type 2 diabetes and both conditions cause cardiovascular issues. Reflecting these associations, the term metabolic syndrome is used to denote patients that suffer a combination of obesity, type 2 diabetes and hypertension [8]. As well as issues with mobility, patients with metabolic syndrome are more likely to suffer from peripheral neuropathy, heart failure and an increased risk of ischaemic stroke [8–10].

1.2. Pharmacological treatments of obesity:

Beyond dietary and exercise interventions, a limited number of pharmacological treatments are available for obesity. Unfortunately, some of these weight loss treatments, such as rimonabant, amphetamine derivatives and sibutramine have been withdrawn from sale due to associated adverse effects [11–13]. A subset of anti-obesity drugs, including examples which have been withdrawn from sale, are described below:

1.2.1. Pancreatic lipase inhibitors - orlistat

Orlistat is an inhibitor of pancreatic lipase (which is involved in lipid digestion) that reduces the absorption of lipids from the small intestine and induces a modest loss in body weight. Additionally, orlistat treatment reduces the incidence of obese patients developing type 2 diabetes [14,15]. This preventative action of orlistat has been associated with weight loss, reduced plasma levels of free fatty acids, increased incretin secretion and modulated release of adipocytokines [16].

1.2.2. Amphetamine derivatives

Amphetamines derivatives are a group of psychoactive agents which have historically been prescribed for weight-loss due to their ability to suppress appetite. Pharmacologically, amphetamine mediates competitive inhibition of monoamine reuptake and displacement of monoamines sequestered into secretory vesicles, increasing monoaminergic (dopaminergic, serotonergic and noradrenergic) neurotransmission [17]. This increased monoaminergic neurotransmission can reduce food intake. Enhancement of dopaminergic neurotransmission, for example, can reduce appetite by increasing hypothalamic expression of the anorexigenic neuropeptide cocaine and amphetamine regulated transcript (CART) whilst decreasing expression of the orexigenic neuropeptide Y (NPY) [18]. Although effective as a weight loss medication, amphetamines are highly addictive with serious side effects associated with long term use somewhat limiting their modern day clinical use [12].

1.2.3. Sibutramine

Like amphetamine derivatives, sibutramine enhances monoaminergic neurotransmission. However, unlike amphetamine derivatives, sibutramine achieves this by blocking monoamine reuptake without displacement of stored monoamines. Sibutramine induced enhancement in monoaminergic neurotransmission is thought to induce weight loss by increasing energy expenditure whilst suppressing appetite [19]. Unfortunately, sibutramine has largely been withdrawn from clinical use including in the Europe and USA due to association with increased morbidity from cardiovascular disease. However, these issues appear largely restricted to obese patients with pre-existing cardiovascular issues with minimal associated risk to those without [13,20]. This suggests that sibutramine treatment should be reconsidered for obese patients without pre-existing cardiovascular issues.

1.2.4. CB1 receptor inverse agonists - rimonabant

Representing an alternative pharmacological approach for obesity treatment, drugs targeting the cannabinoid type 1 receptor (CB1) have been developed such as rimonabant. Activation of CB1 in hypothalamic neurons has an orexigenic effect linked to the sensitisation of neurons producing the appetite stimulating neuropeptide orexin and attenuated expression of anorexigenic neuropeptides such as corticotropin-releasing hormone (CRH) [21]. Conversely, inverse agonism of CB1 by rimonabant mediates an anorexigenic effect that likely reflects increased activity of neurons producing anorexigenic over orexigenic neuropeptides. Unfortunately rimonabant was withdrawn from sale due to severe psychiatric side effects that were observed post-market release [11,22].

1.2.5. Dual treatment with naltrexone and bupropion

A more recently approved drug treatment is combined administration of naltrexone/bupropion. Bupropion is an antidepressant that boosts noradrenergic and dopaminergic neurotransmission by blocking reuptake of noradrenaline and dopamine respectively. These neurotransmitters stimulate pre-opiomelanocortin (POMC) neurons of the arcuate nucleus (in the hypothalamus) that produce the anorexigenic neurotransmitter alpha-MSH and the autoinhibitory peptide beta-endorphin. When combined with naltrexone,

a μ-opioid receptor antagonist which is thought to enhance POMC neuron activity by blocking autoinhibition by beta-endorphin, bupropion induces modest weight loss [22].

1.2.6. Lorcaserin

Lorcaserin is a specific agonist of the 5-HT_{2C} receptor and was approved by the FDA for clinical use as an anti-obesity drug in 2012 [23]. Lorcaserin exerts appetite suppression believed to derive from simulation of anorexigenic POMC neurons within the arcuate nucleus [24]. Preferential activation of 5-HT_{2C} receptors over 5-HT_{2B} receptors by lorcaserin avoids known cardiovascular issues associated with 5-HT_{2B} receptor activation [25]. Such issues have previously led to the withdrawal of other anti-obesity drugs with a serotonergic mode of action such as fenfluramine [23].

1.2.7. Incretin mimetics

Incretin mimetics, which imitate the actions of the gut peptide glucagon-like peptide 1 (GLP-1), such as liraglutide have recently been approved by the FDA for obesity treatment in addition to their pre-existing approval for type 2 diabetes treatment (discussed later) [26]. The weight loss triggered by these injectable drug agents derives from appetite suppression (reducing calorie intake) predominantly mediated by stimulation of GLP-1 receptors (GLP1Rs) within the central nervous system (particularly those of glutamatergic neurons) [27–30]. To maintain a therapeutic dose, liraglutide must be injected once/twice daily. Recent clinical trials have focussed on the potential of incretin mimetics with longer biological half-lives (and therefore longer lasting), such as semaglutide, which could be administered once a week for obesity treatment [31]. Use of such longer lasting injectable agents would likely improve current levels of patient compliance to obesity treatment with incretin mimetics.

1.3. Pharmacological treatments of type 2 diabetes

In common with obesity, type 2 diabetes can be partly managed by dietary and lifestyle alterations. However, there are also a number of pharmacological options including the classical use of insulin analogues, metformin, sulphonylureas and glinides and newer drugs such as incretin mimetics and dipeptidyl peptidase-4 (DPP-4) inhibitors [32]. These examples and their mechanisms of actions are briefly discussed below:

1.3.1. Metformin

The therapeutic benefits of metformin treatment are thought to derive from a combination of suppressed hepatic glucose production (by gluconeogenesis), sensitisation of peripheral tissues to insulin and promotion of beta-cell function. Activation of adenosine monophosphate-activated protein kinase (AMPK) appears key to the effects of metformin on hepatic gluconeogenesis and insulin sensitivity. However, the precise pharmacological mechanisms underlying metformin therapy have not been resolved, despite over 60 years of clinical application [33,34].

1.3.2. Insulin

Insulin and its analogues are the traditional first line treatment for type 1 diabetes, compensating for the loss of endogenous insulin resulting from autoimmune induced beta-cell death. In contrast, most type 2 diabetics produce endogenous insulin on an insulin resistant background. The production of endogenous insulin makes therapeutic dosing of insulin analogues more complex for type 2 than type 1 diabetes. Subsequently, insulin analogues tend to be utilised 10-15 years after initial diagnosis, following behavioural and other pharmacological interventions [35]. Furthermore, patient compliance to insulin treatment is lower than for orally administrable drugs since insulin injections cause discomfort and potentially life-threatening episodes of hypoglycaemia [36]. Recent advances in the closed-loop insulin pump, also known as the ‘artificial pancreas’, may help alleviate dosing issues. This system constantly monitors glycaemic levels and adjusts the administered dose of insulin accordingly avoiding the need for regular self-administered insulin injections [37]. This system was initially designed for treatment of type 1 diabetes, but by using

computational modelling of endogenous insulin release it is hoped that it can be applied successfully to type 2 diabetics [38].

1.3.3. K_{ATP} channel inhibitors - sulphonylureas and glinides

Sulphonylureas (such as glimepiride) and glinides (such as nateglinide) restore normoglycaemia in type 2 diabetic patients through stimulation of endogenous insulin secretion from pancreatic beta-cells. Stimulation of insulin secretion by these pharmacological agents results from inhibition of beta-cell ATP-sensitive potassium (K_{ATP}) channels causing plasma membrane depolarisation and increased insulin exocytosis [39,40]. Although effective insulin secretagogues, sulphonylureas (in common with insulin administration) can trigger a dangerous state of abnormally low glycaemia known as hypoglycaemia [6]. More recent drug development efforts in the diabetes field have focussed on minimising hypoglycaemic risk whilst delivering therapeutic benefit. To this end, the incretin mimetics and DPP-4 inhibitors have been developed.

1.3.4. Incretin mimetics

Newer anti-diabetes drugs include incretin mimetics, such as exenatide, which imitate the actions of the gut peptide glucagon-like peptide 1 (GLP-1) to restore normoglycaemia through the incretin effect. The incretin effect accounts for the higher levels of insulin secretion elicited by oral compared with intravenous administration of glucose under similar glycaemic conditions. It is exerted by the incretin peptides GLP-1 and glucose insulinotropic peptide (GIP) secreted from endocrine cells of the intestinal epithelium known as enteroendocrine cells (EECs). GLP-1 and GIP can act directly on pancreatic islets to stimulate endogenous insulin secretion from beta cells and modulate glucagon secretion from alpha cells (GLP-1 inhibits whilst GIP stimulates glucagon secretion) thus reducing glycaemic levels [41–43]. Whilst incretin mimetic treatment does not generally trigger hypoglycaemia, like insulin they are peptides which must be administered by injection influencing patient compliance [44].

1.3.5. DPP-4 inhibitors

By pharmacological inhibition of the enzyme DPP-4, which rapidly inactivates circulating GLP-1 and GIP, levels of endogenous incretins in the circulation can be enhanced with associated

therapeutic benefits. Gliptins represent a licensed class of such DPP-4 inhibitors. Unlike incretin mimetics, gliptins can be orally administered. However, incretin mimetics are more effective at lowering blood glucose levels and also exert a weight loss effect which DPP-4 inhibitors do not [45].

1.4. Surgical treatment of obesity and type 2 diabetes – bariatric surgery

A more drastic approach to obesity treatment is bariatric (weight-loss) surgery. One of the most commonly employed procedures is the Roux-en-Y gastric bypass (RYGB) [46]. Here the upper part of the stomach is partitioned from the rest of the stomach and the small intestine is divided at the jejunum. Following this, an anastomosis is made between the small pouch formed by the upper stomach and the jejunum forming the alimentary limb (aka Roux limb) which bypasses the majority of the stomach and the duodenum. An additional anastomosis is formed between the excluded stomach and duodenum (biliopancreatic limb) and the alimentary limb [47]. RYGB results in a large reduction in the size of stomach, enhancing the postprandial sensation of fullness and inducing weight-loss by increasing satiety and reducing food intake [48].

RYGB can additionally be used to treat type 2 diabetes which can lead to remission with Purnell et al. finding that 68.7% of patients studied were in remission 3 years post-RYGB [49]. The improvements in glycaemic control following RYGB occur acutely and are therefore unlikely to derive solely from weight loss. The hindgut and foregut hypotheses are the main theories put forward to explain the glycaemic improvements and satiety seen following RYGB. The hindgut hypothesis postulates that by bypassing the early small intestine nutrients are delivered directly to the distal small intestine stimulating release of factors which stimulate insulin secretion acting to restore normoglycaemia and exerting satiety. Conversely, the foregut hypothesis suggests that bypassing the early small intestine reduces secretion of inhibitory factors that negatively affect glycaemic control (perhaps by suppressing incretin release) and that increase appetite [50,51]. These factors are likely peptides produced and secreted by EECs [52]. In the case of the hindgut hypothesis, involvement of proglucagon-expressing (GLP-1 producing) EECs has been implicated. Under this theory, nutrient delivery directly to the distal small intestine which is enriched in proglucagon-expressing EECs enhancing GLP-1 and PYY (another hormone co-secreted with GLP-1) secretion with consequential effects on postprandial insulin secretion and satiety [53]. Investigating the nutrient sensing mechanisms of proglucagon-expressing EECs in particular, which is the

primary objective of this thesis, and of other EECs in general may therefore uncover mechanisms by which type 2 diabetes remission is achieved following RYGB.

1.5. Targeting the enteroendocrine system – a novel therapeutic approach

Pharmacological targeting of enteroendocrine cells may achieve therapeutic benefit through modulated secretion of endogenous gut hormones. Such an approach might achieve the aforementioned clinical benefits of RYGB by stimulating the release of incretins or suppressing release of as-of-yet uncharacterised anti-incretin factors. Indeed, oral administration of a class of known GLP-1 secretagogues known as free fatty acid receptor 1 (FFAR1) agonists also capable of acting as positive allosteric modulators (AgoPAMs) reduced food intake and body weight in diet-induced obese (DIO) mice. AgoPAM administration to GLP1R knockout mice did not induce these effects suggesting that GLP-1 release underlies AgoPAM-induced satiety [54]. Therefore, as this example demonstrates, characterisation of the molecular mechanisms regulating secretion from EECs may aid identification of novel drug targets for obesity and type 2 diabetes treatment.

1.6. Enteroendocrine cells – chemosensitive epithelial cells

EECs represent around 1% of all epithelial cells of the gastrointestinal tract and are electrically excitable cells characterised by their endocrine products. These hormones exert a variety of physiological effects both in a local paracrine fashion and at distant sites via the systemic circulation. One key characteristic of EECs is the ability to chemosense luminal contents of the gastrointestinal tract, neurotransmitters and systemic factors and modulate secretory activity accordingly. Many EECs, for example, respond to dietary stimuli such as carbohydrates, peptides and lipids regulating satiety, glycaemia and gastrointestinal motility [52,55]. EEC chemosensory responses are largely regulated by G-protein coupled receptor (GPCR) signalling and more specifically the G_q, G_s and G_i signalling pathways which modulate exocytosis through the secondary messengers IP_3, DAG and cAMP (figure 1) [55]. Example modulations include changes to intracellular calcium (Ca^{2+}) levels (critical to exocytosis) directly through IP_3-dependent release of intracellular Ca^{2+} stores and indirectly by modulating the activities of voltage-gated calcium channels through which Ca^{2+} influx occurs [56,57]. An increase in intracellular Ca^{2+} triggers secretion by acting on SNARE proteins directly involved in mediating fusion of secretory vesicles with the plasma membrane [58].

EECs can also chemosense stimuli in a GPCR-independent fashion. For example, L-cell glucose-sensing involves the transporter sodium-glucose transport protein 1 (SGLT1) which mediates sodium-dependent active transport of glucose and accordingly depolarises the plasma membrane triggering GLP-1 secretion [59]. Likewise, the potent GLP-1 secretion triggered by the amino acid L-glutamine partly derives from the electrogenic activities of a sodium-dependent amino acid transporter (the precise identity of this transporter has not yet been clarified) [60,61].

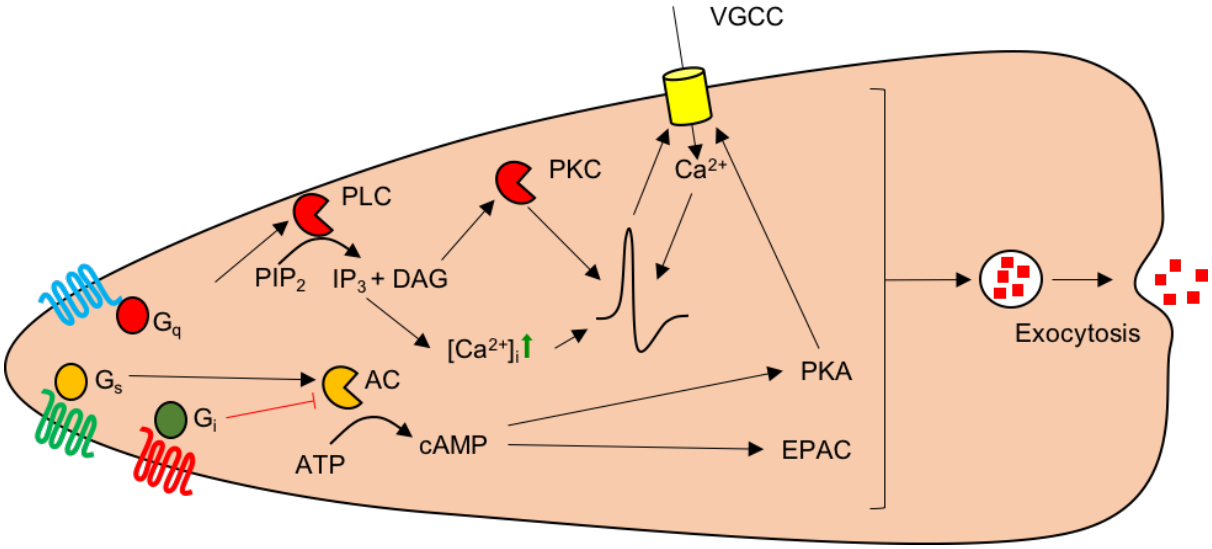

***Figure 1**: Schematic illustrating the G_q, G_s and G_i signalling pathways underlying chemosensation in enteroendocrine cells. Stimulation of the G_q pathway stimulates phospholipase C (PLC) activity which catalyses PIP_2 hydrolysis to the secondary messengers IP_3 and DAG. IP_3 triggers release of intracellular calcium stores which increases membrane excitability (indicated by the waveform) and triggers secretory vesicle fusion. DAG activates protein kinase C (PKC) which can increase membrane excitability by modulating the activities of other proteins. Stimulation of the G_s pathway stimulates adenylate cyclase (AC) to produce the secondary messenger cAMP from ATP. cAMP activates protein kinase A (PKA) and EPAC which in turn mediates calcium influx including voltage gated calcium channels (VGCCs) and may modulate the activities of proteins involved in the fusion mechanism. A combination of these downstream effects yields exocytosis of EEC peptides/factors (represented by red squares). Stimulation of the G_i pathway, contrastingly to the G_s pathway, inhibits AC activity repressing exocytosis. G_q, G_s and G_i-coupled GPCRs represented respectively by blue, green and red shapes with 7 transmembrane intersections. Black arrows reflect stimulatory effects whilst red T-shaped lines indicate inhibitory effects.*

1.7. Enteroendocrine cell subtypes

Historically the EECs were thought to produce one particular gut hormone and split into subtypes according to which gut hormone they produced. However, this canonical view has been challenged by transcriptomic and immunohistological studies indicating a large degree of overlap in the gut hormone profiles produced and secreted by the historical EEC subdivisions [62–65]. In light of these findings Fothergill and Furness propose that a new classification system is required for EECs [66]. For simplicity, in this thesis the classical terms are used to refer to proglucagon-expressing, somatostatin-expressing and serotonin-producing EECs respectively as L-cells, D-cells and enterochromaffin (EC) cells (see figure 2).

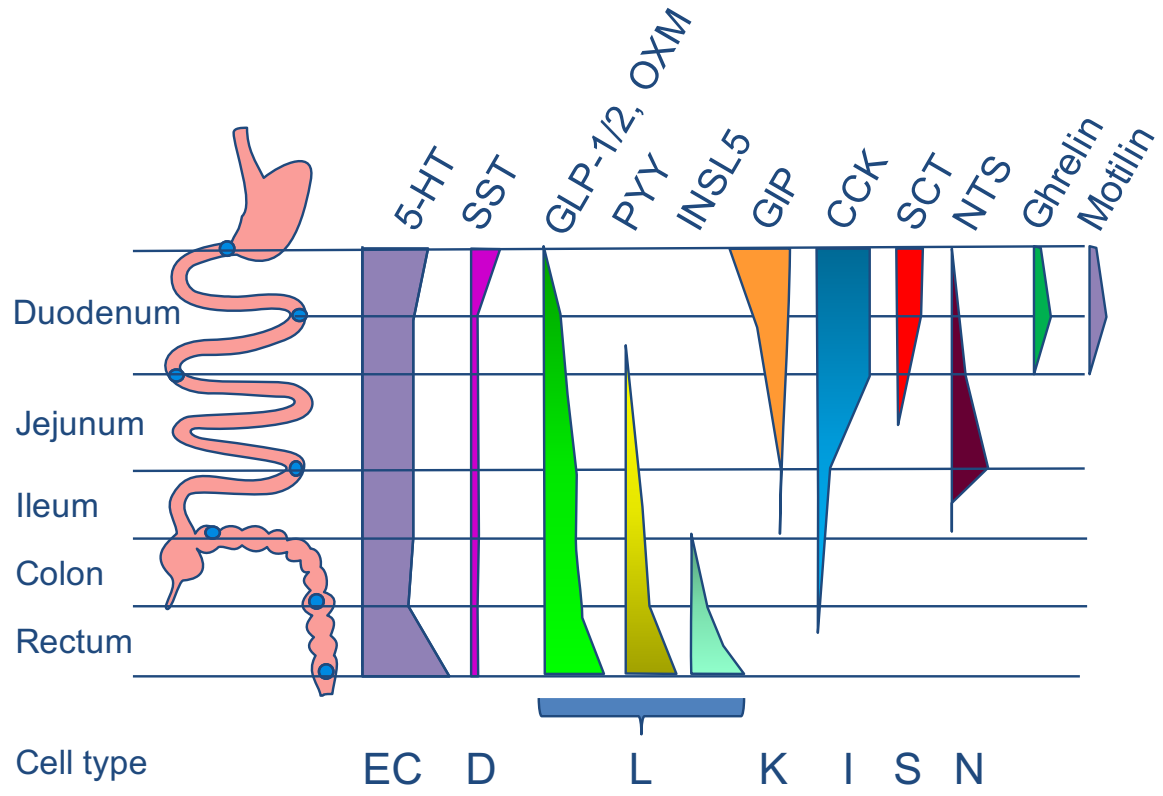

***Figure 2**: Frequency distribution of enteroendocrine cell subtypes through the human small and large intestines. Established through immunolabelling of key endocrine products (labelled at the top) of each subtype in samples taken at the intestinal sites labelled by blue circles on the schematic. Width of coloured shapes indicates frequency of cell type. Produced by Fiona Gribble.*

The following sections briefly describe the key gut hormones covered in this thesis:

1.7.1. Proglucagon derived peptides

Proglucagon-expressing cells, referred to henceforth as 'L-cells' (a classical term for proglucagon-expressing cells of the gastrointestinal tract), are localised to the epithelium of the small and large intestines and secrete a range of proglucagon derived peptides (peptides derived from post-translational processing of the proglucagon precursor polypeptide) into the circulation (see figures 2 and 3) [67,68]. Proglucagon and its derivatives are produced in alpha-cells of the pancreas, a subset of central neurons and intestinal L-cells. Whilst pancreatic alpha-cells produce glucagon and glicentin-related pancreatic polypeptide (GRPP) from proglucagon, L-cells do not. Conversely, L-cells produce GLP-1, GLP-2, glicentin and oxyntomodulin which are not produced by alpha-cells. These differences in proglucagon processing derive from differential expression of different prohormone convertases (Pcsk) that cleave at different sites along the proglucagon polypeptide chain. Alpha-cells express Pcsk2 which favours glucagon and GRPP production whilst L-cells express Pcsk1/3 which favours GLP-1, GLP-2, glicentin and oxyntomodulin production [69].

Secretion of GLP-1 from L-cells is triggered by a range of nutrients digested and absorbed from the intestinal lumen including free fatty acids (FFAs), glucose and peptides [70–72]. Additional GLP-1 secretagogues include circulating factors such as angiotensin II and arginine vasopressin (AVP; hormones involved in blood pressure regulation and osmoregulation) and bacterial metabolites such as SCFAs produced by fermentation in the distal gastrointestinal tract [73–75]. As detailed earlier, GLP-1 is an incretin peptide which restores normoglycaemia postprandially by triggering insulin secretion and suppression of glucagon secretion. GLP-1 stimulated insulin secretion likely results from direct activation of beta cell GLP1R. In contrast, suppression of glucagon secretion from alpha-cells may result indirectly from GLP-1 stimulated somatostatin secretion from delta-cells mediating paracrine inhibition [76]. Regarding the anorexigenic effects of GLP-1, these effects can be mediated by activation of GLP1R on peripheral vagal afferents innervating the gastrointestinal tract and on central

neurons of the lateral hypothalamus. Due to the short half-life of GLP-1, it is likely that signalling through local vagal afferents is more physiologically relevant to gastrointestinal GLP-1 mediated satiation than direct action on the central nervous system [77,78].

Regarding the other proglucagon-derived peptides that are secreted together with GLP-1 from L-cells, whilst glicentin has no known receptor or physiological role, GLP-2 has an intestinotrophic effect via the G_s-coupled GLP-2 receptor. This effect appears important to the recovery of intestinal mucosa following injury [79,80]. Furthermore, oxyntomodulin in both rodent models and human volunteers, mediates loss in body weight (through appetite suppression and increases in energy expenditure) and restoration of normoglycaemia. Oxyntomodulin treatment also appeared to have superior therapeutic effects to GLP1R-selective incretin mimetics. These effects do not appear to be mediated by a specific oxyntomodulin receptor (which has not been identified to date), but by dual agonism of GLP1R and the glucagon receptor (GCGR) by oxyntomodulin [80,81]. Aiming to replicate the weight loss and improvements in glucose tolerance seen with oxyntomodulin administration, synthetic GLP1R/GCGR dual agonists have recently been developed, an example being MEDI0382. In recent clinical trials, MEDI0382 administration induced significant weight loss and restored normoglycaemia in type 2 diabetic patients demonstrating the therapeutic potential of GLP1R/GCGR dual agonism [82].

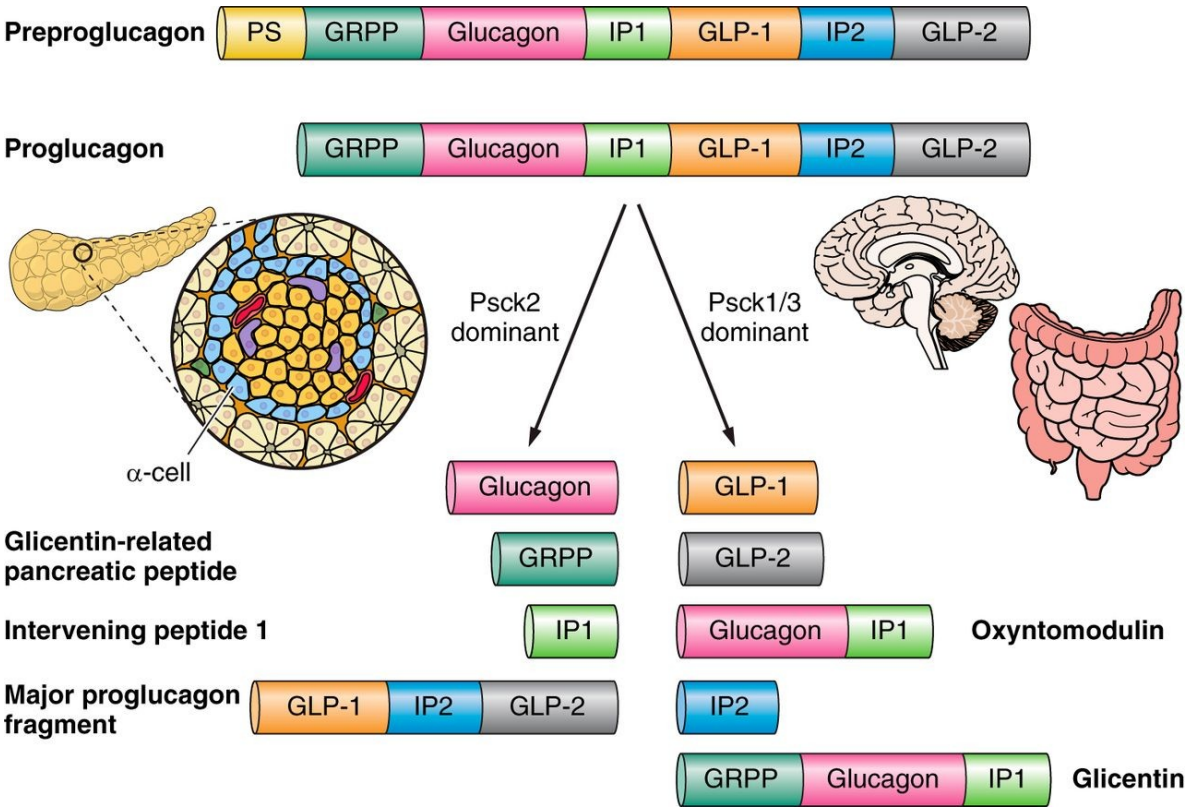

***Figure 3**: Post-translational processing of the preproglucagon polypeptide in alpha cells, neurons and L-cells of the gastrointestinal tract. Prohormone convertase 2 (Psck2) activity in alpha cells produces glucagon, GRPP, IP1 and major proglucagon fragment. Contrastingly, Psck1/3 activity in neurons and L-cells favours production of GLP-1, GLP-2, oxyntomodulin, IP2 and glicentin. Figure adapted from Sandoval et al. (2015)* [69].

1.7.2. Peptide YY

Peptide YY (PYY) is structurally related to neuropeptide Y (NPY) and activates NPY receptors. The secreted form is 36 amino acids in length (PYY 1-36) and is truncated to the predominant active form found in the circulation PYY 3-36 by DPP-4. PYY 3-36 has a much higher binding affinity for NPY2R than the other NPY receptors. Similarly to GLP-1, activation of NPY2R by PYY 3-36 in the hypothalamic arcuate nucleus and vagal afferents reduces food intake in rodent models [83–85]. Furthermore, both GLP-1 and PYY appear involved in the 'ileal brake' mechanism. This is a feed forward mechanism by which arrival of nutrients such as lipids in the proximal small intestine trigger GLP-1 and PYY release that attenuates gastric emptying, aiding with complete digestion and absorption of ingested nutrients [86]. The physiological effects of GLP-1 and PYY therefore seem to complement one another in reducing appetite, aiding in digestion and restoring normoglycaemia post-prandially. Indeed PYY is produced and co-secreted into the circulation with GLP-1 by L-cells [67,68,70–72]. Given that recent

immunohistological examinations of L-cells suggest that PYY and GLP-1 are packaged into separate secretory vesicle pools it is likely that the co-secretion of GLP-1 and PYY observed derives from regulation of the GLP-1 and PYY vesicle pools by common molecular secretory mechanisms [87].

1.7.3. Insulin-like peptide 5

Recent examination of colonic L-cells has revealed a subpopulation, representing roughly half of large intestinal L-cells, express and produce the gut peptide insulin-like peptide 5 (INSL5) [88]. The etymology of INSL5 relates to structural similarities between insulin and INSL5, with both consisting of two polypeptide chains (referred to as the A and B chains) linked together by disulphide bonds [89]. Regarding physiological relevance, INSL5 is thought to modulate hepatic glucose production, potentially stimulate insulin secretion from beta cells and to act, in contrast to GLP-1 and PYY, as an orexigenic gut peptide [88,90,91]. These actions are likely through the G_i-coupled cognate receptor of INSL5 relaxin family peptide receptor 4 (Rxfp4) with knockout of Rxfp4 in mice abolishing INSL5-induced increases in food intake [88]. Whether INSL5 is secreted together with GLP-1 and PYY to known colonic L-cell stimulants is unknown with investigations hampered by an inability to accurately quantify INSL5 from secretion and plasma samples [89].

1.7.4. Cholecystokinin

Cholecystokinin (CCK) is a gut peptide produced and secreted in response to luminal stimuli by a subset of enteroendocrine cells concentrated in the duodenum canonically referred to as I-cells. Through stimulation of CCK1 receptors on vagal neurons, like GLP-1 and PYY, CCK can exert a anorexigenic effect. However, this effect appears to be acute as after 24 hours of continuous administration of CCK no sustained change in food intake is observed [92]. Locally, CCK stimulates the release of digestive enzymes (from the pancreas) and bile (by triggering contraction of the gallbladder) into the duodenum [93]. The pancreatic enzymes released catalyse the breakdown of macromolecules such as complex carbohydrates, proteins and lipids into, respectively, simple sugars, amino acids and free fatty acids (together with cholesterol and monoglycerides) which are absorbed across the small intestinal mucosa [94]. Bile aids in this process by neutralising acidic chyme entering the duodenum from the

stomach and emulsifying ingested lipids into smaller micelles. CCK therefore plays a critical regulatory role in digestion [95].

1.7.5. Neurotensin

Neurotensin (NTS) is a 13 amino acid long peptide produced and secreted by a subset of enteroendocrine cells historically referred to as N-cells [96]. Neurotensin-producing cells are concentrated within the small intestine in rodents with lower numbers found distally in the large intestine [97]. Whilst N-cells are also numerous within the human small intestine, unlike in the rodents, they are very rarely found in the large intestine [98,99]. Neurotensin secretion is triggered by many of the same dietary stimuli as GLP-1/PYY including free fatty acids and glucose and is often produced and co-released by the same cells as GLP-1 and PYY [100,101]. Physiologically neurotensin mediates a range of different effects including promotion of fatty acid absorption from the small intestine, glucose-dependent modulation of insulin secretion (stimulating or reducing insulin secretion in conditions of low and high glycaemia respectively), wound healing and inflammatory responses and satiety [101–105].

The proinflammatory effects of neurotensin are thought relevant to the pathophysiology of inflammatory bowel disease (IBD) with patients displaying elevated expression levels of neurotensin and neurotensin receptor 1 [106]. Furthermore, neurotensin has also been linked to the development of obesity and type 2 diabetes. The evidence for such a link comes from physiological examinations of neurotensin knockout mice. When fed a high fat diet (HFD; used to model obesity), the neurotensin knockout mice displayed significantly attenuated weight gain, liver triglyceride/cholesterol accumulation and obesity-related insulin resistance compared to wild type mice on HFD. In part, these discrepancies appear to result from the absence of neurotensin facilitated absorption of lipids from the small intestine. Consistently, intestinal absorption of fatty acids following olive oil gavage (as measured by triglyceride accumulation) was attenuated in neurotensin knockout mice relative to wild type mice in a manner reversible through co-administration with neurotensin peptide [102].

Further evidence of the clinical relevance of neurotensin comes from studies investigating the effect of RYGB on the secretion profile of gut peptides. RYGB performed on rats yielded an

expected decrease in food intake associated with increased plasma levels of GLP-1 and neurotensin. Post-operative pharmacological antagonism of peripheral neurotensin signalling reversibly increased food intake [105]. Complimenting these findings, RYGB in humans is associated with elevated plasma GLP-1 and neurotensin levels. GLP-1 and neurotensin levels were particularly pronounced in patients with a longer biliopancreatic limb whereby nutrients are delivered directly to more distal regions of the small intestine rich in L and N-cells, relative to patients with shorter biliopancreatic limbs [107]. Combined, these findings imply that neurotensin may represent one of the aforementioned hindgut factors which enhances satiety following RYGB.

1.7.6. Somatostatin

Somatostatin is a cyclic polypeptide which has two active isoforms derived from the precursor peptide preprosomatostatin, a 28 amino acid variant (SST-28) and 14 amino acid variant (SST-14) produced by truncation of SST-28 [108,109]. Cells which produce and secrete somatostatin are referred to henceforth as D-cells (historical term for somatostatin-producing EECs). Radioimmunoassay analysis identified that gastrointestinal somatostatin equates to roughly 65% of the total somatostatin produced in the body with the highest concentrations found in the gastric antrum and distal colon. The remaining somatostatin is partitioned between delta cells in pancreatic islets (5%) and neurons of central nervous system (30%) [110]. Further immunohistological studies imply that the SST-14 isoform predominates in the stomach, pancreas and somatostatin-producing neurons whilst SST-28 predominates in the small and large intestines likely reflecting SST-28 as the terminal peptide product of preprosomatostatin in these regions [111]. Physiologically, somatostatin acts as a global inhibitor of exocrine and endocrine secretions inhibiting the release of all enteroendocrine hormones, pancreatic glucagon and insulin secretion and gastric acid production (both through direct action on parietal cells and indirectly through reduced secretion of stimulants of gastric acid secretion such as gastrin). The inhibitory properties of somatostatin are harnessed clinically by use of somatostatin analogues (such as octreotide) in neuroendocrine tumour treatment, suppressing the adverse effects of ectopic hormone production such as hypoglycaemia resulting from insulinoma [112]. In addition to dietary nutrients, such as small peptides, many endocrine and exocrine hormones, including GLP-1

and CCK, stimulate somatostatin secretion forming negative feedback loops [113–115]. As such, gastrointestinal somatostatin is involved in a wide range of physiological processes including glucose homeostasis, and regulation of gastric pH and gastrointestinal motility.

1.7.7. Serotonin

More than 90% of the total serotonin (5-HT) in the body is produced by EECs of the gastrointestinal epithelium referred to in this thesis as enterochromaffin cells (EC cells) [116]. These cells are found with highest incidence in the pylorus of the stomach and a fairly consistent distribution throughout the rest of the GI tract [117]. EC cells release 5-HT in response to a variety of different stimuli including neurotransmitters, bacterial metabolites and irritants. The 5-HT released modulates physiological activities via direct paracrine action and indirect action through neuromodulation. Serotonergic neuromodulation of the enteric nervous system (ENS) is known to regulate gut motility and peristaltic contractions (coordinated waves of circular and longitudinal smooth muscle contraction). Additional 5-HT functions include paracrine stimulation of gastrointestinal secretions with an example being mucous secretion from goblet cells. [118]. Clinically, dysfunction of gut serotonergic signalling has previously been linked to conditions such as irritable bowel syndrome (IBS), potentially reflecting the role of 5-HT in gut motility regulation. Furthermore, Bellono et al. hypothesise that EC cells may act as primary detectors of irritants before damage to the mucosa occurs suggesting that EC cells might be involved in gastrointestinal inflammatory responses [118,119].

1.8. Modelling the enteroendocrine system *in vitro*

In order to examine the secretory mechanisms of human enterendocrine cells *in vitro*, immortalised cell line models, primary murine and human tissue samples and recently developed gastrointestinal organoid models have been used. The following sections will briefly cover each of these approaches:

1.8.1. Immortalised cell line models

Immortalised cell lines provide *in vitro* physiological models which are self-renewing and can easily be scaled up and repeatedly passaged for new experiments. The self-renewing properties derive from genetic mutations which prevent cellular senescence which normally prevents cells from dividing indefinitely. Immortalised cell lines can either be generated by artificially inducing these genetic mutations through genetic engineering or from cancerous cells in which such mutations have already occurred. Additional experimental genetic perturbations can also be induced. The primary immortalised cell line models used to replicate L-cell physiology are GLUTags, STC-1 and NCI-H716 cells. GLUTags and STC-1 cells were derived from tumours of the murine colon and small intestine respectively [120,121]. Whereas NCI-H716 cells were generated from a colorectal cancer from a human patient [122]. Kuhre et al. compared EEC peptide production and secretory responses of these cell lines to native L-cells. Whilst GLP-1 was produced and released from all three cell lines, none of the cell lines produced PYY, the other main characteristic L-cell peptide. Furthermore, all three cell lines produced pancreatic glucagon which is absent in L-cells. This is consistent with GLUTag and STC-1 expression of proprotein convertase 2 (PC2) which is not expressed in L-cells (figure 3) [123]. Thus, whilst GLUTag, STC-1 and NCI-H716 cell are fairly inexpensive models of L-cells they do not completely recapitulate the physiology of native L-cells.

1.8.2. Primary tissue

Primary tissue based investigations of EEC secretory mechanisms have principally been conducted through generation of mixed primary cultures, Ussing chamber experiments and perfusion of isolated segments of gastrointestinal tissue. 2D mixed primary cultures are generated from isolated gastrointestinal secretory glands and have been successfully generated from all regions of the murine and human gastrointestinal tracts enabling analysis

of EEC peptide secretory and secondary messenger responses [114,124]. Ussing chamber experiments allow measurements of ionic fluxes across strips of gut epithelium suspended between isolated apical (replicating the lumen) and basolateral (replicating the extracellular fluid) chambers of buffer and subsequent identification of active transport processes [125]. Furthermore, the polarity of sensory transduction by EECs can be determined by application of stimuli/and or antagonists of specific transporters to either the apical or basolateral chambers (which is not possible in the 2D primary cultures) [126]. The epithelial polarity of EEC responses can also be examined using buffer perfused isolated sections of intestine with the added advantage that the structural integrity of the intestine and the blood vessels supplying it are largely preserved (for Ussing chamber experiments intestinal tissue must be opened up and flattened and usually the muscle layers and vasculature are removed). This allows stimuli to be directly administered either to the lumen or intravascularly [127]. A further benefit of the perfused intestine system derives from preservation of the smooth muscle layers enabling characterisation of the mechanisms underpinning gut motility [128].

1.8.3. Gastrointestinal organoids

The lifespan of the gastrointestinal epithelial cells is roughly 3-5 days with continual turnover driven by division and differentiation of stem cells found within the base of the intestinal secretory glands (crypts/pits) [129]. One population of such intestinal stem cells are marked by expression of leucine-rich repeat-containing G-protein coupled receptor 5 (LGR5+ cells) which is involved in Wnt signalling [130]. By culturing isolated LGR5+ cells or gastrointestinal glands in media that replicates the *in vivo* stem cell niche (different for each region) self-renewing mini-guts replicating the structural composition and polarity of native epithelium termed organoids can be generated [130,131].

Proliferation and differentiation of LGR5+ cells is regulated by exposure to various modulators, principally by the signalling peptides Wnt, bone morphogenetic protein (BMP), epidermal growth factor (EGF) as well as direct cell-cell Notch signalling (figure 4) [131]. The typical composition of small intestinal organoid media (subsequently referred to as ENR media) reflects this with inclusion of EGF, the BMP inhibitor Noggin and R-spondin1 which promotes Wnt signalling [132]. Inclusion of EGF in organoid media promotes proliferation of

stem cells and progenitor cells whilst suppressing apoptosis [133]. Likewise Wnt activity, which is promoted by R-spondin, promotes LGR5+ proliferation and stemness maintaining a pool of stem cells at the base of intestinal crypt [131]. Repression of BMP signalling by Noggin promotes crypt fission *in vivo* and is required for long term maintenance and passaging of organoids [130,134]. BMP signalling can also determine the hormone repertoire produced by small intestinal enteroendocrine cells according to placement along the crypt-villus axis where a gradient of BMP exists with highest levels found in the villus [132]. Additionally, Notch signalling drives LGR5+ stem cells towards an enterocyte fate through upregulation of *Hes1* expression. *Hes1* represses expression of *Math1* and *Dil1* which drive LGR5+ cells toward a secretory cell fate, including enteroendocrine cells. Reflecting this, inclusion of inhibitors of Notch signalling, such as DAPT and DBZ, in the organoid culture media decreases numbers of LGR5+ stem cells whilst increasing the numbers of enteroendocrine and goblet cells [135,136].

Regarding the use of gastrointestinal organoids to investigate enteroendocrine cell physiology, Petersen et al. have shown that L-cells of both murine and human small intestinal organoids exhibit similar secretory responses to SCFAs and glucose as native L-cells and imply that organoid-derived L-cells recapitulate native L-cell physiology. This suggests that intestinal organoids provide a valid platform for investigating enteroendocrine cell physiology which combines the advantages of using cell lines (e.g. indefinite propagation, genetic modification) with those of using primary tissue (e.g. contains all epithelial cell types, preserves polarity).

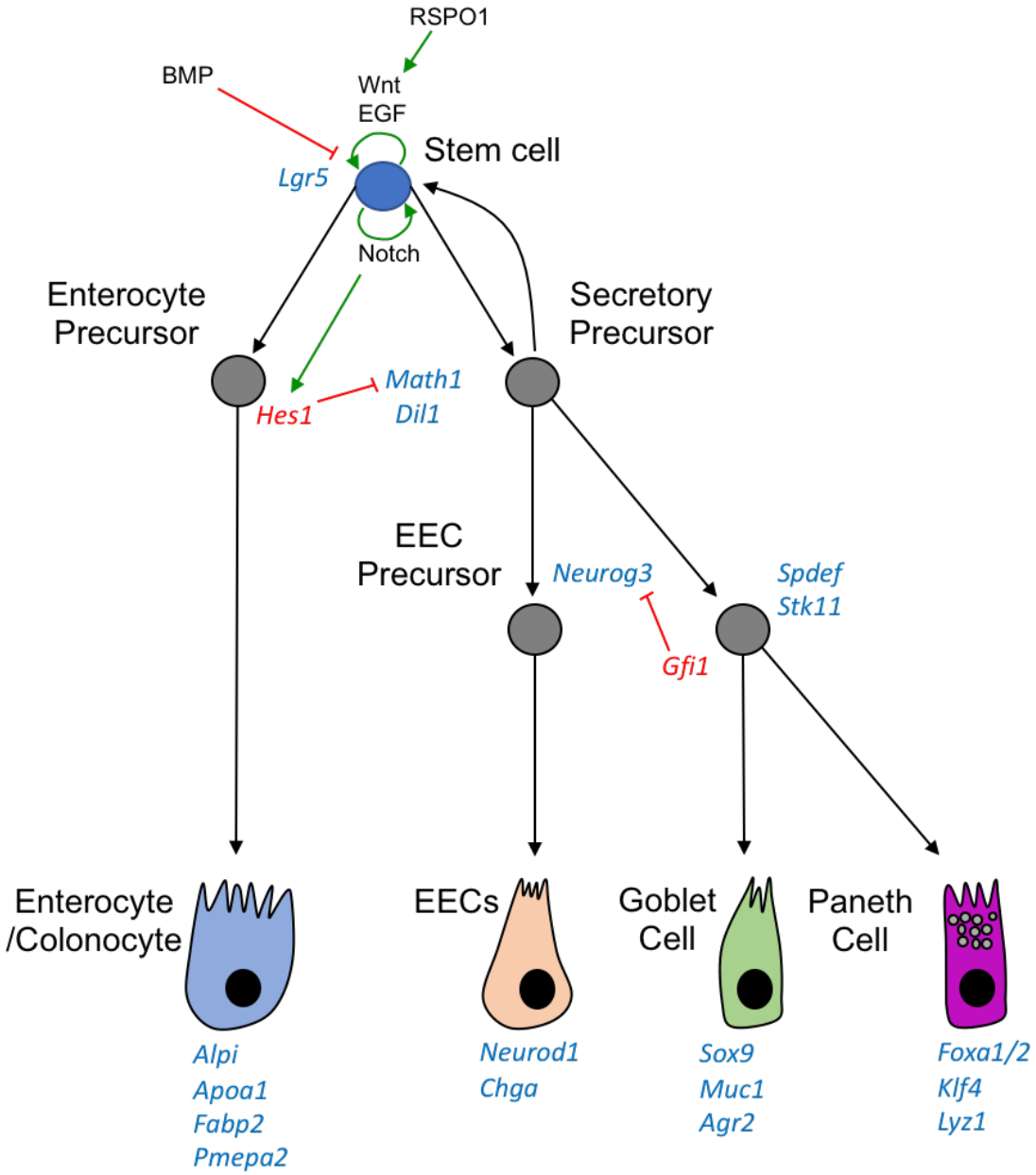

***Figure 4**: Schematic illustrating LGR5+ cell differentiation into mature absorptive cells (enterocytes/colonocytes) and secretory cells (enteroendocrine cells, goblet cells and Paneth cells). Wnt, epidermal growth factor (EGF) and Notch signalling promote LGR5+ cell proliferation whilst bone morphogenetic protein (BMP) inhibits proliferation. Notch signalling additionally promotes Hes1 expression which represses expression of the secretory cell determinants Math1 and Dil1. Secretory precursors can provide a reserve population of intestinal stem cells, dedifferentiating to stem cells upon tissue injury. Key transcription factors marking each cell population are indicated in blue and red text. Green arrows indicate stimulatory activity whilst T-shaped red lines indicate inhibitory activity. Based on Brunschwig et al. (2003), Grun et al. (2015), Haramis et al. (2004), Kim et al. (2016), Li et al. (2011), Noah et al. (2011), Suzuki et al. (2010), Yamane et al. (2016), Van es et al. (2012) and Buczacki et al. (2013)* [65,133,134,137–143].

1.9. Hypotheses explored in this thesis

The investigations detailed in chapters 3, 4 and 5 were designed to expand the current understanding of enteroendocrine cell physiology with a focus on L-cell secretory mechanisms by testing the following hypotheses:

Chapter 3:

1. Co-activation of the G_s-coupled bile acid receptor GPBAR-1 and the G_q-coupled receptor for medium chain fatty acids (MCFAs) and long chain fatty acids (LCFAs), FFAR1, potentiates resulting intracellular Ca^{2+} and GLP-1 secretory responses.

Chapter 4:

1. INSL5-expressing L-cells exhibit intracellular Ca^{2+} transients and secrete INSL5 in response to application of known GLP-1 secretagogues.
2. INSL5 is co-secreted with PYY and GLP-1.
3. INSL5, PYY and GLP-1 are stored in separate vesicle populations which are regulated by common release mechanisms.

Chapter 5:

1. Colonic enteroendocrine cells can be subdivided beyond the canonical L-cell, D-cell and EC cell subtypes.
2. INSL5-expressing L-cells are concentrated in the distal large intestine.
3. Colonic enteroendocrine cell subgroups display functional differences in GPCR repertoire.

Chapter 2. Materials and Methods

N.B.: All reagents, unless stipulated, were obtained from Sigma-Aldrich. Quantities listed as percentages refer to $volume_{reagent}/volume_{total}$. All statistical analyses were run on GraphPad Prism 7.0 (GraphPad Software) unless otherwise stated.

2.1. Solutions and culture media

Saline buffer:

4.5mM KCl, 138mM NaCl, 4.2mM $NaHCO_3$, 1.2mM NaH_2PO_4, 2.6mM $CaCl_2$, 1.2mM $MgCl_2$, 10mM HEPES. Adjusted to pH 7.4 with 1M NaOH.

30mM KCl

30mM KCl, 113.6mM NaCl, 4.2mM $NaHCO_3$, 1.2mM NaH_2PO_4, 2.6mM $CaCl_2$, 1.2mM $MgCl_2$, 10mM HEPES. N.B. titrated to pH 7.4 using 1M NaOH.

Lysis buffer

0.25g deoxycholic acid, 0.5ml Igepal CA-630, 2.5ml 1M Tris-HCl, 1.5ml 5M NaCl, 1 EDTA-free protease inhibitor cocktail, made up to 50ml with H_2O.

ENR media

Murine 50ng/ml EGF (Invitrogen), 100ng/ml murine noggin (Peptrotech), 1μg/ml human R-Spondin-1 (Peprotech), 1% penicillin/streptomycin (100 units/ml; Invitrogen), 2mM L-glutamine (Invitrogen), N2 supplement (1x; Invitrogen), 1μM N-acetyl-L-cysteine (Sigma) diluted in advanced DMEM/F-12 (ADF; Invitrogen).

N.B. 10μM Y-27632 (Tocris) was added to media used to feed organoids immediately following seeding to limit anoikis.

Neutralisation media

ADF enriched with 10% fetal bovine serum and 10μM Y-27632.

Cryopreservation media

45% ADF, 45% FBS, 10% DMSO and 10μM Y-27632.

Primary culture media

Dulbecco's modified Eagle's medium (DMEM) high (4500mg/L) glucose enriched with 10% fetal calf serum, 1% glutamine and 1% penicillin/streptomycin.

Demucifying solution

10% glycerol, 10% 0.1M Tris titrated to pH 8.2, 20% ethanol, 30% H_2O, 92mM NaCl and 20mM DTT.

2.2. Animal procedures and ethics

All animal procedures were approved by the University of Cambridge Animal Welfare and Ethical Review Body and carried out in accordance with the Animals (Scientific Procedures) Act 1986 Amendment Regulations (SI 2012/3039). The animal work was performed under the UK Home Office project licence 70/7824. Mice were sacrificed by asphyxiation and cervical dislocation.

A local ethics review committee (09/H0308/24) approved all human studies. Human tissue samples were obtained from patients undergoing surgical resection and acquired from the Human Research Tissue Bank at Addenbrooke's Hospital, Cambridge, UK. All human tissue samples were utilised on the day of collection.

2.3. Transgenic mice

For intracellular calcium imaging of organoid-derived L-cells, organoids were generated from mice specifically expressing the genetically encoded intracellular calcium indicator GCaMP3 in L-cells. GCaMPs (including GCaMP3) are chimeric proteins consisting of circularly permutated GFP, calmodulin and M13 (from myosin light chain kinase) domains [144–146]. Under the condition of elevated intracellular calcium levels, calcium ions binding to the calmodulin moiety of GCaMP causes a conformational change in GCaMP that reduces solvent quenching of GFP fluorescence (when excited with 488nm light) [147]. Thus, when intracellular calcium levels increase GCaMP fluorescence (when excited with 488nm light) also increases providing a proxy measure for intracellular calcium levels. Selective L-cell expression of GCaMP3 was achieved by crossing Glu-Cre12 mice with ROSA26-GCaMP3 reporter mice (Jax stock 014538) [148,149]. In these Glu-Cre12/ROSA26-GCaMP3 mice expression of Cre recombinase drives specific expression in proglucagon expressing cells (i.e. L-cells) by excision of a floxed stop codon within the ROSA26-GCaMP3 cassette.

Transcriptomic and intracellular calcium imaging based scrutiny of *Insl5*-expressing L-cells was achieved through development of two novel transgenic mouse models based on the Tet-on system. As described in Billing et al. (2018), Insl5-rtTA mice were developed by Frank Reimann in which expression of the reverse tetracycline transactivator (rtTA) is placed under control

of the *Insl5* promoter (figure 1A). These Insl5-rtTA mice were crossed with mice expressing the bidirectional tetracycline reporter Tre-lacZ/GFP to produce Insl5-rTA/TET-GFP mice [150]. Similarly the Insl5-rTA mice were crossed with TET-GCaMP6F and CMV-Cre mice generating Insl5-rTA/TET-GCaMP6FΔCMV mice (the CMV-Cre cross produced germ line deletion of a floxed stop codon within the TET-GCaMP6F cassette) [151]. GCaMP6F was developed from pre-existing GCaMP variants by mutagenesis and exhibits greater sensitivity and faster responses to intracellular calcium than GCaMP3 [152]. In the Insl5-rTA/TET-GFP and Insl5-rTA/TET-GCaMP6FΔCMV mice conditional expression of GFP and GCaMP6F is limited to *Insl5*-expressing cells upon administration of tetracyclines such as doxycycline (figure 1B) [153]. For FACS-isolation and model verification by tissue section immunofluorescent labelling mice were orally induced for 5-7 days with 3mg/ml doxycycline dissolved in drinking water supplemented with 5% sucrose to improve palatability.

Isolation of mature colonic enteroendocrine cells for scRNA-seq analysis was achieved based on FACS-purification of cells expressing the enteroendocrine cell marker *Neurod1*. For this, NeuroD1-Cre mice were crossed with ROSA26-EYFP mice yielding selective expression of EYFP in *Neurod1*-expressing cells via Cre recombinase excision of a stop codon within the ROSA26-EYFP cassette [139,154].

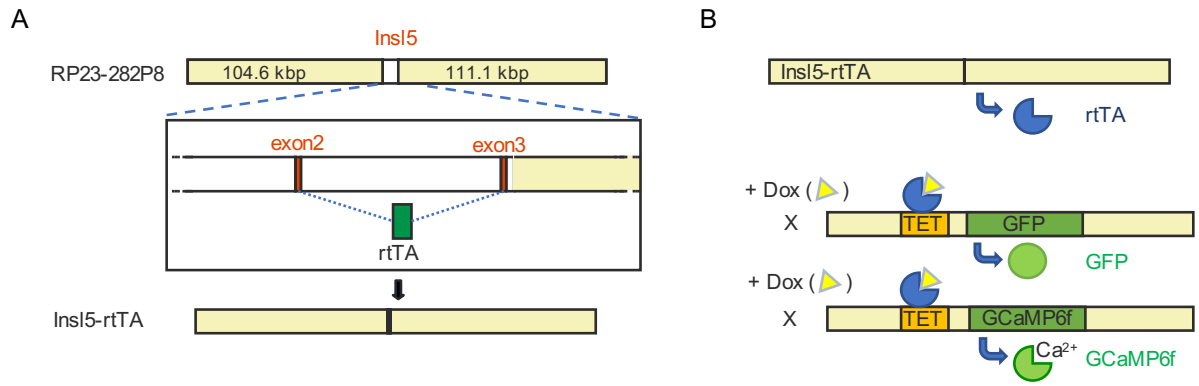

Figure 1: *(A) Scaled diagram of the BAC-transgene used to make Insl5-rtTA mice. The reverse tetracycline transactivator (rtTA) coding sequence replaced the Insl5-coding sequence. (B) Schematic illustrating the tetracycline dependent expression of GFP and the calcium indicator GCaMP6F in Insl5-rTA/TET-GFP and Insl5-rTA/TET-GCaMP6FΔCMV mice. Dox = doxycycline. Figure adapted from Billing et al. (2018)* [153].

2.4. Fluorescence activated cell sorting

2.4.1. Collagenase Digestion

Single cell digests of murine colon were prepared for FACS purification by collagenase digestion. For purification of *Insl5*-expressing cells digests from mice orally dosed with doxycycline prior to sacrifice (as described previously) were used. Single cell digests were produced by serial incubation of colonic tissue with 1mg/ml collagenase (dissolved in calcium-free HBSS) at 37°C and filtration through 50µm filters (to remove larger debris). The final digest was spun at 300g for 10 minutes, resuspended in HBSS (calcium-free) with 10% FBS (to reduce cell clumping and adhesion to plasticware) and 10µM Y-27632 (to prevent anoikis) and transferred to 5ml polypropylene round-bottomed tubes (Corning). Prior to FACS purification, samples were spiked with DAPI (to label dead cells) and for the NeuroD1-EYFP sort only, DRAQ5 (live cell marker; BioLegend UK).

2.4.2. Flow cytometry

Single cell suspensions were sorted using an Influx Cell Sorter (BD Biosciences) at the Cambridge Institute of Medical Research (CIMR) Flow Cytometry Core Facility. DAPI-staining, DRAQ5-staining (only for the NeuroD1-EYFP sort), side scatter, forward scatter and pulse width gates were applied to remove clustered cells and any cellular debris present. *Insl5*-expressing cells (from Insl5-rTA/TET-GFP and Insl5-rTA/TET-GCaMP6FΔCMV mice) were isolated by GFP fluorescence into RLT plus lysis buffer (Qiagen) enriched with 1% β-mercaptoethanol. GFP-ve cells were also isolated as a control population for the transcriptomic analysis of INSL5-producing cells. *Neurod1*-expressing cells (from a NeuroD1-EYFP mouse) were purified by EYFP fluorescence into LoBind tubes (Eppendorf) with 40µl HBSS (calcium-free), 10% FBS and 10µM Y-27632.

2.5. Tissue culture methods

2.5.1. Primary cultures

Excised tissue (both murine and human) was collected in Leibovitz's L-15 media. Collected tissue was cleaned of contents in PBS containing $CaCl_2$ and $MgCl_2$ and any adipose tissue was removed. The epithelium layer was separated from the outer muscle layers and vasculature by manual stripping. Following this the tissue was cut into small chunks ~2mm^2 in size and rinsed with PBS. Intestinal crypts were isolated through serial digestion at 37˚C with filtered collagenase (0.25mg/ml for mouse and 0.5mg/ml for human tissue) dissolved in high glucose DMEM. At the end of each digest the tissue was agitated through shaking. Digest fractions containing crypts (as examined by light microscopy) were centrifuged at 100g for 5 minutes and resuspended in primary culture media (neutralising collagenase activity). Subsequently these fractions were pooled and filtered through a 100µm filter. Following centrifugation at 100g for 5 minutes, intestinal crypts were resuspended in primary culture media enriched with 10µM Y-27632 (Tocris). These crypt suspensions were plated on 2% matrigel (Corning) precoated 12 well plates for secretion experiments, 35mm glass-bottomed dishes (MatTEK) for intracellular calcium imaging experiments and 18x18mm 1.5H glass coverslips (Zeiss) for immunohistochemistry. Plated crypt suspensions were placed into a 37˚C humidified incubator with 5% CO_2 to settle overnight prior to experimentation. For experiments using Insl5-rTA/TET-GFP and Insl5-rTA/TET-GCaMP6FΔCMV mice, cultures were seeded in primary culture media with added 2µg/ml doxycycline hyclate.

N.B.: For chapter 5, regional murine colonic crypt cultures were generated by division of the colon into proximal (first 1.5-2cm from the caecocolic junction), intermediate and distal (most distal 2 cm of the large intestine) segments. Segments from 2 mice were pooled together to ensure there was enough tissue for each secretion plate.

2.5.2. Small intestinal organoids culture

Generation

Excised murine small intestines were washed in ice cold PBS (with $CaCl_2$ and $MgCl_2$) using a glass pipette to remove luminal contents. Following washing, the small intestines were

opened up using scissors and cut into 3-5mm sections. These sections were transferred to ice cold 30mM EDTA (0.5M EDTA stock diluted in PBS) for 5 minutes. Subsequently, the sections were moved to fresh PBS in 50ml falcon tubes and shaken for ~12 seconds. The resulting digest fractions were transferred to FBS pre-coated (reduces crypt adhesion) Petri dishes (Corning) and examined under the light microscope for villi/crypt presence. The sections were then transferred back to EDTA for a further 4 rounds of EDTA digestion. Fractions with the greatest crypt yield and lower levels of villi were pooled, passed through a 70µm filter (to remove debris and villi) and centrifuged at 100g for 5 minutes in a 15ml Falcon tube. Following centrifugation, the supernatant was discarded and the crypt pellet was resuspended in ~200-300µl matrigel (Corning) and seeded onto a 48-well plate (15-20µl of crypts per well). These 48-well plates were incubated at 37˚C for 30 minutes to enable matrigel polymerisation. Following this, each well was overlaid with 200-300µl ENR media (enriched with 10µM Y-27632) and placed in a 37˚C humidified incubator with 5% CO_2.

Maintenance

Organoids were refed with fresh ENR media every 2-3 days and split roughly every 7 days. For splits, ENR media was removed and organoid wells were scrapped and collected with TrypLE express enzyme (Gibco) into a 15ml Falcon tube and incubated in a water bath at 37°C for 2-3 minutes. Subsequently the TrypLE express enzyme was neutralised by addition of neutralisation media and titriated with P1000 tips. The digest was then centrifuged at 200g for 5 minutes and the majority of the supernatant was discarded leaving around 30-40µl solution. Using P200 tips the organoid pellet was mechanically disrupted through titriation. 200-300µl matrigel was added and the broken-up organoids were seeded in the same manner as the isolated crypts.

2D culture generation

7-10 day old organoids cultured in matrigel domes were scrapped and collected with ice cold ADF to dissolve the matrigel matrix. Following centrifugation at 200g for 5 minutes, the supernatant was discarded and organoids were enzymatically digested in TrypLE express enzyme for 2 minutes at 37°C. The digest was then neutralised with neutralisation media and

titriated to break-up the organoids into smaller chunks. These chunks were centrifuged at 200g for 5 minutes and resuspended in an appropriate volume of ENR media enriched with 10µl Y-27632 and plated onto 2% matrigel precoated 48-well plates for secretion assays and glass-bottomed dishes for intracellular calcium imaging experiments. Plated 2D cultures were then left to settle in a humidified 37°C incubator (with 5% CO_2) overnight before experimental use. See figure 2 for a cartoon summarising organoid generation, maintenance and seeding of 2D cultures.

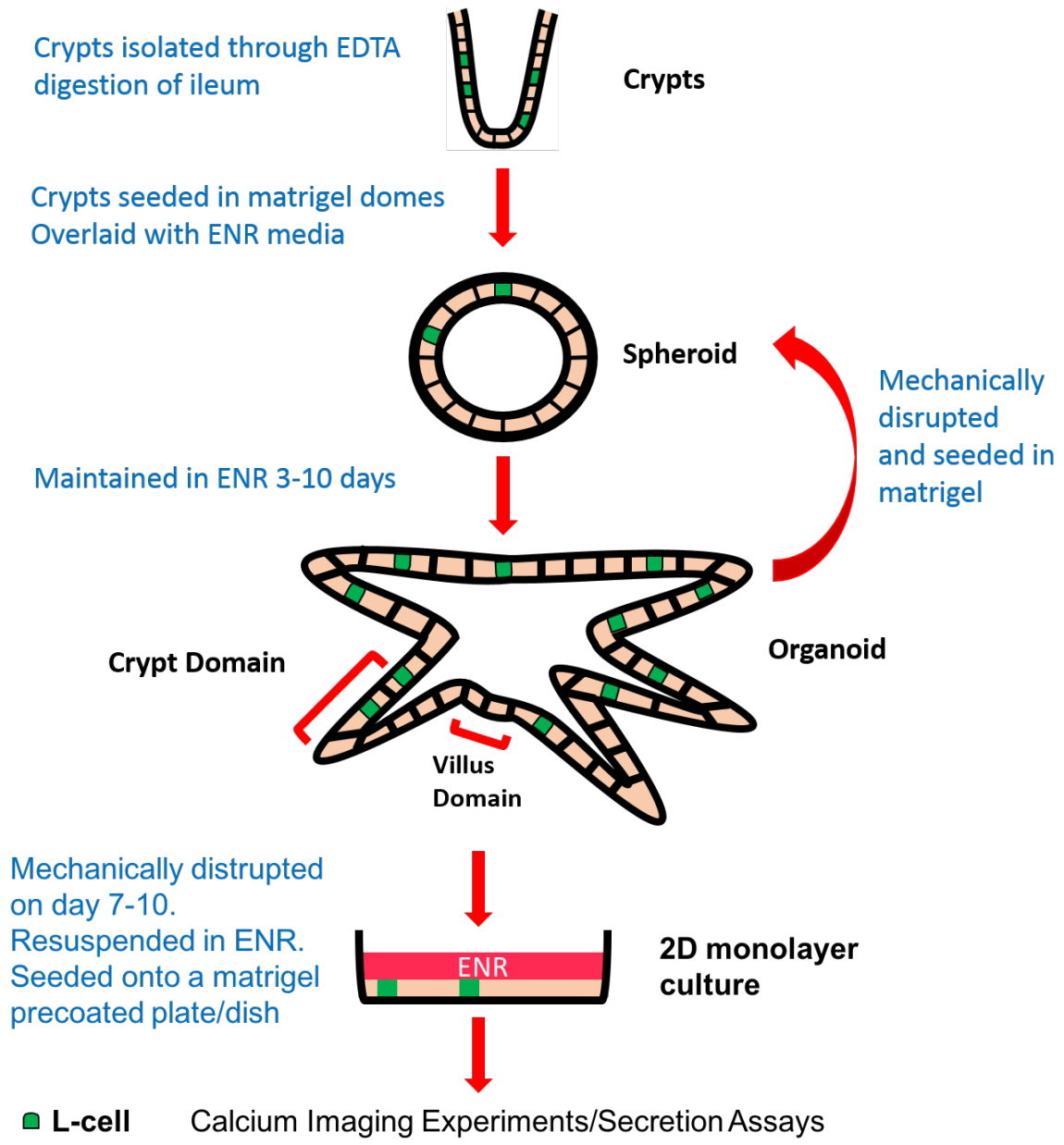

***Figure 2**: Schematic illustrating organoid generation, maintenance and 2D culture seeding.*

Cryopreservation

Stocks of generated organoids were made through cryopreservation. For this, organoids were scrapped and collected using cold TrypLE express enzyme and immediately neutralised using neutralisation media. Following centrifugation at 200g for 5 minutes and subsequent discarding of the supernatant, organoid pellets were resuspended in an appropriate volume of cryopreservation media and aliquoted into cryogenic vials. These vials were frozen in Mr. Frosty (Thermo Scientific) containers and transferred to liquid nitrogen filled tanks.

Frozen organoid stocks were thawed by briefly heating cryogenic vials in a 37°C water bath and transferring the contents to a 15ml Falcon tube containing neutralisation media. Following centrifugation at 200g for 5 minutes, the defrosted organoids were resuspended in matrigel and seeded as described for isolated crypts.

2.6. Secretion assays

2.6.1. Measuring GLP-1 secretion from organoid cultures

N.B: These experiments were performed as a collaborative effort with Deborah Goldspink.

2D organoid cultures were washed 3 times with warm saline buffer containing 1mM glucose and 0.1% fatty acid free BSA. In the final wash the cultures were incubated at 37°C for 20 minutes. Subsequently, 150µl of drug treatments were added to each well (all test agents were dissolved in wash buffer) and the plates were incubated at 37°C for 2 hours in a humidified incubator. Following this the plate was placed on ice and the cell supernatants transferred to 1.5ml tubes. These tubes were spun at 350g for 5 minutes at 4°C to remove cellular debris and the supernatants was harvested. Meanwhile, 150µl lysis buffer was added to each well and the plate was left on ice for 30 minutes to allow for complete cell lysis. The lysates were then collected from each well following scraping and spun at 8000g for 5 minutes at 4°C with the supernatants retained. The treatment and lysate supernatants were stored at -70°C prior to analysis. GLP-1 quantification was achieved through the use of total GLP-1 ELISA kits (MesoScale) as per the manufacturer's instructions.

GLP-1 secretory responses for each stimulus were calculated as the amount of GLP-1 secreted as a percentage of the total GLP-1 content of each well (sum of GLP-1 secreted and lysate GLP-1 content). Relative GLP-1 secretion was calculated by dividing these secretory responses by the percentage GLP-1 secretion in the basal condition (to control for inter-plate variability). Statistically significant GLP-1 responses ($p<0.05$) were identified by two-tailed t-tests assessing deviation of mean of relative GLP-1 secretion from 1 (i.e. basal GLP-1 secretion). The statistical significance of inter-group differences in GLP-1 responses were assessed using one-way ANOVA tests with Dunnett's correction on log transformed values ($p<0.05$). In order to assess the effect of combined GPBAR-A and TAK-875 treatment on GLP-1 secretion, the actual GLP-1 responses to GPBAR-A and TAK-875 co-application were divided by the expected GLP-1 responses (sum of GLP-1 responses to isolated GPBAR-A and TAK-875 treatment). Statistically significant ($p<0.05$) deviation of these ratios from 1 (i.e. no potentiation) were assessed using two-way t-tests.

2.6.2. Measuring GLP-1, PYY and INSL5 secretion from colonic crypt cultures

N.B: The murine and human secretions detailed in chapter 4 were performed and analysed by Pierre Larraufie.

Primary murine and human colonic crypt cultures were washed 3 times with warm saline buffer containing 1mM glucose and 0.001% fatty acid free BSA. In the final wash cultures were incubated at 37°C for 30 minutes. The lower concentration of BSA (relative to that used for the organoid cultures), prevented saturation of the downstream LC/MS analysis with BSA-derived peptides. Following discarding of the final wash, 600µl of each treatment (made up in saline buffer with 1mM glucose and 0.001% BSA) was added to each well and the plate was incubated at 37°C for 1 hour. The plate was then placed on ice and treatments were transferred to LoBind 1.5ml tubes (Eppendorf; reduced peptide loss) and centrifuged at 2000g for 5 minutes at 4°C to remove cellular debris. 500µl of each supernatant were collected into fresh 1.5ml LoBind tubes. Meanwhile, 200µl lysis buffer was added to each well. After 30 minutes on ice the plates were snap frozen and defrosted to ensure complete cell lysis. Lysates were collected following cell scraping and spun at 8000g for 5 minutes at 4°C and the supernatants were retained.

For LC-MS/MS peptide quantification, treatment supernatants were first acidified with 50µl 1% formic acid and spiked with internal standards. The samples were then loaded into primed µElution SPE plates (Waters) according to the manufacturer's instructions. Elution was achieved by twice running through 20µl of methanol/acetic acid/water (60%/10%/30%) applying positive pressure.

For the peptide quantification in chapter 4, murine samples were analysed intact whereas the human samples were dried and reduced and alkylated. Reduction and alkylation was achieved by incubation with 40µl 10mM DTT in 50mM ammonium bicarbonate for 1 hour at 60°C followed by 30 minutes with 10µl 100mM iodoacetamide. 50µl of 0.1% formic acid (dissolved in H_2O) was then added. 40µl of sample were injected. Murine samples were analysed by LC/MS on a high-flow rate and human samples analysed by LC-MS/MS on a nano-flow rate by

a ThermoFisher Ultimate 3000 nano LC system coupled to a Q Exactive Plus Orbitrap mass spectrometer (Thermo Scientific). Peptide quantification was achieved using XCalibur (ThermoFisher) to integrate the peak area for selected sets of m/z values at specific retention times corresponding to amidated GLP-1, PYY 1-36 and intact INSL5 for murine samples and the C-chain N-terminus of INSL5 for human samples (fragment most consistently detected).

For chapter 5, murine samples were dried and reduced and alkylated using 50µl DTT and 10µl iodoacetamide in the same manner as for human samples. These samples were then topped up with 10µl 1% formic acid and 30µl injected for nano-flow LC/MS analysis. In these samples the A-chain of INSL5 was quantified (fragment most consistently detected) and NTS (with terminal glutamine transformed into pyroglutamate) was additionally quantified. All readings were normalised by the internal standard measurements. Total protein content was calculated from lysate supernatants using a BCA protein assay (Thermo Fisher Scientific) which was used to normalise secretory responses between different wells (account for differences in cellular content).

For chapter 4, secretory responses were normalised to basal secretion and the statistical significance ($p<0.05$) of murine colonic crypt secretory responses were assessed using a Dunn test. Pair-wise correlation between GLP-1, INSL5 and PYY secretory responses were assessed for both murine and human colonic crypt cultures using Pearson correlation. RStudio was used for these statistical evaluations.

For the regionals secretions detailed in chapter 5, given that in some cases basal levels of NTS and INSL5 secretion were undetectable, statistical tests were run on the secretory responses normalised by total protein content only. Using square root transformed data, statistically significant INSL5, PYY and NTS secretory responses (compared to basal secretion) were identified by one-way ANOVA tests. Likewise, statistical differences in regional secretory responses were assessed using one-way ANOVA tests (with the exception of INSL5 responses to angiotensin II and all NTS secretory responses where one-way t-tests were used).

2.7. Immunohistochemistry

2.7.1. Organoid cultures

For IHC, organoids were seeded onto coverslips in a 48-well plate. Following PBS washing, they were fixed in 4% PFA (Alfa Aesar) for 1.5 hours. Afterwards they were permeabilised using a wash solution containing 0.1% Triton-X 100 dissolved in PBS and blocked using wash solution containing 10% donkey serum for 1 hour at room temperature. They were then incubated with primary antibodies to proglucagon and GFP (table 1) diluted in wash buffer with 1% donkey serum overnight at 4°C. The next day, following further washes the organoids were incubated with donkey secondary antibodies (conjugated to AlexaFluor 488 and 555) for 1 hour at room temperature. This was followed by a 10 minute treatment with 1:1300 Hoescht nuclear stain, further washes and mounting on microscope slides using Hydromount (National Diagnostics).

2.7.2. Primary cultures

For immunofluorescent labelling, primary cultures were seeded onto 2% matrigel precoated 18x18mm 1.5H glass coverslips (Zeiss). They were fixed for 1 hour at room temperature with 4% PFA (Alfa Aesar) followed by 3 PBS washes. The cultures were then detergent treated with 0.1% Triton-X 100 (was used as wash solution in subsequent steps) dissolved in PBS. Following a 15 minute block in 10% goat serum (diluted in PBS), the primary cultures were incubated at room temperature with primary antibodies to INSL5 and GFP for verification of GCaMP6F induction and INSL5, PYY and GLP-1 for 3D-SIM analysis (table 1) for 45 minutes diluted in wash solution containing 1% goat serum. Subsequently, cultures were washed for 30 minutes and incubated at room temperature with 1:300 (1:100 for cultures imaged by 3D-SIM) goat secondary antibodies (conjugated to AlexaFluor 488, 555, 633 and 647) for 30 minutes with an additional 10 minute incubation with 1:2000 Hoescht nuclear stain (in PBS). After further PBS washes, the coverslips were mounted onto microscope slides using Hydromount (National Diagnostics).

2.7.3. Tissue sections

Insl5-rtTA/TET-GCaMP6FΔCMV mice were orally treated with 3mg/ml doxycycline for 5-7 days prior to sacrifice and whole colon excision. Following removal of adipose tissue and muscle layers colons were fixed in 4% PFA (Alfa Aesar) overnight at 4°C. The tissue was subsequently dehydrated using a sucrose gradient firstly by placement in 15% sucrose (dissolved in PBS) for 5-6 hours at 4°C, followed by incubation in 30% sucrose (dissolved in PBS) overnight at 4°C. Following dehydration, the tissue was embedded in OCT creating blocks for sectioning and was stored at -70°C prior to further processing. A cryostat was used to create 6-10µm sections. Sections were mounted onto glass microscope slides for cell counting and onto Poly-Lysine (VWR) coated 18x18mm 1.5H glass coverslips (Zeiss) for 3D-SIM analysis.

Immunofluorescent labelling of tissue sections was achieved in a similar manner as for primary cultures except: 1 hour block steps, overnight incubation with primary antibodies (table 1) to INSL5 and GFP for cell counting and INSL5, GLP-1 and PYY for 3D-SIM at 4°C primary (table 1) and room temperature incubation with secondary antibodies for 1 hour.

2.7.4. Colonic Wholemounts

The following method was adapted from that developed by Winton et al. (1990) [155]:

Excised colons were stripped of adipose tissue and muscle layers (removal of the muscle layer greatly reduces immunofluorescent background). Colons were pinned onto 3% agar filled petri dishes, cut open and washed with PBS using a plastic pipette. The colons were then fixed for 3 hours at room temperature using 4% PFA (Alfa Aesar) and subsequently washed with PBS. Next, residual mucus was removed from the fixed tissue by incubation with 50mls of demucifying solution for 20 minutes at room temperature followed by 4 PBS washes.

The fixed colons were transferred to 50ml Falcon tubes containing blocking solution (PBS with 0.1% Triton-X 100 and 10% goat serum) and left overnight at 4°C. The following morning the colons were incubated for 4 hours at room temperature with primary antibodies to PYY, INSL5 and NTS diluted in wash solution containing 1% goat serum and 0.1% Triton-X 100 in PBS

(table 1). After this the colons were placed in wash solution overnight. Then the tissue was incubated with goat secondary antibodies (conjugated to AlexFluor 488, 555 and 633; 1:300) for 3 hours at room temperature. Following further washing overnight at 4°C, the colons were incubated with 1:2000 Hoescht nuclear stain (in PBS) for 30 minutes at room temperature followed by 1 hour period of PBS washes. Finally, the colons were divided in half and mounted onto microscope slides using Hydromount (National Diagonistics).

N.B: all steps for wholemount staining involving washing or incubation with primary and secondary antibodies involved the use of a rocker to promote washout and equalise antibody exposure across the length of the tissue.

Antigen	**Raised in**	**Concentration**	**Source**
Proglucagon	Rabbit	1:200	Santa Cruz sc13091
GFP	Goat	1:1000	AbCam Ab5450
INSL5	Rat	1:1000/1:2000	Takeda
PYY	Guinea Pig	1:500	Progen 16066
NTS	Rabbit	1:100	Merck AB4596
GLP-1	Rabbit	1:100	AbCam Ab22625

Table 1*: Primary antisera used for immunofluorescent labelling. Note 1:1000 of the INSL5 primary antibody was used for the 3D-SIM and wholemount samples whilst 1:2000 was used for verification of the Insl5-rTA/TET-GFP and Insl5-rTA/TET-GCaMP6FΔCMV mice by cell counting.*

2.8. Imaging

2.8.1. Confocal microscopy

For cell counting and verification of transgenic mouse models, slides were imaged using the Leica TCS SP8 X confocal microscope with x20/x40/x60 objectives. Images are presented as individual z-slices (tissue sections) or maximal z-stack projections (organoids).

Cell counts of immunofluorescently labelled tissue from doxycycline-induced Insl5-rtTA/TET-GCaMP6FΔCMV mice were carried out manually on x20 images using the Leica Application Suite X (n=3 mice).

2.8.2. Intracellular calcium imaging

Prior to analysis, primary and 2D organoid cultures were equilibrated with saline buffer containing 1mM glucose for 30 minutes. Following this, treatments were applied at a perfusion rate of 1ml/minute. All treatments were made up in saline with added 1mM glucose. Changes in GCaMP3/GCaMP6F fluorescence (proxy to intracellular Ca^{2+} levels) emitted upon excitation with 488nm laser light were measured through a long-pass filter (>510nm) every 2 seconds using a Nikon Eclipse TE2000-5. MetaFluor was used to coordinate GCaMP3/GCaMP6F excitation to record GCaMP3/GCaMP6F emissions from marked L-cells. L-cells were imaged 1-2 days after plating. After the first day of imaging, dishes were topped up with primary culture media (with 10μM Y-27632 and 2μg/ml doxycycline hyclate) and ENR (with 10μM Y-27632) for the primary and 2D organoid cultures respectively. Intracellular calcium responses were computed as ratio of maximum GCaMP3/GCaMP6F fluorescence measured during treatment to the maximum GCaMP3/GCaMP6F fluorescence during the 30 seconds prior to treatment (basal).

To examine the effect of concomitant activation of GPBAR-1 on intracellular calcium responses to 10μM TAK-875 and 30mM KCl cells were first stimulated with either 10μM TAK-875 or 30mM KCl alone. Following saline buffer washout, cells were pre-treated with 3μM GPBAR-A (GPBAR-1 agonist) for 10 minutes prior to co-application of 3μM GPBAR-A with 10μM TAK-875 or 30mM KCl for up to 5 minutes depending on whether responses in GCaMP3 fluoresence were observed. Subsequent TAK-875/KCl washout was achieved by a 3-5 minute

washout period with 3µM GPBAR-A followed by a 5 minute saline washout. After this period, 10µM TAK-875 or 30mM KCl was applied for a third time to allow comparison of intracellular calcium responses prior, during and after 3µM GPBAR-A co-application. The magnitude of the GPBAR-A and TAK-875 or KCl co-application effect was calculated by dividing the observed fold change in GCaMP3 fluorescence to co-application by the anticipated fold change (estimated from the individual GCaMP3 responses to GPBAR-A during the 30 seconds prior to TAK-875 addition and initial TAK-875 application) relative to basal GCaMP3 fluorescence (30 seconds prior to GPBAR-A application).

Statistical significance of intracellular calcium responses was assessed using a Kruskal-Wallis test comparing responses to the basal 0.1% DMSO condition or Wilcoxon tests (H_0: median=1). Inter-group comparisons were made using Kruskal-Wallis tests and potentiation was assessed using a Wilcoxon test (H_0: median=1, i.e. no synergy).

2.8.3. 3D-SIM imaging of GLP-1, PYY and INSL5 vesicles

3D super resolution microscopy

3D super resolution microscopy (3D-SIM) was used to examine the overlap between L-cell secretory vesicles containing INSL5, GLP-1 and PYY in both primary culture and tissue sections. This was facilitated by using the ELYRA S.1 microscope (Zeiss) to take 0.11µm spaced z-stack images of immunofluorescently labelled L-cells. These raw images were processed using ZEN Black (Zeiss). For the surfaces analysis, chromatic abberations were adjusted for by comparison with similarly imaged 100nm TetraSpeck fluorescent microspheres (ThermoFisher).

Vesicle analysis by 3D surface mapping

The surfaces analysis of overlap between INSL5, GLP-1 and PYY vesicles is based on methods employed by Cho et al. (2014) [87]. Using the ‘create surfaces’ function of Imaris (Bitplane), INSL5, GLP-1 and PYY vesicles were rendered in 3D from the 3D-SIM z-stack images. The ‘surface-surface colocalization’ function was then applied to create new surfaces from the

overlap in INSL5, GLP-1 and PYY surfaces. Using these surfaces, overlap in INSL5, GLP-1 and PYY vesicle volume was calculated as a percentage of total vesicle volume.

Vesicle analysis based on fitted 3D Gaussian distributions

This analysis was performed by Christopher Smith using MATLAB and is described in Billing et al. (2018) [6]. In brief, 3D Gaussian distributions were fitted onto the individual channel data from the 3D-SIM acquired z-stack images [156,157]. This enabled the determination of vesicle centre points for each channel. Chromatic aberration was accounted for by coinciding the mean 3D positions of all the vesicles in each of the channels for every image analysed. To remove erroneously localised vesicles, if the positions of the channel signals for a particular identified vesicle were >200nm apart they were considered to originate from different vesicles and therefore discarded. The channel intensities of each image were normalised to a 0-1 scale by reference to the image's maximum intensity pixel. Subsequently the channel intensities were determined for each vesicle by calculating the mean pixel intensity within a 150 nm radius sphere centred at the identified vesicle centre point, followed by background subtraction (mean intensity per image per channel across the whole z-stack). If the normalised intensity calculated for a particular channel exceeded 0.05 then the vesicle was deemed to contain the corresponding peptide. In contrast, if the channel intensity was lower than 0.02 then the vesicle was considered devoid of the corresponding peptide. The vesicle intensity profiles produced for each channel were derived in the x-axis plane centred on the identified vesicle centre point. The standard deviation of 1D Gaussian distributions fitted to these cross-sectional intensity profiles was used to estimate vesicle size.

N.B: Search https://bitbucket.org/cwissmiff/travis/src for the code used for the 3D Gaussian distribution analysis.

2.8.4. Imaging of colonic wholemounts

Image acquisition

Wholemounts were imaged using the Axio Scan.Z1 system (Zeiss). Tiles of extended depth of focus (EDF) images were taken for each of the three labelled channels using a Plan-ApoChromat 20x/0.8 M27 objective, a Hamamatsu Orca Flash camera and an inbuilt autofocus function. The depths used for the EDF images were customised for each wholemount and depended on tissue thickness. Following acquisition, the tiled images were stitched together with shading correction.

Counting of immunofluorescently labelled cells

Immunofluorescently labelled cells within the wholemount images were counted using HALO (Indica Labs). Following manual removal of damaged tissue or bubbles within each image, spatial analysis was used to identify cells labelled in each of the three channels (reflecting staining for NTS, PYY and INSL5). Afterwards, using INSL5 and NTS staining as the primary labels, dual labelled cells were identified. Following on from this, triple labelled cells were identified using NTS staining as the primary label. Finally, the infiltration analysis function (HALO) was applied to determine the density distribution of each type of cell (single, dual and triple labelled) within proximal (P1-P2), intermediate (P3-P5) and distal (P6-P7) subdivisions of the wholemounted tissue.

Downstream processing and statistical analysis of the cell density distributions was achieved using a combination of Excel (Microsoft Office) and GraphPad Prism 7.0 (GraphPad Software). One-sample t-tests were used to detect statistically significant ($p<0.05$) fold changes in cell density in each region of colon examined relative to those measured in the proximal colon.

2.9. Transcriptomic techniques

2.9.1. Real-time quantitative PCR

FACS-purified cells were lysed in RLT plus buffer with RNA extracted using the RNeasy plus micro kit (Qiagen) according to the manufacturer's instructions. TRI reagent was used to extract RNA from tissue homogenates (murine colons segmented into 7x 1cm pieces) with an additional step using DNA-free DNA removal kit (Invitrogen) to remove residual genomic DNA.

RNA was reverse transcribed using SuperScript II for homogenate samples and SuperScript III for samples from FACS-purified cells using a Peltier Thermal Cycler-225 (MJ Research) according to standard protocols. All RNA samples from FACS-purified cells were quality checked by using a Bioanalyser RNA Pico Kit (Agilent) with all RIN values above 7.3. RT-qPCR was undertaken using the QuantStudio 7 flex RT-qPCR system (Applied Biosystems). The RT-qPCR reaction mix consisted of template cDNA, TaqMan Universal Master Mix (Applied Biosystems) and specific primers (Applied Biosystems) which are detailed in table 2.

Relative expression was evaluated by calculating the difference in cycle threshold (ΔCT) between the housekeeper gene β-actin and the gene of interest ($CT_{\beta\text{-actin}}$-CT_{Gene}). With the exception of the regional expression analysis in the colon, statistical analysis was carried out on $2^{\Delta CT}$ values using ratio paired t-tests ($p<0.05$). For examination of differences in relative gene expression along the colonic proximal-distal axis (P1-P7 segments), statistically significant ($p<0.05$) differences in regional ΔCT values, with reference to the most proximal segment (P1), were evaluated using repeated-measures one-way ANOVA with Dunnett's correction.

Gene	Reference
ß-actin	Mm02619580_g1
Insl5	Mm00442241_m1
Gcg	Mm01269055_m1
Pyy	Mm00520716_g1
Ffar1	Mm00809442_s1
Casr	Mm00443375_m1
Gpbar1	Mm04212121_s1
Agtr1a	Mm01957722_s1
Avpr1b	Mm01700416_m1
Ffar2	Mm02620654_m1
Bb2r	Mm01157247_m1
Ppy	Mm01250509_g1
Nts	Mm00481140_m1
Olfr78	Mm00453733_s1
Slc5a8	Mm00520629_m1
Cck	Mm00446170_m1
Tph1	Mm01202614_m1
Sct	Mm00441235_g1
Sst	Mm00436671_m1
Calcrl	Mm0051986_m1

Table 2: *Identities of the TaqMan probes (Applied Biosystems) used for real time quantitative PCR.*

2.9.2. Single-cell RNA-sequencing

10x Chromium system

Following FACS isolation, 3500 EECs together with reverse transcription (RT) master mix reagents and gel beads, each containing primers with the same unique barcode and different unique molecular identifiers (UMIs), were fed into a microfluidics chip (see figure 3). 3500 cells were loaded rather than the total 7000 cells FACS-isolated due to cost restrictions. The flow rate was optimised to enable capture of single cells by each individual gel bead forming gel beads in emulsion (GEMs) separated by supplied partitioning oil. Within each GEM the captured cells were lysed and RNA transcripts were reverse transcribed into barcoded cDNA. The first strand cDNA generated from each GEM were then pooled together and amplified using PCR yielding a cDNA library ready for sequencing.

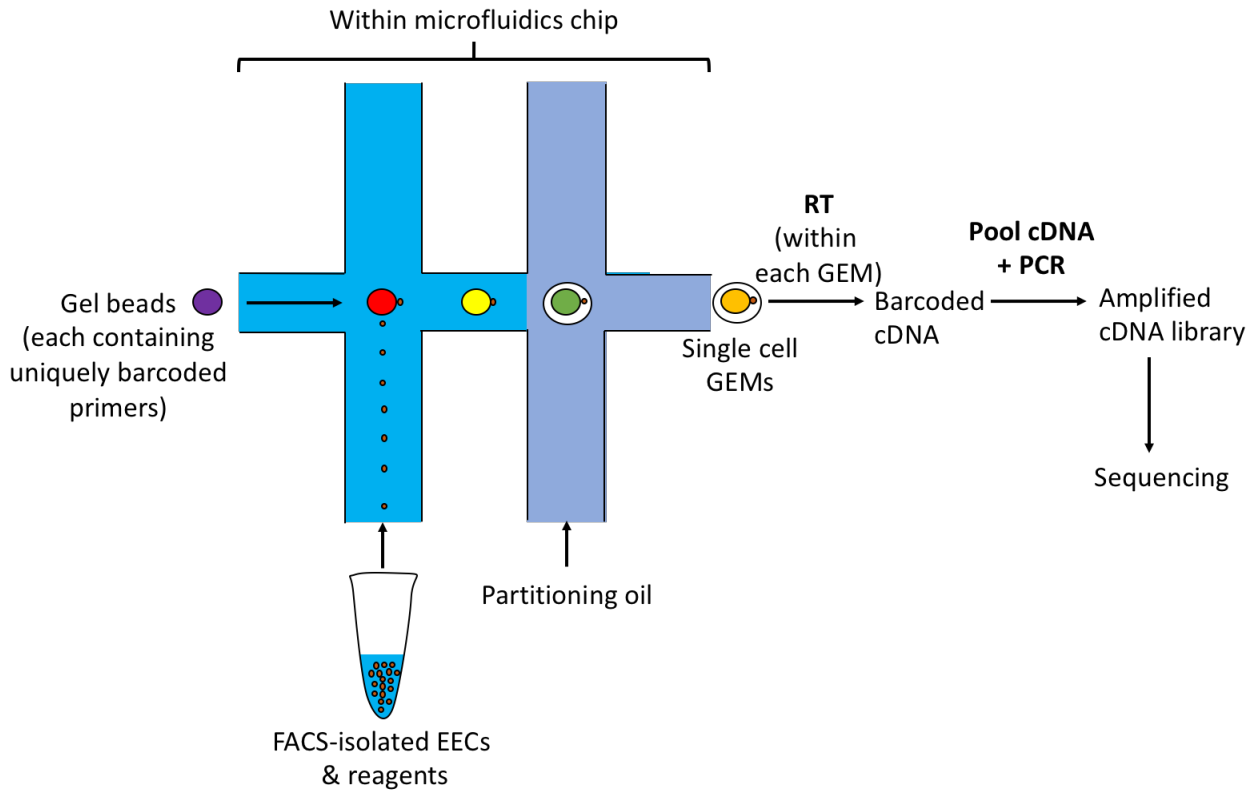

Figure 3: *Schematic illustrating how the 10x Chromium system generated single cell transcriptomes from FACS-isolated enteroendocrine cells (EECs). Gel beads in emulsion – GEMs.*

N.B. All the single-cell RNA-sequencing analyses were achieved using Bioconductor Software Packages on RStudio.

Library preparation

3500 FACS-purified NeuroD1-EYFP cells (from a single mouse colon) were used as input into the Chromium system (10x Genomics) producing cDNA libraries which were paired-end sequenced by a HiSeq 4000 (Illumina) at the Cancer Research UK Cambridge Institute (CRUK CI). Quality control, read alignment (with reference to the mm10 genome) and raw count quantification for each cell was achieved by Brian Lam using the CellRanger pipeline (10x Genomics). Cells with less than 2000 unique molecular identifier (UMI) counts were discarded yielding transcriptomes from 1779 cells for downstream analysis. Note that the Chromium system has a cell capture rate of up to 65% so many of the 3500 cells initially inputted were likely within the microfluidics chip. A mean of 190279 reads was achieved for the cells sequenced with transcripts from 17621 different genes detected and a median of 2099

different genes detected per cell. The median unique molecular identified (UMI) counts per cell was 5134.

K-means clustering

Prior to clustering, raw counts were normalised to UMI counts. K-means clustering (k=9) was then run on a t-distributed stochastic neighbour embedding (t-SNE) plot (seed=0, dims=2, perplexity=30) using the Rtsne package [158].

Differential expression

Differential expression analysis between identified groups was conducted using the edgeR package [159]. Raw counts were firstly normalised using the trimmed mean of M-values normalisation method (TMM) and then fitted to a negative binomial generalised log-linear model (using the glmFit function). Following this, gene-wise likelihood ratio tests were performed (using the glmLRT function) to examine statistical differences in gene expression between one reference group and all the other groups. These tests were repeated so that gene expression was compared between all groups. Subsequently, genes with a false discovery rate (FDR) above 0.01 were excluded and the top 10 most differentially expressed genes were identified for each group. Additionally, by subsetting genes encoding GPCRs (appendix 3) and transporters, the top 10 most differentially expressed GPCRs and transporters were identified for each group. Visual representation of differentially expressed genes was achieved by plotting heatmaps of the $\log_2$ UMI-normalised counts using the heatmap.2 function of the gplots package.

Correlation of gene expression

To assess correlation in expression between pairs of genes (namely *Insl5, Gcg, Pyy* and *Nts*) in L-cells, Pearson's product moment correlation coefficients (R) were calculated. For graphical representation, linear regression plots were created of the correlated pairs of genes using ggplot.

Chapter 3. Synergy between FFAR1 and GPBAR-1 signalling in L-cells

3.1. Introduction

As previously discussed, luminal contents of the intestine and circulating factors can be sensed by L-cells through activation of both G_q and G_s coupled GPCRs [55]. Simultaneous activation of the G_q and G_s signalling pathways by dietary stimuli raises the possibility of cross-talk between the two pathways and consequential synergistic effects on secretion (i.e. greater secretion than the sum of the responses to activation of the pathways individually). Ekberg et al. have identified such synergy in the GLP-1 secretory responses of small intestinal L-cells upon concomitant activation of the G_q-coupled free fatty acid receptor 1 (FFAR1) and the G_s-coupled GPR119 (receptor for 2-monoacylglycerol) with the synthetic agonists TAK-875 (AKA fasiglifam) and AR231453 respectively [160]. In this chapter, the hypothesis that synergy exists between the signalling pathways of FFAR1 and the G_s-coupled bile acid receptor GPBAR-1 is examined through intracellular calcium imaging and GLP-1 secretion assays. Clinically, combination therapy might enable exploitation of such synergy for type 2 diabetes treatment. This approach could potentially reduce adverse effects associated with monotherapy by yielding therapeutic benefits at lower doses of each individual drug administered.

3.2. Aims

1. To identify potential synergistic effects on intracellular calcium responses to FFAR1 and GPBAR1 co-activation
2. To examine possible synergistic effects on GLP-1 secretion to FFAR1 and GPBAR1 co-activation

3.3. Background

3.3.1. Lipid digestion and free fatty acid absorption

Animal and plant derived fatty acids form an essential dietary component and are ingested as esters such as triglycerides, phospholipids and cholesterol. Ingested triglycerides are digested to 2-monoacylglycerol (2-MAG) and free fatty acids (FFAs). Free fatty acids (FFAs) compose a group of hydrocarbons divided by the number of constituent carbon atoms into small (<8 carbons; SCFAs), medium (8-12 carbons; MCFAs) and long (>12 carbons; LCFAs) chain fatty acids [161]. Unlike MCFAs and LCFAs, volatile SCFAs are products of bacterial fermentation in the large intestine and contribute ~10% total daily calorie intake in humans [162]. FFAs modulate the activities of EEC cells and consequently gut hormone release through a diverse range of GPCRs [86].

Lipid digestion and absorption (figure 1) occurs primarily in the small intestine, facilitated by the action of pancreatic lipases. Pancreatic lipases catalyse the cleavage of ester bonds thus liberating free fatty acids (and 2-MAG) which are absorbed across the epithelium [163]. Lipase action is facilitated through lipid emulsification by bile acids produced by the liver from cholesterol. Produced bile acids are stored in the gallbladder between meals and enter the duodenum via the common bile duct. CCK, released postprandially in the proximal small intestine, stimulates gallbladder contraction and subsequent bile secretion into the duodenum [164]. These amphipathic molecules act as surfactants forming small micelles thus increasing the relative surface area of exposed lipid for lipase action [165,166]. Following liberation, FFAs are absorbed by enterocytes. The precise mechanisms by which this uptake occurs is not clear but appears to rely on a diffusion based mechanism known as ‘flip-flop’ and/or protein mediated transport mechanisms [167]. Once uptaken, FFAs bind to free acid binding proteins (FABPs) in the cytosol which act as chaperones [168]. Directed to the endoplasmic reticulum (ER), triglycerides are synthesised from the FFAs and 2-MAG and packaged into prechylomicrons. Following Golgi processing, prechylomicrons are transformed into mature chylomicrons which are exocytosed into the lacteals (vessels of the lymphatic system) and transport lipids to various tissues of the body [167].

Reabsorption and recycling of bile acids secreted into the intestinal lumen (summarised in figure 1) is highly efficient with roughly 95% of the secreted bile acids reabsorbed acting to reduce the metabolic burden of producing new bile acids [126]. The majority of bile acids (>95%) are reabsorbed by enterocytes through active transport. The key protein involved in this uptake is apical sodium-dependent bile acid transporter (ASBT) which imports 2 sodium ions for every bile acid molecule [169]. ASBT represents a potential therapeutic drug target in conditions such as functional constipation since ASBT inhibition attenuates bile acid reabsorption resulting in accelerated colonic transport [170]. Alternatively, bile acids conjugated to taurine or glycine can be passively absorbed across the apical brush border via diffusion [171]. As with FFAs, bile acids are sequestered within the cytosol by ileal bile acid binding proteins. Transportation across the baslolateral membrane of bile acids into the circulation is achieved by various solute transporter proteins enabling bile acid recycling by hepatocytes [95].

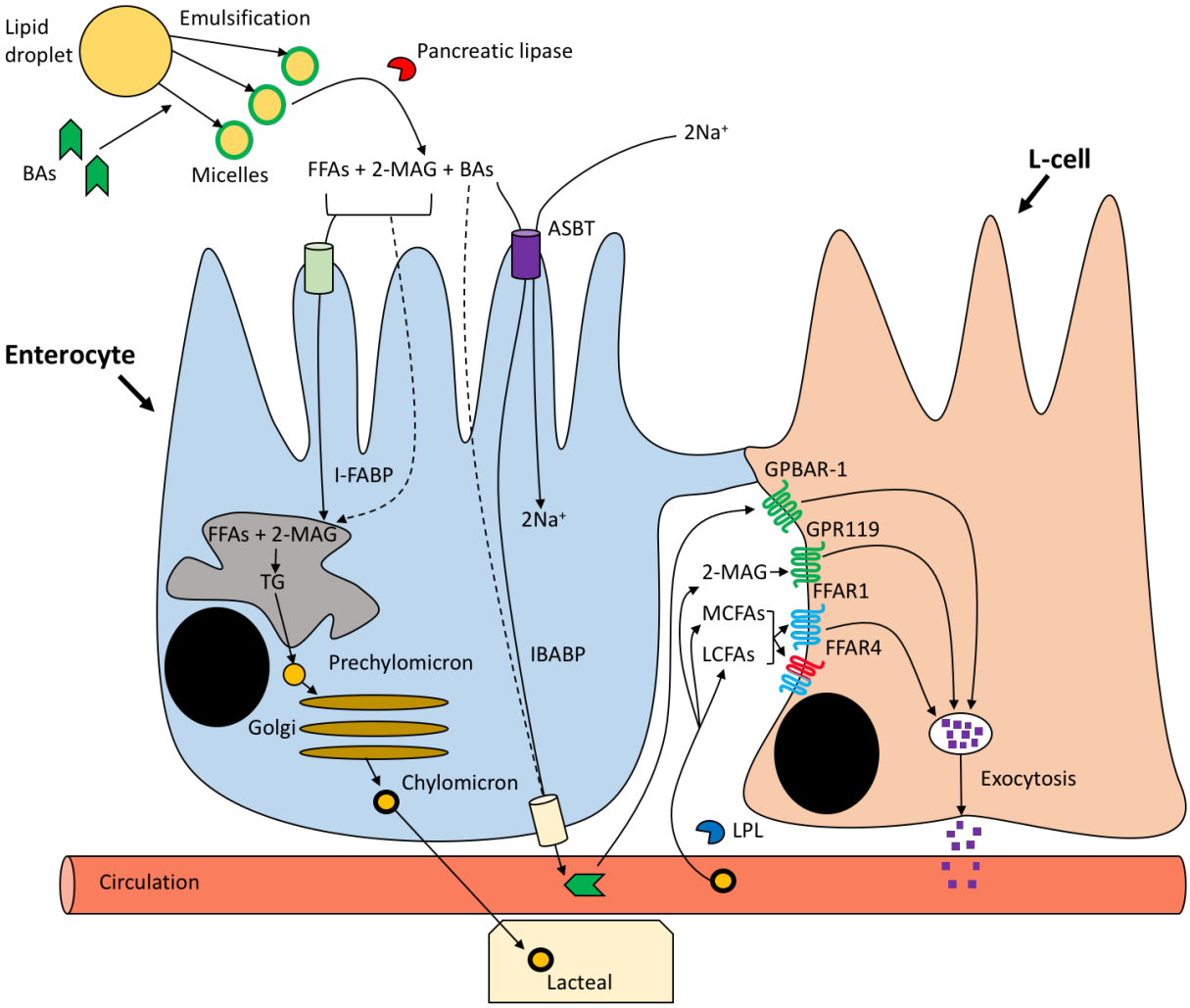

Figure 1: *Schematic illustrating the mechanisms involved in lipid digestion and absorption within the small intestine and receptors involved in L-cell chemosensation of free fatty acids (FFAs) and bile acids (BAs). Lipids droplets entering the small intestine are emulsified into micelles by released bile acids enhancing pancreatic lipase breakdown of triglycerides (TGs) to free fatty acids (FFAs) and 2-monoacylglycerol (2-MAG). FFAs and 2-MAG are absorbed by both passive diffusion and protein mediated mechanisms into enterocytes. Triglycerides are synthesised from absorbed FFAs and 2-MAG and packaged into prechylomicrons in the endoplasmic reticulum. These prechylomicrons are subsequently processed by the Golgi complex into chylomicrons which are exocytosed from the basolateral membrane into neighbouring lacteals. FFAs and 2-MAG are released from circulating chylomicrons by the action of local lipoprotein lipase (LPL). BAs are co-transported into enterocytes with sodium ions (2 Na^+ ions per bile acid molecule) from the lumen via apical sodium-dependent bile acid transporter (ASBT) and subsequently across the basolateral membrane into the circulation via protein-mediated mechanisms. FFAs, 2-MAG and bile acids can modulate secretion of gut hormones (red squares) from L-cells through GPCRs on the basolateral membrane. GPCRs are indicated by shapes with 7 transmembrane passes (blue = G_q-coupled, green = G_s-coupled and red = G_i-coupled). Cylindrical shapes indicate transporter proteins.*

3.3.2. L-cell FFA and bile acid sensing

Physiologically, detection of free fatty acids in the distal small intestine acts as an important initiation step of the 'ileal-brake' mechanism (which inhibits gastric emptying) through stimulation of GLP-1 and PYY release [86]. The resulting reduction in gastric emptying aids the complete digestion and absorption of ingested nutrients [172]. Previously, L-cells have been found to express functional receptors for FFAs and bile acids including receptors for medium and long chain fatty acids (e.g. linoleic acid) such as FFAR1 (AKA GPR40) and FFAR4 (AKA GPR120) and the bile acid receptor GPBAR-1 (AKA TGR5) [126,173–175]. FFAR1 and FFAR4 are primarily G_q-coupled GPCR whilst GPBAR-1 is G_s-coupled though FFAR4 can also couple to G_i signalling pathways [126,176]. *Ffar1* expression has been identified as enriched in both L and K-cells of the small intestine. Accordingly, *Ffar1* knockout in mice significantly attenuated plasma GIP/GLP-1 responses to high fat diet (administered via gavage) [175]. Additionally, application of FFAR1/FFAR4 dual agonists to human colonic crypt cultures triggered GLP-1 secretion [70]. FFAR4 appears to be play a less significant role in FFA-mediated GLP-1 secretion, as although the FFAR4-selective agonist Metabolex209 acted as a weak GLP-1 secretagogue from primary cultures, *in vivo* murine GLP-1 responses to corn oil gavages were abolished in *Ffar1* but not *Ffar4* knockout mice [160]. In fact, the weak GLP-1 responses seen to Metabolex209 could derive indirectly from inhibition of D-cell secretion of somatostatin which acts as a global inhibitor of enteroendocrine secretions [115,176].

Interestingly, FFAR1 appears to be basolaterally located in L-cells since in experiments where FFAR1 agonists, including TAK-875 and linoleic acid, were applied to perfused rat small intestine, GLP-1 secretion was only triggered by vascular administration and not luminal administration [127]. Such results imply that FFAs are not sensed by L-cells luminally but basolaterally following absorption. In support of this Psichas et al. suggest that FFA liberation from chylomicrons at the basolateral membrane by local lipoprotein lipase facilitates FFA sensing through FFAR1 [177]. However, support for this mechanism is compounded by evidence that orlistat (lipase inhibitor) does not attenuate GLP-1 secretion from murine intestinal cultures [177]. Furthermore, given the low bioavailability of orlistat, a study by Ellrichmann et al. (2008) on healthy humans suggests that pancreatic lipases might be more significant to FFA-mediated GLP-1 release as oral orlistat administration attenuated

postprandial increases in plasma GLP-1 [178]. Contrastingly, Damci et al. (2004) found that oral orlistat administration increased postprandial plasma GLP-1 levels in type 2 diabetic patients [179]. This increase in GLP-1 release could derive from increased delivery of lipids to the L-cell rich distal gastrointestinal tract. It is possible that the discrepancies in findings between the Damci et al. (2004) and Ellrichmann et al. (2008) studies reflect nutritional differences in the diets employed. The diet in the Damci et al. study, for example, contained higher levels of fat than in the Ellrichmann et al. study. In light of the contrasting findings detailed here, more *in vivo* and *in vitro* studies will be required to establish the precise molecular mechanisms which mediate basolateral L-cell FFA-sensing.

Functional *Ffar1* expression has also been identified in both rodent and human pancreatic islets whereby stimulation of FFAR1 with the FFAR1 specific agonist TAK-875 enhanced glucose-induced insulin stimulation from isolated islets [180,181]. Under physiological conditions it appears that glucose-induced production and release of 20-hydroxyeicosatetraenoic acid (20-HETE) by beta-cells potentiates glucose stimulated insulin secretion in an autocrine fashion by stimulating FFAR1 [182]. Kalis et al. (2007) claim that they have identified SNPs in human *FFAR1* that are associated with impaired beta cell function and Kristinsson et al. (2017) hypothesise that FFAR1 signalling may contribute to obesity and type 2 diabetes pathology [183,184]. Indeed Tunaru et al. (2018) found that glucose-induced 20-HETE production was attenuated in islets isolated from human patients with type 2 diabetes likely contributing to the impairment in glucose stimulated insulin secretion seen in patients with type 2 diabetes [182]. Together these results further highlight the physiological and clinical relevance of FFAR1.

With regards to the effects of bile acids on intestinal L-cells, treatment of primary small intestinal crypt cultures with bile acids such as taurodeoxycholic acid (TDCA) stimulates GLP-1 secretion. This stimulation appears GPBAR-1 dependent as GPBAR-A (a specific agonist of GPBAR-1) triggers GLP-1 secretion and primary cultures generated from *Gpbar1* knockout mouse did not display GLP-1 responses to TDCA (or GPBAR-A). Acute L-cell secretory responses to bile acids appear not to be mediated by the nuclear receptor for bile acids, FXR [126]. Ussing chamber experiments whereby a piece of suspended small intestine epithelium separates two chambers of buffer, one apically facing and the other basolaterally facing,

enabled the polarity of the small intestinal bile acid responses to be examined. GPBAR-A only triggered GLP-1 secretion when applied to the basolateral facing chamber whereas TDCA triggered GLP-1 secretion when applied to either side. However, in the presence of an ASBT (which does not transport GPBAR-A) inhibitor TDCA only stimulated GLP-1 secretion when applied to the basolateral chamber. These results suggest that as with free fatty acids, bile acids are first absorbed across the small intestinal epithelium and sensed basolaterally [126].

3.3.3. Synergistic effects of coactivation of G_q and G_s signalling pathways on GLP-1 secretion

FFAs and bile acids reach the small intestinal mucosa in parallel raising the prospect of concomitant activation of the G_s and G_q signalling pathways under physiological conditons. Synthetic full agonists of FFAR1 such as AM-1638, which can employ both the G_q and G_s signalling pathways trigger significantly greater GLP-1 secretion, from colonic crypt cultures and *in vivo* following oral gavage, than partial agonists like TAK-875 which activate G_q-signalling alone [173,185]. It should be noted that in experiments where AM-1638 was applied to L-cells in primary culture increases in intracellular cAMP were not observed contrasting with previous studies (unpublished data by Gwen Tolhurst). This discrepancy might be explained by utilisation of non-physiological overexpression of *Ffar1* in cell lines (such as HEK293 and COS7 cells) to assess cAMP responses to AM-1638 in previous studies [173,185]. Consequently, it is unclear whether AM-1638 triggers elevations in cAMP through G_s-signalling *in vivo*.

An example of synergy between the L-cell G_q and G_s signalling pathways comes from findings that co-activation of FFAR1 and the G_s-coupled 2-MAG receptor GPR119 potentiates GLP-1 secretion from murine colonic crypt cultures [160]. *In vivo,* 2-MAG should arrive at the small intestinal apical brush border simultaneously with FFAs meaning GPR119-mediated potentiation of FFAR1-mediated GLP-1 release has physiological relevance. TAK-875 was withdrawn from phase III clinical investigations because of issues with liver toxicity and such synergy suggests that a lower, possibly non-toxic, therapeutic dose of TAK-875 could be achieved when co-administered with a stimulus of the G_s signalling pathway [186]. Alternatively, dual-agonists of FFAR1 and GPR119/GPBAR-1 could be developed whereby a

single drug activates both receptors. Dual-agonists for the GLP-1 and glucagon receptors have recently been developed for the treatment of obese type 2 diabetes and appear more effective at reducing body weight and restoring normoglycaemia than standard GLP-1 receptor agonists. Glucagon receptor agonism alone acts to elevate blood glucose levels by increased liver glycogenolysis and gluconeogenesis, however co-agonism of GLP-1 receptor counteracts this adverse effect and appears to improve glucose tolerance overall [81,82,187].

The precise mechanism by which synergy between the G_q and G_s signalling pathways arises has not been explored but likely reflects molecular cross-talk between signalling pathways. In G_s signalling pathways, elevated levels of cAMP activate the effector proteins PKA and EPAC2. These proteins modulate the activities of proteins involved in exocytosis affecting peptide secretion [188]. EPAC2 in beta cells for example is known to potentiate glucose stimulated insulin secretion by increasing the density of insulin granules at the plasma membrane (ready to be secreted) [189,190]. Similarly, whilst G_q activation increases IP_3 production, leading to release of intracellular Ca^{2+} and subsequent exocytosis, the other secondary messenger of G_q signalling, DAG, activates protein kinase C and can directly activate certain TRP cation channels which depolarise the plasma membrane [191]. This could explain how inhibition of the protein kinase C variant PKCzeta, significantly attenuated oleic acid (a LCFA) induced GLP-1 secretion from GLUTag cells [192]. Synergistic interactions between G_q and G_s signalling likely arise from integration of the actions of their effector proteins resulting in increased exocytotic activity. Such cross-talk has been observed before for example in cardiac fibroblasts and mast cells [193,194]. Potential synergistic effects of FFAR1 and GPBAR-1 co-activation on L-cell responses are explored in this chapter using the FFAR1 and GPBAR-1 agonists TAK-875 and GPBAR-A.

3.4. Results

N.B: The secretory experiments presented here were carried out in conjunction with Deborah Goldspink. Responses are quoted as mean fold changes (from basal) ± SEM. All the fold changes in fluorescence quoted in the following sections reflect median values with 95% confidence interval (CI) in parentheses.

3.4.1. Bile acids and FFAR1 agonists elicit intracellular calcium responses in organoid-derived L-cells

Immunofluorescent labelling of proglucagon and GCaMP3 revealed selective expression of GCaMP3 in organoid cultured ileal L-cells (figure 2A). Organoid-derived L-cells exhibited significant calcium responses (figure 2B&C) to application of 10μM of the bile acid TDCA which triggered a median fold increase of 1.63 (CI=1.07-2.04) in GCaMP3 fluorescence. Similarly, application of 3μM AM-1638 drove a 1.45 (CI=1.16-3.01) fold increase in GCaMP3 fluorescence. All cells included in the analysis responded to one of the positive controls which were 100nM bombesin and 30mM KCl. 100nM bombesin and 30mM KCl application triggered 1.51 (CI=1.32-1.65) and 1.35 (CI=1.22-1.55) fold increases in GCaMP3 fluorescence respectively. The 0.1% DMSO vehicle control triggered significant changes in intracellular calcium levels (though the effect was minimal) resulting in a 1.03 fold (CI=1.028-1.136) increase in overall GCaMP3 fluorescence.

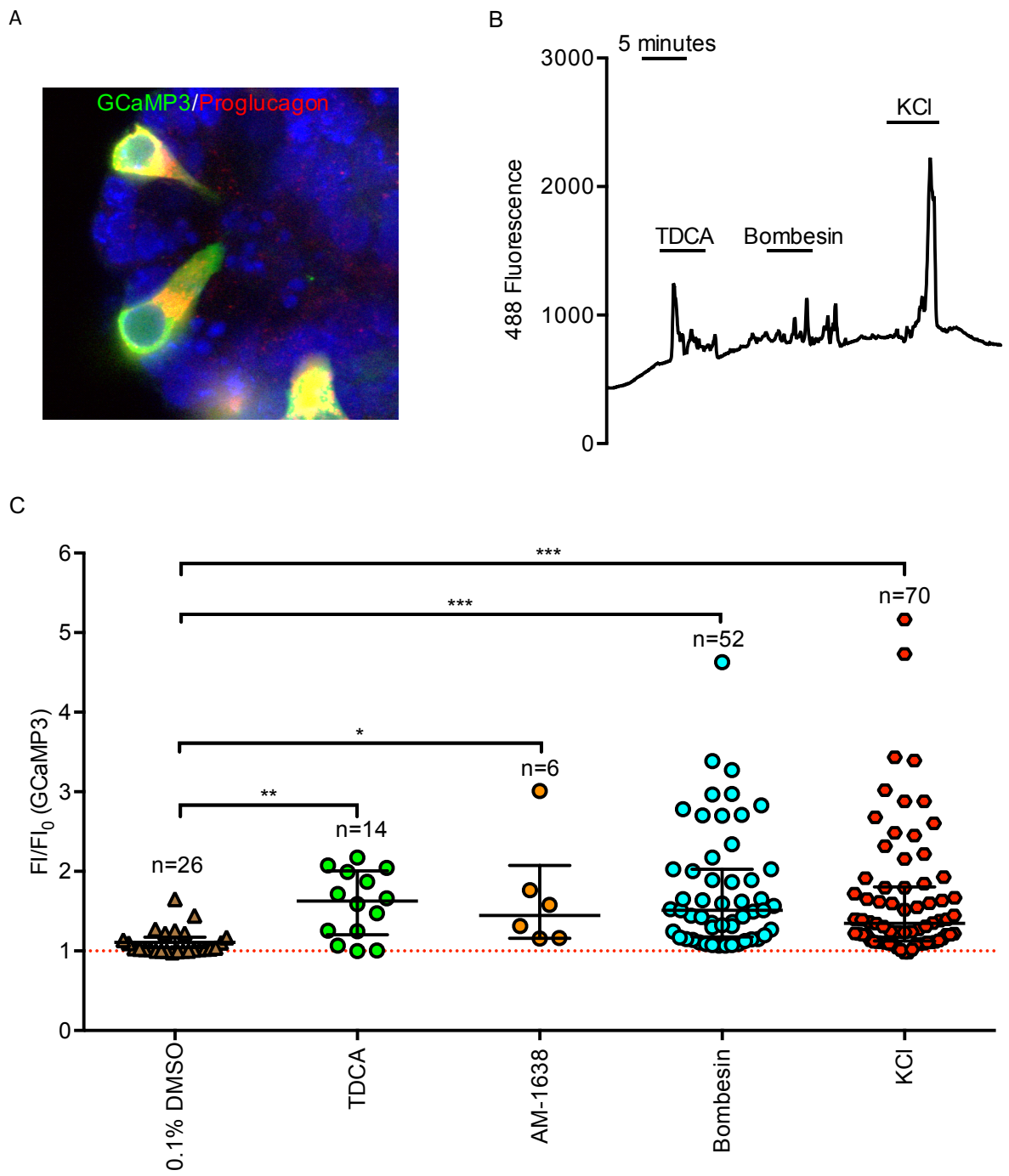

***Figure 2**: (A) Immunohistochemistry indicates GCaMP3 expression is limited to L-cells in 4 day old ileal organoids derived from Glu-Cre x Rosa26-GCaMP3 mice. Organoids were fixed in 4% PFA for 1.5 hours. Following this fixed organoids were incubated overnight at 4°C with primary antibodies to GFP (raised in goat; Ab5450; 1:1000) and proglucagon (raised in rabbit; sc13091; 1:200). Fluorescent labelling of GCaMP3 and proglucagon was achieved by incubation for 1 hour at room temperature with 1:300 of goat-raised secondary antibodies conjugated to AlexaFluor 488 and 555 respectively. Nuclear staining was achieved by a further 10 minute incubation with 1:1300 Hoescht nuclear stain. (B) Representative trace from a calcium imaging experiment on 2D monolayer cultured ileal organoids derived from Glu-Cre x Rosa26-GCaMP3 mice. (C) Summary of intracellular calcium responses recorded to 0.1% DMSO (vehicle control), 10µM taurodeoxycholic acid (TDCA), 3µM AM-1638, 100nM bombesin and*

*30mM potassium chloride (KCl). FI/FI_0 plotted on y-axis reflects the maximum measured GCaMP3 fluorescence during drug application divided by the maximum measured during a 30 second period prior to drug application i.e. fold change in fluorescence. Median and IQR reflected by central line and whiskers. Red dotted line marks $FI/FI_0=1$ i.e. no change in fluorescence from baseline. n = number of cells. Statistical significance assessed using Kruskal-Wallis test with comparisons made to the 0.1% DMSO control group. *p<0.05, **p<0.01, ***p<0.001.*

3.4.2. GPBAR-A potentiates L-cell intracellular calcium responses to TAK-875

Application of 10µM TAK-875 and 3µM GPBAR-A individually triggered significant, if small, 1.12 (CI=1.03-1.32) and 1.07 (CI=1.02-1.42) fold increases in GCaMP3 fluorescence respectively (figure 3B). Following pre-incubation with 3µM GPBAR-A, co-application of 10µM TAK-875 with 3µM GPBAR-A elicited 1.33 (CI=1.26-1.98) fold increases in GCaMP3 fluorescence (figure 3B). On average these responses were 4.91 (CI=1.28-11.81) fold higher than the anticipated response in 488 fluorescence (sum of the steady state GPBAR-A and 1st TAK-875 responses) indicating that GPBAR-A potentiated L-cell intracellular calcium responses to TAK-875 (figure 3C). Comparison of responses to the 1st TAK-875 (before GPBAR-A addition) and 3rd TAK-875 (after GPBAR-A washout) applications did not identify a significant difference ($p>0.05$), suggesting that the potentiated responses seen are reversible upon GPBAR-A washout (figure 3B).

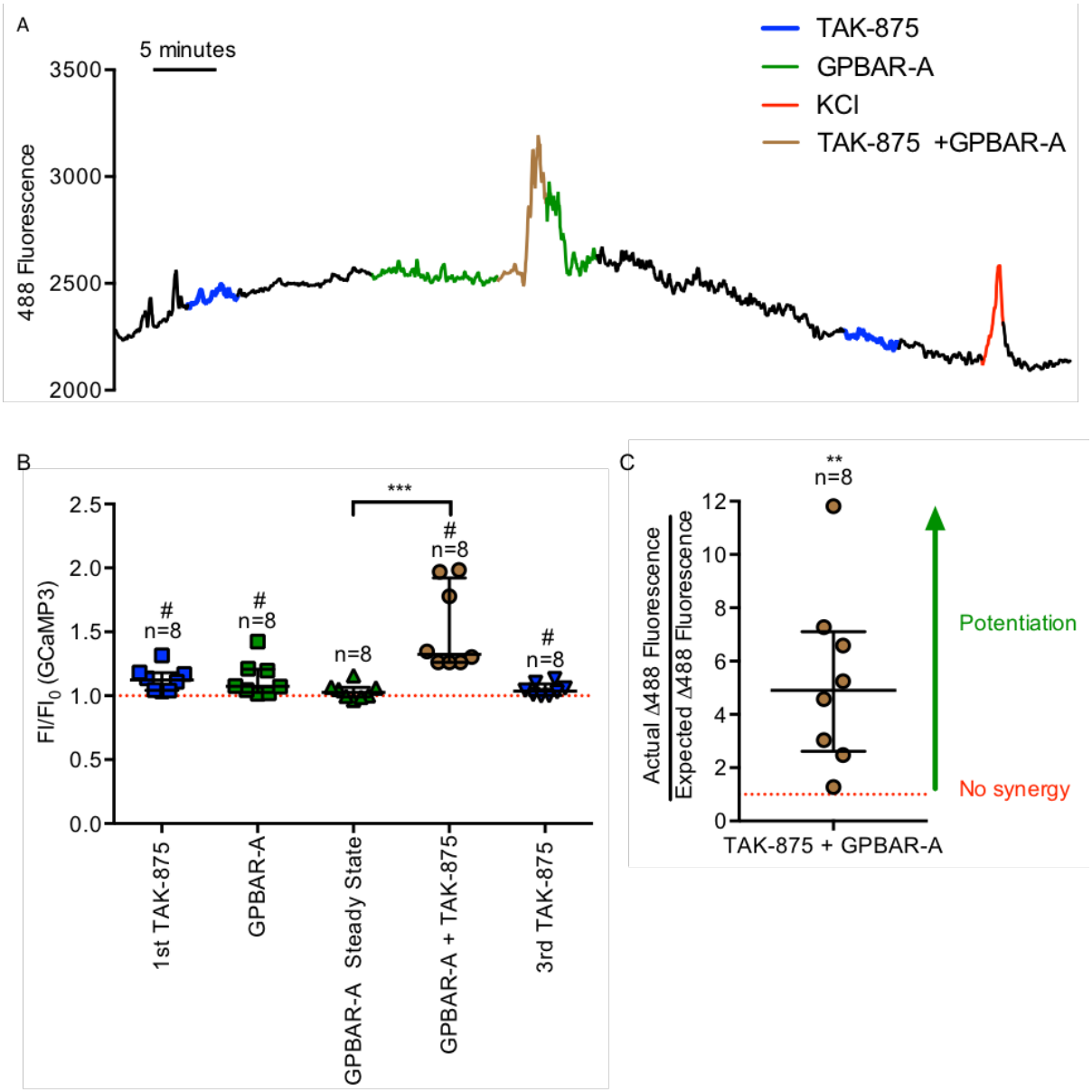

***Figure 3**: (A) Representative trace from a calcium imaging experiment on 2D monolayer cultured ileal organoids derived from Glu-Cre x Rosa26-GCaMP3 mice. Colour coded according to drug application. (B) Summary of the L-cell intracellular calcium responses to 3µM TAK-875 and 3µM GPBAR-A application individually and simultaneously. GPBAR-A steady state refers to the maximum fold change in fluorescence of GPBAR-A measured in the 30 seconds preceding simultaneous TAK-875 addition using 30 seconds before GPBAR-A application as the baseline. Fl/Fl_0 plotted on y-axis reflects the maximum measured GCaMP3 fluorescence during drug application divided by the maximum measured during a 30 second period prior to drug application i.e. fold change in fluorescence. Red dotted line marks $Fl/Fl_0=1$ i.e. no change in fluorescence from baseline. n = number of cells. Statistical significance assessed between GPBAR-A steady state and other groups assessed using Kruskal-Wallis test. # indicates significant ($p<0.05$) individual responses for each group assessed via Wilcoxon test examining deviation of median values from 1 (i.e. no change in GCaMP3 fluorescence). (C) Degree of potentiation of responses to TAK-875 by co-application with GPBAR-A. y-axis reflects the ratio between the maximum fold change in GCaMP3 fluorescence during TAK-875 and GPBAR-A co-application and the anticipated fold change in fluorescence, calculated from the sum of the*

*GPBAR-A and TAK-875 responses individually. Median and IQR reflected by central line and whiskers. Statistics calculated using a Wilcoxon test assessing deviation from 1 (no synergy). **p<0.01, ***p<0.001.*

3.4.3. GPBAR-A potentiates L-cell intracellular calcium responses to KCl

30mM KCl triggered 1.10 (CI= 1.03-1.73) fold increases whilst 3µM GPBAR-A triggered 1.11 (CI=1.02-1.25) fold increases in GCaMP3 fluorescence (figure 4B). Responses to 30mM KCl were significantly enhanced by co-application with 3µM GPBAR-A with responses 1.18 (CI=1.09-1.96) fold above baseline reflecting a median potentiation of 1.47 (CI=0.84-4.39) fold above the anticipated response (figure 4B&C). As with TAK-875, no significant difference was found between responses elicited by 30mM KCl prior to GPBAR-A application and following GPBAR-A washout (p>0.05; figure 4B).

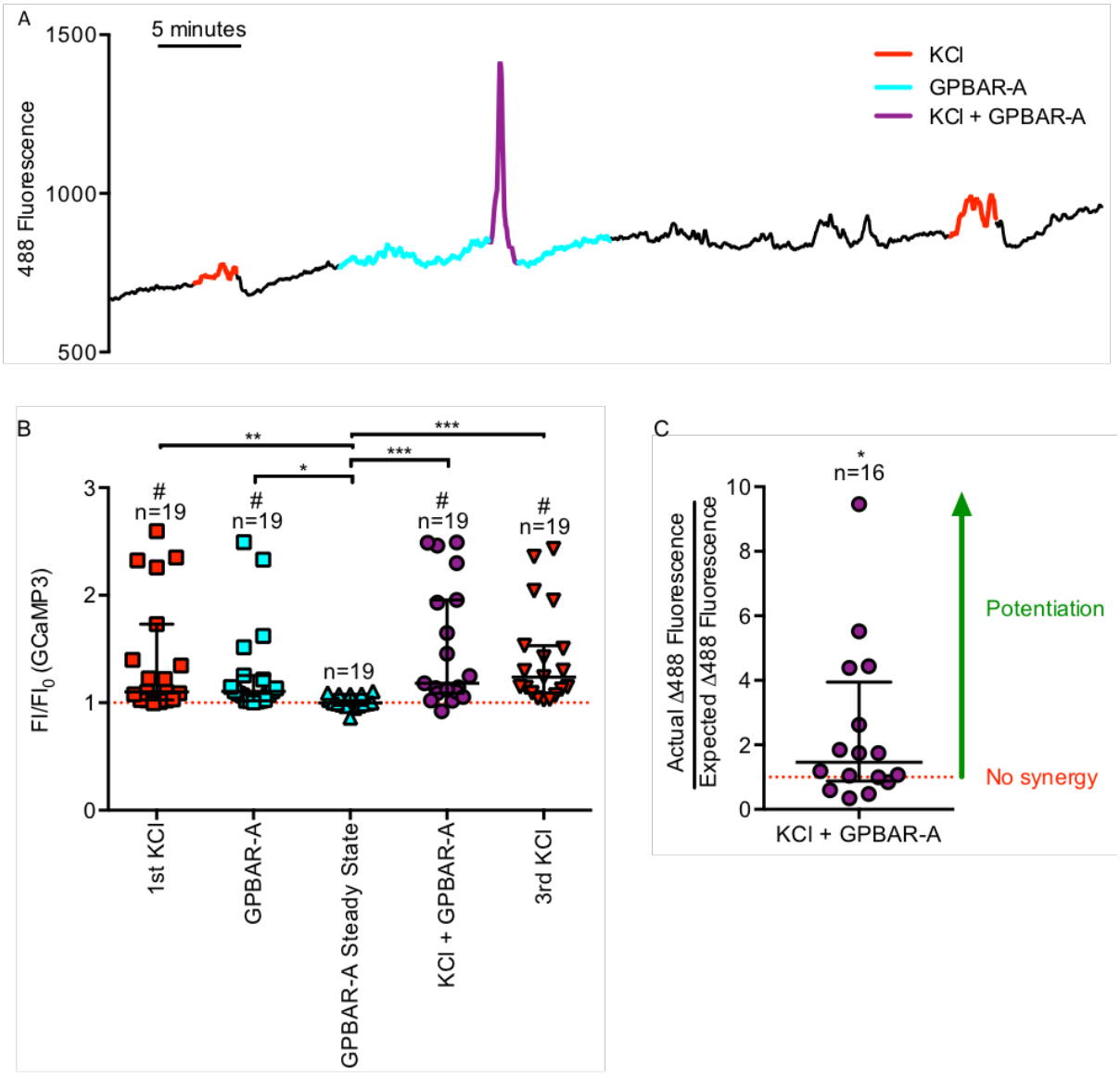

Figure 4*: (A) Representative trace from a calcium imaging experiment on 2D monolayer cultured ileal organoids derived from Glu-Cre x Rosa26-GCaMP3 mice. Colour coded according to drug application. (B) Summary of the L-cell intracellular calcium responses to 30mM KCl and 3µM GPBAR-A application individually and simultaneously. GPBAR-A steady state refers to the maximum fold change in fluorescence of GPBAR-A measured in the 30 seconds preceding simultaneous KCl addition using 30 seconds before GPBAR-A application as the baseline. FI/FI_0 plotted on y-axis reflects the maximum measured GCaMP3 fluorescence during drug application divided by the maximum measured during a 30 second period prior to drug application i.e. fold change in fluorescence. Red dotted line marks $FI/FI_0=1$ i.e. no change in fluorescence from baseline. n = number of cells. Statistical significance assessed between GPBAR-A steady state and other groups assessed using Kruskal-Wallis test. # indicates significant ($p<0.05$) individual responses for each group assessed via Wilcoxon test examining deviation of median values from 1 (i.e. no change in GCaMP3 fluorescence). (C) Degree of potentiation of responses to KCl by co-application with GPBAR-A. y-axis reflects the ratio between the maximum fold change in GCaMP3 fluorescence during KCl and GPBAR-A co-*

*application and the anticipated fold change in fluorescence, calculated from the sum of the GPBAR-A and KCl responses individually. Median and IQR reflected by central line and whiskers. Statistics calculated using a Wilcoxon test assessing deviation from 1 (no synergy). *p<0.05, **p<0.01, ***p<0.001.*

3.4.4. GPBAR-A potentiates GLP-1 secretory responses to TAK-875

10μM TDCA and 3μM GPBAR-A respectively triggered 2.90 ± 0.19 and 4.82 ± 0.32 fold increases in GLP-1 secretion from 2D monolayer cultures of ileal organoids (figure 5A). The positive control 10μM forskolin (Fsk)/IBMX increased GLP-1 secretion by 10.79 ± 0.32 fold. Only plates containing Fsk/IBMX responsive wells were included in the final analysis.

10μM TAK-875 application elicited 1.49 ± 0.08 fold increases in GLP-1 secretion. Co-application of 3μM GPBAR-A with 10 μM TAK-875 yielded a 6.41 ± 0.78 fold increase in GLP-1 secretion reflecting a mean potentiation in GLP-1 secretion of 1.58 ± 0.17 fold above anticipated additive GLP-1 secretion (figure 5B&C).

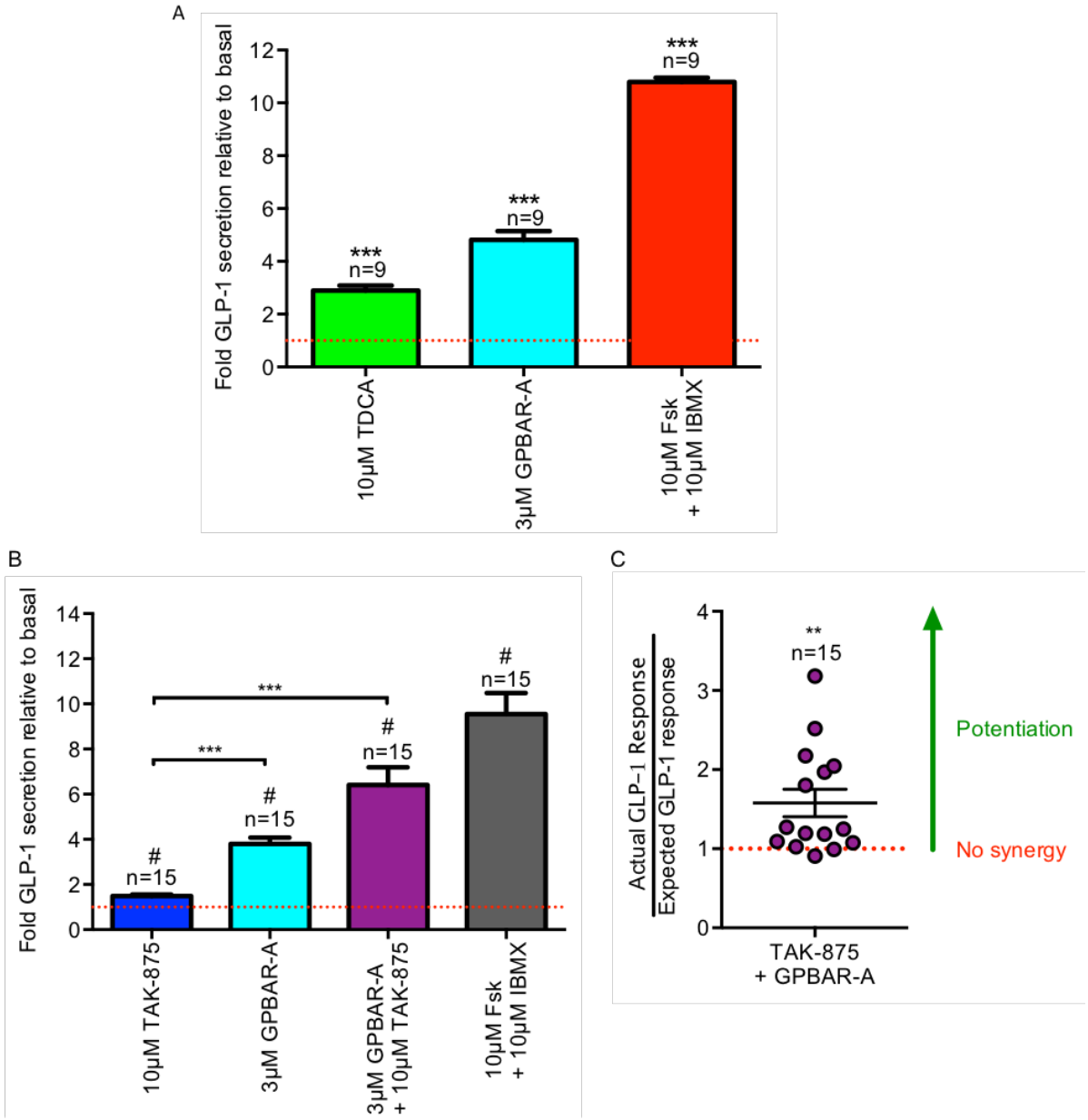

Figure 5: *(A) GLP-1 secretion responses (over 2 hours) to 10μM TDCA (A) and 3μM GPBAR-A relative to the basal condition (saline buffer enriched with 1mM glucose). Two-tailed t-test run to assess statistical deviation of means from 1 (i.e. basal GLP-1 secretion). (B) Relative GLP-1 secretion responses to 10μM TAK-875 and 3μM GPBAR-A applied with 10μM TAK-875. Statistical significance assessed on log transformed values. Two-tailed t-test used to assess deviations in individual group means from 1 (no change in secretion). Intergroup comparisons made using a one-way ANOVA test with Dunnett's correction. 10μM forskolin (fsk)/IBMX acted as a positive control for GLP-1 secretion. (C) Potentiation of TAK-875 induced GLP-1 secretion by GPBAR-A. Values plotted derive from percentage of GLP-1 secretion measured from the combined TAK-875/GPBAR-A condition divided by that anticipated from the individual GLP-1 secretory responses to TAK-875 and GPBAR-A. A two-tailed t-test was used to assess deviation from 1 (no potentiation). **p<0.01, ***p<0.001, #p<0.05. n=number of wells. Bars represent mean ± SEM. Red dotted line marks y=1. Secretions performed in conjunction with Deborah Goldspink.*

3.5. Discussion

3.5.1. Organoid L-cells replicate native L-cell physiology

The intracellular calcium and GLP-1 secretory responses from 2D small intestinal organoid cultures to TDCA and GPBAR-A application are consistent with previous findings by Brighton et al. using primary cultures [126]. Petersen et al. also found that small intestinal organoids resuspended in test solutions (i.e. 3D structure maintained) display similar GLP-1 secretory responses to glucose and SCFAs as L-cells in primary culture [195]. Furthermore, Zietek et al. (2015) used small intestinal organoids to examine GLP-1 secretory responses to applied glucose and the dipeptide gly-sar. Small intestinal organoids developed from *Sglt1* and *Pept1* knockout mice exhibited impaired GLP-1 secretory responses to glucose and gly-sar respectively. The *Sglt1* and *Pept1* knockout organoids also demonstrated impaired epithelial transport of radiolabelled glucose and gly-sar respectively [196]. Therefore L-cells from organoid culture appear to recapitulate intracellular calcium and GLP-1 secretory responses as well as epithelial nutrient transport mechanisms found in primary cultures and likely, by extension, L-cells *in vivo*.

3.5.2. GPBAR1 and FFAR1 stimulation triggers L-cell intracellular Ca^{2+} and GLP-1 secretory responses

The small, but significant, intracellular calcium transients seen following GPBAR-A application could result from coupling of GPBAR-1 to G_q activation, even though GPBAR-1 is not classically coupled to G_q. GPBAR-A induced calcium transients could also reflect indirect signalling of GPBAR-A via other cells (since organoid cultures contain a mixture of epithelial cells) releasing paracrine signals that trigger elevate intracellular calcium levels in neighbouring L-cells. Alternatively, the GPBAR-A induced intracellular calcium transients observed here (figure 4B) may reflect incomplete washout of TAK-875/KCl prior to GPBAR-A application. Further intracellular calcium experiments employing longer washout periods or application of GPBAR-A prior to addition of TAK-875/KCl would help explore this possibility.

Physiologically, bile acids may also signal through GPBAR-1 independent mechanisms since TDCA appears to elicit larger intracellular calcium responses than GPBAR-A in L-cells [126]. This raises the possibility that a component of bile acid stimulated GLP-1 secretion might

occur independently of GPBAR-1 signalling. However, Brighton et al. (2015) found that bile acid triggered GLP-1 secretion was abolished in *Gpbar1* knockout mice implying GPBAR-1 signalling as essential to GLP-1 responses to bile acids. Thus, it is unlikely that any potential GPBAR-1 independent bile sensing mechanism triggers GLP-1 secretion in the absence of functional GPBAR-1. Alternatively, the larger intracellular calcium transients elicited by TDCA compared to GPBAR-A application may reflect modulation of GPBAR-1 signalling by GPBAR-1 independent bile sensing mechanisms. Brighton et al. have ruled out, through pharmacological manipulation, contribution of farnesoid X receptor (the other known bile acid receptor expressed in L-cells) and the electrogenic effects of apical sodium-bile acid transporter (ASBT) to the intracellular calcium responses to bile acids [126].

We found that generally AM-1638 triggered larger intracellular calcium and GLP-1 secretory responses than TAK-875 reflecting the results of previous studies [173,197,198]. The weak ability of TAK-875 to induce calcium transients could in part relate to the low concentration of glucose (1mM) used in the saline buffer since Sakuma et al. (2016) highlighted that TAK-875 applied to MIN6 cells (a cell line model of beta cells) elicited weak intracellular calcium responses in 1mM glucose but strong responses in the presence of 3mM glucose [197]. Sakuma et al. attribute the basis of this dependency on glucose-dependent closure of K_{ATP} channels studding the plasma membrane. This has the effect of depolarising the plasma membrane and activating voltage gated calcium channels. L-cells are known to express functional K_{ATP} channels and tolbutamide, a sulfonylurea drug which blocks K_{ATP}, triggers GLP-1 secretion from primary cultured small intestinal L-cells [59]. However, the importance of K_{ATP}-channels to L-cell responses to glucose appears to be minor [148].

3.5.3. Co-activation of GPBAR-1 and FFAR1 potentiates L-cell intracellular Ca^{2+} and GLP-1 responses

Co-application of GPBAR-A (activating GPBAR-1) and TAK-875 (activating FFAR1) triggered significantly greater than anticipated intracellular calcium and GLP-1 secretory responses. These findings imply that simultaneous activation of the G_s and G_q signalling pathways has synergistic effects on GLP-1 secretion as previously suggested by Ekberg et al. [160]. Using different agonists of GPBAR-1 and FFAR1, Hauge et al. have replicated our findings regarding

potentiation of GLP-1 secretion from small intestinal cultures and extended our findings through *in vivo* studies with oral administration of GPBAR-1 and FFAR1 agonists to mice. These agonists all elevated plasma levels of GLP-1 and when co-administered resulting plasma levels of GLP-1 exceeded anticipated levels demonstrating potentiation *in vivo* [199]. These results indicate that pharmacological exploitation of synergy between GPBAR-1 and FFAR1 signalling could have therapeutic benefits. More recent *in vivo* work on mice by Briere et al. (2018) further highlights the clinical potential of combination therapy. In this study, co-administration of a SSTR5 antagonist (inhibiting SSTR5 mediated G_i signalling) together with GPBAR-1 and FFAR1 agonists (stimulating G_s and G_q signalling) and a DPP-4 inhibitor enhanced GLP-1 release. These findings suggest that the synergy between GPBAR-1 and FFAR1 activation might be further enhanced by suppression of G_i-signalling (which is likely to increase intracellular cAMP levels further). The combinational therapy was associated with improved glucose tolerance in $Lepr^{db/db}$ mice (diabetic mouse model) beyond that seen with monotherapy (i.e. each drug administered in isolation) [200].

Curiously, L-cells from *Gpbar1* knockout mice exhibit attenuated intracellular calcium responses to KCl application raising the possibility that GPBAR-1 can enhance intracellular calcium responses by raising intracellular cAMP levels in the absence of bile acids (unpublished data by Cheryl Brighton). GPBAR-1 may possess constitutive G_s-signalling activity or endogenous agonists other than bile acids. Given the synergy observed between the GPBAR-1 and FFAR1 signalling pathways, GLP-1 responses to FFAs might be influenced by basal activity of GPBAR-1. This could be investigated by examining L-cell intracellular calcium and GLP-1 secretory responses to FFAR1 activation in *Gpbar1* knockout mice.

The synergistic effects mediated by co-activation of the G_s and G_q signalling pathways implies signalling crosstalk exists which enhances exocytosis of GLP-1 containing vesicles. The precise molecular basis of this crosstalk is unclear. Transcriptomics and further electrophysiological examination of ileal L-cells (in organoid culture) suggests that the non-selective cation channel TRPC3 and voltage gated calcium channels are involved [201]. Transcripts for P/Q calcium channel subunit such as *Cacna1a* predominate the calcium channel profiles in both ileal and colonic L-cells (highest in ileal L-cells). Transcripts encoding L and T-type calcium channel subunits were also present but at lower levels. Consistent with this profile, in voltage

clamp studies of ileal L-cells, the P-type calcium channel blocker ω-agatoxin IVA blocked most measured Ca^{2+} currents whereas the L-type calcium channel blocker isradipine had only a marginal effect. However, GPBAR-A induced inward calcium currents (~20% increase) which were blocked by the L-type calcium channel blocker nifedipine implying L-type calcium channel modulation by GPBAR-A. This likely reflects downstream PKA activity as phosphorylation by PKA is known to increase the activity of L-type calcium channels [202]. Supporting this hypothesis, application of H-89 (a PKA inhibitor) to ileal crypt cultures significantly attenuated GPBAR-A dependent GLP-1 secretion. Concerning FFAR1 signalling, pharmacological blockade of TRPC3 using pyr3 significantly attenuated TAK-875 induced inward currents and GLP-1 secretion from primary ileal crypt cultures [201]. Further experiments examining the effects of the membrane permeable TRPC3 activator 1-oleoyl-2-acetyl-sn-glycerol (OAG), pyr3 and H-89 on GLP-1 secretion and L-cell electrophysiological responses would allow the potential roles of TRPC3 and PKA in mediating synergy between FFAR1 and GPBAR-1 to be assessed.

Goldspink et al. (2018) suggest these results indicate that co-agonism of FFAR1 and GPBAR-1 drives increased L-type voltage gated calcium channel activity through activation of TRPC3 and PKA-mediated phosphorylation. In turn, this leads to calcium influx and exocytosis of GLP-1 containing vesicles (the proposed molecular mechanism is illustrated in figure 6). GPBAR-A potentiation of the intracellular calcium responses to 30mM KCl application may similarly reflect GPBAR-A mediated modulation of L-type calcium channel kinetics. However, the proposed mechanism (figure 6) is questioned by evidence that co-application of the L-type calcium channel activator Bayk8644 with TAK-875 did not trigger synergy in GLP-1 secretion [201]. Whilst Bayk8644 is known to have off-target effects on voltage-gated potassium channels, these results could reflect alternative cross-talk mechanisms downstream of GPBAR-1 and FFAR1 activation [203].

Alternative cAMP-dependent signalling mechanisms potentially involved include PKA modulation of the activities of SNARE proteins involved in vesicle docking, priming and exocytosis. Such mechanisms are known to promote neurotransmission and possibly renin secretion from juxtaglomerular cells [204,205]. PKA-independent mechanisms are also likely involved since H-89 application does not completely abolish GLP-1 responses to GPBAR-A

[201]. cAMP is also known to directly modulate the activities of hyperpolarisation-activated cyclic nucleotide-gated (HCN) channels. However, whilst cAMP appeared to activate hyperpolarisation currents in GLUTags, no such currents were observed in ileal L-cells following GPBAR-A addition, implying these channels are not involved in GPBAR-1 induced GLP-1 secretion [201,206].

Another possibility is that the PKA-independent effects of GPBAR-1 activation observed involve the cAMP effector EPAC2. EPAC2 function has been examined in pancreatic islets through knockdown of *Rapgef4* (the gene encoding EPAC2). Interestingly, these studies indicate that a significant component of GLP-1 induced potentiation of glucose-stimulated insulin secretion depends on EPAC2 activity (PKA involvement was also identified). Furthermore, islet knockdown of *Rapgef4* blunted potentiation of insulin secretion by combined application of 8-Br-cAMP (a stable cAMP analogue) with carbachol (which activates G_q-coupled muscarinic receptors) or with high levels of external K^+. Contrastingly, *Rapgef4* knockdown did not attenuate responses to carbachol or high K^+ applied individually [207]. These results suggest that EPAC2 (together with PKA) is involved in mediating synergy between G_q and G_s signalling pathways in pancreatic beta-cells. One can therefore postulate that EPAC2 may perform an analogous role in L-cells, mediating synergy between GPBAR-1 and FFAR1 signalling. This hypothesis is questioned by investigations by Islam et al. since application of the EPAC activator EPAC-selective cAMP analogue (ESCA) did not trigger GLP-1 secretion from GLUTag cells. It should be noted though that ESCA was found to increase GLP-1 production in GLUTag cells implying that whilst EPAC may not mediate GLP-1 secretion from L-cells directly it might modulate the magnitude of GLP-1 secretory responses [208]. Targeted knockout of *Rapgef4* using CRISPR-Cas9 techniques in intestinal organoids would allow the potential involvement of EPAC2 in synergistic interactions between GPBAR-1 and FFAR1 signalling to be assessed and could be carried out with human-derived organoids [209,210].

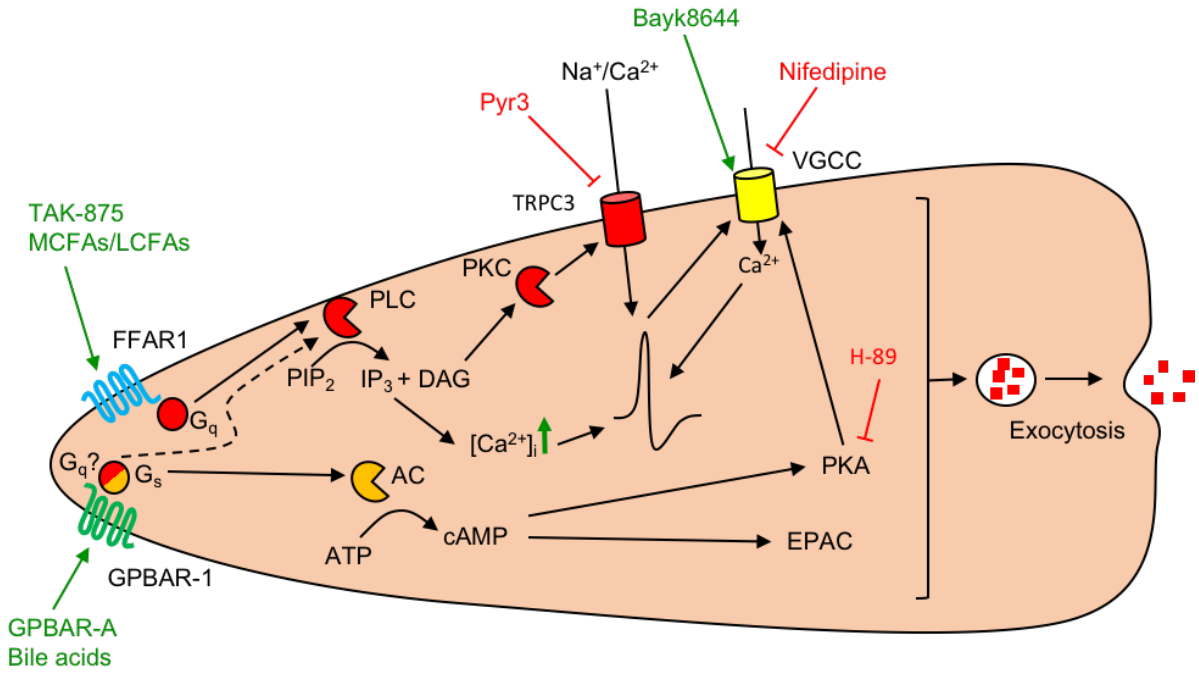

Figure 6: *Schematic illustrating downstream signalling mechanisms of FFAR1 and GPBAR-1. Agonists/activators indicated in green text. Dashed arrow indicates possible G_q activation by GPBAR-1. Inhibitors indicated in red text. Waveform drawn represents action potential firing. Exocytosis of GLP-1 (represented by red squares) is triggered downstream of the illustrated signalling mechanisms.*

3.6. Concluding remarks

Small intestinal organoids provide a physiologically relevant platform to investigate L-cell physiology as evidenced here by observed intracellular calcium and GLP-1 responses to known GLP-1 secretagogues. Using this platform, synergistic effects of GPBAR-1 and FFAR1 co-activation on both intracellular calcium responses and GLP-1 secretion were identified confirming the primary hypothesis of this chapter. Such synergy likely occurs physiologically as bile acids and FFAs arrive in the small intestinal lumen concomitantly. Further electrophysiological probing of the molecular mechanisms underlying this synergy imply involvement of TRPC3 activation downstream of FFAR1 and PKA downstream of GPBAR-1. There also appears to be PKA-independent components of GPBAR-1 signalling involved that could include EPAC2 activity. Further experiments utilising pharmacological agents, genetic modification and electrophysiological techniques will help illuminate the precise molecular basis of downstream cross-talk between the GPBAR-1 and FFAR1 signalling pathways. Exploitation of GPBAR-1/FFAR1 synergy through combination therapy or administration of a dual agonist may yield novel therapeutic treatments of type 2 diabetics.

Chapter 4. Characterisation of INSL5-producing cells

4.1. Introduction

INSL5-producing cells comprise roughly half of the colonic L-cell population. It has not previously been established whether these cells express a similar or different repertoire of GPCRs to non-INSL5 producing colonic L-cells. Attempts to measure INSL5 secretory responses have previously been hampered by a lack of reliable quantification assays [88]. Physiologically, INSL5 has been implicated in regulation of appetite, hepatic glucose production and insulin secretion [88,90,91]. Regarding appetite regulation, INSL5 is believed to have an orexigenic effect, contrasting with the anorexigenic effects of the canonical L-cell hormones GLP-1 and PYY [88,211,212]. In this chapter, novel murine transgenic models were used to interrogate the expression profile of INSL5 cells and the hypothesis that GLP-1 secretagogues can trigger intracellular Ca^{2+} responses in INSL5 cells. Employment of LC/MS allowed quantification of INSL5 secretory responses and also enabled simultaneous quantification of other peptide molecules including GLP-1 and PYY. This allowed the hypothesis that INSL5 is co-secreted with GLP-1 and PYY in response to applied GLP-1 secretagogues to be tested. Finally, using 3D structured illumination microscopy (3D-SIM) to examine immunofluoresecently labelled crypt cultures and tissue sections, the hypothesis that INSL5, GLP-1 and PYY are stored in separate secretory vesicle pools was explored.

4.2. Aims:

1. To validate the novel INSL5 mouse models Insl5-rtTA/TET-GFP and Insl5-rtTA/TET-GCaMP6FΔCMV
2. To compare the GPCR repertoire of canonical L-cells with that of INSL5 cells
3. To examine intracellular Ca^{2+} and INSL5 secretory responses to known GLP-1 secretagogues
4. To compare the secretory response profiles of INSL5, GLP-1 and PYY
5. To examine whether INSL5, GLP-1 and PYY are stored separately or together in secretory vesicles

4.3. Background

4.3.1. Physiological stimuli of colonic L-cells:

Secretion of GLP-1 and PYY by L-cells is triggered by a diverse range of physiological stimuli as detailed previously in chapter 1. The following sections provide background on a subset of known colonic GLP-1 secretagogues that were utilised to examine INSL5 cell intracellular calcium and secretory responses:

Angiotensin II

The renin-angiotensin system performs a critical role in osmoregulation and blood pressure maintenance. When blood volume drops (e.g. due to dehydration) renal blood flow also drops leading to a decrease in blood pressure in the arterioles supplying the renal glomeruli. This in turn triggers mechanosensitive juxtaglomerular cells in the arteriole walls to release the enzyme renin into the bloodstream. Renin catalyses the cleavage of the circulating precursor angiotensinogen into angiotensin I. This is subsequently processed by angiotensin converting enzymes (ACE) when passing through the lung circulation to angiotensin II. Angiotensin II acts to sustain adequate blood pressure by directly acting on vascular smooth muscle narrowing blood vessel lumens through vasoconstriction, stimulating sodium reabsorption from renal nephrons and triggering the release of other osmoregulatory hormones including AVP and aldosterone [213,214].

In the context of the gastrointestinal tract, angiotensin II strongly stimulates GLP-1 and PYY secretion when applied to both murine and human colonic crypt cultures. Agtr1a, a G_q-coupled GPCR, appears to be the key angiotensin receptor variant involved in colonic L-cell responses as the specific Agtr1 blocker candesartan significantly attenuates GLP-1 and PYY secretion. Accordingly, expression of *Agtr1a* is significantly enriched in FACS-isolated colonic L-cells compared with the control cell group with low expression (100-fold lower) found in small intestinal L-cells implying Agtr1a is specifically enriched in colonic L-cells. Such localisation to the large intestine may reflect a suggested role in reducing net fluid secretion into the colonic lumen via paracrine action of released PYY [73].

Arginine vasopressin (AVP)

Arginine vasopressin (AVP; also known as anti-diuretic hormone) is produced and secreted directly into the systemic circulation by neurosecretory cells of the hypothalamus in response to a drop in blood pressure and/or hyperosmolarity. AVP counteracts these homeostatic perturbations by increasing water reabsorption from the kidneys and by vasoconstriction [215].

In the same vein as angiotensin II, AVP appears to reduce net water loss from the distal gastrointestinal tract via stimulation of PYY secretion. *In vitro,* AVP stimulated GLP-1 and PYY secretion from murine and human colonic crypt cultures inhibited by the Avpr1b inhibitor SSR. *Avpr1b* expression is particularly enriched in colonic L-cells compared with small intestinal L-cells. *Avpr1b* is a GPCR which couples both to G_q and G_s. This is reflected by observed L-cell elevations in intracellular Ca^{2+} and cAMP levels upon AVP application. In healthy human participants, serum levels of copeptin (a stable equimolar biproduct of AVP production) and PYY levels were found to be positively correlated potentially suggesting human physiological relevance to the hypothesis that AVP reduces colonic water loss through paracrine PYY action [74].

Short chain fatty acids (SCFAs)

SCFAs are products of bacterial fermentation which occurs in the colon. The most abundantly produced SCFAs are acetate, butyrate and proprionate with concentrations which can exceed 100mM in the colon and acetate being the most dominant. Acetate's predominance likely arises due to acetate producing pathways present in the majority of bacterial groups whilst butyrate and proprionate production are restricted to fewer groups [216].

Regarding L-cells, SCFAs and specific agonists of the SCFA receptors FFAR2 and FFAR3 trigger GLP-1 secretion from murine crypt cultures [75,217]. FFAR2 is a G_q coupled whilst FFAR3 is G_i coupled GPCR. Tolhurst et al. (2012) found that both *Ffar2* and *FFar3* are enriched in L-cells and that knockout mice for *Ffar2* and *Ffar3* both exhibited attenuated GLP-1 responses to SCFAs with *Ffar2* knockout having the larger effect. Pre-treatment with pertussis toxin (which

blocks the G_i) pathway did not attenuate responses to proprionate implying that FFAR3 can couple to other downstream signalling pathways triggering GLP-1 secretion or perhaps that the *Ffar3* knockout had downregulatory effects on *Ffar2* [75].

MCFA/LCFAs

As previously discussed, MCFA/LCFAs trigger GLP-1 secretion from colonic L-cells through activation of FFAR1. In this chapter, the FFAR1 full agonist AM-1638 was applied in secretion and intracellular calcium assays to assess the function of FFAR1 in INSL5 cell responses [173].

Bile acids

Chapter 3 explored the synergistic effects of GPBAR-1 and FFAR1 coactivation on small intestinal GLP-1 secretion. Previous studies have found that GPBAR-1 agonists also act as GLP-1 secretagogues in the colon [126]. In the setting of the distal intestine, whilst the levels of luminal bile acids are lower than in the small intestine due to reabsorption, some primary bile acids are likely present together with secondary bile acids such as lithocholic acid produced from modifications made by bacterial metabolism. These modifications are an example of symbiosis between bacteria and the host as the secondary bile acids are highly hydrophobic and easily pass across the colonic epithelium reducing loss of bile acids in faeces to about 1-3% of the total secreted [218]. Secondary bile acids also have higher potency at GPBAR-1 than primary bile acids [219]. Here we explore whether GPBAR-1 activation by GPBAR-A also triggers INSL5 secretion from colonic L-cells.

Gastrin releasing peptide (GRP) and Neuromedin B (NMB)

GRP and NMB are neuropeptides related to the peptide bombesin isolated from the skin of the *Bombina bombina*. Whilst NMB is largely produced by neurons of the central nervous system, GRP is the predominant bombesin-like peptide produced by neurons innervating the small and large intestine. GRP receptor (GRPR) also known as BB2R is activated by both GRP and NMB but GRP is more potent an agonist [220]. This receptor is enriched in L-cells and likely underlies GLP-1 responses seen to bombesin administration from both murine small

intestinal cultures and perfused tissue [221]. This GLP-1 secretion could underlie the anorectic effect of intraperitoneal administration of bombesin-like peptides including GRP in rats which are blocked by previous intraperitoneal injections of BB2R antagonists such as BW2258U89 [222,223]. Whilst bombesin is also known to trigger both intracellular calcium responses and GLP-1 secretion in colonic L-cells its effect on INSL5-producing cells specifically are unclear [59].

4.3.2. Vesicular localisation of GLP-1 and PYY

Early attempts to examine GLP-1 and PYY relative localisation within L-cells using immunogold labelling and electron microscopy suggested co-storage between the two peptides [224]. Habib et al. also found overlap between the GLP-1 and PYY vesicle pool in human colonic crypt cultures using confocal microscopy [70]. However, the resolving power of confocal microscopy is limited around the diffraction limit of 200nm. This means that if the GLP-1 and PYY vesicles were smaller than this then it would be difficult to differentiate close together but separate vesicles of GLP-1 and PYY from vesicles dual labelled for GLP-1 and PYY [225,226].

Subsequent application of 3D structured illumination microscopy (3D-SIM) imaging by Cho et al. overcame this diffraction limit yielding roughly double the resolving power of confocal microscopy [87,225]. In this study, immunofluorescently labelled tissue from mouse, rat, pig and human intestine GLP-1 and PYY were imaged. Images were thresholded across each 3D stack by the brightest background (identified manually) in each channel (corresponding to GLP-1 and PYY labelling). GLP-1 and PYY vesicles were subsequently detected and rendered in 3D based on fluorescence intensity in each channel (background subtraction was applied manually) using the 'create surfaces' function on the software package Imaris. The 'surface-surface colocalisation' function was then applied to render regions of overlap between the detected GLP-1 and PYY vesicles in 3D. Following this the total volume of space occupied by detected GLP-1 and PYY vesicles and by identified regions of overlap were computed as the sum of the individual voxels occupied by each. By using these values, the degree of overlap between detected GLP-1 and PYY vesicles was calculated as a percentage of total volume (i.e. of all identified vesicles). Using this methodology, henceforth dubbed the 'surfaces method',

Cho et al. found that the majority of GLP-1 and PYY was stored separately in all the samples examined with, for example, only ~8% overlap in the murine colon [87]. The GLP-1 and PYY vesicles in human L-cells were found to be 160-170nm in diameter (using the spot detection method in Imaris), below the resolving power of confocal microscopy but within the range of 3D-SIM. Mouse GLP-1 and PYY vesicles were about 10nm smaller. Fothergill et al. have built on these results, using similar methods to those of Cho et al. to examine 5-HT, secretin, CCK, ghrelin, CgA and GLP-1 co-localisation in the murine small intestine and found separation of each into different vesicle populations [227]. These results raise the possibility that INSL5 could be stored in a separate pool of vesicles from PYY and GLP-1 which are differentially regulated and respond to different stimuli. Since GLP-1 and PYY are anorexigenic and INSL5 is orexigenic such differential regulation could have physiological significance.

4.4. Results

N.B: FACS isolation of INSL5 cells was conducted by staff at the CIMR Flow Cytometry Core. The secretion assays detailed here were conducted and analysed by Pierre Larraufie (see methods for details of the secretion assay and LC-MS/MS analysis). Analysis and identification of INSL5, PYY and GLP-1 vesicles based on 3D Gaussian fitting was carried out by Christopher Smith.

4.4.1. Induction of specific GFP/GCaMP6F expression within INSL5-producing cells

Fixed tissue sections from Insl5-rtTA/TET-GFP mice (orally induced with 3mg/ml doxycycline over 5-7 days) and crypt cultures generated from Insl5-rtTA/TET- GCaMP6FΔCMV reporter mice (incubated overnight with 2µg/ml doxycycline) were immunofluorescently labelled for GFP (GCaMP6F is a chimeric protein with GFP domains) and INSL5 (figure 1A&C). Confocal imaging of these samples and subsequent cell counting revealed that 167 of the 232 INSL5-positive cells counted co-stained with GFP, indicating an average *in vivo* induction rate of 72% (figure 1B). Similarly, 205 out of 233 labelled INSL5 cells from crypt cultures co-labelled for GCaMP6F, indicating an induction rate of 88% (figure 1D). Off-target labelling was minimal in examined crypt cultures and tissue sections with average rates of 2.3% and 1.4% respectively (figure 1B&D).

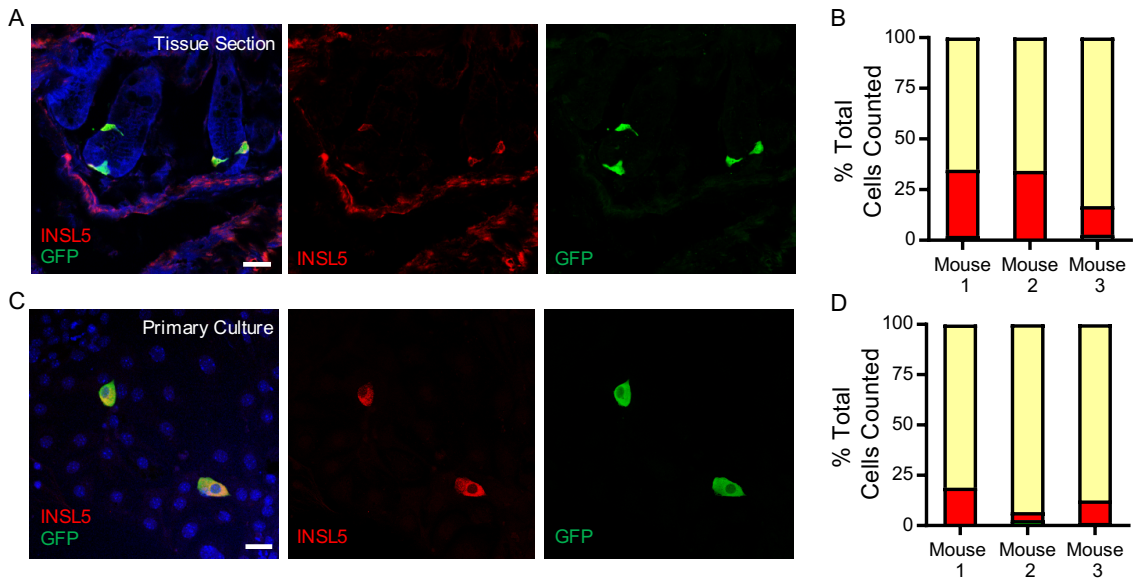

***Figure 1**: Verification of in vitro and in vivo induction of GFP/GCaMP6F expression by doxycycline administration. Representative confocal images of cells immunofluorescently labelled for INSL5 and GFP/GCaMP6F in tissue sections from mice (n=3) induced in vivo (A) and primary cultures (n=3) induced in vitro (C). Proportion of cells labelled solely for INSL5 (red), both INSL5 and GFP/GCaMP6F (yellow) or just GFP/GCaMP6F (grey) in tissue sections (B) and primary crypt cultures (D). 236 cells were manually assessed for both tissue sections and crypt cultures from the confocal images taken. All cells were 4% PFA fixed and subsequently incubated with INSL5 (1:2000) and GFP (1:1000) primary antibodies respectively labelled by goat secondary antibodies (1:300) conjugated to AlexaFluor 488 and 647 followed by exposure to Hoechst nuclear stain (1:2000). Figure adapted from Billing et al. (2018)* [153].

FACS-isolated GFP positive cells from colonic digests generated from both doxycycline induced Insl5-rtTA/TET-GFP and Insl5-rtTA/TET- GCaMP6FΔCMV mice constituted an average of 0.21 ± 0.05% (n=6 mice) of the total digest cell population (an example FACS output can be seen in figure 2C). Since roughly half of colonic L-cells are INSL5-producing, this proportion is consistent with previous FACS-analysis of L-cells in murine colonic digests which found 0.46 ± 0.07% cells were tagged when using a GLP-1 antibody [62]. RT-qPCR confirmed that the FACS-isolated GFP/GCaMP6F cells were INSL5-producing cells as they were significantly enriched for *Insl5*, *Gcg* and *Pyy* transcripts (figure 2A). *Insl5*, *Gcg* and *Pyy* transcripts had relative expression levels 712, 508 and 2052 fold higher in the GFP positive cells than in the control GFP-negative cell population (relative to ß-actin; fold measurements based on geometric means). Relative expression ($2^{\Delta CT}$, +SEM, -SEM) was highest of *Pyy* (46.64, +4.56, -2.95), followed by *Gcg* (8.39, +33.6, -19.5) and *Insl5* (2.89, +1.07, -0.78).

4.4.2. INSL5 cells express cognate GPCRs of known GLP-1 secretagogues

FACS-purified INSL5 cells were enriched for expression ($2^{\Delta CT}$, +SEM, -SEM) of *Agtr1a* (0.0140, +0.0036, -0.0001), *Avpr1b* (0.0303, +0.0180, -0.000115), *Ffar1*(0.00657, +0.000453, -0.000002)*, Gpbar1* (0.00869, +0.000824, -0.000040), *Grpr* (0.00261, +0.00146, -0.00084) and *Casr* (0.000541, +0.000512, -0.0000191) which encode the *c*ognate receptors for angiotensin II, vasopressin, MCFA/LCFAs, bile acids, bombesin and small peptides respectively (n=3 mice; figure 2B). Relative expression of the SCFA receptor *Ffar2* was not significantly different ($p>0.05$) in INSL5 cells (0.00186, +0.000789, -0.000522) compared with controls (0.000683, +0.0000418, - 0.000826).

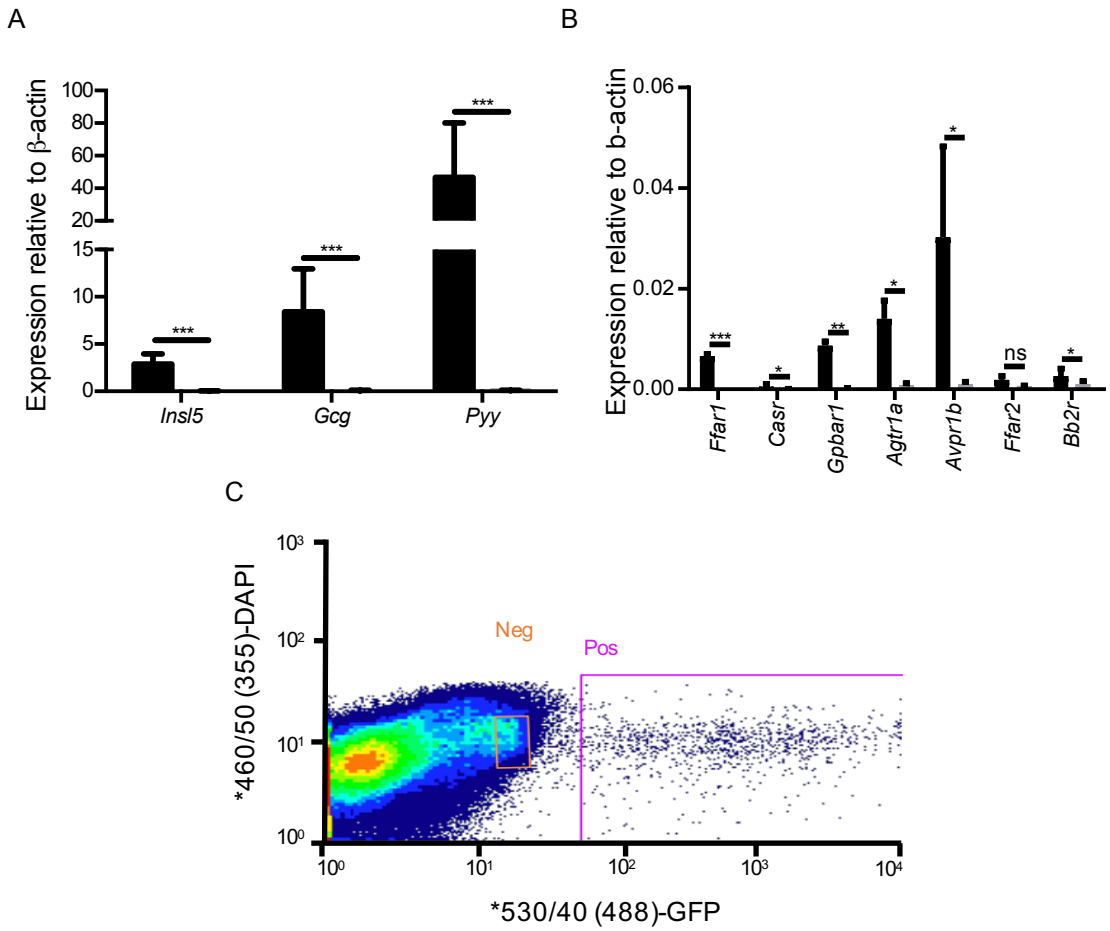

***Figure 2**: RT-qPCR expression analysis of FACS-isolated INSL5 cells. (A) Expression of Insl5, Gcg and Pyy (n=6 mice) relative to the housekeeper β-actin was enriched in the GFP cell population isolated by FACS. (B) Relative expression of a known subset of colonic L-cell GPCRs (n=3 mice). Difference in cycle threshold (ΔCT) was evaluated between the gene of interest and the housekeeper β-actin. These values were used to derive relative expression as $2^{\Delta CT}$. Bars represent mean relative expression with error bars reflecting SEM derived from ΔCT. Ratio paired t-tests run on $2^{\Delta CT}$ values. Black coloured bars represent INSL5 cells whilst grey coloured bars represent control cells. n.s. = p>0.05, *p<0.05, **p<0.01, ***p<0.001. (C) Representative FACS output indicating sampled populations of GFP negative and positive cells. Figures adapted from Billing et al. (2018)* [153].

4.4.3. Physiological stimuli trigger intracellular Ca^{2+} transients in cultured INSL5 cells

In calcium imaging experiments significant intracellular calcium responses were recorded in INSL5 cells to, in descending order of median fold increase in GCaMP6F fluorescence, 10nM angiotensin II (3.59 fold, 95% CI=2.74-4.51; n=50), 10nM AVP (1.65 fold, 95% CI=1.48-1.96; n=20), 100nM bombesin (1.56 fold, 95% CI=1.49-1.86; n=76), 5mg/ml peptones (1.56 fold, 95% CI=1.35-2.08; n=34), 2mM butyrate (1.18 fold, 95% CI=1.09-1.24; n=38) and 1μM AM-

1638 (1.06 fold 95% CI=1.02-1.16; n=40; figure 3C). The AM-1638 and butyrate intracellular calcium responses were variable between cells tested, with responses (defined as eliciting more than a 1.1 fold increase in GCaMP6F fluorescence) triggered in 17/40 cells and 25/38 cells, respectively (figure 3D).

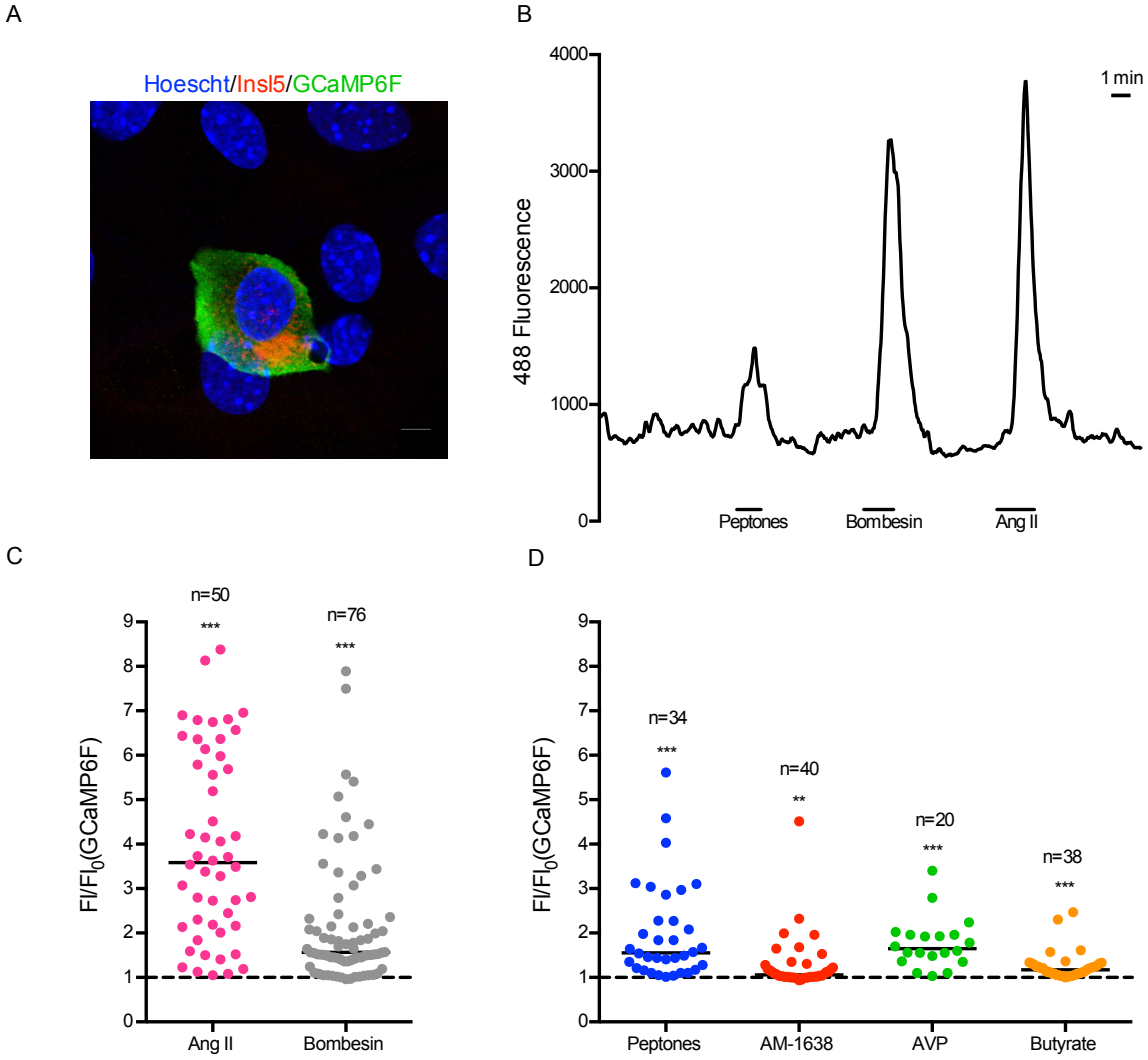

Figure 3: *(A) Example of an immunofluorescently labelled INSL5 cell which has been doxycycline induced for GCaMP6F expression in primary culture overnight. Fixed in 4% PFA and incubated with primary antibodies for INSL5 (1:2000) and GFP (1:1000) respectively labelled by goat secondary antibodies (1:300) conjugated to AlexaFluor 488 and 647 followed by treatment with Hoescht nuclear stain (1:2000). (B) Representative calcium imaging trace. (C) Fold changes in GCaMP6F fluorescence following addition of positive controls (10nM angiotensin II and 100nM bombesin). (D) Fold changes in GCaMP6F fluorescence following addition of a select range of agonists for identified G_q-coupled GPCR expressed in INSL5 cells. Fold change in fluorescence calculated as the peak fluorescence achieved during treatment divided by baseline fluorescence (an average of maximum fluorescence measured 30 seconds before and after treatment). Bold lines in 3C and 3C indicate the median of calculated fold changes in fluorescence. Statistical significance assessed using a Wilcoxon test. **p<0.01, ***p<0.001. Figure adapted from Billing et al. (2018)* [153].

4.4.4. GLP-1 secretagogues induce concomitant PYY and INSL5 secretion

The following GLP-1 secretagogues, listed from the strongest to weakest stimulus, triggered simultaneous INSL5 and PYY release from murine crypt cultures (figure 4A): forskolin/IBMX/glucose (10µM/10µM/10mM), arginine vasopressin (10nM), AM-1638 (1µM), angiotensin II (10nM), PMA (1µM), IBMX/glucose (100µM/10mM), GPBAR-A (3µM), SCFA mix (3mM acetate, 1mM butyrate and 1mM propionate), bombesin (100nM), KCl (70mM), l-glutamine (10mM), linoleic acid (100µM) and glucose (10mM). Addition of 100nM somatostatin (SST) significantly attenuated responses to IBMX/glucose. Pearson correlation (R) indicated strong positive correlation between the three peptide secretory responses with values of 0.91 for GLP-1/INSL5 (figure 4B), INSL5/PYY (figure 4C) and PYY/GLP-1 (figure 4D).

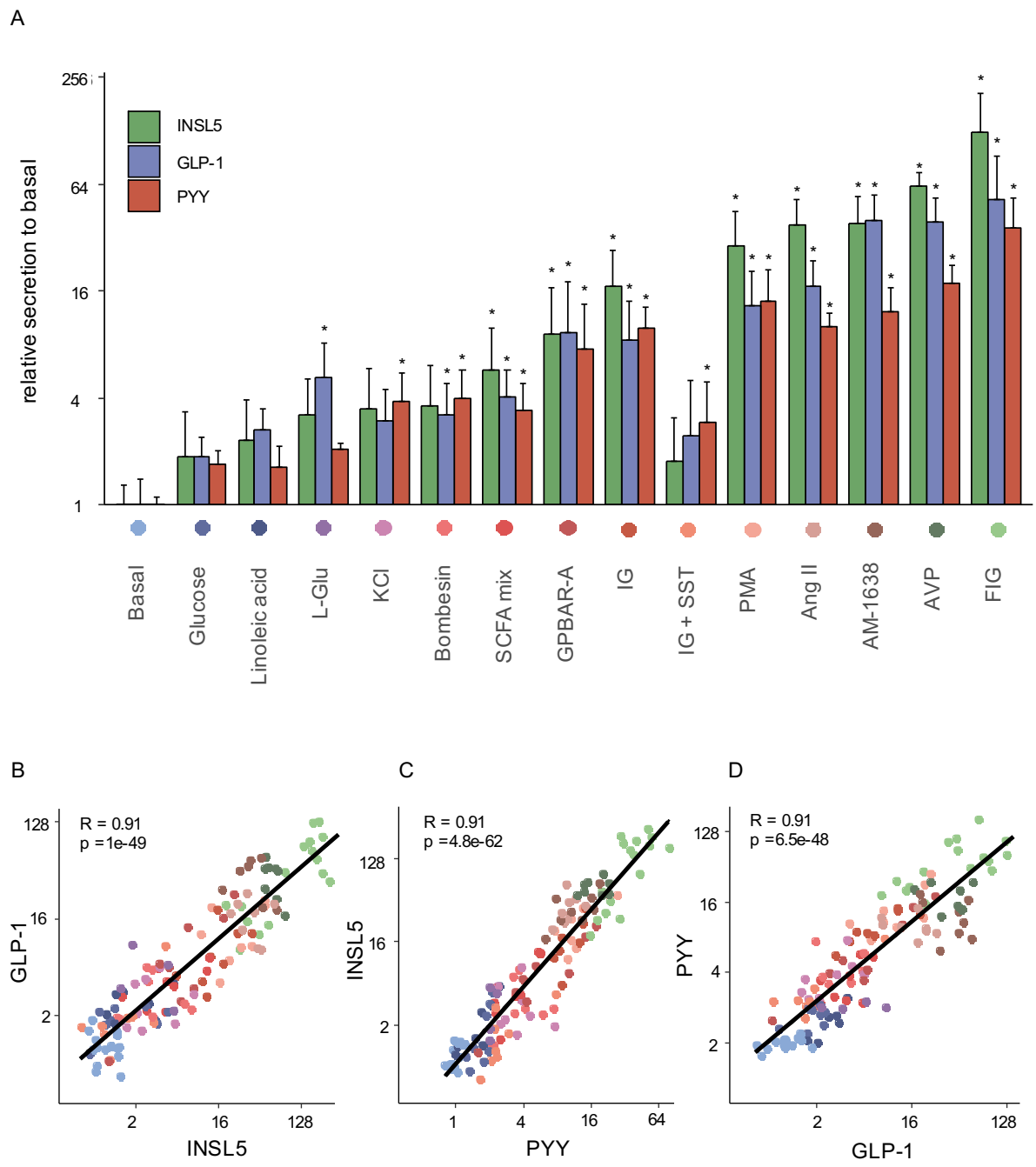

***Figure 4**: (A) Relative secretion of INSL5, GLP-1 and PYY from murine colonic crypt cultures in response to a range of stimuli as assessed by LC/MS analysis. Values derived from integration of the peak found for each peptide identified by retention time and m/z value. These values were firstly normalised to protein content assessed by a BCA protein assay and subsequently normalised by secretion in the basal condition (saline buffer with 1mM glucose). Statistically significant deviation from basal secretion was assessed using a Dunn test. n=duplicates from at least 3 different crypt cultures for each test condition. Bars represent mean + SD. *p<0.05. Linear regression between GLP-1/INSL5 (B), INSL5/PYY (C) and PYY/GLP-1 (D) responses with Pearson correlation coefficient shown (R) and each test condition using the same colour code and data as (A). Experimental data collected and analysed by Pierre Larraufie. Figure from Billing et al. (2018)* [153].

Human crypt cultures displayed a similar secretion profile to the murine crypt cultures with strong positive correlation between GLP-1, PYY and INSL5 secretory responses. Pearson correlation coefficients (R) for GLP-1/INSL5 (figure 5A), INSL5/PYY (figure 5B) and PYY/GLP-1 (figure 5C) were 0.72, 0.75 and 0.9 respectively. These results are derived from 4 different human crypt cultures (total of 11 crypt cultures were produced but INSL5 was only detectable in 4).

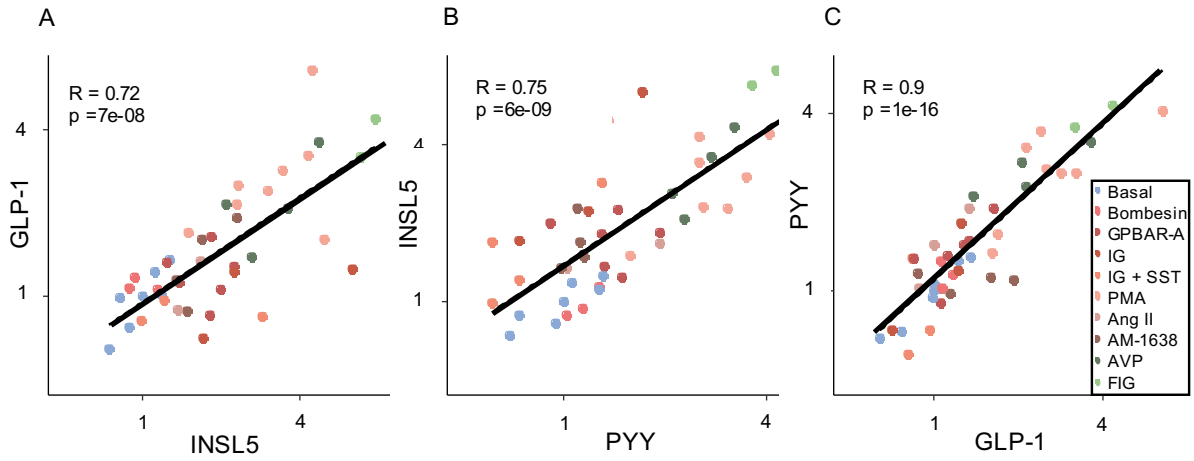

***Figure 5**: INSL5, GLP-1 and PYY secretory responses of human colonic crypt cultures to a range of stimuli. Linear regression between GLP-1/INSL5 (A), INSL5/PYY (B) and PYY/GLP-1 (C). Experimental data collected and analysed by Pierre Larraufie. Figure from Billing et al. (2018)* [153].

4.4.5. The majority of INSL5, GLP-1 and PYY secretory vesicles label for all three peptides

Initial surfaces based analysis of INSL5, GLP-1 and PYY immunofluorescent labelling in cultured murine colonic crypts indicated that roughly ~50% of vesicle volume was labelled for one peptide alone whilst ~30% was labelled for two peptides and the remaining ~20% vesicle volume was labelled for all three peptides (n=14 cells from 3 different mice; figure 6B). The surfaces analysis was also applied to cultured cells stained with a single primary antibody against GLP-1 and 3 secondary antibodies, AlexaFluor 488, 555 and 633, with the expectation that the three channels would strongly overlap in 3 dimensions. However, the degree of

overlap found was poor with only ~45% of the total vesicular volume triple labelled, ~15% dual labelled and ~40% single labelled (figure 6H).

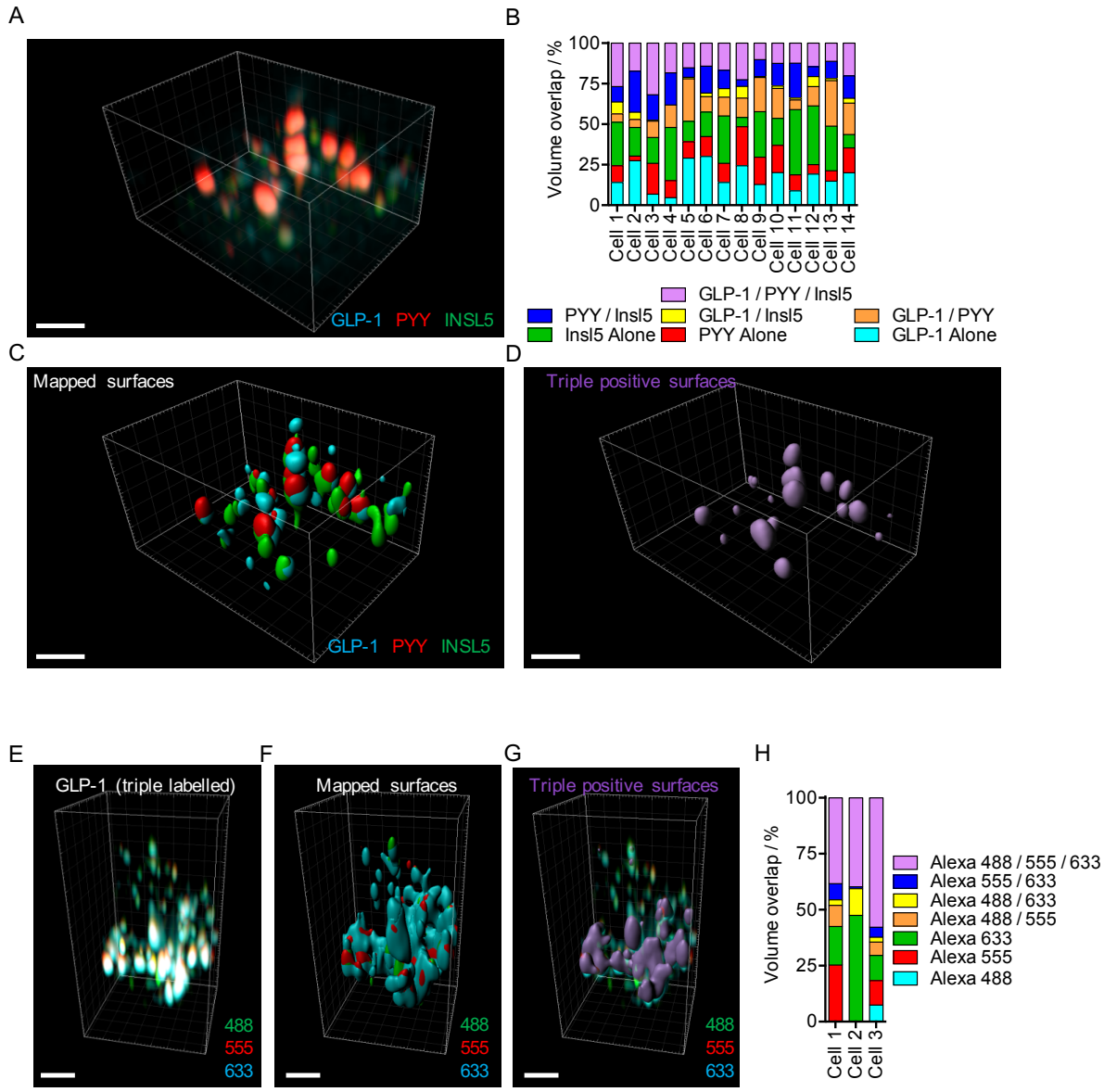

***Figure 6**: Surfaces based analysis of immunofluorescently labelled murine colonic crypt cultures. (A) Representative subsection of labelled GLP-1, PYY and INSL5 vesicles imaged using 3D-SIM and rendered in 3D using Imaris. (B) Mapped vesicle volume occupied by labelled GLP-1, PYY and INSL5 fractionated by single, dual and triple labelling. (C) Example image of surfaces rendered on Imaris from the individual channels for GLP-1, PYY and INSL5 shown in A. (D) Surfaces rendered from identified areas of triple labelling from C. Analysis of GLP-1 labelled with three different secondaries conjugated to Alexa 488, 555 and 633 with raw channel data (E), mapped surfaces (F) and triple positive surfaces (G) shown. (H) Percentage overlap between volume of the mapped surfaces for GLP-1 labelled with Alexa 488, 555 and 633. Scale bar = 1µm. Figure adapted from Billing et al. (2018)* [153].

An alternative methodology, developed by Chris Smith, fitted 3D Gaussian distributions onto the channel data from the 3D-SIM imaging allowing identification of INSL5, PYY and GLP-1 vesicles and of single, dual or triple labelled vesicles (see methods) [156,157]. Using fitted 3D Gaussian distributions to analyse the samples labelled for GLP-1 with AlexaFluor 488, 555 and 633 (the same samples used to examine the surfaces method) >95% of identified vesicles (1175 vesicles examined) were triple labelled, suggesting that this method was reliable analysis of co-labelled vesicles (figure 7C).

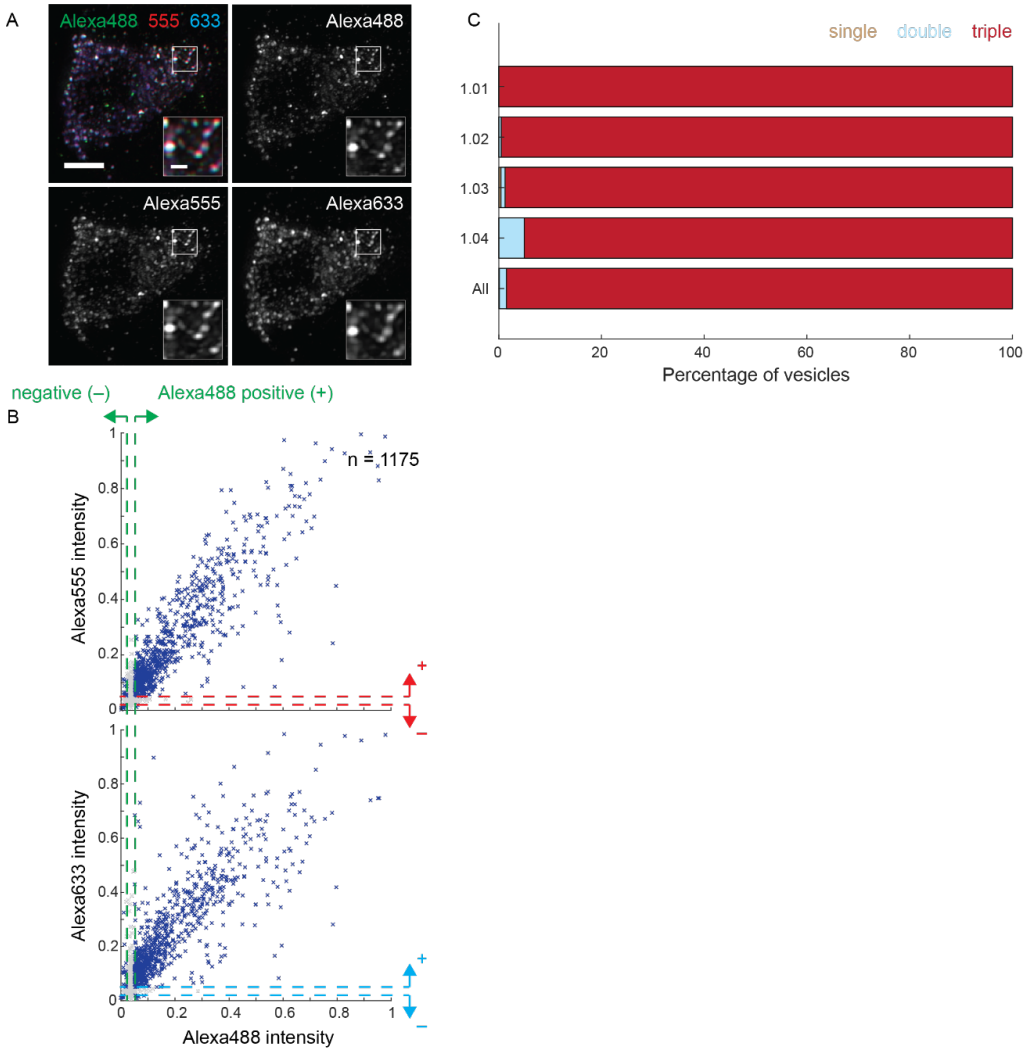

Figure 7: *Reanalysis of GLP-1 labelled with secondary antibodies conjugated to AlexaFluor 488, 555 and 633 using an alternative method which utilises fitted 3D Gaussian distributions. (A) Example 3D-SIM image of immunofluorescently stained crypt cultures. Images projected in z (scale bar = 3µm). Insets are individual z-planes of vesicle clusters in each channel (scale bar = 500nm). (B) Scatterplots showing normalised intensity of the AlexaFluor 555 and 633 against AlexaFluor 488. Dashed lines represent 5% (+) and 2% (-) of maximum intensity. Vesicles with intensities above 5% were classified as containing the relevant peptide whereas those below 2% were considered empty of that peptide. (C) Proportion of identified vesicles labelled with one, two or all three AlexFluor conjugated secondary antibodies. 1175 identified vesicles analysed from crypt cultures generated from a single mouse. Analysis conducted by Christopher Smith. Figure from Billing et al. (2018)* [153].

In contrast to the surfaces method, ~90% of the total INSL5, PYY and GLP-1 containing vesicles (total of 9860 vesicles examined from 16 cells) identified using 3D-Gaussian fitting were found to contain all three peptides, ~5% were double labelled and the remaining ~5% single labelled (figure 8C). A similar pattern was observed in stained tissue sections, in which for 13/14 cells analysed >80% of the vesicles (total of 4147 vesicles examined) were triple labelled (figure 9C). The remaining cell however showed a different pattern with ~54% of vesicles triple labelled, ~10% dual labelled and 36% single labelled which were almost all GLP-1 labelled (35.5% GLP-1). The diameters of GLP-1 vesicles labelled with AlexaFluor 488 (the wavelength least affected by chromatic aberration) were 205±92nm. As also found by Cho et al. (2014), we identified some irregular 'doughnut' shaped vesicles in both the tissue sections and primary cultures (examples can be seen in figure 10).

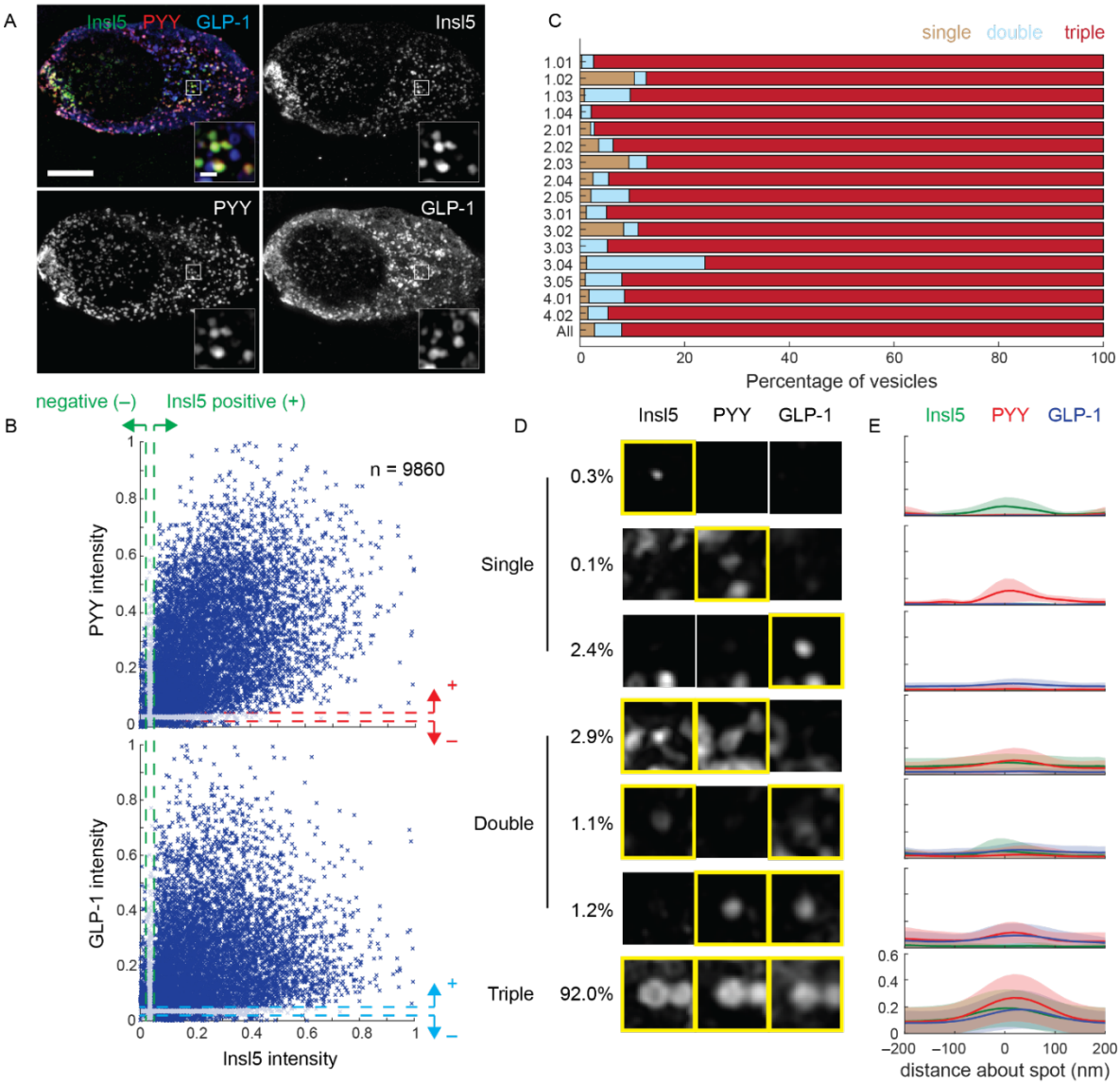

***Figure 8**: Analysis of INSL5, PYY and GLP-1 vesicle co-labelling in immunofluorescently labelled primary colonic crypt cultures. (A) Example image of a z-slice through a 3D-SIM imaged cell. Scale bar = 5µm (B) Scatterplot showing normalised intensity of the PYY and GLP-1 channels against that of INSL5. Dashed lines represent 5% (+) and 2% (-) of maximum intensity. Vesicles with intensities above 5% were classified as containing the relevant peptide whereas those below 2% were considered empty of that peptide. (C) Proportion of vesicles for each cell examined which were single, double and triple labelled. The first digit of the y-axis labels refers to the particular crypt culture examined whilst the digits after the full stop refer to the particular cell examined within that experiment. 9860 identified vesicles examined from 4 crypt cultures generated from 4 different mice. (D) Example images of the different variants of single and double labelled vesicles together with triple labelled vesicles. Percentages reflect the proportion each variant identified in the analysis. (E) Cross-sectional intensity profiles of INSL5, PYY and GLP-1 vesicles. Shading reflects standard deviation. Analysis conducted by Christopher Smith. Figure from Billing et al. (2018)* [153].

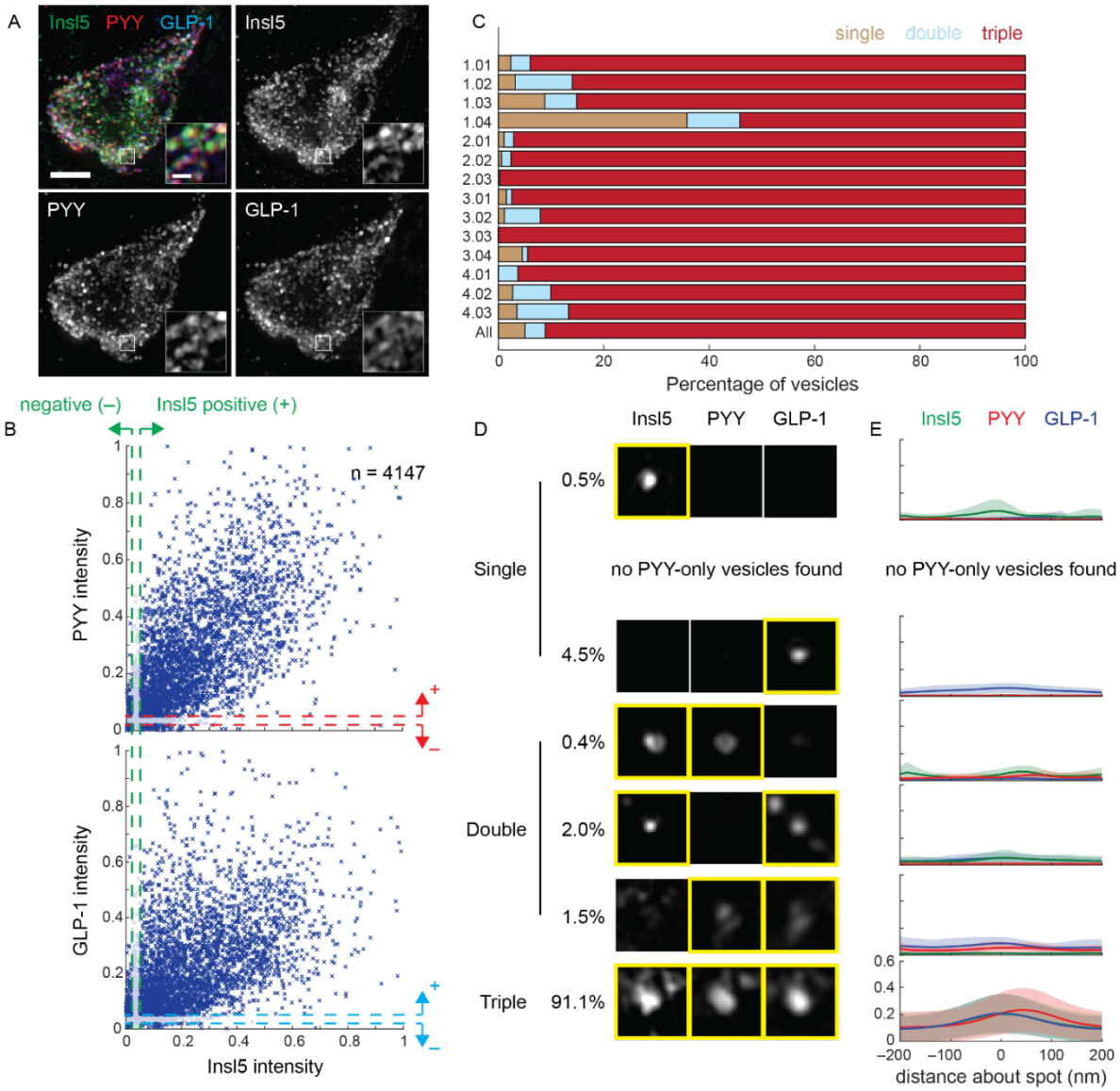

Figure 9: *Analysis of INSL5, PYY and GLP-1 vesicle co-labelling in immunofluorescently labelled colonic tissue sections. (A) Example image of a z-slice through a 3D-SIM imaged cell. Scale bar = 3µm (B) Scatterplot showing normalised intensity of the PYY and GLP-1 channels against that of INSL5. Dashed lines represent 5% (+) and 2% (-) of maximum intensity. Vesicles with intensities above 5% were classified as containing the relevant peptide whereas those below 2% were considered empty of that peptide. (C) Proportion of vesicles for each cell examined which were single, double and triple labelled. The first digit of the y-axis labels refers to the particular tissue section examined whilst the digits after the full stop refer to the particular cell examined within that experiment. 4147 identified vesicles examined from tissue sections from 4 different mice. (D) Example images of the different variants of single and double labelled vesicles together with triple labelled vesicles. Percentages reflect the proportion each variant identified in the analysis. (E) Cross-sectional intensity profiles of INSL5, PYY and GLP-1 vesicles. Shading reflects standard deviation. Analysis conducted by Christopher Smith. Figure from Billing et al. (2018)* [153].

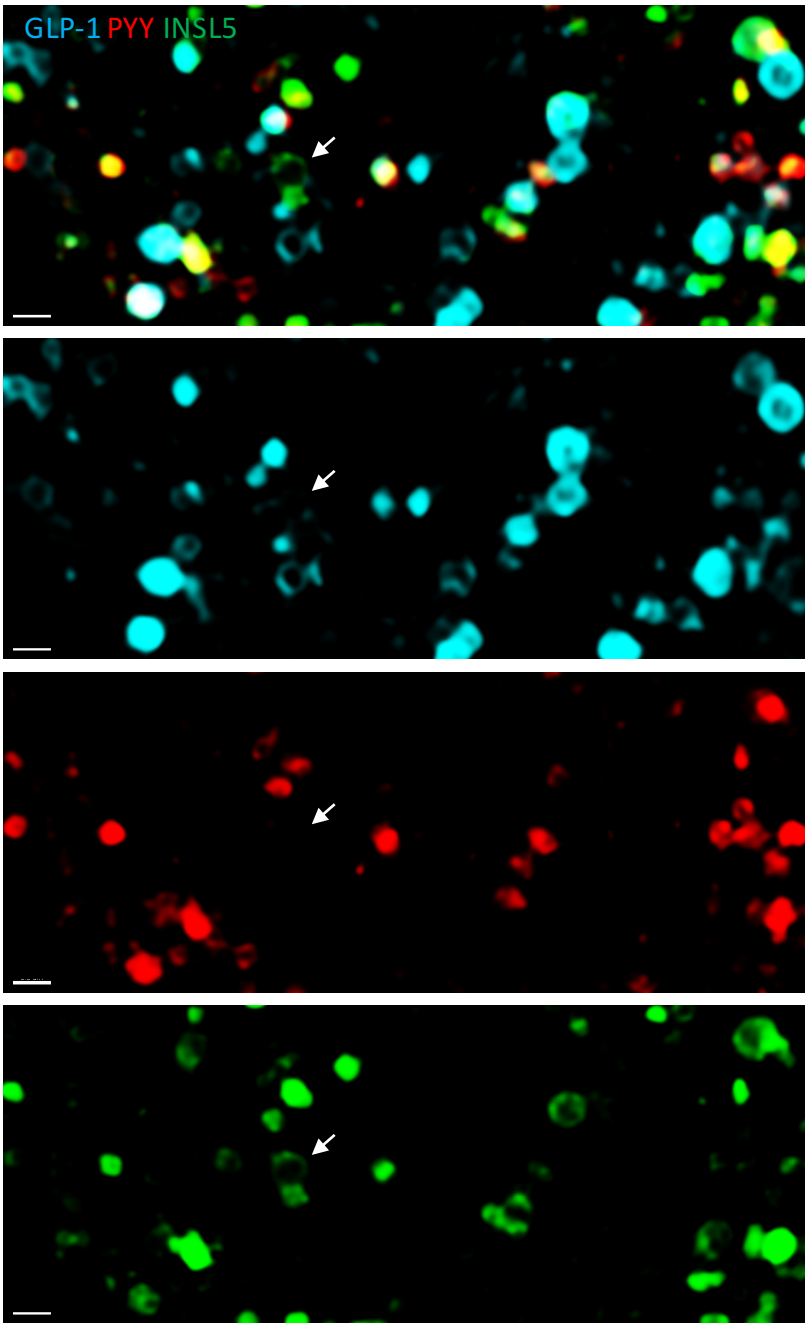

***Figures 10**: Example 3D-SIM images across a single z-plane of doughnut shaped vesicles in primary cultured L-cells. Scale bar = 0.5µm. An example doughnut shaped vesicle is indicated by the white arrow.*

4.5. Discussion

4.5.1. Verification of the Insl5-rtTA/TET-GCaMP6FΔCMV and Insl5-rTA/TET-GFP mouse models in vivo and ex vivo

The results of the IHC experiments both from tissue sections and primary cultures indicate that the doxycycline induction of the GFP/GCaMP6F fluorescent reporter was almost entirely limited to INSL5-producing cells with minimal non-specific labelling. The inducible Tet-on system minimises non-specific cell labelling issues associated with other systems such as Cre-lox recombination [228]. The induction rate *in vivo* was slightly lower than that in doxycycline treated *ex vivo* cultures (72% vs. 88%) though both rates are consistent with previous levels of penetrance observed in Glu-Venus mice (~80%) [62].

The transcriptomic profile of cells FACS-purified from Insl5-rtTA/TET-GFP and Insl5-rtTA/TET-GCaMP6FΔCMV mice was also consistent with specific INSL5 cell induction of GFP/GCaMP6F expression as these cells were enriched for *Insl5* as well as *Gcg* and *Pyy* (classical markers of L-cells) [88]. The tissue section staining however suggests that potentially around 30% of INSL5 cells were not isolated as they did not express the GFP reporter. This could mean that a subset of INSL5 cells are excluded from downstream RT-qPCR experiments.

4.5.2. INSL5 cells display intracellular Ca^{2+} responses to GLP-1 secretagogues

The results of the intracellular calcium imaging experiments reflect the expression of characterised L-cell GPCRs in INSL5 cells. In particular, on average angiotensin II and AVP application induced the largest of all the intracellular calcium responses, larger in fact than the positive control bombesin. Subsequently, the exclusion criteria were widened so that cells which did not respond to angiotensin II or bombesin were excluded from the final analysis. Interestingly, past investigations found that peripheral administration of angiotensin-converting enzyme (ACE) inhibitors such as captopril to fasted rats decreased subsequent food intake. The authors imply that this action is due to increased central angiotensin II concentrations (since captopril poorly passes across the blood brain barrier and angiotensin II is anorexigenic when centrally administered). However, it could also be driven by decreased INSL5 secretion resulting from decreased peripheral levels of angiotensin II [229].

The SCFA butyrate triggered calcium transients in spite of low levels of *Ffar2* expression in INSL5 cells. This could potentially reflect SCFA signalling through a different pathway, perhaps the aforementioned FFAR3 acting via an alternative signalling pathway (i.e. not via G_i-signalling). However, since the responses observed to butyrate were small and recorded in 25/38 cells it could be that expression of *Ffar2* is limited to a subset of a INSL5 cells and at levels beyond the sensitivity of the RT-qPCR used.

Comparing the intracellular Ca^{2+} responses of colonic INSL5 cells observed here with those small intestinal L-cells observed in chapter 3 it appears that the INSL5 cell responses are more robust than those the small intestinal L-cells. The reasons behind this are unclear but could relate to inherent differences between small and large intestinal L-cells and/or methodological differences. Regarding methodological differences, it should be noted that the L-cells examined in chapter 3 were derived from organoids grown in ENR media whereas examined INSL5 cells were derived from primary cultures grown in primary culture media. It is plausible that residual matrigel or insufficient disruption of the 3D organoid structure may have impaired access of applied stimuli to the cell surface of L-cells in 2D organoid cultures and consequently added noise to observed intracellular Ca^{2+} responses not observed in primary cultures. Chronic exposure of organoid derived L-cells to ENR media (containing multiple different growth factors) could also have reduced the robustness of observed responses through downregulation of G_q-signalling pathways. Beyond differences in the culture systems employed, different genetically encoded calcium sensors were used to examine intracellular Ca^{2+} responses with GCaMP3 used for the small intestinal L-cells and GCaMP6F used for INSL5 cells. GCaMP6F is much more sensitive to Ca^{2+} and exhibits greater signal to noise ratios than GCaMP3 which could explain why the intracellular Ca^{2+} responses recorded from INSL5 cells (using GCaMP6F) were more robust than those from the small intestinal L-cells (using GCaMP3) [152].

4.5.3. GLP-1 secretagogues trigger concomitant PYY and INSL5 secretion

The stimuli applied in the intracellular calcium imaging experiments, which are known to trigger GLP-1 and PYY secretion, also triggered INSL5 secretion implying that the intracellular calcium transients elicited may couple to INSL5 secretion (INSL5 secretory responses to peptones could not be tested as the mixture of peptides would obscure the LC/MS output) [73–75,173,221]. Consistent with these previous studies, LC/MS analysis confirmed that GLP-1 and PYY were also secreted. The murine and human colonic crypt cultures also showed largely the same secretory profiles of these three peptides. These results imply that murine INSL5 cells are a faithful model of human INSL5 cells, at least in the context of peptide secretion. Interestingly only 4/11 human crypt cultures examined had measurable levels of INSL5 in the secretory supernatants. This could reflect smaller INSL5 secretory responses in some samples (below the LC/MS detection threshold) or the number of INSL5 cells surviving in primary culture. Indeed, in other studies, L-cells derived from human colonic crypt cultures appear ~4 times less responsive than murine L-cells in terms of GLP-1 and PYY secretory responses [70]. Further refinement of the culture conditions and INSL5 peptide extraction may therefore help improve INSL5 detection for future examinations of human INSL5 cell responses. The low number of human crypt cultures secreting measurable levels of INSL5 could also reflect the source of the tissue samples used for each crypt culture, for example the precise region of colon sampled or the particular patient that samples were taken from. Any such issues could be minimised by obtaining tissue samples from the same region of colon and from patients matched for characteristics such as age and gender.

4.5.4. Co-storage of INSL5, PYY and GLP-1 likely underlies co-secretion

The co-release of INSL5, PYY and GLP-1 observed implies that the three peptides are either stored in separate vesicle pools with a common release mechanism or stored together resulting in concomitant secretion upon exocytosis. Previous findings suggest the former, as colonic GLP-1 and PYY were observed in separate vesicles in some studies [87]. However, our results are not consistent with these particular studies as 3D-SIM analysis illustrated that INSL5, PYY and GLP-1 are mostly co-stored in the same vesicles. These results suggest that co-secretion observed from human crypt cultures also arises as a consequence of co-storage, though no immunofluorescent investigations were conducted here on human L-cells. These

results fit with older studies employing electron microscopy and immunogold labelling where enteroglucagon and PYY were found to be co-stored in rabbit colon [224].

Whilst studies which concluded GLP-1 and PYY are stored in separate vesicles also used 3D-SIM techniques, they used a volume based approach to assess the degree of peptide co-storage. Using similar methods we similarly found a high percentage of single labelled vesicles in primary crypt cultures, albeit considerably less than found by Cho et al. [230]. Application of this method to samples with triple labelled GLP-1 illuminated a major flaw with this strategy. The three channels imaged for each of the different AlexaFluor labels used should in theory overlap exactly and as such one would expect the surfaces analysis to reflect this. In practice however, only ~45% of the total vesicle volume mapped contained overlapping signals from all three channels. This can, in part, be explained by the different wavelengths of the channels used. The longer wavelength channels, 555nm and 633nm, will occupy greater 3D space when imaged than the shorter 488nm channel due to chromatic aberration. This appears to have occurred despite correction using fluorescent beads as the largest proportions of single labelled vesicular volume were from the 633nm and 555nm channels (figure 6H). Our new methodology overcame these issues as evidenced by the >95% overlap between the channels of the same GLP-1 stained samples. GLP-1 vesicles, labelled with AlexaFluor 488, measured 205±92nm in diameter using this method, which is ~40-50nm larger than found by Cho et al. (2014) [87]. This difference may arise as a consequence of the different methodology applied with Cho et al. using spot detection to estimate the diameter of the vesicles. Alternatively, it may reflect the precise pool of vesicles examined as Cho et al. found the diameters of the vesicles measured varied from 90-440nm. Interestingly, not all GLP-1, PYY and INSL5 vesicles were spherical in shape, with some (as seen in figure 10) exhibiting a ring of fluorescence around a dim core similar to a doughnut. Similar findings were made by Cho et al. [87]. The physiological significance of these doughnut shaped vesicles is unclear and they could result from unusual restricted packaging of labelled peptides into the outer edges of secretory vesicles or staining artefacts.

Whilst L-cells immunofluorescently labelled from crypt cultures and tissue sections largely showed the same proportions of triple, dual and single labelled GLP-1, PYY and INSL5 vesicles, there was slightly greater variation between L-cells analysed in the tissue sections than

primary culture. One of the cells in a fixed section had 36% single labelled vesicles which were almost entirely GLP-1 labelled. These variations may have resulted from variations in immunolabelling between different tissue sections, which exhibit greater background staining than primary cultures. It should be noted that the primary antibodies used to target GLP-1, PYY and INSL5 likely exhibit differing detection limits which, despite protocol optimisation, may yield underestimates of the total numbers of GLP-1, PYY and INSL5 vesicles present within analysed cells and the degree of both dual and triple labelled vesicles. Alternatively, temporal differences in *Insl5*, *Pyy*, and *Gcg* expression (influenced by the age and/or environment of the cell) could create variations in the peptide constituents of the L-cell secretory vesicles. Using tissue from transgenic mice or transfected organoids whereby L-cells have been engineered to produce fluorescently tagged GLP-1, PYY and INSL5 would enable live confocal imaging of vesicle trafficking. In the case of intestinal organoids, this would also enable long-term tracing of vesicle peptide composition within L-cells.

4.5.5. Physiological Implications

Given that INSL5, PYY and GLP-1 are co-stored and likely co-secreted *in vivo* from INSL5 cells, interesting questions arise regarding how exactly the opposing effects of INSL5 and PYY/GLP-1 on appetite are exerted. One possible explanation relates to the differential distribution of GLP-1, PYY and INSL5 production along the GI tract with GLP-1 and PYY produced throughout the small and large intestines and INSL5 limited to the large intestine [88,231]. Post-prandially, acute delivery of the nutrients to the small intestine likely stimulates L-cells to secrete GLP-1 and PYY but not INSL5, exerting a net anorexigenic effect. In the long term, nutrients entering the colon and bacterial fermentation may stimulate INSL5 secretion (together with GLP-1 and PYY) with net orexigenic effects. It is possible that the combined action of the three peptides could yield different effects on appetite to the actions of the three individual peptides. GLP-1 and PYY co-secretion with INSL5 may also provide autoinhibitory feedback on the orexigenic effects of INSL5.

INSL5 may act as an autoinhibitor of L-cell activities by activation of the G_i-coupled RXFP4. Indeed, in support of the potentially auto-inhibitory nature of INSL5, in NCI-H716 cells (a model of human L-cells) INSL5 application attenuates acute forskolin-induced secretion of

GLP-1 [232]. Unpublished RNA-seq data (Cheryl Brighton), further supports this hypothesis as enrichment of *Gcg, Pyy* and *Insl5* transcripts was found in cells expressing *Rxfp4*. The autoinhibitory nature of INSL5 could be explored by application of a modified version to murine crypt cultures in combination with a stimulant such as forskolin, or of murine INSL5 to human crypt cultures, with subsequent LC/MS analysis to distinguish exogenous from endogenous INSL5 peptides. Using these protein isoforms would allow identification of any autoinhibitory effects on endogenous INSL5 secretion.

5-HT producing enterochromaffin cells were identified as expressing *Rxfp4*, as transcripts of the enterochromaffin marker *Tph1* were enriched in Rxfp4 labelled cells (unpublished work by Cheryl Brighton). This suggests that INSL5 can act as a paracrine modulator of 5-HT secretion and might subsequently influence motility in the colon, likely in an inhibitory manner. Changes in colonic motility can influence the composition of the present microbiota as well as fermentation, with SCFAs in particular affected [233–235].

Bariatric surgery (such as RYGB) increases delivery of dietary L-cell stimulants (including bile acids) to more L-cell rich distal regions of the GI tract, modulates the microbiota and increases GLP-1 secretion which potentially underlies increased glucose tolerance in people with type 2 diabetes [48,236]. It is possible that INSL5 levels are also modulated though this has not been investigated. Given that plasma levels of the other known orexigenic gut hormone, ghrelin, are greatly attenuated by RYGB and absent in patients with gastrectomy, INSL5 could play a key compensatory role in appetite regulation in such patients [237].

4.6. Concluding remarks

In summary, INSL5 cells express a range of known colonic L-cell GPCRs for physiological stimuli. Confirming my hypothesis that INSL5 cells exhibit responses to known GLP-1 secretagogues, application of these secretatogues triggered INSL5 secretion and a G_q-stimulating subset triggered intracellular Ca^{2+} transients in INSL5 cells. Secretion of INSL5 was observed in parallel with GLP-1 and PYY which our results suggest arises from co-storage of these peptides in the same secretory vesicles refuting the hypothesis that INSL5, GLP-1 and PYY are stored in separate secretory vesicle pools. The differential plasma dynamics of GLP-

1, PYY and INSL5 post-prandially likely reflect the regional expression profile of *Insl5* with activation of different L-cell populations along the gastrointestinal tract. The physiological significance of the co-secretion of orexigenic INSL5 with anorexigenic GLP-1 and PYY is unclear but we postulate that INSL5 may modulate responses to GLP-1 and PYY potentially acting as an autoinhibitor of L-cells. The establishment of a reliable LC/MS method for quantifying INSL5 is a significant step towards untangling INSL5's physiological actions. Application of a modified version of this LC/MS method will be especially useful when applied to further *in vivo* investigations of the physiological functions of INSL5.

Chapter 5. A single cell RNA-seq based examination of colonic enteroendocrine cells

5.1. Introduction

The diversity of EECs in the large intestine is lower than in upper regions of the gastrointestinal tract, predominantly consisting of 5-HT-producing enterochromaffin cells, followed by L-cells and D-cells [238]. The frequency of L-cells is particularly high when compared with the rest of the GI tract with highest abundance in the rectum. Roughly 50% of these L-cells express *Insl5* [88]. Whilst intracellular Ca^{2+} and INSL5 secretory responses detailed in chapter 4 were broadly consistent with those seen for colonic L-cells, it is still unclear whether *Insl5*-expressing cells form a transcriptomically distinct subgroup of L-cells. In this chapter, the hypothesis that the colonic EECs can be subdivided into distinct subgroups (beyond the canonical L-cell, D-cell and EC cell subdivisons) is examined through single cell RNA-seq (scRNA-seq) analysis. Furthermore, using a combination of RT-qPCR, immunohistochemistry and secretion experiments the hypotheses that the different L-cell subgroups exhibit differences in terms of regional distribution within the colon and functional GPCR repertoire were preliminarily tested.

5.2. Aims

1. To identify colonic enteroendocrine cell subgroups using transcriptomics
2. To examine the proximal-distal distribution of EEC subgroups within the colon
3. To examine the functional consequences of differences in GPCR repertoire between EEC subgroups

5.3. Background

5.3.1. Colonic EEC subtypes:

Enterochromaffin cells

5-HT-producing enterochromaffin cells (EC cells) dominate the profile of EECs in the colon representing around 70% of the total EEC population in the proximal colon decreasing to 40% in the rectum [238]. Immunohistological examination of colonic EC cells by Roth et al. (1992) identified no overlap between 5-HT and PYY, GLP-1, CCK or neurotensin staining and imply that EC cells derive from a separate branch of EEC progenitor differentiation than L-cells [239].

Lund et al. (2018) have recently investigated the GPCR repertoire of FACS-isolated murine small intestinal and colonic EC cells using RT-qPCR. Surprisingly, unlike other EECs, they found that small intestinal and colonic EC cells lack expression of receptors for dietary nutrients such as lipids (e.g. FFAR1) and protein metabolites. However, colonic EC cells did express *Ffar2* (the receptor for the SCFAs), *Gpbar1* (a bile acid receptor) and *Glp1r*. Consistent with functional *Glp1r* expression, application of the GLP-1 analogue liraglutide triggered 5-HT release from isolated pieces of murine colon [240]. Physiologically, 5-HT plays a critical role in regulating gastrointestinal motility and peristalsis [241]. Dysfunction of the local colonic serotonergic system has been implicated in a range of gastrointestinal disorders including irritable bowel syndrome (IBS) and inflammatory bowel disease (IBD) [242].

L-cells

L-cells are the second most abundant type of EEC in the colon with increasing frequency moving through the proximal-distal axis [238]. Roughly half of the total colonic L-cell population express *Insl5* [88]. Immunohistochemistry experiments in mouse have shown that the number of INSL5-positive cells increases moving from the caecum down to the rectum. Consistently, semi-quantitative PCR examination of human biopsy samples indicates that *INSL5* expression increases moving from the proximal to the distal colon [243]. These results imply that at least 2 subgroups of L-cells exist, those which express *Insl5* and those that do not and display discrepancies in regional distribution.

Comparison of the nutrient sensor expression profiles of small intestinal and colonic L-cells reveals that whilst there are similarities, for example in the expression of functional FFARs, there are notable discrepancies [86]. For example, expression of the key L-cell glucose sensor SGLT1 is 9-fold higher in small intestinal than colonic L-cells. Reflecting this, murine colonic primary cultures display smaller GLP-1 secretory responses to glucose and to the non-metabolisable glucose analogue α-methylglucopyranoside (transported by SGLT1) than small intestinal primary cultures [59]. Furthermore, in *in vivo* experiments using mice, direct intraluminal application of glucose to the colon did not trigger increased plasma GLP-1 whereas intraluminal application of glucose to the small intestine did [244]. Likewise, no significant increase in GLP-1 secretion was measured from human colonic primary cultures to glucose application [245]. Contrastingly, *Agtr1a* and *Avpr1b*, genes encoding receptors for angiotensin II and AVP respectively, are highly enriched in murine colonic L-cells compared with small intestinal L-cells [73,74]. These results provide further evidence for regional differences in nutrient sensing by intestinal L-cells. scRNA-seq analysis of the total colonic EEC population should aid identification of different subregional populations of L-cells in the colon.

D-cells

Colonic D-cells compose ~3-5% of all colonic EECs and predominantly produce the 28 amino acid form of somatostatin (SST-28) [238]. As with EC cells, intestinal D-cells appear to derive from a separate branch of EEC progenitor differentiation to L-cells. Evidence for this comes in part from IHC of the small intestine showing that SST labelling does not overlap with labelling of other EEC peptide products such as GLP-1, PYY and CCK. Furthermore, selective ablation of L-cells, through *in vivo* application of diphtheria toxin to transgenic mice expressing human diphtheria toxin receptor under the control of the proglucagon promoter, had no significant effect on SST immunoreactivity whilst greatly reducing immunoreactivity for GLP-1 and PYY, demonstrating separation of SST-producing D-cells and GLP-1/PYY-producing L-cells [246].

As in other regions of the gastrointestinal tract, somatostatin acts as a global inhibitor of colonic enteroendocrine secretions, including INSL5, as observed in chapter 4 [247]. Additionally, somatostatin regulates smooth muscle contraction in the colon and therefore

colonic motility. However, previous findings are mixed as to whether somatostatin increases or decreases intestinal muscle contractions and whether these effects are due to direct action of somatostatin on smooth muscle or indirectly via myenteric neurons [248–250]. In the clinical setting, colonic somatostatin may be involved in regulating intestinal inflammation in IBD as the number of immunohistologically labelled D-cells in colonic samples from patients inversely correlated with the grade of mucosal inflammation [251]. Thus, scRNA-seq aided insights into colonic D-cell secretory mechanisms could have implications for understanding IBD pathophysiology.

5.3.2. Single cell RNA-seq techniques

Cell isolation: plate-based vs droplet-based

Unlike bulk RNA-seq, whereby transcriptomes of entire cell populations are analysed and compared, single cell RNA-seq (scRNA-seq) enables the examination of the transcriptome of each individual cell within a cell population. Cluster analysis of these individual transcriptomes in turn enables identification of cellular subgroups within the analysed population. Currently scRNA-seq techniques depend on separation of cells either by FACS into individual wells on a plate, microfluidics or encapsulation into separate reaction droplets (drop-seq based techniques). Plate-based methods such as SMART-seq2 yield higher coverage and lower dropout rates (number of non-zero reads misread as zero reads) than droplet based method such as drop-seq or 10x Genomic's Chromium platform, translating to greater sensitivity and ability to detect to genes with low transcript abundance such as those encoding GPCRs. However, the throughput of SMART-seq2 is considerably lower than droplet based methods (100s vs. 1000-10000s of cells) due to the use of plates (typically 96 or 384 well plates) and consequently more expensive per cell sequenced.

Investigating EEC diversity using scRNA-seq

Glass et al. (2017) used SMART-seq2 to examine the diversity of *Gcg* expressing cells of the murine duodenum [64]. Analysis of transcriptomic profiles of FACS-isolated cells from duodenal digests generated from Glu-venus mice identified 3 main subgroups. The predominant group (51%) was highly enriched for *Gcg* and *Pyy* transcripts, the second most abundant (35%) was identifiable by *Tph1* and *Pzp* enrichment whilst the remaining group (14% total) was particularly enriched for *Gip* transcripts. These results imply that in the proximal small intestine alongside the classical L-cells, which express high levels of *Gcg* and *Pyy*, a small percentage of L-cells overlap with K-cells and the remainder appear to overlap with 5-HT producing EC cells (*Tph1* encodes tyrosine hydroxylase which is critical in 5-HT synthesis). Meanwhile Haber et al. (2017) characterised epithelial cells of the small intestine (including EECs) using a combination of high-throughput drop-seq and high sensitivity SMART-seq2 scRNA-seq [63]. This enabled broad subclustering of EECs by hormone expression profile using the drop-seq data followed by comparison of the GPCR repertoire of each group using the higher sensitivity SMART-seq2 data. EC cells, as anticipated, formed a separate subgroup from the other EECs cells. The other EECs clustered consisted of variations in *Gcg*, *Pyy, Gip, Sst, Ghrl* and *Cck* co-expression. Interestingly, *Sct* appeared to mark all mature EEC lineages including EC cells. These results demonstrate the ability of scRNA-seq to identify novel subclusters of EECs.

Here we employ the use of the Chromium platform for scRNA-seq analysis of colonic cells FACS-isolated based on expression of the mature enteroendocrine cell marker NeuroD1 [139]. For this purpose, single cell digests were prepared from a whole colon (from the caecocolic junction to the end of the rectum) extracted from a NeuroD1-EYFP mouse (see methods). The Chromium platform was chosen over plate-based methods because it allows high throughput analysis of 1000s cells at an affordable cost per cell screened and we hypothesised that the main EEC subdivisions would be identifiable by genes with high transcript abundance, such as hormones and enzymes, which are readily detectable by drop-seq. Use of the lower throughput of plate-based techniques in this case could potential restrict the ability to identify colonic EEC subclusters as EC cells, which are the most abundant cell type making up 40-70% of the total EEC population in the colon, would likely predominate [238].

5.4. Results

N.B: FACS isolation of NeuroD1-EYFP cells was conducted by staff at the CIMR Flow Cytometry Core and sorted cells were subsequently loaded into the Chromium system (10x Genomics) by staff at Cancer Research UK Cambridge Institute. Quality control, read alignment and raw count quantification for each cell analysed by scRNA-seq was carried out by Brian Lam.

Cluster analysis of colonic NeuroD1 scRNA-seq Cluster analysis of the t-SNE output from the NeuroD1 scRNA-seq identified 9 EEC subgroups (figure 1B). edgeR was subsequently used for differential expression analysis allowing transcriptomic variations between each subset to be explored. The following sections cover each of the EEC subgroups identified from this analysis and key genes that distinguish them (figure 2).

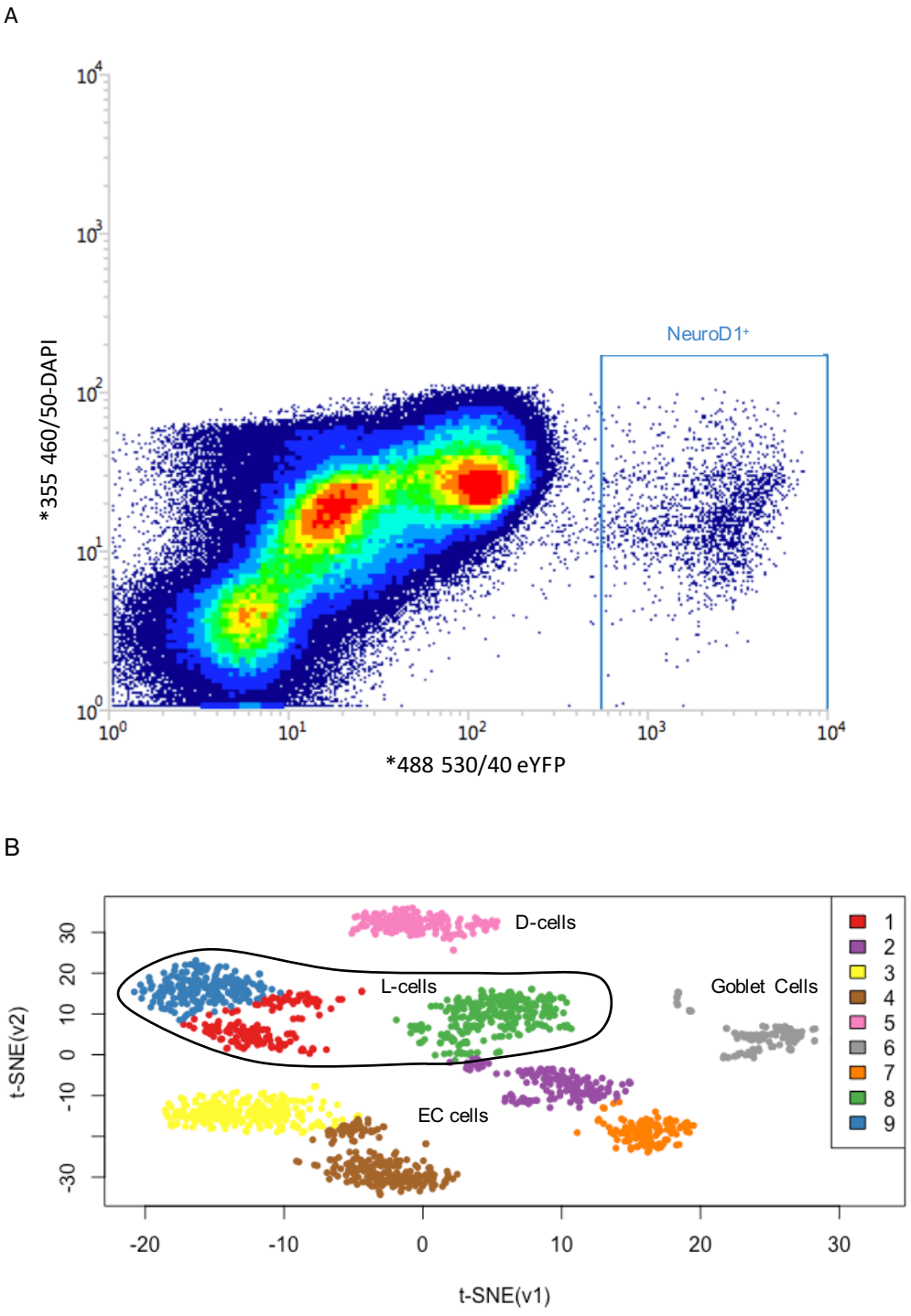

Figure 1: *(A) FACS output from the NeuroD1 sort. Sorted fluorescent EYFP cells ~0.58% of parent population following forward/side scatter, DRAQ5 and DAPI gating. 7000 EYFP+ve cells were isolated in one FACS run from one NeuroD1-EYFP mouse. 3500 of these cells were put into the Chromium system. (B) t-SNE plot of identified cell clusters from scRNA-seq analysis of FACS-isolated NeuroD1 expressing colonic cells (n=1779 cells). K-means clustering was applied to t-SNE coordinates with k=9.*

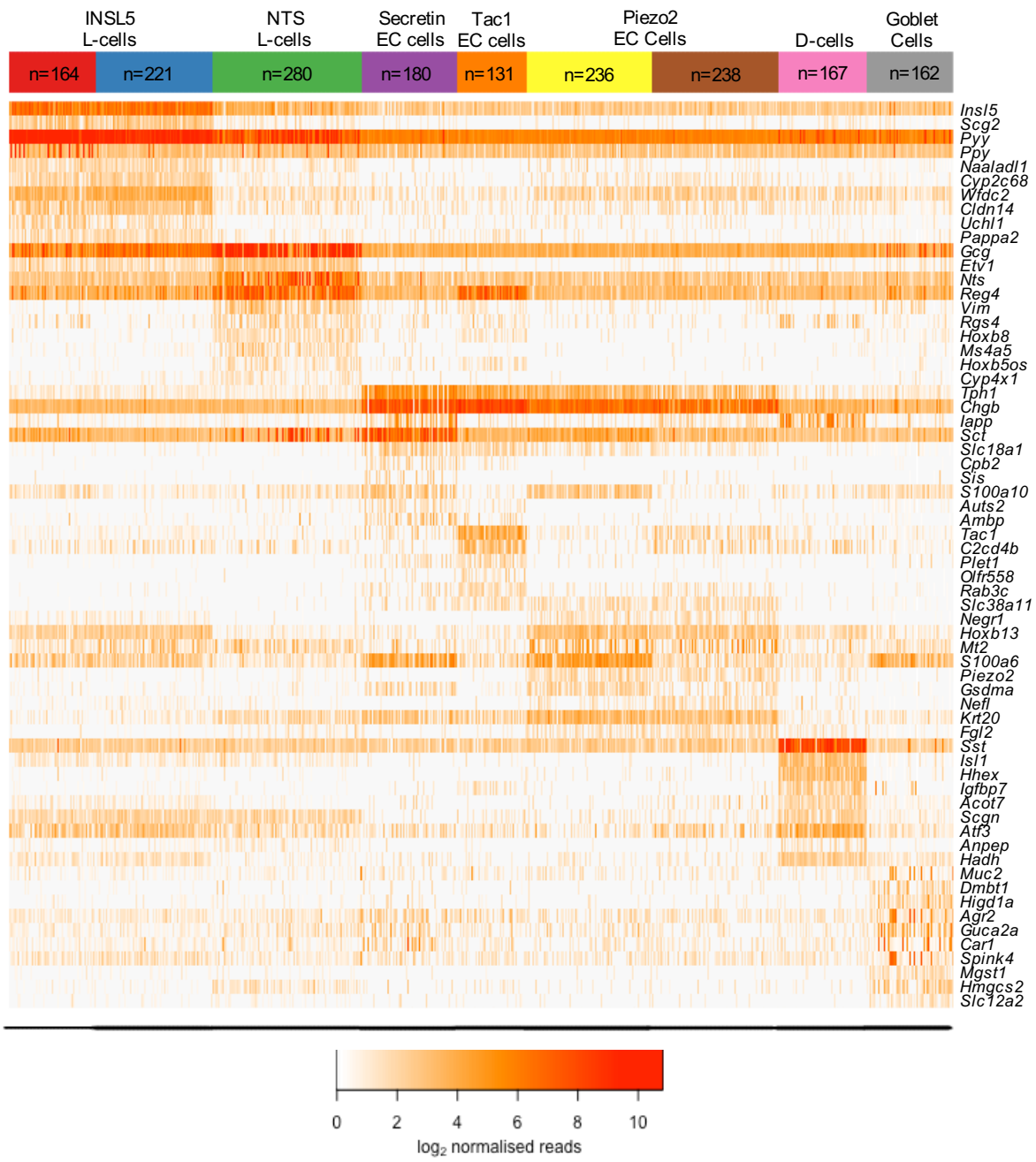

Figure 2: *Heat-map of log_2 normalised reads for each cell for the top differentially expressed genes of the INSL5 and NTS L-cells together with the secretin, Tac1 and piezo2 EC cell subgroups, D-cells and goblet cells. The top 10 differentially expressed genes were identified for each group using edgeR. Likelihood ratio tests were applied to statistically examine differences in transcript abundance between each cluster and all other clusters. Only genes with an FDR<0.01 were included for representation. The top 10 differentially expressed genes were identified for each cluster by ranking calculated log fold changes in transcript abundance between each group. Colours of top bar indicate cluster assignment of cells.*

L-cells

The classical markers of L-cells, *Gcg* and *Pyy* were both differentially enriched in clusters 1, 8 and 9 in comparison to the other clusters, identifying them as L-cells (figure 2). All L-cell clusters (together with D-cells) were also enriched for *Scgn*. Based on proximity on the t-SNE plot the clusters 1 and 9 were combined yielding 2 separate L-cell subgroups from the cluster analysis (figure 1B). Differential expression analysis of all the EEC subgroups revealed that the subgroup comprised of clusters 1 and 9 was enriched for *Insl5* expression marking them as INSL5 cells. On the other hand, cluster 8 was enriched for *Nts* expression and low in *Insl5* expression and are referred to as NTS cells. 385 of 665 cells (~58%) L-cells fell into the INSL5 cell subgroup roughly consistent with previous data implying half the colorectal L-cell population are INSL5 producing [88]. Beyond differential expression of *Insl5* and *Nts*, the INSL5 cells are distinguishable by enrichment in transcripts for various gut associated peptides and proteins such as *Scg2, Naaladl1* and *Cldn14* whilst NTS cells are distinguished by enrichment for *Reg4*, the transcription factor *Etv1* and *Cck* expression (figure 2 and appendix 1). A subgroup of INSL5 cells (cluster 1) are enriched for *Ppy* transcripts encoding pancreatic polypeptide which is associated with glucose homeostasis and appetite regulation [252].

Following identification, linear correlation between measured levels of *Gcg, Pyy, Insl5* and *Nts* transcripts were assessed for the colonic L-cells. Correlation between *Gcg* and *Pyy* (figure 3A) in L-cells was negative (R=-0.46) and interestingly, whilst only weak positive correlation (R=0.15) was identified between *Insl5* and *Gcg* levels (figure 3B), stronger positive correlation between *Insl5* and *Pyy* levels was found (R=0.55; figure 3C). Contrastingly, *Insl5* was negatively correlated with *Nts* (R=-0.61; figure 3D) and whilst *Gcg* was only weakly positively correlated with *Nts* (R=0.093; figure 3E), *Pyy* was negatively correlated with *Nts* (R=-0.29; figure 3F). These results are consistent with the cluster analysis which separated out INSL5 and NTS producing L-cells into distinct subgroups which respectively exhibited the highest levels of measured *Pyy* and *Nts* (figures 1B and 2).

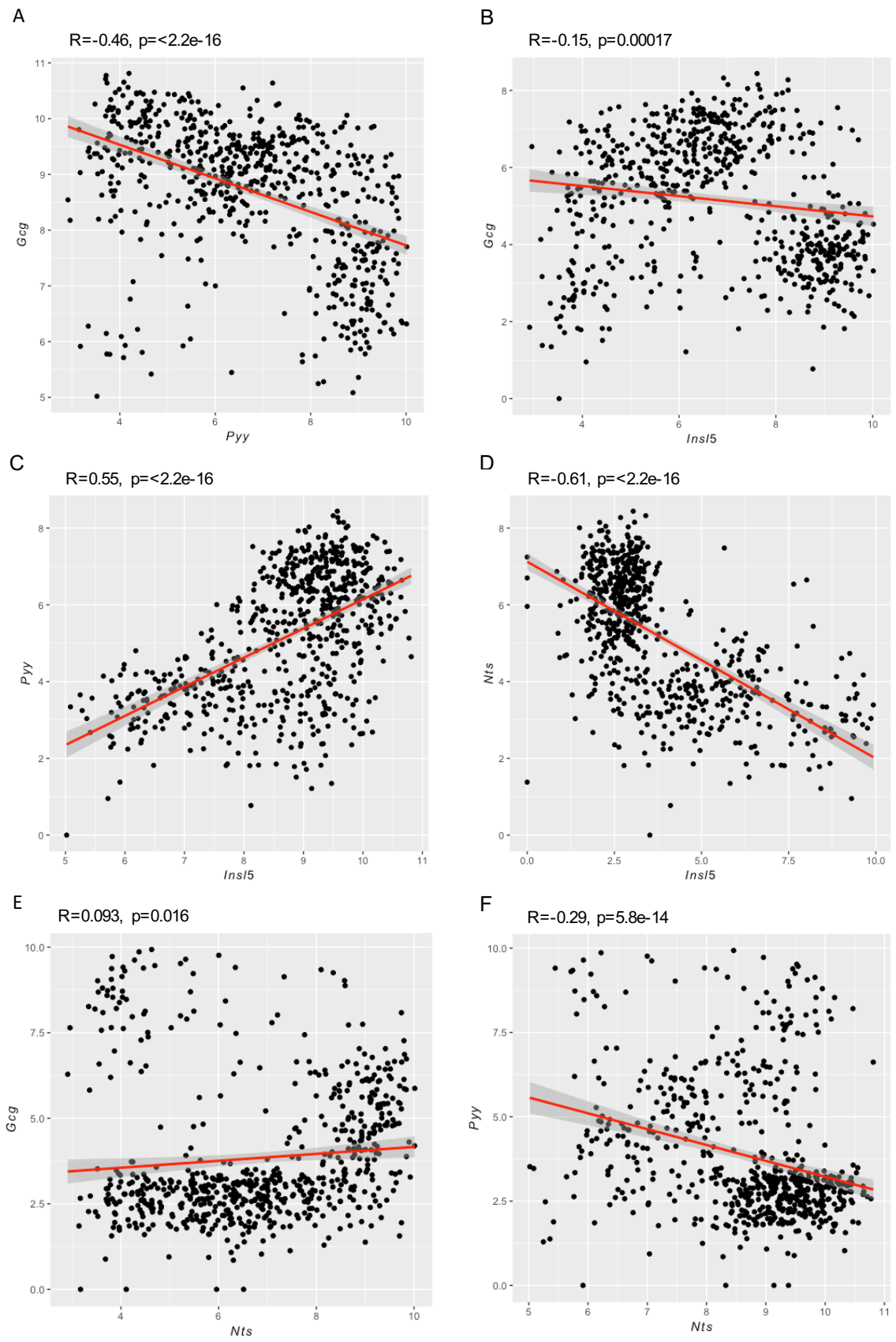

Figure 3: *Linear regression plots of log_2 normalised reads for (A) Pyy vs. Gcg, (B) Insl5 vs. Gcg, (C) Insl5 vs. Pyy, (D) Insl5 vs. Nts, (E) Nts vs. Gcg and (F) Nts vs. Pyy* measured *from all L-cells. R= Pearson correlation coefficient. n=665 cells.*

Enterochromaffin cells

Clusters 2, 3, 4 and 7 were all determined to be EC cells from enrichment of *Tph1* transcripts (figure 2). *Tph1* encodes the tryptophan hydroxylase 1, an enzyme which catalyses the rate limiting step in serotonin production in EC cells [253]. Based on the t-SNE plot and differential expression analysis of these combinations suggested existence of three main subgroups of colonic EC cells represented by clusters 2 and 7 and a combined group of clusters 3 and 4.

Cluster 2 is distinguished by enriched *Sct* expression whilst cluster 7 is selectively enriched for *Tac1* and *Reg4* transcripts (figure 2). Transcripts of *Tac1* encode for tachykinin peptide precursors, including substance P and have been previously been linked with EC cells. A subset of these *Tac1*-expressing EC cells were found to express high levels of *Reg4* in other scRNA-seq based studies [65]. Immunohistological examinations of serotonin, secretin and substance P have previously identified secretin and substance P production in separate populations of EC cells, consistent with our cluster analysis results [254]. Cluster 2 also shares enriched levels of *Iapp* expression with D-cells. *Iapp* encodes amylin and co-expression with intestinal *Sst* has been identified before by scRNA-seq [63,132].

Contrastingly, the third combined group of EC cells, comprised of clusters 3 and 4, is largely distinguished by selective enriched expression of the transcription factor *Hoxb13* and the mechanosensitive ion channel *Piezo2* (figure 2). As previously discussed, some EC cells are mechanosensitive and regulate gastrointestinal motility through 5-HT release. Recent Ussing chamber based experiments on murine jejeunum suggest that EC cell mechanosensation depends on Piezo2 activity, highlighting this group of EC cells as potentially mechanosensitive [255].

All three groups of EC cells were distinguishable by higher abundance of *Chgb* transcripts compared with the other EEC groups.

D-cells

Cluster 5 formed a distinctive and small group of 167 cells on the t-SNE map when compared with the other clusters (figure 1B). Enrichment of *Sst* transcripts within this cluster of cells identifies them as D-cells. These cells are also distinguishable by expression of the transcription factors *Isl1* and *Hhex* (figure 2). Consistent with this selective enrichment, *Isl1* expression has previously been identified as specific to mature D-cells in the murine gastrointestinal tract whilst *Hhex* is selectively expressed in somatostatin-producing pancreatic delta-cells where it maintains delta cell differentiation [256,257].

Goblet Cells

Cluster 6 appears to largely consist of goblet cells as this group was differentially enriched for *Muc2* and *Agr2* expression. Mucin 2 (MUC2) is the predominant form of mucin produced and secreted by intestinal goblet cells forming a protective mucous barrier around the intestinal lumen [258]. *Agr2* encodes a protein essential for MUC2 production by intestinal goblet cells and is therefore another marker of intestinal goblet cells [259]. Likewise, goblet cells are known to express high levels of *Spink4* and *Guca2a,* the latter of which encodes the gut peptide guanylin and these two genes are also enriched in cluster 6 [260,261].

5.4.1. Differential expression of GPCRs in colonic EEC subgroups

Differential expression analysis allowed differences in GPCR repertoires between identified colonic EEC subgroups to be identified. As GPCRs play a critical role in EEC nutrient sensing and secretory mechanisms, identification of such differences may reflect potentially differing secretory response profiles of EEC products to particular stimuli. Figure 4 denotes expression of the top 10 GPCRs in each subgroup in heat-map form (appendix 3 contains a list of the GPCRs examined). The following sections describe key receptors identified within each subgroup:

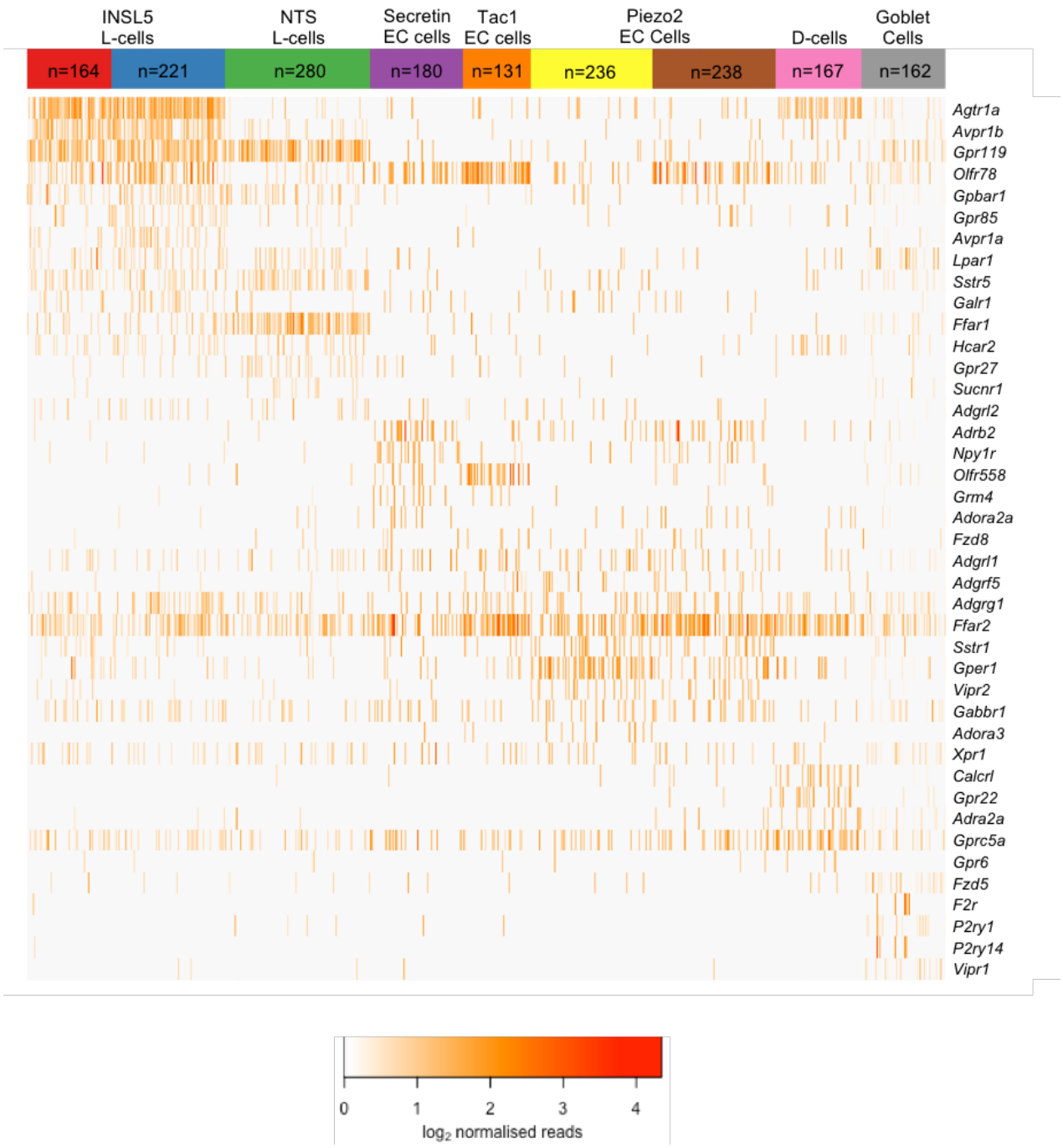

Figure 4: *Heat-map of log_2 normalised reads from each cell for the top differentially expressed GPCRs for each colonic EEC subgroup identified using edgeR.*

Insl5-expressing L-cells

The highest and most differentially expressed GPCRs in *Insl5*-expressing L-cells were *Agtr1a* and *Avpr1b* the cognate receptors for angiotensin II and arginine vasopressin (AVP) respectively (figure 4). Functional expression of these receptors in *Insl5*-expressing L-cells was illustrated in chapter 4 through RT-qPCR and secretion experiments. Interestingly, examination of the scRNA-seq data suggests that these receptors are largely absent from the *Nts*-expressing L-cells, implying differential responsiveness to angiotensin II/AVP by the L-cell subgroups. Like *Agtr1a/Avpr1b*, selective expression of the G_q-coupled SCFA receptor *Olfr78*, the orphan GPCR *Gpr85* and the galanin receptor *Galr1* was found in *Insl5*-expressing L-cells over the other L-cell subgroups (figure 4) [262–264]. Previous RT-qPCR and immunohistological based studies indicate that Olfr78 is restricted to the colon of mice and overlaps with GLP-1 and PYY labelling with increased numbers of labelled Olfr78 cells moving distally along the colon. Together with evidence that co-labelling of Olfr78 with PYY was greater than with GLP-1 (35% of PYY-labelled cells vs. 17% of GLP-1 labelled cells), the findings are consistent with selective expression of *Olfr78* in *Insl5*-expressing L-cells which are enriched for *Pyy* over *Gcg* expression [262]. Regarding *Galr1*, functional expression of *Galr1* has been identified in L-cells of the murine small and large intestine and has an inhibitory effect on GLP-1 and GIP secretion through G_i-signalling [264]. This suggests that galanin application may suppress INSL5 secretory responses from colonic L-cells.

Nts-expressing L-cells

Nts-expressing L-cells share expression of receptors such as *Gpr119*, *Gpbar1* and *Sstr5* with *Insl5*-expressing L-cells over the other colonic EEC subgroups (figure 4). These findings are reflected by the secretion data from chapter 4 which indicated that GPBAR-A, a specific agonist of GPBAR-1, stimulates simultaneous colonic INSL5, PYY and GLP-1 secretion whilst application of somatostatin suppressed INSL5, PYY and GLP-1 secretory responses to IBMX application. Furthermore, selective expression of *Gpr119*, a receptor for oleoylethanolamide (OEA) has previously been reported in intestinal L-cells and appears to play a key role in OEA-stimulated GLP-1 secretion [265]. Likewise, *Nts* and *Insl5*-expressing L-cells are selectively enriched for *Ffar1* expression, reflected by co-secretion of GLP-1, PYY and INSL5 observed

when the selective FFAR1 agonist AM-1638 was added to murine and human colonic crypt cultures (chapter 4).

GPCRs transcripts differentially abundant in *Nts*-expressing L-cells compared with *Insl5*-expressing L-cells include those for *Gpr*27 and *Sucnr1* (figure 4). The orphan GPCR GPR27 is a poorly characterised G_q-coupled receptor but appears to modulate glucose-stimulated insulin secretion from beta-cells since knockdown of *Gpr27* significantly attenuated glucose-stimulated insulin secretion from isolated murine islets [266]. Likewise, glucose-tolerance tests applied in murine knockout studies of *Sucnr1* (encoding the preferentially G_i-coupled succinate receptor 1 – SUCNR1) suggest that SUCNR1 is a modulator of insulin secretion (though interestingly plasma levels of GLP-1 appeared unaffected in the knockout mice) [267,268].

Sct-*expressing* enterochromaffin cells

Differentially expressed GPCRs in *Sct*-expressing EC cells include *Npy1r*, a G_i-coupled NPY/PYY receptor and *Adora2a* which encodes the G_s-coupled adenosine A_{2A} receptor [269,270]. Expression of both receptors has been identified previously in colonic EC cells [240,271]. Expression of *Adrb2* encoding beta-2 adrenergic receptor, which is G_s-coupled, was enriched in *Sct*-expressing and also in *Piezo2*-expressing EC cells (figure 4).

Tac1-expressing enterochromaffin cells

Examination of differentially expressed GPCRs in *Tac1*-expressing cells found limited differences. These differences include *Olfr78* and *Olfr558* (figure 4). Previous RT-qPCR analysis of FACS-isolated colonic EC cells revealed enrichment for both genes with ~640 fold higher levels of *Olfr78* than *Olfr558* [240]. Our results appear to reflect these findings as *Olfr78* expression was higher in *Tac1*-expressing cells than *Olfr558* and unlike *Olfr558, Olfr78* was also enriched in *Piezo2*-expressing EC cells (and *Insl5*-expressing L-cells). Olfr558 itself has been poorly characterised but functional expression in intestinal EC cells has previously been observed with Olfr558 appearing to respond to the bacterial metabolite isovalerate [119].

Piezo2-expressing enterochromaffin cells

As previously mentioned *Piezo2*-expressing EC cells are enriched for *Adrb2* and *Olfr78* as are the *Sct* and *Tac1*-expressing subgroups respectively (figure 4). The *Piezo*-expressing group is distinguishable from the other EC cell subgroups by enriched expression of *Gper1*, *Vipr2* and *Adora3* (figure 4). *Gper1* encodes a G_s-coupled GPCR for estrogen and has previously been identified in mucosal cells of the human colon. Expression levels of *Gper1* are significantly higher in IBS patients relative to controls suggesting that GPER1 activity may contribute to IBS-related dysfunctional gastrointestinal motility through modulation of 5-HT secretion from this particular subset of cells [272,273]. *Vipr2* encodes vasoactive intestinal peptide receptor 2 (VIPR2) which like GPER1 is G_s-coupled. With regards to the effects of VIP on 5-HT secretion, findings are mixed with one study indicating that intravenously delivered VIP may trigger colonic 5-HT secretion in rats whilst other studies using isolated guinea pig small intestine found VIP administration reduced 5-HT secretion [274,275]. Unlike *Adora2a,* which encodes a G_s-coupled GPCR and was enriched in the *Sct*-expressing EC cell subgroup, *Adora3* encodes a G_i-coupled adenosine receptor [276]. This discrepancy suggests that adenosine may have differential 5-HT secretory effects on the *Sct* and *Piezo2*-expressing subgroups. However, stimulation of Adora3 could actually increase EC cell secretory activity since activation of another G_i-coupled GPCR, alpha-2 adrenergic receptor increases EC cell activity (indicated by triggered intracellular Ca^{2+} transients) [119].

D-cells

Like *Insl5*-expressing L-cells, D-cells were enriched with *Agtr1a* transcripts. Identified GPCRs specifically enriched in D-cells included *Calcrl*, *Adra2a* and *Hcar2* (figure 4). *Calcrl* encodes calcitonin receptor-like receptor which forms functional GPCRs with different ligand affinities for adrenomedullin and calcitonin gene-related peptide (CGRP) when bound to one of three proteins known as receptor activity-modifying proteins (RAMPs) [277]. Transcripts of *Ramp1* were enriched within the D-cell population (appendix 2) suggesting that CALCRL and RAMP1 form a functional receptor for CGRP in colonic D-cells. Correspondingly, *Calcrl* and *Ramp1* expression have previously been identified in gastric D-cells and CGRP acted as a potent somatostatin secretagogue when applied to murine primary cultures of gastric pits [114,115].

Adra2a encodes the G_i-coupled alpha2 adrenergic receptor expression of which has also been previously identified in gastric D-cells [115]. RT-qPCR and immunohistochemistry has found that hydroxycarboxylic acid receptor (HCAR2) a G_i-coupled SCFA receptor, encoded by *Hcar2*, is expressed within murine and human colonic epithelial cells where it potentially acts as a tumour suppressor [278].

Goblet cells

The purinergic receptors *P2ry1* and *P2ry14* appear to be enriched these cells (figure 4). Consistently, *P2ry1* expression has previously been detected in the rat colonic epithelium [279]. Also enriched within this population was *Fzd5* encoding the Wnt5A receptor frizzled-5 (figure 4). One previous study found that *Fzd5* was particularly enriched within goblet cells within the colonic mucosa further supporting that cluster 6 contains goblet cells [280].

5.4.2. RT-qPCR examination of INSL5 cells

scRNA-seq analysis identified a selection of genes for which transcripts were enriched and other genes such as *Nts* which had a low abundance of transcripts specifically in clusters enriched for INSL5 transcripts when compared with other L-cell subgroups. We sought to confirm the transcriptomic profile of INSL5 cells identified by scRNA-seq using RT-qPCR analysis (figure 5). For this analysis, the same cDNA samples from FACS-purified INSL5 cells detailed in chapter 4 were used.

Relative expression ($2^{\Delta CT}$, +SEM, -SEM) of the peptides *Ppy* and *Nts* was 0.199 (+0.0902, -0.0836) and 0.0383 (+0.0319, -0.0309) respectively, reflecting a 93.2 and 58.5 fold enrichment in the INSL5 cells compared with control cells. Likewise, relative expression of the SCFA receptor *Olfr78* and the SCFA transporter *Slc5a8* (see appendix 2) was 0.0478 (+0.0276, -0.0269) and 0.107 (+0.0295, -0.0288) respectively, representing expression 1390 and 13.9 fold greater in INSL5 cells than in the control population.

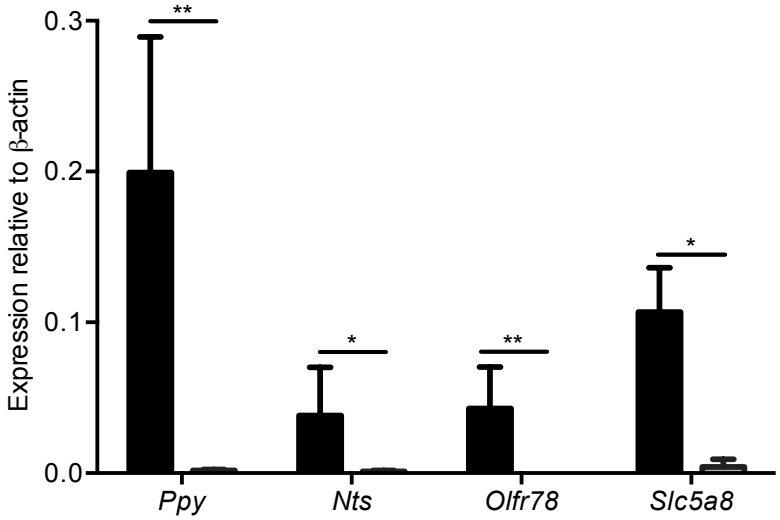

Figure 5: *Relative expression of a selection of genes enriched within identified L-cell clusters by FACS-purified INSL5 cells (n=3 mice). Difference in cycle threshold (ΔCT) was evaluated between the gene of interest and the housekeeper β-actin. These values were used to derive relative expression as* $2^{\Delta CT}$*. Bars represent mean relative expression with error bars reflecting SEM derived from ΔCT. Black coloured bars represent INSL5 cells and grey coloured bars represent control cells. Ratio paired t-tests run on* $2^{\Delta CT}$ *values. *p<0.05, **p<0.01. To obtain these results RT-qPCR was run on the same cDNA samples characterised in chapter 4.*

5.4.3. Regional expression of EEC markers

RT-qPCR analysis along the proximal-distal axis of the colon allowed regional profiling of key gene markers of the L-cell subgroups identified through t-SNE clustering (figure 6). For this analysis, whole murine colons (from the caecocolic junction to distal rectum) were sampled at ~1cm intervals along the proximal-distal axis. This yielded 7 segments for analysis denoted as, in proximal-distal order, P1-P7 (see methods for more details). For each of the analysed L-cell markers, statistically significant deviations were identified between expression in each segment with that of P1.

Relative expression of *Insl5* was highest in the distal segments of colon (P4-P7) with expression levels ~50 times greater than in P1. Conversely, relative expression of *Nts* was lowest in the distal segments of colon (P4-P7) with expression levels ~140 times lower than in P1. Relative expression of *Gcg* was significantly lower in P6 and P7 dropping to a tenth of that in P1. *Pyy* expression was largely consistent in each of the colonic segments examined with peak expression (3.6 fold higher than in P1) found in P5 (figure 6A). Expression of *Cck*,

which like *Nts* is enriched within the *Nts*-expressing L-cell subgroup (appendix 1), was lowest in the distal colon (P4-P7) with around one fifth of the levels of expression seen in P1 (figure 6B).

In addition to markers of L-cell subgroups, regional expression of *Sst* and *Tph1*, markers of D-cells and EC cells respectively, was examined (figure 6B). *Sst* expression was reasonably consistent across the length of the colon though in P7 expression levels were significantly lower (6.5 fold lower) than in P1. *Tph1* displayed lower expression in distal colon (P5-P7) relative to P1 (dropping down ~10 fold). Similarly, *Sct* showed lowest levels of expression in P6-P7 (28 fold less in P7 compared with P1). These results could reflect a decrease in total mature EECs along the proximal-distal axis particularly of EC cells and *Nts*-expressing L-cells.

5.4.4. Regional expression of GPCRs highlighted by scRNA-seq analysis

Expression of genes encoding various functional L-cell receptors highlighted in the scRNA-seq cluster analysis were evaluated across the proximal-distal axis of the colon in the same manner as for the EEC markers (figure 6C). Expression of *Agtr1a* (transcripts of which were enriched in the INSL5 cluster) did not significantly differ between the segments of colon along the proximal-distal axis analysed (P1-P7). Neither did expression of *Ffar1* or *Gpbar1* (receptors expressed within all colonic L-cell subpopulations) or that of *Calcrl* (specifically enriched within the D-cell subcluster). On the other hand, whilst expression of *Avpr1b* (which like *Agtr1a* is highly enriched within the INSL5-producing L-cell subpopulation) was notably lower in all the colonic segments analysed than for the other receptors examined, it was significantly higher in more distal segments of colon (P3-P7) relative to P1 (peaking at 34 fold higher in P6).

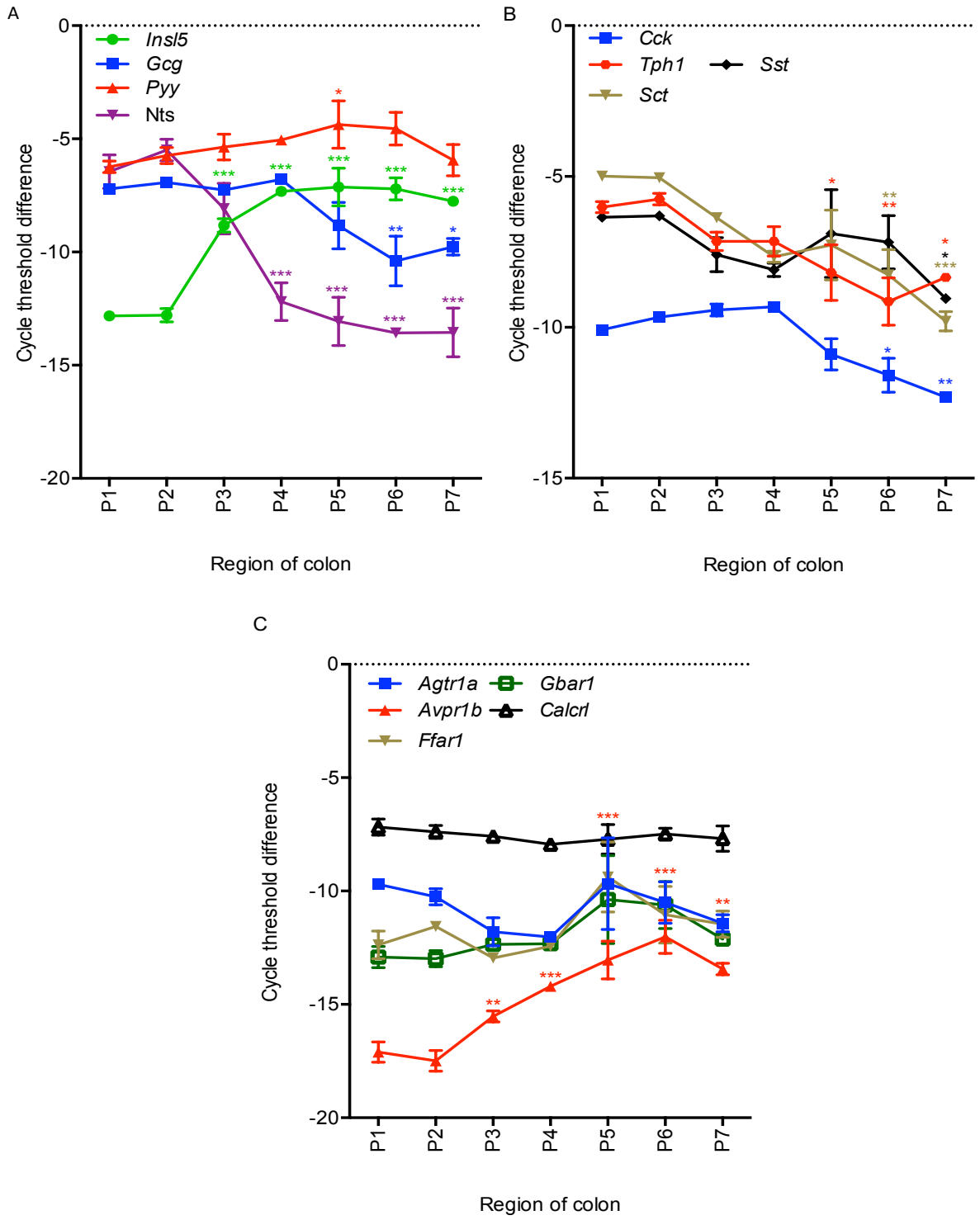

Figure 6: *Relative expression of identified L-cell subgroup (A), enterochromaffin and D-cell markers along with Cck (B) and a subset of identified GPCRs (C) across the proximal-distal axis of the murine colon. Murine colons were sampled every 1cm along the proximal-distal axis (starting from the caecocolic junction). These samples are denoted as P1-P7 (proximal-distal). Cycle threshold difference calculated between the gene of interest and the housekeeper β-actin ($CT_{\beta\text{-}actin}$-CT_{Gene}). n=3 mice. Plotted points and bars represent mean ± SEM. Statistically significant deviations in cycle threshold differences from values in P1 were assessed using repeated-measures one-way ANOVA with Dunnett's correction. *p<0.05, **p<0.01, ***p<0.001.*

5.4.5. Immunofluorescent labelling of INSL5, PYY and NTS in wholemounted murine colon

To examine the distribution of L-cell subgroups along the proximal-distal axis of the colon I immunofluorescently labelled INSL5, PYY and NTS in whole-mounted murine colons (figure 7). Automated cell counts were then made for single, dual and triple labelled cells within proximal (P1-P2), intermediate (P3-P5) and distal (P6-P7) segments of colon using HALO (see methods). The overall cell counts for NTS, PYY and INSL5 labelled cells (figure 7B) were highly variable between the different mice but generally showed trends toward increased INSL5 and PYY cell density in the distal end of the colon (71.8 and 113.8 cells/mm^2 respectively) compared with in proximal colon (36.6 and 76.2 cells/mm^2 respectively). Contrastingly the density of NTS labelled cells was higher in proximal colon (19.6 cells/mm^2) than in distal colon (3.0 cells/mm^2). In all regions, the number of PYY and INSL5 labelled cells was far greater than those labelled for NTS.

Analysis of cells labelled for NTS, INSL5 and PYY revealed that roughly 54% of the total cells counted were labelled with INSL5, 76% with PYY and 7% with NTS. The majority of the INSL5 labelled cells were either dual-labelled with PYY (54%) or singularly labelled for INSL5 (42%) with very few triple labelled (4%) or dual-labelled with NTS (<0.5%; figure 7C). Likewise, roughly 50% of all NTS cells were dual-labelled with PYY, 30% were triple labelled, <2% dual labelled with INSL5 and the remaining 18% single labelled for NTS (figure 7C). Unlike NTS and INSL5 labelled cells, roughly ~54% of all PYY labelled cells were singularly labelled whilst 38% were dual labelled with INSL5, 5% were dual labelled with NTS and 3% were triple labelled (figure 7C).

Figure 7D illustrates the breakdown of single, dual and triple labelled colonic cells across the proximal-distal axis. As anticipated from the decline in NTS-labelled cells, the percentage of triple labelled cells decreases dramatically moving from proximal to distal colon whilst the proportion of INSL5 labelled cells increases, particularly the single labelled variant.

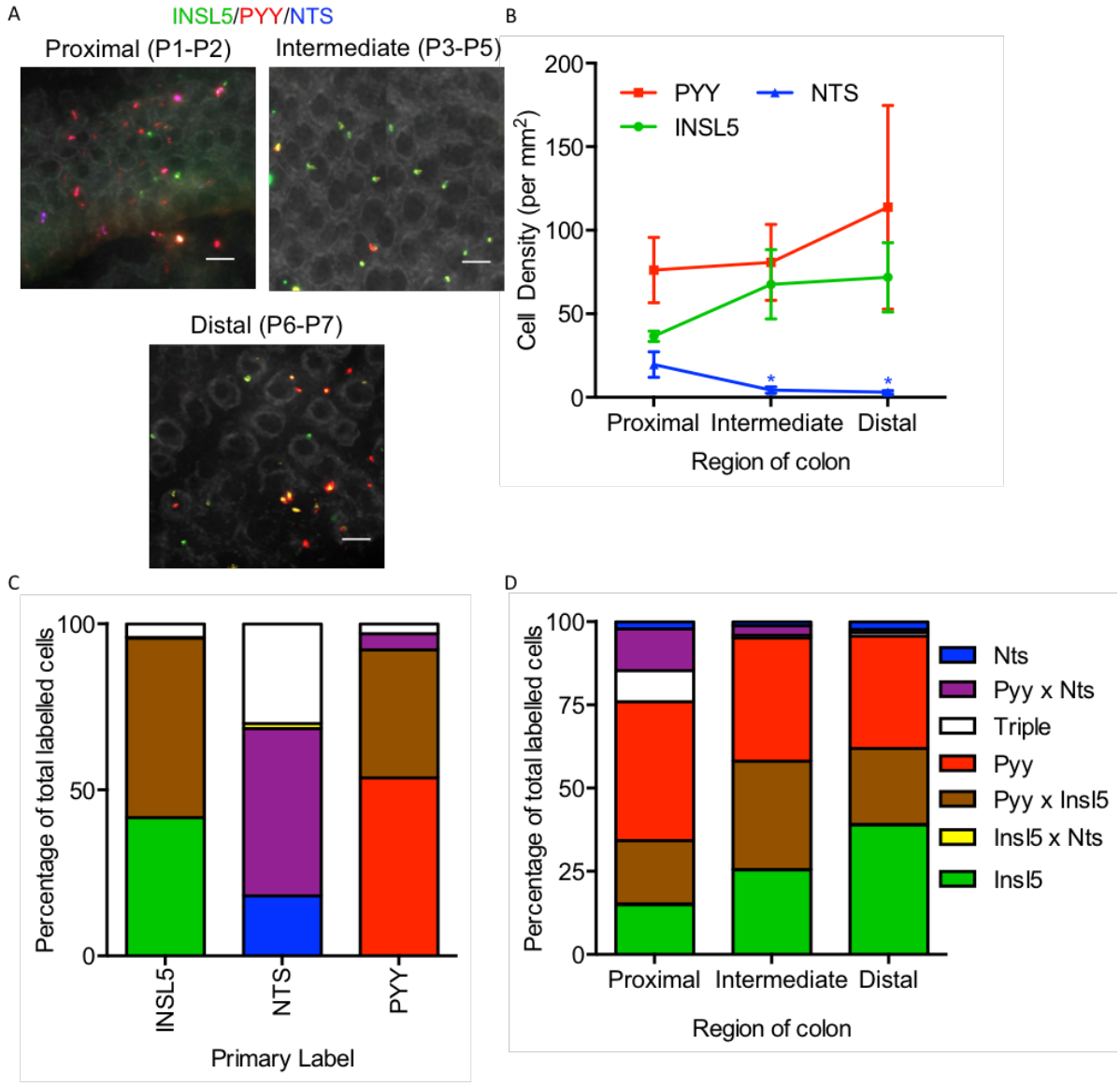

Figure 7: *Immunofluorescent labelled INSL5, PYY and NTS cells in murine wholemounts of colon (see methods). (A) Representative images of proximal (P1-P2), intermediate (P3-P5) and distal (P6-P7) colon. Scale bar = 50µm. (B) Plot showing the density of NTS, PYY and INSL5 cells observed within proximal, intermediate and distal colon. Points and bars plotted represent mean ± SEM. n=3 mice. Statistically significant differences in cell density between each region and proximal colon were identified using repeated measures one-way ANOVA run on square root transformed data. *p<0.05. (C) Co-labelling breakdown of identified INSL5, NTS and PYY cells. Bars reflect average percentage of cells singularly, dual or triple labelled. (D) Colour-coded co-labelling breakdown of cells single, dual and triple labelled for INSL5, PYY and NTS by region of colon.*

5.4.6. Secretory responses

To examine the physiological relevance of the proximal-distal distribution of L-cell subgroups identified in the colon, we examined INSL5, PYY and NTS secretory responses of colonic crypt cultures generated from different regions along the proximal-distal axis. For these regional crypt cultures, murine colons were subdivided into proximal (P1-P2), intermediate (P3-P5) and distal (P6-P7) fractions and for each experiment fractions from 2 different mice were pooled together and seeded onto 12-well plates. The stimuli tested were angiotensin II, AM-1638 and IBMX. Angiotensin II and AM-1638 were selected based on differential expression of *Agtr1a* and *Ffar1* identified between the L-cell subgroups (figure 3). Responses to IBMX acted as a positive control.

Comparison of the basal levels of INSL5 secreted between the different regions highlighted increasing levels of INSL5 moving along the proximal-distal axis. Basal INSL5 levels were significantly ~21 and ~29 times higher in the intermediate and distal colon, respectively, than in the proximal colon. Showing a reverse of this trend, basal NTS levels, though not significantly different, were ~5 times lower in the intermediate colon than in the proximal colon and below the detectable threshold in distal colonic samples. Measurements of basal PYY secretion did not identify any significant difference ($p>0.05$) in basal secretion along the proximal-distal colonic axis.

Responses to the FFAR1 agonist AM-1638 largely reflected the regional pattern of basal INSL5, NTS and PYY secretion. Significant INSL5 responses were only triggered from the intermediate and distal regions. Contrastingly, though not significantly, there was a trend towards elevated levels of NTS measured following AM-1638 administration to proximal and intermediate colon relative to basal. Differences in NTS responses to AM-1638 between the proximal and intermediate colon were significant however. Given that no significant proximal INSL5 or intermediate colonic NTS responses were recorded to the positive control IBMX (compared to basal), these results either reflect insufficient sensitivity of the assay to detect responses to AM-1638 or an absence of FFAR1 responsive INSL5/NTS producing cells in these regions. On the other hand, AM-1638 triggered significant responses to PYY across all regions that

were not significantly different from one another. This implies that consistent numbers of FFAR1 expressing PYY-producing cells are scattered along the length of the colon.

Recorded responses to angiotensin II were more variable than for AM-1638. No significant NTS responses were measured to angiotensin II application in any region. INSL5 did not display significant responses to angiotensin II in the intermediate or distal colon (levels in the proximal colon were undetectable) when compared to basal secretion though levels measured from distal colon were significantly higher than from intermediate colon. PYY responses to angiotensin II were only significantly different from basal levels in the distal colon. Together these results suggest differential L-cell *Agtr1a* expression along the proximal-distal axis of the colon with specific enrichment in INSL5-producing cells.

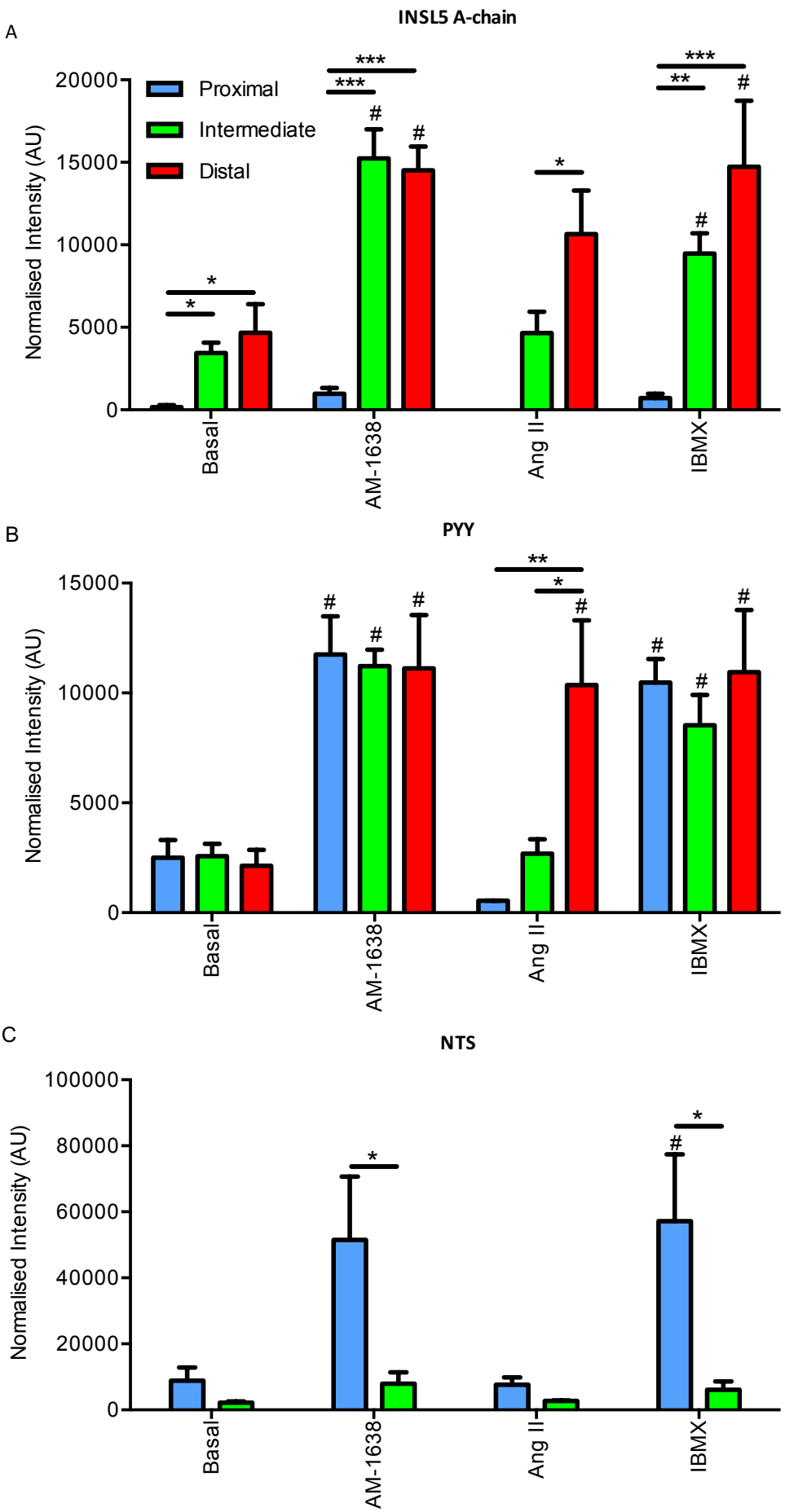
A
INSL5 A-chain
Proximal
Intermediate
Distal
Normalised Intensity (AU)
20000
15000
10000
5000
0
Basal
AM-1638
Ang II
IBMX
B
PYY
Normalised Intensity (AU)
15000
10000
5000
0
Basal
AM-1638
Ang II
IBMX
C
NTS
Normalised Intensity (AU)
100000
80000
60000
40000
20000
0
Basal
AM-1638
Ang II
IBMX

Figure 8: *INSL5 A-chain (A), PYY (B) and NTS (C) secretory responses of murine colonic crypt cultures produced from proximal, intermediate and distal regions of the colon measured by LC/MS. The stimuli tested (over 1 hour) were: 3µM AM-1638, 10nM angiotensin II and 100mM IBMX with 10mM glucose. The basal condition was saline buffer with no added glucose. IBMX acted as a positive control. Normalised intensity reflects measured peptide intensity (integral of signal peak observed at each peptide's specific m/z and retention time) normalised to total protein content for each well measured through a BCA assay. Statistically significant responses (#p<0.05) to a particular stimulus were assessed through comparison to basal responses in each region using one-way ANOVA tests on square root transformed data. Statistical significant differences between regional responses to a particular stimulus were assessed by one-way ANOVA tests on square root transformed data (one-way t-tests used for INSL5 responses to angiotensin II and all NTS responses). *p<0.05, **p<0.01 and ***p<0.001. Bars represent mean + SEM. Results derived from 2 plates of crypt cultures from 4 separate mice with test conditions run in duplicate on each plate. N= 4 independent wells with the following exceptions: n=3 for proximal NTS responses to angiotensin II; n=2 for INSL5 from proximal colon and intermediate colon for NTS in the basal condition together with PYY from the proximal colon and NTS from intermediate colon in the angiotensin II condition. These exceptions (where n<4) reflect undetectable levels of peptides in 1 or more wells analysed.*

5.5. Discussion

5.5.1. Colonic L-cells split into distinct proximal *Nts*-expressing and distal *Insl5*-expressing subgroups

Consistent with evidence that ~50% of colonic L-cells express *Insl5*, our scRNA-seq analysis of colonic EECs indicates that colonic L-cells can be split into two subgroups, one enriched for *Insl5* and low in *Nts* transcripts and one enriched with *Nts* and low in *Insl5* transcripts.

NTS has previously been identified in intestinal L-cells (by immunohistochemistry and expression analysis) and is co-released with GLP-1 and PYY exerting anorexigenic effects [101,239]. In accordance, Ratner et al. suggest that (from *in vivo* experiments with rats using NTS receptor antagonists) part of the weight loss following RYGB results from increased plasma NTS [105]. With respect to the colon, NTS has been linked to colitis and colorectal tumours due to enriched expression of NTS and NTS receptor 1 together with known proinflammatory and trophic effects of NTS [103,104,281]. The *Nts*-expressing cells here may exert these effects through NTS release.

Regional RT-qPCR analysis of the colon suggests that *Nts* expression is concentrated in the proximal part of the colon whilst *Insl5* expression (in accordance with previous studies) is concentrated in the distal colon [88]. Meanwhile, *Pyy* expression was relatively consistent between colonic segments but *Gcg* expression was lower in more distal segments [282]. Furthermore, *Cck* expression was lowest in the most distal segments of colon consistent with a previous examination of regional expression and consistent with a drop in *Nts*-expressing L-cells (*Cck* expression was enriched in *Nts*-expressing L-cells – see appendix 1) [282]. Consistently, previous investigations by Fakhry et al. (2017) found that *Cck* expression dropped moving from proximal to distal colon in mouse. Furthermore Fakhry et al. (2017) using immunostaining and peptidomic analysis detected low levels of bioactive CCK peptides in the colon and that CCK labelled cells often co-stained for PYY suggesting that the L-cell enrichment for CCK transcripts identified in the scRNA-seq analysis here may reflect production and secretion of bioactive CCK peptides [283]. Examination of immunofluorescently labelled murine colonic wholemounts yielded results largely matching these expression patterns with the density of NTS cells significantly decreasing and density of

INSL5 cells showing a trend towards higher levels towards the distal colon. The NTS distribution is supported by analysis of NTS content from proximal and distal murine colon indicating a dramatic drop moving distally [97]. Furthermore, whilst INSL5 and PYY labelled cells displayed considerable overlap, less than 5% of INSL5 cells were also labelled for NTS although ~30% of NTS cells were labelled with INSL5 (this discrepancy is due to the larger number of cells labelled for INSL5 than NTS). The RT-qPCR data suggests low, but significant *Nts* expression in FACS-isolated INSL5 cells which could reflect the small percentage of INSL5 cells co-labelled with NTS observed. When interpreting the observed pattern of co-staining it is important to note that the accuracy of the cell counts depend on the sensitivity of the antibodies used to their respective antigens. For example, the low number of NTS labelled cells identified (when compared with INSL5 and PYY labelled cells) and low proportion of INSL5 and PYY labelled cells co-stained for NTS could reflect that the primary antibody of NTS used had a low sensitivity to NTS leading to an underestimation of NTS positive cells (both single labelled and co-labelled for INSL5 and/or PYY). Indeed, this could explain why despite relatively low numbers of NTS positive cells, in the secretion experiments the measured levels of NTS often exceeded those of INSL5 and PYY (figure 8). Alternatively, though NTS cells might be scarce they may produce and secrete higher quantities of NTS or the higher levels of NTS observed might relate to a more effective extraction of NTS relative to INSL5 and PYY prior to LC/MS analysis. These caveats aside, our findings are consistent overall with the existence of largely separate INSL5 and NTS-producing colonic L-cell subpopulations.

Intriguingly, despite possessing abundant levels of *Pyy* transcripts, as indicated by RT-qPCR (chapter 4) and scRNA-seq analysis (figure 2), roughly 42% of the INSL5 labelled cells did not stain for either PYY or NTS. On the other hand, ~80% of NTS labelled cells co-stained for PYY. The reason for this discrepancy is unclear but could result from sensitivity/specificity issues with the immunofluorescent labelling of PYY/INSL5. An alternative explanation is that a large proportion of the *Pyy* transcripts in the *Insl5*-expressing cells are not translated into functional protein. This second possibility highlights a central issue with interpreting transcriptomic data which is that measured transcript abundance does not always correlate with protein product abundance for a particular gene with large variations in translational efficiency between different genes [284]. Such issues could be overcome by profiling the transcriptomes and

proteomes of individual cells in parallel within a single reaction, allowing direct comparison between expression of genes at the transcript and protein level [285].

Regarding identification of enteroendocrine peptides other than GLP-1, PYY and INSL5 produced by *Insl5*-expressing L-cells, the scRNA-seq analysis highlights secretogranin 2 and pancreatic polypeptide as potential candidates. Secretoneurin, the active peptide derivative of secretogranin 2, has been implicated in a diverse range of physiological functions throughout the body, including regulation of reproductive processes, angiogenesis and in inflammation and has been measured in the rat intestine by radioimmunoassays [286,287]. Hypothalamic expression of *Scg2* increases after a 24-hour fast in mice suggesting involvement in appetite regulation. In fact, secretogranin 2 mediates accumulation of hormones such as orexin into secretory granules implying that it may facilitate release of appetite regulatory peptides [288]. Therefore, *Scg2* enrichment in *Insl5*-expressing cells could indicate secretogranin involvement in INSL5 packaging into secretory vesicles. Alternatively, these cells may secrete secretoneurin directly into the bloodstream exerting direct, INSL5-independent, physiological effects.

The other candidate peptide, pancreatic polypeptide (PP) is predominantly produced and released from PP cells of the pancreatic islets but rare numbers of PP-producing cells have been detected, by immunohistochemistry, in the human colon and rectum [67]. Interestingly the intestinal PP cells do not appear to produce PYY and could comprise some of the immunofluorescently labelled INSL5 cells we observed in murine colon wholemounts that did not overlap with PYY [289]. Regarding function, PP has an anorexigenic effect when administered *in vivo* or overexpressed [252]. Physiologically, PP release has a cephalic and postprandial phase. The cephalic phase depends on vagal innervation as evidenced by abolished PP responses to sham-feeding following vagotomy [290]. Post-prandial, PP release is stimulated by dietary components such as protein and fats as well as gut hormones such as CCK and gastrin [291–293]. Therefore, the PP-expressing subset of INSL5 cells may contribute to PP release following a meal by secreting PP (along with INSL5) in response to dietary stimuli and circulating hormones.

Regarding the relevance of these murine findings to human physiology, whilst INSL5-producing L-cells are found in the large intestines of both humans and mice, in humans NTS-producing cells are largely restricted to the jejenum and are scarce (1 per 100 crypts) in the large intestine [98,99,104]. This suggests that in humans the non-INSL5 producing L-cells, which constitute roughly half all colonic L-cells, are unlikely to be distinguished by NTS. However, it is possible that these human L-cells, with the exception of *NTS*-expression, exhibit the same markers and differences in GPCR repertoire as seen between murine *Insl5* and *Nts*-expressing L-cells. Murine colonic *Nts*-expressing L-cells may also serve as a model of human jejenunal N-cell physiology. Guided by the results from the murine scRNA-seq presented here, further study using human tissue, including secretion assays, should help clarify the physiological relevance of murine colonic NTS-producing L-cells.

5.5.2. *Insl5*-expressing and *Nts*-expressing L-cells display functional differences in GPCR repertoire

The differential expression analysis highlighted, amongst others, *Agtr1a*, *Avpr1b*, *Olfr78* as GPCR genes selectively enriched (at least at the transcript level) within *Insl5*-expressing cells when compared with *Nts*-expressing L-cells. Enrichment of these genes within *Insl5*-expressing L-cells was confirmed by RT-qPCR (figure 4 and chapter 4). Contrastingly many GPCR genes, such as *Ffar1*, *Gpbar1* and *Sstr1* were enriched in both *Insl5* and *Nts*-expressing L-cells, indicating a degree of GPCR overlap between the two populations.

Examination of *Ffar1*, *Gpbar1*, *Agtr1a* and *Avpr1b* expression along the proximal-distal axis of the colon revealed no significant differences in regional expression except for *Avpr1b* which was expressed at higher levels in the distal colon. The results concerning *Ffar1* and *Gpbar1* are backed up by murine expression analysis by Symonds et al. (2015) comparing expression in the proximal (first half) and distal (2nd half) of colon which was also replicated in human colonic samples [282]. Based on the concentration of *Insl5*-expression and INSL5-producing L-cells in the distal colon and the enrichment of *Agtr1a* and *Avpr1b* transcripts in this subgroup, one might have anticipated *Agtr1a* expression to also be enriched in distal colon. This was not found to be the case. However, this possibility still exists given that expression was not determined from isolated colonic L-cells but a mix of different cell types. L-cell specific

Agtr1a expression concentrated in the distal colon might be obscured by *Agtr1a* expression in other more numerous cell types present in the samples analysed.

Functional L-cell expression of *Agtr1a* and *Avpr1b* was described in chapter 4 with angiotensin II and AVP triggering co-secretion of INSL5, PYY and GLP-1 from murine and human colonic crypt cultures. The murine crypt cultures were produced from whole colons from the caecocolic junction down to the end of the rectum. Therefore, based on the data presented here in chapter 5, these cultures would contain a mix of proximal and distal EEC populations including *Nts* and *Insl5*-expressing L-cells. To isolate regional specific secretory responses, we performed secretion assays on crypt cultures produced from proximal, intermediate (middle) and distal (rectum) colon. In the basal condition, we found that, as expected, NTS levels were highest in the proximal colon and undetectable in the distal colon whilst INSL5 levels increased moving from the proximal to distal colon and PYY levels did not significantly vary between regions. Similar regional differences of the NTS, INSL5 and PYY secretory responses to AM-1638 and the positive control 10mM glucose + IBMX were observed. On the other hand, application of angiotensin II appeared to trigger INSL5 and PYY responses only from distal crypt cultures and not from any region for NTS. Consistently, no significant NTS responses were measured in secretions from whole colon generated crypt cultures to angiotensin II (or indeed AVP) application whereas INSL5, GLP-1 and PYY were co-secreted (unpublished data from Pierre Larraufie). Combined with the scRNA-seq and RT-qPCR data these results imply specific functional expression of *Agtr1a* in *Insl5*-expressing over *Nts*-expressing L-cells and non-specific L-cell expression of *Ffar1*. Thus, the *Insl5*-expressing and *Nts*-expressing L-cell subsets are not simply distinguished by differential EEC peptide expression and production but also functional GPCR expression.

Specific pharmacological targeting of the non-*Insl5* expressing L-cell population, avoiding secretion of orexigenic INSL5, may enhance the anorexigenic effects of stimulated GLP-1/PYY release. To this end, future studies should examine the functionality of differentially enriched G_q/G_s-coupled GPCRs in the NTS cell population such as GPR27.

It should be noted that generally expression levels of GPCRs are relatively low compared with other gene families (including hormones and transcription factors) [294–296]. This is indeed

evident from the low levels of GPCR transcripts detected (figure 4) when compared with the levels of detected transcripts encoding hormones and other key EEC biomarkers (appendix 1). As previously discussed droplet-based scRNA-seq platform such as the Chromium system employed here are poor at detecting genes which are expressed at low levels [297]. Consequently, it is likely that the scRNA-seq analysis detailed here did not detect GPCRs with low expression levels within the identified EEC subgroups. Such issues could be avoided by using by using a platform with greater sensitivity to genes with low expression levels such as the plate-based SMART-seq2 platform. For example, in the context of L-cells SMART-seq2 could be used to analyse the transcriptomes of FACS-isolated L-cells (e.g. from Glu-Venus mice for example in a similar manner to that used by Glass et al. (2017)) in order to identify additional GPCRs differentially expressed between the L-cell subgroups described here [64].

5.5.3. Colonic enterochromaffin cells comprise of three subpopulations marked by *Sct*, *Tac1* and *Piezo2* expression

The *Sct*-expressing subgroup of EC cells identified likely constitutes a population of *Sct* expressing cells that were previously found in murine colon using *in situ* hybridisation [298]. Interestingly, these cells often also co-labelled for *Gcg*, Pyy and *Nts* which may reflect *Sct* enrichment in observed in a subset *Nts*-expressing cells (figure 2). Our findings suggest that although *Sct*-expression, as postulated by Haber et al., appears to mark mature enteroendocrine cells (transcripts were picked up in the majority of the scRNA-seq analysed NeuroD1 cells), subsets of EECs appear to display specific enrichment for *Sct* expression [63]. Whether this *Sct*-expression reflects functional secretin production from these subgroups is not clear. Clarification could be obtained through mass spectrometry analysis of colonic sample peptide content together with immunofluorescent experiments. It should be noted that whilst Lund et al. (2018) identified *Sct* expression in small intestinal EC cells, they did not detect *Sct* expression in colonic EC cells [240]. Expression of the NPY/PYY receptor *Npy1r* raises the prospect of L-cell modulation, via PYY release, of 5-HT release from the *Sct*-expressing subgroup of EC cells. *Sct*-expressing EC cells may therefore sense luminal contents indirectly through L-cell activation [240].

The second identified group of EC cells were highly enriched for *Tac1*-expression and unlike the other EC cells may mediate local inflammatory responses to bacterial infection or damage to the mucosa. This prediction derives from the potential production and release of substance P, derived downstream of *Tac1* expression, from these cells which is a known proinflammatory peptide. It is known to trigger cytokine production and release, local vasodilation and algesia and even possesses antimicrobial properties [299–302]. With regards to the intestine, substance P has been implicated in intestinal inflammation with possible significance to the pathphysiology of IBD and as a regulator of circular smooth muscle contractions in human colon [303–305]. Therefore, in addition to potential mediation of local inflammatory responses, substance P release may represent an additional means of modulating colonic contractility to 5-HT release in *Tac1*-expressing cells when compared with the other EC subgroups. Together our findings imply that further study of this subgroup of *Tac1*-expressing EC cells, particularly regarding differential stimulation from the other EC groups by OLFR78/558 stimulation, may yield insight into inflammatory disorders of the intestine including IBD.

Recent findings from Beumer et al. (2018) suggest that *Sct*-expressing and *Tac1*-expressing EC cells may occupy different positions within the crypt axis with *Sct*-expressing EC cells clustered around the distal crypt (i.e. closest to the lumen) and *Tac1*-expressing EC cells clustered around the base of the crypt [132]. In crypts of both the small and large intestines, EECs (along with enterocytes/coloncytes and other secretory cell types) are derived from stem cells located at the base of the crypt. These stem cells function to replenish epithelial cells shed into the intestinal lumen. Newer cells produced from division of these stem cells displace older epithelial cells which move upwards along the crypt towards the lumen where they are shed [306]. Beumer et al. (2018) found a BMP gradient across the crypt axis (highest levels in the distal crypt and lowest at the base of the crypt) that regulates the expression of multiple different gut hormone genes including *Sct*, *Tac1*, *Nts, Pyy* and *Gcg* [132]. Therefore, *Tac1*-expressing EC cells might represent new EC cells in the base of the crypt which become *Sct*-expressing EC cells as they mature and move upwards along the crypt axis (towards the lumen) upregulate *Sct* expression and downregulate *Tac1* according to increasing BMP exposure.

Similarly, *Nts* expression was found to be upregulated whilst expression of *Gcg* was downregulated by BMP signalling by Beumer et al. (2018) supporting previous immunohistological and transcriptomic investigations by Grunddal et al. (2016) indicating that NTS cells were concentrated in the distal crypt whilst GLP-1 producing cells were concentrated at the crypt base. Furthermore, in the Grunddal et al. (2016) study selective ablation of L-cells (via diphtheria toxin administration to transgenic mice engineered to express of human diphtheria toxin receptor under the proglucagon promoter) revealed that numbers of GLP-1 producing L-cells recovered much earlier than those of PYY and NTS producing L-cells [101]. These findings imply that NTS-producing L-cells might be located at the distal end of the crypt and reflect a population of mature L-cells that have moved upwards towards the lumen and acquired the ability to express and produce NTS (thus taking longer to replenish following ablation). It should be noted that the Beumer et al. (2018) and Grunddal et al. (2016) studies investigated small intestinal EECs and that these findings might not translate well to colonic crypts. Indeed, given that *Pyy* expression was negatively correlated with *Nts* expression in colonic L-cells (figure 3E&F) one might have anticipated that *Pyy* expression would be lowest in the distal crypt, however the opposite pattern was observed [101,132].

The third and largest group of EC cells identified were distinguished by *Piezo2* expression. Piezo2 is a non-selective cationic channel which is mechanosensitive, meaning that application of mechanical force induces Piezo2 activation and subsequent membrane depolarisation [307]. In the context of EC cells, this raises the possibility that distension of the colonic mucosa by luminal contents, may stimulate 5-HT secretion by activation of Piezo2. Indeed, recent studies indicate that *Piezo2* is highly expressed within EC cells in both murine and human intestines and that it functions to couple EC mechanosensation to 5-HT release [255]. As a result, these cells may reflect a mechanosensitive subset of EC cells which co-ordinates colonic contractility either by direct effects of 5-HT on colonic smooth muscle or indirectly through signalling through stimulation of the enteric nervous system.

The regional RT-qPCR data suggests that colonic EC cells decline in number moving distally across the colon as *Tph1* expression significantly drops. *Sct* also dropped implying that *Sct*-expressing EC cells might be concentrated in the proximal colon. No similar analysis was

conducted for *Tac1* or *Piezo2* so regional variations in the distribution of these EC cell subpopulations may exist.

5.5.4. D-cells form a transcriptomically distinct group of colonic EECs

D-cells formed a clearly separated cluster on the t-SNE plot and were identifiable by highly specific expression of *Sst.* Relative expression of *Sst* was fairly constant throughout the length of the colon, with a drop in the most distal regions of colon, largely consistent with previous immunohistological data indicating that colonic D-cells are fairly evenly scattered throughout the colon [238]. Colonic D-cells appear to possess similar expression profiles to D-cells from other regions of the gastrointestinal tract. For example, colonic D-cells were enriched for *Iapp*, *Calcrl* and *Adra2a* transcripts, genes which are also expressed in gastric D-cells. This suggests that intestinal D-cells may not display regional differences in expression [63,114,115,132]. Direct comparisons between gastric, small intestinal and colonic D-cell transcriptomes would enable D-cell regional similarities and differences to be assessed.

5.5.5. Unexpected identification of goblet cells in a FACS-purified NeuroD1 cell population

Goblet cells and enteroendocrine cells are derived from separate cell lineages diverging from a common secretory precursor cell. Whilst expression of *Neurog3* commits the common precursor cells to an EEC fate, expression of *Gfi1* commits them to either goblet cell or Paneth cell fates depending on expression of *FoxA1/2* and *Klf4* for goblet cells or *Sox9* for Paneth cells [140]. *Neurod1* is specific transcriptional marker of enteroendocrine cells which are derived from *Neurog3*-expressing EEC precursors, which is absent in goblet cells, therefore it is surprising that our scRNA-seq analysis of cells isolated by NeuroD1 expression identified a cluster of goblet cells. This result could derive from the Cre-recombination system employed to label NeuroD1 cells as all cells which express NeuroD1 and their progeny will express EYFP due to Cre recombinase editing of the genome. Therefore, if precursor cells to these goblet cells expressed *Neurod1*, even briefly, the resulting goblet cells would be EYFP labelled. Some goblet cells may also have produced Cre recombinase in the absence of *Neurod1* expression or due to low levels of *Neurod1* expression and subsequently acquired EYFP labelling. Indeed, from analysis of the scRNA-seq data the goblet cell group appears to express low levels of

Neurod1 (data not shown). Goblet cells may also have been isolated due to issues with the FACS-purification itself. For example, a few autofluorescent goblet cells or doublets containing goblet cells may have been isolated. Alternatively, the goblet cell population may derive from transdifferentiation of mature EECs. To the author's knowledge however, this has not been observed *in vivo* although transdifferentiation of EECs to insulin-producing beta-like cells has been achieved through genetic modification in murine stomach [308].

5.5.6. Concluding remarks

In sum, scRNA-seq analysis of the colonic enteroendocrine cell population identified three main EEC groups: L, D and EC cells. Cluster analysis and differential expression identified that whilst D-cells formed a fairly homogenous group the L and EC cell groups could be divided into subgroups. L-cells divided into two main groups consisting of distally located *Insl5*-expressing and proximally located *Nts*-expressing cells with functional differences in GPCR repertoire. Meanwhile EC cells divided into three groups distinguished by expression of *Sct*, *Tac1* and *Piezo2*. We postulate that the *Tac1* and *Piezo2* groups may reflect pro-inflammatory and mechanosensitive EC subpopulations respectively. Together the findings presented in this chapter largely confirm my initial hypotheses about colonic EECs though the distribution, functional GPCR repertoires and clinical relevance of all the different EEC subgroups identified (particularly of the EC cell subgroups) require further clarification. Significantly these findings suggest that selective pharmacological targeting of particular subsets of colonic EEC cells might be possible, with potential implications for obesity, diabetes and IBD treatment.

Chapter 6. General discussion

6.1. Summary of key findings

6.1.1. GPBAR-1 activation potentiates FFAR1-mediated GLP-1 secretion

In chapter 3, concomitant GPBAR-1 activation was found to potentiate L-cell intracellular calcium responses to FFAR1 activation and 30mM KCl application. Likewise, GPBAR-1 activation potentiated FFAR1-mediated GLP-1 secretion. This suggests coupling of the potentiated intracellular calcium responses observed to increased GLP-1 secretion (since GLP-1 secretion is calcium dependent). These findings were achieved using small intestinal organoids which appear to recapitulate native L-cell physiology. Further application of these small intestinal organoids in secretion and electrophysiological experiments suggests involvement of TRPC3 and L-type VGCCs in the synergy seen between the GPBAR-1 and FFAR1 signalling pathways [201]. However, the precise molecular basis of these synergistic interactions has yet to be determined.

Our findings compliment previous findings by Ekberg et al. (2016) that activation of the G_s-coupled GPR119 (receptor for 2-monoacylglycerol) potentiated GLP-1 secretory responses from colonic crypt cultures to G_q-coupled FFAR1 activation [160]. Furthermore, Hauge et al. (2016) similarly found that GPBAR-1 activation potentiates FFAR1-dependent GLP-1 secretion and found a similar effect on plasma GLP-1 levels *in vivo* using mouse models [199]. Therefore, co-activation of G_q and G_s signalling pathways in L-cells could provide a novel therapeutic approach to type 2 diabetes management.

Future investigations could elucidate the molecular basis of synergy between GPBAR-1 and FFAR1 signalling in L-cells through a combination of pharmacological experiments and genetic modification. Pharmacological experiments could examine PKA-independent effects of GPBAR-1 stimulation through the cAMP effector EPAC2 by applying the EPAC2 selective antagonist ESI-05 in intracellular calcium and secretion assays [309]. Likewise, inhibition of PKC using sphingosine could identify potential involvement of PKC [310]. Concerning genetic modification, CRISPR/Cas9 mediated genetic knockout in intestinal organoids would allow identification of the key VGCC subtypes underlying GPBAR-1 potentiation of FFAR1-mediated

GLP-1 secretion [210]. Using such genetic knockouts would avoid potential off-target effects of VGCC pharmacological modulators such as on potassium channels by the L-type calcium channel agonist Bayk8644 [203]. Future experiments should also establish the clinical relevance of these findings through secretion experiments on primary cultures of human intestine.

6.1.2. INSL5, PYY and GLP-1 are co-stored and co-released from L-cells

In chapter 4, the physiology of INSL5-producing subset of L-cells was initially considered through a combination of transcriptomic profiling, intracellular calcium imaging and secretion assays. RT-qPCR revealed that INSL5 cells express GPCRs previously characterised in L-cells including FFAR1, Agtr1a and Avpr1b [73,74,127]. The functionality of a G_q-coupled subset of these GPCRs, was confirmed by intracellular calcium transients elicited upon specific pharmacological activation. Consistently, stimulation of these GPCRs along with other previously characterised L-cell GPCRs stimulated INSL5 release from both murine and human crypt cultures. The use of LC/MS peptide quantification enabled INSL5 secretion to be accurately measured from colonic crypt cultures for the first time (Pierre Larraufie). Such techniques revealed that GLP-1, PYY and INSL5 were co-released in response to the subset of physiological stimuli tested from both murine and human primary cultures of colonic crypts.

It was hypothesised that GLP-1, PYY and INSL5 co-release either arose from largely separate populations of GLP-1, PYY and INSL5 secretory vesicles regulated by a common release mechanism. This hypothesis was explored in chapter 4 by 3D-SIM analysis of immunofluorescently labelled primary cultures and sections of murine colonic tissue. Overlap between identified GLP-1, PYY and INSL5 vesicles within imaged L-cells was examined by fitting 3D Gaussian distributions (method developed by Christopher Smith) [153]. This method revealed that the majority (more than 80%) of identified vesicles were triple labelled for GLP-1, PYY and INSL5. Consequently, it was concluded that co-release of GLP-1, PYY and INSL5 resulted from co-storage in mouse and likely also in humans (though similar 3D-SIM experiments should be carried out on human tissue to confirm this).

In contrast, Cho et al. (2014) found only a ~8.2% overlap between GLP-1 and PYY vesicles in murine L-cells of the colon [87]. Discrepancies between the findings detailed in chapter 4 and those of Cho et al. (2014) likely arise from the different analytical methods applied. Cho et al. (2014) used an approach (dubbed the surfaces analysis) which examined volume overlap between vesicles rendered in 3D using Imaris (Bitplane). Applying a similar approach to our data indicated roughly 50% of vesicles were single labelled for GLP-1, PYY and INSL5. One potential concern with the surfaces analysis was under-representation of dual or triple labelled vesicles due to differences in the excitation wavelengths of the fluorophores conjugated to the secondary antibodies used. We hypothesised that the surfaces method would yield different vesicle size estimates when labelled with fluorophores with long compared with shorter excitation wavelengths. To test this hypothesis, we applied the surfaces analysis to 3D-SIM images of L-cells labelled for GLP-1 with three different secondary antibodies conjugated to AlexFluor 488, 555 and 633. In theory the 488, 555 and 633 channel profiles should exhibit complete overlap as each channel labels the same vesicles. However, only 45% of total mapped vesicle volume was triple labelled confirming our hypothesis. On the other hand, using our method based on 3D Gaussian fitting, more than 95% of all GLP-1 vesicles identified were triple labelled.

Given that INSL5 has an orexigenic effect whilst GLP-1 and PYY have anorexigenic effects, the significance of simultaneous GLP-1, PYY and INSL5 secretion on food intake regulation is unclear [88,211,212]. One could hypothesise that the restriction of INSL5-producing L-cells to the distal colon may help explain this apparent paradox through differences in the post-prandial plasma dynamics of INSL5, GLP-1 and PYY. Under this hypothesis during the acute phase following a meal, GLP-1 and PYY secretion is stimulated from L-cells of the proximal gastrointestinal tract suppressing further food intake. In between meals and during fasting, INSL5 secretion from colonic L-cells, perhaps stimulated by bacterial fermentation by-products (e.g. SCFAs), results in food seeking behaviour. In support of this, fasted mice exhibit elevated plasma levels of INSL5 reversible upon refeeding (though there have been reported issues with the INSL5 immunoassays used in this study) [88,311].

6.1.3. Murine colonic L-cells divide into *Insl5*-expressing and *Nts*-expressing cells

scRNA-seq analysis of colonic enteroendocrine cells in chapter 5 enabled further characterisation of INSL5-producing L-cells. Cluster and subsequent differential expression analysis revealed 2 subpopulations of colonic L-cells; one characterised by *Insl5* expression and the other characterised by *Nts* expression. Interestingly, the *Insl5*-expressing L-cells were particularly enriched with *Pyy* expression relative to *Nts*-expressing L-cells. *Gcg* expression showed the converse relationship to *Pyy* expression with highest expression found in the *Insl5*-expressing L-cells. Additionally, the two subsets appear to differentially express other appetite regulating peptides with a subset of *Insl5*-expressing cells enriched for *Ppy* expression whilst *Nts*-expressing cells were enriched for *Cck* expression [92,252]. These results suggest that *Insl5*-expressing and *Nts*-expressing L-cells may produce and secrete different subsets of gut peptides with potential physiological consequences.

Through examination of immunofluorescently labelled colon wholemounts and RT-qPCR *Nts*-expressing L-cells were identified as proximally distributed whilst *Insl5*-expressing L-cells were distally distributed along the colon (fitting with findings by Grosse et al.) [88]. The relevance of the identified NTS-producing L-cells to human physiology is unclear, since, unlike in rodents, Nts is scarcely found in the human large intestine (figure 1) [97–99]. However, colonic murine *Nts*-expressing L-cells may act as a useful model for a known subset of human small intestinal L-cells that co-produce NTS with GLP-1 and PYY [101]. Characterisation of these cells might be clinically relevant, particularly for obesity research, since NTS appears to potentiate the anorexigenic actions of GLP-1 and PYY [101].

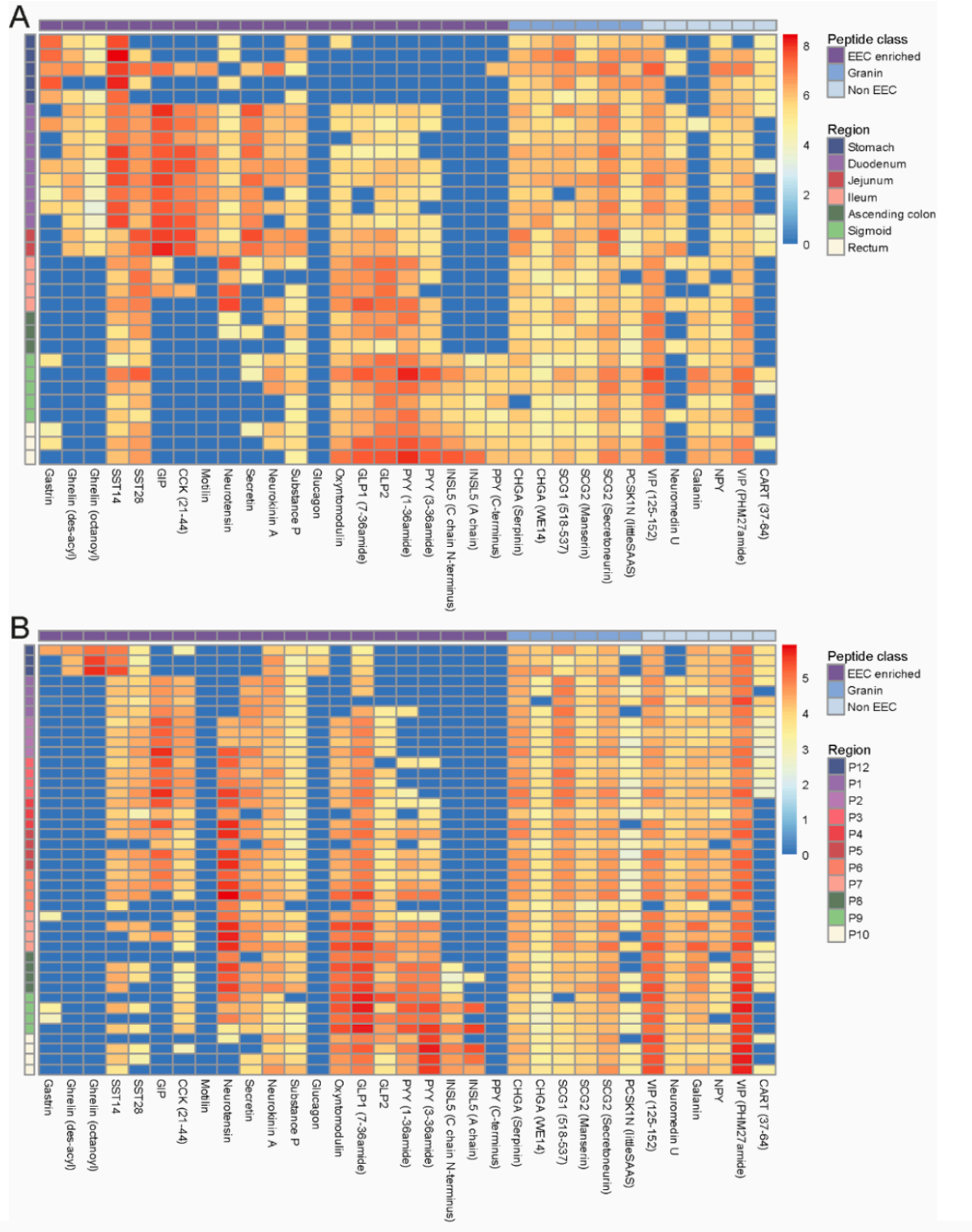

Figure 1: *Heatmap representation of gut hormones across the gastrointestinal tract of (A) humans and (B) mouse. P12 = stomach lesser curvature. P1-P7 = proximal to distal small intestine sampled every 5cm. P8-P10 = large intestine (proximal, middle and distal). Adapted from Roberts et al. (2018)* [296].

6.1.4. Colonic enterochromaffin cells split into 3 distinct subpopulations

The scRNA-seq analysis detailed in chapter 5 identified 3 main subpopulations of colonic EC cells distinguished by *Sct*, *Tac1* or *Piezo2* expression. The *Sct*-expressing EC cell subgroup differentially express the PYY activated receptor *Npy1r* potentially reflecting regulation of this subpopulation by L-cell secretions [269]. This is consistent with recent findings that GLP-1 stimulates 5-HT secretion from intestinal ECs. Interestingly, the same study found expression of *Sct* was restricted to small intestinal EC cells, contrasting with the results presented in chapter 5 [240]. The reasons for this discrepancy are unclear.

We hypothesise that the *Tac1*-expressing EC cell subpopulation responds to local intestinal inflammation. This is based on the production of the pro-inflammatory peptide substance P downstream of *Tac1* expression [299]. Accordingly, *Tac1* expression and substance P production have previously been identified in intestinal enterochromaffin cells by transcriptomic and immunohistological analysis [65,254]. Since substance P has previously been implicated in inflammatory bowel disease pathophysiology, these *Tac1*-expressing EC cells may play a critical role in the development of inflammatory disorders of the intestine [303].

Piezo2 encodes the mechanosensitive cation channel Piezo2 [307]. Recent investigations by Wang et al. (2017) suggest that the mechanosensitivity of EC cells depends on the activity of Piezo2, with activation stimulating 5-HT secretion [255]. In turn, 5-HT regulates gastrointestinal motility and peristaltic contractions [118]. Given this background, the *Piezo2*-expressing EC subset identified in our scRNA-seq could reflect a subset of mechanosensitive colonic ECs that responds to local intestinal distension and modulates gastrointestinal motility accordingly. Such local feedback may play a critical role in co-ordinating peristaltic contractions and transit of luminal contents through the gastrointestinal tract.

6.1.5. Colonic enteroendocrine cells exhibit distinct GPCR repertoires

Differentially expressed GPCRs are identified for each identified EEC subpopulation in chapter 5. *Insl5*-expressing L-cells for example were particularly enriched for *Agtr1a* and *Avpr1b* when compared with *Nts*-expressing L-cells. This difference was found to be functionally relevant since stimulation of Agtr1a and Avpr1b, by angiotensin II and AVP respectively, triggered GLP-1, PYY and INSL5 but not NTS secretion from murine colonic crypt cultures (unpublished data from Pierre Larraufie). This was backed up further in chapter 5 by examining PYY, INSL5 and NTS secretion from crypt cultures prepared from different regions of the colon along the proximal-distal axis. Under these conditions, whilst angiotensin II appeared to stimulate INSL5 and PYY secretion from distal colon, NTS secretion did not appear to be stimulated from any region. Contrastingly, application of AM-1638 (FFAR1 agonist) triggered PYY secretion from all regions, INSL5 from distal colon and NTS from proximal colon. The peptide secretion profiles resulting from FFAR1 activation are consistent with previous results in which NTS, GLP-1 and PYY were co-secreted in response to AM-5262 (FFAR1 agonist) application from small intestinal and colonic crypt cultures [101]. Together the secretion results support functional differences in the proximal-distal colonic distribution and GPCR repertoires of INSL5 and NTS-producing L-cells.

Regarding GPCRs differentially expressed in the other EECs subgroups, as previously mentioned, *Sct*-expressing EC cells express *Npy1r* potentially reflecting L-cell regulation of this subset of EC cells. *Tac1*-expressing EC cells were enriched with transcripts for the SCFA receptor *Olfr78* consistent with findings by Lund et al. (2018) and suggests that this subset of EC cells responds to the bacterial microbiota [240]. *Olfr78* was also highly enriched within *Insl5*-expressing (but not in *Nts*-expressing) L-cells which probably reflects previous identification of Olfr78 expression in a subpopulation of colonic L-cells by Fleischer et al. (2015) [262]. Concerning GPCRs of colonic D-cells, these cells were enriched for transcripts for *Calcrl* and *Ramp1* suggesting that they express the receptor for the neuropeptide CGRP. Functional expression of this receptor has previously been identified in gastric D-cells. Indeed, CGRP application was found to potently stimulate somatostatin secretion from gastric primary cultures [115]. Therefore, since CGRP is produced and released by enteric neurons,

under physiological conditions colonic D-cells might be in part be regulated by the enteric nervous system through CGRP activity [312].

In summary, these results suggest that differences in GPCR repertoire might enable selective pharmacological targeting of specific EEC subpopulations for potential therapeutic benefit.

6.2. Future directions

6.2.1. Establishing the physiological roles of INSL5

The precise physiological role of INSL5 has not been clearly elucidated with various reports suggesting that INSL5 is orexigenic, potentiates glucose-stimulated insulin secretion and modulates hepatic glucose production [88,90,91]. In part, these studies have been hampered by unreliable INSL5 quantification using current immunoassays [311]. The LC-MS approach presented in this thesis presents a solution to this long-running issue. Members of the Gribble/Reimann lab are optimising an LC-MS method to measure plasma INSL5. By using such a method *in vivo* changes in plasma INSL5 could be quantified in both mice and humans following different experimental interventions including bariatric surgery.

A novel approach for investigating INSL5 physiology would be to develop transgenic mouse models expressing designer receptors exclusively activated by designer drugs (DREADDs) specifically in *Insl5* and *Rxfp4*-expressing cells. Activation of DREADDs by the physiologically inert drug CNO can stimulate or inhibit secretory processes depending on coupling to G_q or G_i respectively. Selective expression of these DREADDs in *Insl5* and *Rxfp4* has been achieved in the Gribble/Reimann lab through the use of Cre-dependent DREADDs [313]. Through administration of CNO to such mice, selective stimulation of *Insl5*-expressing cells (through G_q-coupled DREADDs) triggering INSL5 secretion and imitation of elicited G_i signalling by INSL5 in *Rxfp4*-expressing cells (through G_i-coupled DREADD) could be achieved *in vivo*. It is hoped such experiments will elucidate the physiological effects attributable to INSL5**.**

Alternatively, identification of the cell types and tissues expressing Rxfp4 would yield clues as to the physiological role of Rxfp4's cognate ligand INSL5 and guide future investigations. To this end, bulk RNA-seq of Rxfp4 cells FACS purified from novel Rxfp4-cre/Rosa26-EYFP and

Rxfp4-cre/Rosa26-RFP mice was carried out by Cheryl Brighton (unpublished data). This transcriptomic analysis identified enrichment in Rxfp4 cells of *Tph1*, *Pyy, Gcg* and *Insl5*. Subsequent immunofluorescent labelling of colonic tissue from the Rxfp4-cre/Rosa26-EYFP mice indicated that whilst a small proportion of L-cells (stained for INSL5/proglucagon) co-stained for EYFP (Rxfp4 cells), ~60% of all colonic EC cells (labelled by staining 5-HT) co-stained with EYFP. Similar experiments also identified EYFP fluorescence in nodose ganglia extracted from Rxfp4-cre/Rosa26-EYFP mice. This profile of Rxfp4 labelling suggests that INSL5 may autoinhibit a subset of L-cells (through G_i-coupled signalling), regulate gastrointestinal motility (through modulation of EC cells) and modulate activities of the enteric nervous system. However, it should be noted that levels of Rxfp4 transcripts detected by RT-qPCR were very low or undetectable in FACS-purified L-cells and nodose ganglia (unpublished data from Cheryl Brighton). This discrepancy likely reflects historical and transient expression of Rxfp4 yielding permanent expression of RFP/EYFP in the precursors of labelled cells. Development of a transgenic mouse line in which selective expression of RFP/EYFP in Rxfp4 cells is achieved using the conditional Tet-on system would avoid such issues [228].

6.2.2. Selective pharmacological targeting of EEC subtypes

Building on the results from chapter 5, future experiments could attempt to selectively stimulate/inhibit specific subsets of EECs with secretory responses quantified by LC/MS analysis. For example, the scRNA-seq analysis indicates that subunits of the CGRP receptor are specifically expressed in D-cells. This suggests that selective secretion of SST-28 might be achieved by CGRP application. Furthermore, enrichment of *Galr1*, the G_i-coupled galinin receptor mRNA, in *Insl5*-expressing over *Nts*-expressing L-cells suggests that selective inhibition of INSL5 secretion might be achievable [264]. Given the orexigenic effects of INSL5, suppression of INSL5 secretion may yield therapeutic benefits to obese patients. Likewise, selective stimulation of non-INSL5 producing L-cells may prove advantageous through the stimulated release of anorexigenic GLP-1 and PYY without release of orexigenic INSL5. To this end, the G_q-coupled orphan receptor GPR27 appears to be a potential target for further investigation [266].

Technical limitations restrict droplet-based scRNA-seq reads to a relative shallow depth, likely hiding further differences in GPCR repertoire between the different EEC subtypes. Using more sensitive scRNA-seq techniques such as SMART-seq2 could therefore enable detection of further differences in GPCR repertoire between different EEC subtypes. For example, FACS-purified colonic cells from Glu-Venus mice could be analysed by SMART-seq2 to identify differences in GPCR expression between *Insl5*-expressing L-cells and other L-cell subgroups.

All the scRNA-seq investigations into EEC physiology detailed so far, including this thesis, have examined murine EECs. In order to examine the single cell transcriptomes of human EECs, differentiated intestinal organoids could be analysed. By using intestinal organoids rather than primary tissue for scRNA-seq analysis, the transcriptomes of epithelial cells can be isolated without contamination with other cell types e.g. smooth muscle cells and enteric neurons [65]. To enhance this approach, fluorescent tags expressed under the control of specific cell-type markers (e.g. NeuroD1 for EECs) could be knocked into human intestinal organoids using CRISPR/Cas9 genome editing [314]. This would enable selective scRNA-seq analysis of human EECs isolated through FACS-purification. Such analyses of human EECs would yield direct insight into human EEC physiology and allow comparison with murine EECs to examine the relevance of murine models.

6.3. Concluding remarks

This thesis has expanded the current comprehension of synergy between the G_s and G_q-coupled signalling pathways in L-cells and colonic enteroendocrine cell diversity. It is hoped that by pharmacologically replicating the synergistic effects of GPBAR-1 activation on FFAR1-mediated GLP-1 secretion new type 2 diabetes treatments could be developed. Similarly, pharmacological exploitation of identified differences between enteroendocrine cell subtypes in GPCR repertoire may yield therapeutic benefits through modulated release of specific enteroendocrine hormones. This thesis has additionally provided novel insight into the secretory mechanisms of INSL5-producing L-cells. Further complimentary studies *in vivo* will help to clarify the physiological significance of INSL5, a hitherto poorly characterised gut peptide.

Bibliography

[1] Health and Social Care Information Centre., 2014. Statistics on Obesity , Physical Activity and Diet. vol. 1.

[2] Diabetes UK., 2017. Diabetes Prevalence 2017. https://www.diabetes.org.uk/professionals/position-statements-reports/statistics.

[3] Kanavos, P., Van Den Aardweg, S., Schurer, W., 2012. Diabetes expenditure, burden of disease and management in 5 EU countries.

[4] Public Health England., 2017. Health matters: obesity and the food environment. https://www.gov.uk/government/publications/health-matters-obesity-and-the-food-environment/health-matters-obesity-and-the-food-environment--2.

[5] Purnell, J.Q., 2000. Definitions, Classification, and Epidemiology of Obesity. MDText.com, Inc.

[6] Chatterjee, S., Khunti, K., Davies, M.J., 2017. Type 2 diabetes. Lancet (London, England) 389(10085): 2239–51, Doi: 10.1016/S0140-6736(17)30058-2.

[7] Röder, P. V., Wu, B., Liu, Y., Han, W., 2016. Pancreatic regulation of glucose homeostasis. Experimental & Molecular Medicine 48(3): e219, Doi: 10.1038/emm.2016.6.

[8] Kaur, J., 2014. A comprehensive review on metabolic syndrome. Cardiology Research and Practice 2014: 943162, Doi: 10.1155/2014/943162.

[9] Callaghan, B., Feldman, E., 2013. The metabolic syndrome and neuropathy: therapeutic challenges and opportunities. Annals of Neurology 74(3): 397–403, Doi: 10.1002/ana.23986.

[10] Ingelsson, E., Arnlöv, J., Lind, L., Sundström, J., 2006. Metabolic syndrome and risk for heart failure in middle-aged men. Heart (British Cardiac Society) 92(10): 1409–13, Doi: 10.1136/hrt.2006.089011.

[11] Horn, H., Böhme, B., Dietrich, L., Koch, M., Horn, H., Böhme, B., et al., 2018. Endocannabinoids in Body Weight Control. Pharmaceuticals 11(2): 55, Doi: 10.3390/ph11020055.

[12] Müller, T.D., Clemmensen, C., Finan, B., DiMarchi, R.D., Tschöp, M.H., 2018. Anti-Obesity Therapy: from Rainbow Pills to Polyagonists. Pharmacological Reviews 70(4): 712–46, Doi: 10.1124/pr.117.014803.

[13] Hayes, J.F., Bhaskaran, K., Batterham, R., Smeeth, L., Douglas, I., 2015. The effect of sibutramine prescribing in routine clinical practice on cardiovascular outcomes: a cohort study in the United Kingdom. International Journal of Obesity 39(9): 1359–64, Doi: 10.1038/ijo.2015.86.

[14] Martin, J., Paquette, C., Marceau, S., Hould, F.-S., Lebel, S., Simard, S., et al., 2011. Impact of Orlistat-Induced Weight Loss on Diastolic Function and Heart Rate Variability in Severely Obese Subjects with Diabetes. Journal of Obesity 2011: 1–8, Doi: 10.1155/2011/394658.

[15] Padwal, R.S., Majumdar, S.R., 2007. Drug treatments for obesity: orlistat, sibutramine, and rimonabant. The Lancet 369(9555): 71–7, Doi: 10.1016/S0140-6736(07)60033-6.

[16] Mancini, M.C., Halpern, A., 2008. Orlistat in the prevention of diabetes in the obese patient. Vascular Health and Risk Management 4(2): 325–36.

[17] Heal, D.J., Smith, S.L., Gosden, J., Nutt, D.J., 2013. Amphetamine, past and present--a pharmacological and clinical perspective. Journal of Psychopharmacology (Oxford, England) 27(6): 479–96, Doi: 10.1177/0269881113482532.

[18] Chu, S.-C., Chen, P.-N., Ho, Y.-J., Yu, C.-H., Hsieh, Y.-S., Kuo, D.-Y., 2015. Both neuropeptide Y knockdown and Y1 receptor inhibition modulate CART-mediated appetite control. Hormones and Behavior 67: 38–47, Doi: 10.1016/j.yhbeh.2014.11.005.

[19] Araújo, J.R., Martel, F., 2012. Sibutramine effects on central mechanisms regulating energy homeostasis. Current Neuropharmacology 10(1): 49–52, Doi: 10.2174/157015912799362788.

[20] Williams, G., 2010. Withdrawal of sibutramine in Europe. BMJ (Clinical Research Ed.) 340: c824, Doi: 10.1136/BMJ.C824.

[21] Di Marzo, V., Matias, I., 2005. Endocannabinoid control of food intake and energy balance. Nature Neuroscience 8(5): 585–9, Doi: 10.1038/nn1457.

[22] Christou, G., Kiortsis, D., 2015. The efficacy and safety of the naltrexone/bupropion combination for the treatment of obesity: an update. HORMONES, Doi: 10.14310/horm.2002.1600.

[23] Ingelfinger, J.R., Rosen, C.J., 2018. Lorcaserin — Elixir or Liability? New England Journal of Medicine 379(12): 1174–5, Doi: 10.1056/NEJMe1810855.

[24] Gustafson, A., King, C., Rey, J.A., 2013. Lorcaserin (Belviq): A Selective Serotonin 5-HT2C Agonist In the Treatment of Obesity. P & T : A Peer-Reviewed Journal for Formulary Management 38(9): 525–34.

[25] Halford, J.C.G., Boyland, E.J., Lawton, C.L., Blundell, J.E., Harrold, J.A., 2011. Serotonergic Anti-Obesity Agents. Drugs 71(17): 2247–55, Doi: 10.2165/11596680-000000000-00000.

[26] Mehta, A., Marso, S.P., Neeland, I.J., 2017. Liraglutide for weight management: a critical review of the evidence. Obesity Science & Practice 3(1): 3–14, Doi: 10.1002/osp4.84.

[27] Davies, M.J., Bergenstal, R., Bode, B., Kushner, R.F., Lewin, A., Skjøth, T.V., et al., 2015. Efficacy of Liraglutide for Weight Loss Among Patients With Type 2 Diabetes. JAMA 314(7): 687, Doi: 10.1001/jama.2015.9676.

[28] Astrup, A., Rössner, S., Van Gaal, L., Rissanen, A., Niskanen, L., Al Hakim, M., et al., 2009. Effects of liraglutide in the treatment of obesity: a randomised, double-blind, placebo-controlled study. Lancet (London, England) 374(9701): 1606–16, Doi: 10.1016/S0140-6736(09)61375-1.

[29] van Can, J., Sloth, B., Jensen, C.B., Flint, A., Blaak, E.E., Saris, W.H.M., 2014. Effects of the once-daily GLP-1 analog liraglutide on gastric emptying, glycemic parameters, appetite and energy metabolism in obese, non-diabetic adults. International Journal of Obesity 38(6): 784–93, Doi: 10.1038/ijo.2013.162.

[30] Adams, J.M., Pei, H., Sandoval, D.A., Seeley, R.J., Chang, R.B., Liberles, S.D., et al., 2018. Liraglutide Modulates Appetite and Body Weight Through Glucagon-Like Peptide 1 Receptor-Expressing Glutamatergic Neurons. Diabetes 67(8): 1538–48, Doi: 10.2337/db17-1385.

[31] Blundell, J., Finlayson, G., Axelsen, M., Flint, A., Gibbons, C., Kvist, T., et al., 2017. Effects of once-weekly semaglutide on appetite, energy intake, control of eating, food preference and body weight in subjects with obesity. Diabetes, Obesity and Metabolism 19(9): 1242–51, Doi: 10.1111/dom.12932.

[32] Chaudhury, A., Duvoor, C., Reddy Dendi, V.S., Kraleti, S., Chada, A., Ravilla, R., et al., 2017. Clinical Review of Antidiabetic Drugs: Implications for Type 2 Diabetes Mellitus Management. Frontiers in Endocrinology 8: 6, Doi: 10.3389/fendo.2017.00006.

[33] Hadden, D.R., 2005. Goat's rue - French lilac - Italian fitch - Spanish sainfoin: gallega officinalis and metformin: the Edinburgh connection. The Journal of the Royal College of Physicians of Edinburgh 35(3): 258–60.

[34] Zhou, T., Xu, X., Du, M., Zhao, T., Wang, J., 2018. A preclinical overview of metformin for the treatment of type 2 diabetes. Biomedicine & Pharmacotherapy 106: 1227–35, Doi: 10.1016/J.BIOPHA.2018.07.085.

[35] Swinnen, S.G., Hoekstra, J.B., DeVries, J.H., 2009. Insulin therapy for type 2 diabetes. Diabetes Care 32 Suppl 2(Suppl 2): S253-9, Doi: 10.2337/dc09-S318.

[36] Sarbacker, G.B., Urteaga, E.M., 2016. Adherence to Insulin Therapy. Diabetes Spectrum : A Publication of the American Diabetes Association 29(3): 166–70, Doi: 10.2337/diaspect.29.3.166.

[37] Bekiari, E., Kitsios, K., Thabit, H., Tauschmann, M., Athanasiadou, E., Karagiannis, T., et al., 2018. Artificial pancreas treatment for outpatients with type 1 diabetes: systematic review and meta-analysis. BMJ (Clinical Research Ed.) 361: k1310, Doi: 10.1136/BMJ.K1310.

[38] Ruan, Y., Thabit, H., Wilinska, M.E., Hovorka, R., 2015. Modelling endogenous insulin concentration in type 2 diabetes during closed-loop insulin delivery. Biomedical Engineering Online 14: 19, Doi: 10.1186/s12938-015-0009-5.

[39] Khunti, K., Chatterjee, S., Gerstein, H.C., Zoungas, S., Davies, M.J., 2018. Do sulphonylureas still have a place in clinical practice? The Lancet Diabetes & Endocrinology, Doi: 10.1016/S2213-8587(18)30025-1.

[40] Seino, S., Sugawara, K., Yokoi, N., Takahashi, H., 2017. β-Cell signalling and insulin secretagogues: A path for improved diabetes therapy. Diabetes, Obesity and Metabolism 19: 22–9, Doi: 10.1111/dom.12995.

[41] Hare, K.J., Vilsbøll, T., Asmar, M., Deacon, C.F., Knop, F.K., Holst, J.J., 2010. The glucagonostatic and insulinotropic effects of glucagon-like peptide 1 contribute equally to its glucose-lowering action. Diabetes 59(7): 1765–70, Doi: 10.2337/db09-1414.

[42] Holst, J.J., Orskov, C., 2004. The incretin approach for diabetes treatment: modulation of islet hormone release by GLP-1 agonism. Diabetes 53 Suppl 3(suppl 3): S197-204, Doi: 10.2337/DIABETES.53.SUPPL_3.S197.

[43] Holst, J.J., Christensen, M., Lund, A., de Heer, J., Svendsen, B., Kielgast, U., et al., 2011. Regulation of glucagon secretion by incretins. Diabetes, Obesity and Metabolism 13: 89–94, Doi: 10.1111/j.1463-1326.2011.01452.x.

[44] Nori Janosz, K.E., Zalesin, K.C., Miller, W.M., Mccullough, P.A., 2009. Treating type 2 diabetes: incretin mimetics and enhancers. Therapeutic Advances in Cardiovascular Disease 3(5): 387–95, Doi: 10.1177/1753944709341377.

[45] Brown, D.X., Evans, M., 2012. Choosing between GLP-1 Receptor Agonists and DPP-4 Inhibitors: A Pharmacological Perspective. Journal of Nutrition and Metabolism 2012: 381713, Doi: 10.1155/2012/381713.

[46] Kang, J.H., Le, Q.A., 2017. Effectiveness of bariatric surgical procedures: A systematic review and network meta-analysis of randomized controlled trials. Medicine 96(46): e8632, Doi: 10.1097/MD.0000000000008632.

[47] Furtado, L.C. do R., 2010. Procedure and outcomes of Roux-en-Y gastric bypass. British Journal of Nursing 19(5): 307–13, Doi: 10.12968/bjon.2010.19.5.47083.

[48] Holst, J.J., Madsbad, S., Bojsen-Møller, K.N., Svane, M.S., Jørgensen, N.B., Dirksen, C., et al., 2018. Mechanisms in bariatric surgery: Gut hormones, diabetes resolution, and weight loss. Surgery for Obesity and Related Diseases 14(5): 708–14, Doi: 10.1016/J.SOARD.2018.03.003.

[49] Purnell, J.Q., Selzer, F., Wahed, A.S., Pender, J., Pories, W., Pomp, A., et al., 2016. Type 2 Diabetes Remission Rates After Laparoscopic Gastric Bypass and Gastric Banding: Results of the Longitudinal Assessment of Bariatric Surgery Study. Diabetes Care 39(7): 1101–7, Doi: 10.2337/dc15-2138.

[50] Rubino, F., Gagner, M., Gentileschi, P., Kini, S., Fukuyama, S., Feng, J., et al., 2004. The early effect of the Roux-en-Y gastric bypass on hormones involved in body weight regulation and glucose metabolism. Annals of Surgery 240(2): 236–42.

[51] Rubino, F., Forgione, A., Cummings, D.E., Vix, M., Gnuli, D., Mingrone, G., et al., 2006. The Mechanism of Diabetes Control After Gastrointestinal Bypass Surgery Reveals a Role of the Proximal Small Intestine in the Pathophysiology of Type 2 Diabetes. Annals of Surgery 244(5): 741–9, Doi: 10.1097/01.sla.0000224726.61448.1b.

[52] Gribble, F.M., Reimann, F., 2016. Enteroendocrine Cells: Chemosensors in the Intestinal Epithelium. Annual Review of Physiology 78(1): 277–99, Doi: 10.1146/annurev-physiol-021115-105439.

[53] Jirapinyo, P., Jin, D.X., Qazi, T., Mishra, N., Thompson, C.C., 2018. A Meta-Analysis of GLP-1 After Roux-En-Y Gastric Bypass: Impact of Surgical Technique and Measurement Strategy. Obesity Surgery 28(3): 615–26, Doi: 10.1007/s11695-017-2913-1.

[54] Gorski, J.N., Pachanski, M.J., Mane, J., Plummer, C.W., Souza, S., Thomas-Fowlkes, B.S., et al., 2017. GPR40 reduces food intake and body weight through GLP-1. American Journal of Physiology-Endocrinology and Metabolism 313(1): E37–47, Doi: 10.1152/ajpendo.00435.2016.

[55] Psichas, A., Reimann, F., Gribble, F.M., 2015. Gut chemosensing mechanisms. The Journal of Clinical Investigation 125(3): 908–17, Doi: 10.1172/JCI76309.

[56] Mace, O.J., Tehan, B., Marshall, F., 2015. Pharmacology and physiology of gastrointestinal enteroendocrine cells. Pharmacology Research & Perspectives 3(4): e00155, Doi: 10.1002/prp2.155.

[57] Rogers, G.J., Tolhurst, G., Ramzan, A., Habib, A.M., Parker, H.E., Gribble, F.M., et al., 2011. Electrical activity-triggered glucagon-like peptide-1 secretion from primary murine L-cells. The Journal of Physiology 589(Pt 5): 1081–93, Doi: 10.1113/jphysiol.2010.198069.

[58] Wheeler, S.E., Stacey, H.M., Nahaei, Y., Hale, S.J., Hardy, A.B., Reimann, F., et al., 2017. The SNARE Protein Syntaxin-1a Plays an Essential Role in Biphasic Exocytosis of the Incretin Hormone Glucagon-Like Peptide 1. Diabetes 66(9): 2327–38, Doi: 10.2337/db16-1403.

[59] Reimann, F., Habib, A.M., Tolhurst, G., Parker, H.E., Rogers, G.J., Gribble, F.M., 2008. Glucose sensing in L cells: a primary cell study. Cell Metabolism 8(6): 532–9, Doi: 10.1016/j.cmet.2008.11.002.

[60] Reimann, F., Williams, L., da Silva Xavier, G., Rutter, G.A., Gribble, F.M., 2004. Glutamine potently stimulates glucagon-like peptide-1 secretion from GLUTag cells. Diabetologia 47(9): 1592–601, Doi: 10.1007/s00125-004-1498-0.

[61] Tolhurst, G., Zheng, Y., Parker, H.E., Habib, A.M., Reimann, F., Gribble, F.M., 2011. Glutamine triggers and potentiates glucagon-like peptide-1 secretion by raising cytosolic Ca2+ and cAMP. Endocrinology 152(2): 405–13, Doi: 10.1210/en.2010-0956.

[62] Habib, A.M., Richards, P., Cairns, L.S., Rogers, G.J., Bannon, C.A.M., Parker, H.E., et al., 2012. Overlap of Endocrine Hormone Expression in the Mouse Intestine Revealed by Transcriptional Profiling and Flow Cytometry. Endocrinology 153(7): 3054–65, Doi: 10.1210/en.2011-2170.

[63] Haber, A.L., Biton, M., Rogel, N., Herbst, R.H., Shekhar, K., Smillie, C., et al., 2017. A single-cell survey of the small intestinal epithelium. Nature 551(7680): 333–9, Doi: 10.1038/nature24489.

[64] Glass, L.L., Calero-Nieto, F.J., Jawaid, W., Larraufie, P., Kay, R.G., Göttgens, B., et al., 2017. Single-cell RNA-sequencing reveals a distinct population of proglucagon-expressing cells specific to the mouse upper small intestine. Molecular Metabolism 6(10): 1296–303, Doi: 10.1016/j.molmet.2017.07.014.

[65] Grün, D., Lyubimova, A., Kester, L., Wiebrands, K., Basak, O., Sasaki, N., et al., 2015. Single-cell messenger RNA sequencing reveals rare intestinal cell types. Nature 525(7568): 251–5, Doi: 10.1038/nature14966.

[66] Fothergill, L.J., Furness, J.B., 2018. Diversity of enteroendocrine cells investigated at cellular and subcellular levels: the need for a new classification scheme. Histochemistry and Cell Biology: 1–10, Doi: 10.1007/s00418-018-1746-x.

[67] Sjölund, K., Sandén, G., Håkanson, R., Sundler, F., 1983. Endocrine cells in human intestine: an immunocytochemical study. Gastroenterology 85(5): 1120–30.

[68] Gribble, F.M., Reimann, F., 2017. Signalling in the gut endocrine axis. Physiology & Behavior 176: 183–8, Doi: 10.1016/J.PHYSBEH.2017.02.039.

[69] Sandoval, D.A., D'Alessio, D.A., 2015. Physiology of Proglucagon Peptides: Role of Glucagon and GLP-1 in Health and Disease. Physiological Reviews 95(2): 513–48, Doi: 10.1152/physrev.00013.2014.

[70] Habib, A.M., Richards, P., Rogers, G.J., Reimann, F., Gribble, F.M., 2013. Co-localisation and secretion of glucagon-like peptide 1 and peptide YY from primary cultured human L cells. Diabetologia 56(6): 1413–6, Doi: 10.1007/s00125-013-2887-z.

[71] Svendsen, B., Pedersen, J., Albrechtsen, N.J.W., Hartmann, B., Toräng, S., Rehfeld, J.F., et al., 2015. An Analysis of Cosecretion and Coexpression of Gut Hormones From Male Rat Proximal and Distal Small Intestine. Endocrinology 156(3): 847–57, Doi: 10.1210/en.2014-1710.

[72] Gribble, F.M., Williams, L., Simpson, A.K., Reimann, F., 2003. A Novel Glucose-Sensing Mechanism Contributing to Glucagon-Like Peptide-1 Secretion From the GLUTag Cell Line. Diabetes 52: 1147–54.

[73] Pais, R., Rievaj, J., Larraufie, P., Gribble, F., Reimann, F., 2016. Angiotensin II Type 1 Receptor-Dependent GLP-1 and PYY Secretion in Mice and Humans. Endocrinology 157(10): 3821–31, Doi: 10.1210/en.2016-1384.

[74] Pais, R., Rievaj, J., Meek, C., De Costa, G., Jayamaha, S., Alexander, R.T., et al., 2016. Role of enteroendocrine L-cells in arginine vasopressin-mediated inhibition of colonic anion secretion. The Journal of Physiology 594(17): 4865–78, Doi: 10.1113/JP272053.

[75] Tolhurst, G., Heffron, H., Lam, Y.S., Parker, H.E., Habib, A.M., Diakogiannaki, E., et al., 2012. Short-chain fatty acids stimulate glucagon-like peptide-1 secretion via the G-protein-coupled receptor FFAR2. Diabetes 61(2): 364–71, Doi: 10.2337/db11-1019.

[76] Lee, Y.-S., Jun, H.-S., 2014. Anti-diabetic actions of glucagon-like peptide-1 on pancreatic beta-cells. Metabolism 63(1): 9–19, Doi: 10.1016/J.METABOL.2013.09.010.

[77] López-Ferreras, L., Richard, J.E., Noble, E.E., Eerola, K., Anderberg, R.H., Olandersson, K., et al., 2017. Lateral hypothalamic GLP-1 receptors are critical for the control of food reinforcement, ingestive behavior and body weight. Mol Psychiatry 23(5): 1157–68, Doi: 10.1038/mp.2017.187.

[78] Kanoski, S.E., Fortin, S.M., Arnold, M., Grill, H.J., Hayes, M.R., 2011. Peripheral and Central GLP-1 Receptor Populations Mediate the Anorectic Effects of Peripherally Administered GLP-1 Receptor Agonists, Liraglutide and Exendin-4. Endocrinology 152(8): 3103–12, Doi: 10.1210/en.2011-0174.

[79] Patel, A., Yusta, B., Matthews, D., Charron, M.J., Seeley, R.J., Drucker, D.J., 2018. GLP-2 receptor signaling controls circulating bile acid levels but not glucose homeostasis in Gcgr-/- mice and is dispensable for the metabolic benefits ensuing after vertical sleeve gastrectomy. Molecular Metabolism 0(0): 1–10, Doi: 10.1016/j.molmet.2018.06.006.

[80] Gribble, F.M., Reimann, F., Roberts, G.P., 2018. Gastrointestinal Hormones. Physiology of the Gastrointestinal Tract: 31–70, Doi: 10.1016/B978-0-12-809954-4.00002-5.

[81] Pocai, A., 2014. Action and therapeutic potential of oxyntomodulin. Molecular Metabolism 3(3): 241–51, Doi: 10.1016/J.MOLMET.2013.12.001.

[82] Ambery, P., Parker, V.E., Stumvoll, M., Posch, M.G., Heise, T., Plum-Moerschel, L., et al., 2018. MEDI0382, a GLP-1 and glucagon receptor dual agonist, in obese or overweight patients with type 2 diabetes: a randomised, controlled, double-blind, ascending dose and phase 2a study. The Lancet 391(10140): 2607–18, Doi: 10.1016/S0140-6736(18)30726-8.

[83] Guida, C., Stephen, S., Guitton, R., Ramracheya, R.D., 2017. The Role of PYY in Pancreatic Islet Physiology and Surgical Control of Diabetes. Trends in Endocrinology & Metabolism 28(8): 626–36, Doi: 10.1016/J.TEM.2017.04.005.

[84] Karra, E., Chandarana, K., Batterham, R.L., 2009. The role of peptide YY in appetite regulation and obesity. The Journal of Physiology 587(1): 19–25, Doi: 10.1113/jphysiol.2008.164269.

[85] Koda, S., Date, Y., Murakami, N., Shimbara, T., Hanada, T., Toshinai, K., et al., 2005. The Role of the Vagal Nerve in Peripheral PYY3-36 -Induced Feeding Reduction in Rats. Endocrinology 146(5): 2369–75, Doi: 10.1210/en.2004-1266.

[86] Lu, V.B., Gribble, F.M., Reimann, F., 2018. Free-fatty acid receptors in enteroendocrine cells. Endocrinology, Doi: 10.1210/en.2018-00261.

[87] Cho, H.-J., Robinson, E.S., Rivera, L.R., McMillan, P.J., Testro, A., Nikfarjam, M., et al., 2014. Glucagon-like peptide 1 and peptide YY are in separate storage organelles in enteroendocrine cells. Cell and Tissue Research 357(1): 63–9, Doi: 10.1007/s00441-014-1886-9.

[88] Grosse, J., Heffron, H., Burling, K., Akhter Hossain, M., Habib, A.M., Rogers, G.J., et al., 2014. Insulin-like peptide 5 is an orexigenic gastrointestinal hormone. Proceedings of the National Academy of Sciences of the United States of America 111(30): 11133–8, Doi: 10.1073/pnas.1411413111.

[89] Kay, R.G.G., Galvin, S., Larraufie, P., Reimann, F., Gribble, F.M.M., 2017. Liquid chromatography/mass spectrometry based detection and semi-quantitative analysis of INSL5 in human and murine tissues. Rapid Communications in Mass Spectrometry 31(23): 1963–73, Doi: 10.1002/rcm.7978.

[90] Lee, Y.S., De Vadder, F., Tremaroli, V., Wichmann, A., Mithieux, G., Bäckhed, F., 2016. Insulin-like peptide 5 is a microbially regulated peptide that promotes hepatic glucose production. Molecular Metabolism 5(4): 263–70, Doi: 10.1016/j.molmet.2016.01.007.

[91] Luo, X., Li, T., Zhu, Y., Dai, Y., Zhao, J., Guo, Z.-Y., et al., 2015. The insulinotrophic effect of insulin-like peptide 5 *in vitro* and *in vivo*. Biochemical Journal 466(3): 467–73, Doi: 10.1042/BJ20141113.

[92] Kim, G.W., Lin, J.E., Valentino, M.A., Colon-Gonzalez, F., Waldman, S.A., 2011. Regulation of appetite to treat obesity. Expert Review of Clinical Pharmacology 4(2): 243–59, Doi: 10.1586/ecp.11.3.

[93] Chandra, R., Liddle, R.A., 2007. Cholecystokinin. Current Opinion in Endocrinology 14: 63–7.

[94] Whitcomb, D.C., Lowe, M.E., 2007. Human Pancreatic Digestive Enzymes. Digestive Diseases and Sciences 52(1): 1–17, Doi: 10.1007/s10620-006-9589-z.

[95] Dawson, P.A., Karpen, S.J., 2015. Intestinal transport and metabolism of bile acids. Journal of Lipid Research 56(6): 1085–99, Doi: 10.1194/jlr.R054114.

[96] Barchetta, I., Cimini, F., Capoccia, D., Bertoccini, L., Ceccarelli, V., Chiappetta, C., et al., 2018. Neurotensin Is a Lipid-Induced Gastrointestinal Peptide Associated with Visceral Adipose Tissue Inflammation in Obesity. Nutrients 10(4): 526, Doi: 10.3390/nu10040526.

[97] Wewer Albrechtsen, N.J., Kuhre, R.E., Toräng, S., Holst, J.J., 2016. The intestinal distribution pattern of appetite- and glucose regulatory peptides in mice, rats and pigs. BMC Research Notes 9(1): 60, Doi: 10.1186/s13104-016-1872-2.

[98] Martins, P., Fakhry, J., de Oliveira, E.C., Hunne, B., Fothergill, L.J., Ringuet, M., et al., 2017. Analysis of enteroendocrine cell populations in the human colon. Cell and Tissue Research 367(2): 161–8, Doi: 10.1007/s00441-016-2530-7.

[99] Yamashita, Y., Pedersen, J.H., Hansen, C.P., 1990. Distribution of Neurotensin-Like Immunoreactivities in Porcine and Human Gut. Scandinavian Journal of Gastroenterology 25(5): 481–8, Doi: 10.3109/00365529009095519.

[100] Kuhre, R.E., Bechmann, L.E., Wewer Albrechtsen, N.J., Hartmann, B., Holst, J.J., 2015. Glucose stimulates neurotensin secretion from the rat small intestine by mechanisms involving SGLT1 and GLUT2, leading to cell depolarization and calcium influx. American Journal of Physiology-Endocrinology and Metabolism 308(12): E1123–30, Doi: 10.1152/ajpendo.00012.2015.

[101] Grunddal, K. V., Ratner, C.F., Svendsen, B., Sommer, F., Engelstoft, M.S., Madsen, A.N., et al., 2016. Neurotensin Is Coexpressed, Coreleased, and Acts Together With GLP-1 and PYY in Enteroendocrine Control of Metabolism. Endocrinology 157(1): 176–94, Doi: 10.1210/en.2015-1600.

[102] Li, J., Song, J., Zaytseva, Y.Y., Liu, Y., Rychahou, P., Jiang, K., et al., 2016. An obligatory role for neurotensin in high-fat-diet-induced obesity. Nature 533(7603): 411–5, Doi: 10.1038/nature17662.

[103] Brun, P., Mastrotto, C., Beggiao, E., Stefani, A., Barzon, L., Sturniolo, G.C., et al., 2005. Neuropeptide neurotensin stimulates intestinal wound healing following chronic intestinal inflammation. American Journal of Physiology-Gastrointestinal and Liver Physiology 288(4): G621–9, Doi: 10.1152/ajpgi.00140.2004.

[104] Qiu, S., Pellino, G., Fiorentino, F., Rasheed, S., Darzi, A., Tekkis, P., et al., 2017. A Review of the Role of Neurotensin and Its Receptors in Colorectal Cancer. Gastroenterology Research and Practice 2017: 6456257, Doi: 10.1155/2017/6456257.

[105] Ratner, C., Skov, L.J., Raida, Z., Bächler, T., Bellmann-Sickert, K., Le Foll, C., et al., 2016. Effects of Peripheral Neurotensin on Appetite Regulation and Its Role in Gastric Bypass Surgery. Endocrinology 157(9): 3482–92, Doi: 10.1210/en.2016-1329.

[106] Bakirtzi, K., West, G., Fiocchi, C., Law, I.K.M., Iliopoulos, D., Pothoulakis, C., 2014. The neurotensin-HIF-1α-VEGFα axis orchestrates hypoxia, colonic inflammation, and intestinal angiogenesis. The American Journal of Pathology 184(12): 3405–14, Doi: 10.1016/j.ajpath.2014.08.015.

[107] Patrício, B.G., Morais, T., Guimarães, M., Veedfald, S., Hartmann, B., Hilsted, L., et al., 2018. Gut hormone release after gastric bypass depends on the length of the biliopancreatic limb. International Journal of Obesity: 1, Doi: 10.1038/s41366-018-0117-y.

[108] Brazeau, P., Vale, W., Burgus, R., Ling, N., Butcher, M., Rivier, J., et al., 1973. Hypothalamic polypeptide that inhibits the secretion of immunoreactive pituitary growth hormone. Science (New York, N.Y.) 179(4068): 77–9.

[109] Pradayrol, L., Chayvialle, J.A., Carlquist, M., Mutt, V., 1978. Isolation of a porcine intestinal peptide with C-terminal somatostatin. Biochemical and Biophysical Research Communications 85(2): 701–8.

[110] Kronheim, S., Berelowitz, M., Pimstone, B.L., 1976. A radioimmunoassay for growth hormone release-inhibiting hormone: method and quantitative tissue distribution. Clinical Endocrinology 5(6): 619–30, Doi: 10.1111/j.1365-2265.1976.tb03865.x.

[111] Francis, B.H., Baskin, D.G., Saunders, D.R., Ensinck, J.W., 1990. Distribution of somatostatin-14 and somatostatin-28 gastrointestinal-pancreatic cells of rats and humans. Gastroenterology 99(5): 1283–91.

[112] Vezzosi, D., Bennet, A., Rochaix, P., Courbon, F., Selves, J., Pradere, B., et al., 2005. Octreotide in insulinoma patients: efficacy on hypoglycemia, relationships with Octreoscan scintigraphy and immunostaining with anti-sst2A and anti-sst5 antibodies. European Journal of Endocrinology 152(5): 757–67, Doi: 10.1530/eje.1.01901.

[113] Van Op den bosch, J., Adriaensen, D., Van Nassauw, L., Timmermans, J.-P., 2009. The role(s) of somatostatin, structurally related peptides and somatostatin receptors in the gastrointestinal tract: a review. Regulatory Peptides 156(1): 1–8, Doi: 10.1016/j.regpep.2009.04.003.

[114] Adriaenssens, A., Lam, B.Y.H., Billing, L., Skeffington, K., Sewing, S., Reimann, F., et al., 2015. A Transcriptome-Led Exploration of Molecular Mechanisms Regulating Somatostatin-Producing D-Cells in the Gastric Epithelium. Endocrinology 156(11): 3924–36, Doi: 10.1210/en.2015-1301.

[115] Egerod, K.L., Engelstoft, M.S., Lund, M.L., Grunddal, K. V., Zhao, M., Barir-Jensen, D., et al., 2015. Transcriptional and Functional Characterization of the G Protein-Coupled Receptor Repertoire of Gastric Somatostatin Cells. Endocrinology 156(11): 3909–23, Doi: 10.1210/EN.2015-1388.

[116] De Ponti, F., Ponti, D., 2004. PHARMACOLOGY OF SEROTONIN: WHAT A CLINICIAN SHOULD KNOW. Gut 53: 1520–35, Doi: 10.1136/gut.2003.035568.

[117] Maria Portela-Gomes, G., Grimelius, L., Petersson, R., Bergström, R., Maria Portela-Gornes, G., Grirnelius, L., et al., 1984. Enterochromaffin Cells in the Rat Gastrointestinal Tract. Upsala Journal of Medical Sciences 89: 189–203, Doi: 10.3109/03009738409179499org/10.3109/03009738409179499.

[118] Mawe, G.M., Hoffman, J.M., 2013. Serotonin signalling in the gut--functions, dysfunctions and therapeutic targets. Nature Reviews. Gastroenterology & Hepatology 10(8): 473–86, Doi: 10.1038/nrgastro.2013.105.

[119] Bellono, N.W., Bayrer, J.R., Leitch, D.B., Castro, J., Zhang, C., O'Donnell, T.A., et al., 2017. Enterochromaffin Cells Are Gut Chemosensors that Couple to Sensory Neural Pathways. Cell 170(1): 185–198.e16, Doi: 10.1016/j.cell.2017.05.034.

[120] Rindi, G., Grant, S.G., Yiangou, Y., Ghatei, M.A., Bloom, S.R., Bautch, V.L., et al., 1990. Development of neuroendocrine tumors in the gastrointestinal tract of transgenic mice. Heterogeneity of hormone expression. The American Journal of Pathology 136(6): 1349–63.

[121] Grant, S.G., Seidman, I., Hanahan, D., Bautch, V.L., 1991. Early invasiveness characterizes metastatic carcinoid tumors in transgenic mice. Cancer Research 51(18): 4917–23.

[122] Park, J.G., Oie, H.K., Sugarbaker, P.H., Henslee, J.G., Chen, T.R., Johnson, B.E., et al., 1987. Characteristics of cell lines established from human colorectal carcinoma. Cancer Research 47(24 Pt 1): 6710–8.

[123] Kuhre, R.E., Wewer Albrechtsen, N.J., Deacon, C.F., Balk-Møller, E., Rehfeld, J.F., Reimann, F., et al., 2016. Peptide production and secretion in GLUTag, NCI-H716, and STC-1 cells: a comparison to native L-cells. Journal of Molecular Endocrinology 56(3): 201–11, Doi: 10.1530/JME-15-0293.

[124] Psichas, A., Tolhurst, G., Brighton, C.A., Gribble, F.M., Reimann, F., 2017. Mixed Primary Cultures of Murine Small Intestine Intended for the Study of Gut Hormone Secretion and Live Cell Imaging of Enteroendocrine Cells. Journal of Visualized Experiments : JoVE (122), Doi: 10.3791/55687.

[125] Clarke, L.L., 2009. A guide to Ussing chamber studies of mouse intestine. American Journal of Physiology. Gastrointestinal and Liver Physiology 296(6): G1151-66, Doi: 10.1152/ajpgi.90649.2008.

[126] Brighton, C.A., Rievaj, J., Kuhre, R.E., Glass, L.L., Schoonjans, K., Holst, J.J., et al., 2015. Bile Acids Trigger GLP-1 Release Predominantly by Accessing Basolaterally Located G Protein–Coupled Bile Acid Receptors. Endocrinology 156(11): 3961–70, Doi: 10.1210/en.2015-1321.

[127] Christensen, L.W., Kuhre, R.E., Janus, C., Svendsen, B., Holst, J.J., Jens Juul Holst, C., 2015. Vascular, but not luminal, activation of FFAR1 (GPR40) stimulates GLP-1 secretion from isolated perfused rat small intestine. Physiol Rep 3(9), Doi: 10.14814/phy2.12551.

[128] Ellis, M., Chambers, J.D., Gwynne, R.M., Bornstein, J.C., 2013. Serotonin and cholecystokinin mediate nutrient-induced segmentation in guinea pig small intestine. American Journal of Physiology-Gastrointestinal and Liver Physiology 304(8): G749–61, Doi: 10.1152/ajpgi.00358.2012.

[129] Park, J.-H., Kotani, T., Konno, T., Setiawan, J., Kitamura, Y., Imada, S., et al., 2016. Promotion of Intestinal Epithelial Cell Turnover by Commensal Bacteria: Role of Short-Chain Fatty Acids. PloS One 11(5): e0156334, Doi: 10.1371/journal.pone.0156334.

[130] Sato, T., Vries, R.G., Snippert, H.J., van de Wetering, M., Barker, N., Stange, D.E., et al., 2009. Single Lgr5 stem cells build crypt-villus structures in vitro without a mesenchymal niche. Nature 459(7244): 262–5, Doi: 10.1038/nature07935.

[131] Merker, S.R., Weitz, J., Stange, D.E., 2016. Gastrointestinal organoids: How they gut it out. Developmental Biology 420(2): 239–50, Doi: 10.1016/j.ydbio.2016.08.010.

[132] Beumer, J., Artegiani, B., Post, Y., Reimann, F., Gribble, F., Nguyen, T.N., et al., 2018. Enteroendocrine cells switch hormone expression along the crypt-to-villus BMP signalling gradient. Nature Cell Biology 20(8): 909–16, Doi: 10.1038/s41556-018-0143-y.

[133] Suzuki, A., Sekiya, S., Gunshima, E., Fujii, S., Taniguchi, H., 2010. EGF signaling activates proliferation and blocks apoptosis of mouse and human intestinal stem/progenitor cells in long-term monolayer cell culture. Laboratory Investigation 90(10): 1425–36, Doi: 10.1038/labinvest.2010.150.

[134] Haramis, A.-P.G., Begthel, H., van den Born, M., van Es, J., Jonkheer, S., Offerhaus, G.J.A., et al., 2004. De Novo Crypt Formation and Juvenile Polyposis on BMP Inhibition in Mouse Intestine. Science 303(5664): 1684–6, Doi: 10.1126/science.1093587.

[135] Basak, O., Beumer, J., Wiebrands, K., Seno, H., van Oudenaarden, A., Clevers, H., 2017. Induced Quiescence of Lgr5+ Stem Cells in Intestinal Organoids Enables Differentiation of Hormone-Producing Enteroendocrine Cells. Cell Stem Cell 20(2): 177–190.e4, Doi: 10.1016/J.STEM.2016.11.001.

[136] Petersen, N., Reimann, F., van Es, J.H., van den Berg, B.M., Kroone, C., Pais, R., et al., 2015. Targeting development of incretin-producing cells increases insulin secretion. The Journal of Clinical Investigation 125(1): 379–85, Doi: 10.1172/JCI75838.

[137] Brunschwig, E.B., Wilson, K., Mack, D., Dawson, D., Lawrence, E., Willson, J.K. V., et al., 2003. PMEPA1, a transforming growth factor-beta-induced marker of terminal colonocyte differentiation whose expression is maintained in primary and metastatic colon cancer. Cancer Research 63(7): 1568–75.

[138] Kim, C.-K., Bialkowska, A.B., Yang, V.W., 2016. Intestinal stem cell resurgence by enterocyte precursors. Stem Cell Investigation 3: 49, Doi: 10.21037/sci.2016.09.01.

[139] Li, H.J., Ray, S.K., Singh, N.K., Johnston, B., Leiter, A.B., 2011. Basic helix-loop-helix transcription factors and enteroendocrine cell differentiation. Diabetes, Obesity & Metabolism 13 Suppl 1(0 1): 5–12, Doi: 10.1111/j.1463-1326.2011.01438.x.

[140] Noah, T.K., Donahue, B., Shroyer, N.F., 2011. Intestinal development and differentiation. Experimental Cell Research 317(19): 2702–10, Doi: 10.1016/j.yexcr.2011.09.006.

[141] Yamane, S., Inagaki, N., 2016. Control of intestinal stem cell fate: A novel approach to treating diabetes. Journal of Diabetes Investigation 7(2): 166–8, Doi: 10.1111/jdi.12390.

[142] van Es, J.H., Sato, T., van de Wetering, M., Lyubimova, A., Yee Nee, A.N., Gregorieff, A., et al., 2012. Dll1+ secretory progenitor cells revert to stem cells upon crypt damage. Nature Cell Biology 14(10): 1099–104, Doi: 10.1038/ncb2581.

[143] Buczacki, S.J.A., Zecchini, H.I., Nicholson, A.M., Russell, R., Vermeulen, L., Kemp, R., et al., 2013. Intestinal label-retaining cells are secretory precursors expressing Lgr5. Nature 495(7439): 65–9, Doi: 10.1038/nature11965.

[144] Nakai, J., Ohkura, M., Imoto, K., 2001. A high signal-to-noise Ca2+ probe composed of a single green fluorescent protein. Nature Biotechnology 19(2): 137–41, Doi: 10.1038/84397.

[145] Nagai, T., Sawano, A., Park, E.S., Miyawaki, A., 2001. Circularly permuted green fluorescent proteins engineered to sense Ca2+. Proceedings of the National Academy of Sciences 98(6): 3197–202, Doi: 10.1073/pnas.051636098.

[146] Tian, L., Hires, S.A., Mao, T., Huber, D., Chiappe, M.E., Chalasani, S.H., et al., 2009. Imaging neural activity in worms, flies and mice with improved GCaMP calcium indicators. Nature Methods 6(12): 875–81, Doi: 10.1038/nmeth.1398.

[147] Akerboom, J., Rivera, J.D.V., Guilbe, M.M.R., Malavé, E.C.A., Hernandez, H.H., Tian, L., et al., 2009. Crystal structures of the GCaMP calcium sensor reveal the mechanism of fluorescence signal change and aid rational design. The Journal of Biological Chemistry 284(10): 6455–64, Doi: 10.1074/jbc.M807657200.

[148] Parker, H.E., Adriaenssens, A., Rogers, G., Richards, P., Koepsell, H., Reimann, F., et al., 2012. Predominant role of active versus facilitative glucose transport for glucagon-like peptide-1 secretion. Diabetologia 55(9): 2445–55, Doi: 10.1007/s00125-012-2585-2.

[149] Zariwala, H.A., Borghuis, B.G., Hoogland, T.M., Madisen, L., Tian, L., De Zeeuw, C.I., et al., 2012. A Cre-dependent GCaMP3 reporter mouse for neuronal imaging in vivo. The Journal of Neuroscience : The Official Journal of the Society for Neuroscience 32(9): 3131–41, Doi: 10.1523/JNEUROSCI.4469-11.2012.

[150] Krestel, H.E., Mayford, M., Seeburg, P.H., Sprengel, R., 2001. A GFP-equipped bidirectional expression module well suited for monitoring tetracycline-regulated gene expression in mouse. Nucleic Acids Research 29(7): E39.

[151] Madisen, L., Garner, A.R., Shimaoka, D., Chuong, A.S., Klapoetke, N.C., Li, L., et al., 2015. Transgenic mice for intersectional targeting of neural sensors and effectors with high specificity and performance. Neuron 85(5): 942–58, Doi: 10.1016/j.neuron.2015.02.022.

[152] Chen, T.-W., Wardill, T.J., Sun, Y., Pulver, S.R., Renninger, S.L., Baohan, A., et al., 2013. Ultrasensitive fluorescent proteins for imaging neuronal activity. Nature 499(7458): 295–300, Doi: 10.1038/nature12354.

[153] Billing, L.J., Smith, C.A., Larraufie, P., Goldspink, D.A., Galvin, S., Kay, R.G., et al., 2018. Co-storage and release of insulin-like peptide-5, glucagon-like peptide-1 and peptideYY from murine and human colonic enteroendocrine cells. Molecular Metabolism 16: 65–75, Doi: 10.1016/J.MOLMET.2018.07.011.

[154] Li, H.J., Kapoor, A., Giel-Moloney, M., Rindi, G., Leiter, A.B., 2012. Notch signaling differentially regulates the cell fate of early endocrine precursor cells and their maturing descendants in the mouse pancreas and intestine. Developmental Biology 371(2): 156–69, Doi: 10.1016/j.ydbio.2012.08.023.

[155] Winton, D.J., Ponder, B.A.J., 1990. Stem-cell organization in mouse small intestine. Proceedings of the Royal Society of London. Series B: Biological Sciences 241(1300): 13–8, Doi: 10.1098/rspb.1990.0059.

[156] Armond, J.W., Vladimirou, E., McAinsh, A.D., Burroughs, N.J., 2016. KiT: a MATLAB package for kinetochore tracking. Bioinformatics (Oxford, England) 32(12): 1917–9, Doi: 10.1093/bioinformatics/btw087.

[157] Thomann, D., Rines, D.R., Sorger, P.K., Danuser, G., 2002. Automatic fluorescent tag detection in 3D with super-resolution: application to the analysis of chromosome movement. Journal of Microscopy 208(Pt 1): 49–64.

[158] Krijthe, J.H., 2015. Rtsne: T-Distributed Stochastic Neighbor Embedding using Barnes-Hut Implementation. https://github.com/jkrijthe/Rtsne. [accessed September 18, 2018].

[159] Robinson, M.D., McCarthy, D.J., Smyth, G.K., 2010. edgeR: a Bioconductor package for differential expression analysis of digital gene expression data. Bioinformatics 26(1): 139–40, Doi: 10.1093/bioinformatics/btp616.

[160] Ekberg, J.H., Hauge, M., Kristensen, L. V., Madsen, A.N., Engelstoft, M.S., Husted, A.-S., et al., 2016. GPR119, a Major Enteroendocrine Sensor of Dietary Triglyceride Metabolites Coacting in Synergy With FFA1 (GPR40). Endocrinology 157(12): 4561–9, Doi: 10.1210/en.2016-1334.

[161] Montgomery, M.K., Osborne, B., Brown, S.H.J., Small, L., Mitchell, T.W., Cooney, G.J., et al., 2013. Contrasting metabolic effects of medium- versus long-chain fatty acids in skeletal muscle. Journal of Lipid Research 54(12): 3322–33, Doi: 10.1194/jlr.M040451.

[162] den Besten, G., van Eunen, K., Groen, A.K., Venema, K., Reijngoud, D.-J., Bakker, B.M., 2013. The role of short-chain fatty acids in the interplay between diet, gut microbiota, and host energy metabolism. Journal of Lipid Research 54(9): 2325–40, Doi: 10.1194/jlr.R036012.

[163] Iqbal, J., Hussain, M.M., 2009. Intestinal lipid absorption. American Journal of Physiology. Endocrinology and Metabolism 296(6): E1183-94, Doi: 10.1152/ajpendo.90899.2008.

[164] SCHJOLDAGER, B.T.-B.G., 1994. Role of CCK in Gallbladder Function. Annals of the New York Academy of Sciences 713(1 Cholecystokin): 207–18, Doi: 10.1111/j.1749-6632.1994.tb44067.x.

[165] Russell, D.W., 2003. THE ENZYMES, REGULATION, AND GENETICS OF BILE ACID SYNTHESIS, Doi: 10.1146/annurev.biochem.72.121801.161712.

[166] Hundt, M., John, S., 2018. Physiology, Bile Secretion. StatPearls Publishing.

[167] Ii, C.M.M., Gorelick, F., 2007. Development and Physiological Regulation of Intestinal Lipid Absorption. II. Dietary lipid absorption, complex lipid synthesis, and the intracellular packaging and secretion of chylomicrons. Am J Physiol Gastrointest Liver Physiol 293: 645–50, Doi: 10.1152/ajpgi.00299.2007.-Research.

[168] Furuhashi, M., Hotamisligil, G.S., 2008. Fatty acid-binding proteins: role in metabolic diseases and potential as drug targets. Nature Reviews Drug Discovery 7(6): 489–503, Doi: 10.1038/nrd2589.

[169] Balakrishnan, A., Polli, J.E., 2006. Apical sodium dependent bile acid transporter (ASBT, SLC10A2): a potential prodrug target. Molecular Pharmaceutics 3(3): 223–30, Doi: 10.1021/mp060022d.

[170] Wong, B.S., Camilleri, M., McKinzie, S., Burton, D., Graffner, H., Zinsmeister, A.R., 2011. Effects of A3309, an Ileal Bile Acid Transporter Inhibitor, on Colonic Transit and Symptoms in Females With Functional Constipation. The American Journal of Gastroenterology 106(12): 2154–64, Doi: 10.1038/ajg.2011.285.

[171] ALDINI, R., RODA, A., LENZI, P.L., USSIA, G., VACCARI, M.C., MAZZELLA, G., et al., 1992. Bile acid active and passive ileal transport in the rabbit: effect of luminal stirring. European Journal of Clinical Investigation 22(11): 744–50, Doi: 10.1111/j.1365-2362.1992.tb01439.x.

[172] Maljaars, P.W.J., Peters, H.P.F., Mela, D.J., Masclee, A.A.M., 2008. Ileal brake: A sensible food target for appetite control. A review. Physiology & Behavior 95(3): 271–81, Doi: 10.1016/J.PHYSBEH.2008.07.018.

[173] Hauge, M., Vestmar, M.A., Husted, A.S., Ekberg, J.P., Wright, M.J., Di Salvo, J., et al., 2015. GPR40 (FFAR1) - Combined Gs and Gq signaling in vitro is associated with robust incretin secretagogue action ex vivo and in vivo. Molecular Metabolism 4(1): 3–14, Doi: 10.1016/j.molmet.2014.10.002.

[174] Hirasawa, A., Tsumaya, K., Awaji, T., Katsuma, S., Adachi, T., Yamada, M., et al., 2005. Free fatty acids regulate gut incretin glucagon-like peptide-1 secretion through GPR120. NATURE MEDICINE 11(1), Doi: 10.1038/nm1168.

[175] Edfalk, S., Steneberg, P., Edlund, H., 2008. Gpr40 is expressed in enteroendocrine cells and mediates free fatty acid stimulation of incretin secretion. Diabetes 57(9): 2280–7, Doi: 10.2337/db08-0307.

[176] Engelstoft, M.S., Park, W.-M., Sakata, I., Kristensen, L. V., Husted, A.S., Osborne-Lawrence, S., et al., 2013. Seven transmembrane G protein-coupled receptor repertoire of gastric ghrelin cells. Molecular Metabolism 2(4): 376–92, Doi: 10.1016/j.molmet.2013.08.006.

[177] Psichas, A., Larraufie, P.F., Goldspink, D.A., Gribble, F.M., Reimann, F., 2017. Chylomicrons stimulate incretin secretion in mouse and human cells. Diabetologia 60(12): 2475–85, Doi: 10.1007/s00125-017-4420-2.

[178] Ellrichmann, M., Kapelle, M., Ritter, P.R., Holst, J.J., Herzig, K.-H., Schmidt, W.E., et al., 2008. Orlistat Inhibition of Intestinal Lipase Acutely Increases Appetite and Attenuates Postprandial Glucagon-Like Peptide-1-(7–36)-Amide-1, Cholecystokinin, and Peptide YY Concentrations. The Journal of Clinical Endocrinology & Metabolism 93(10): 3995–8, Doi: 10.1210/jc.2008-0924.

[179] Damci, T., Yalin, S., Balci, H., Osar, Z., Korugan, U., Ozyazar, M., et al., 2004. Orlistat augments postprandial increases in glucagon-like peptide 1 in obese type 2 diabetic patients. Diabetes Care 27(5): 1077–80, Doi: 10.2337/DIACARE.27.5.1077.

[180] Yashiro, H., Tsujihata, Y., Takeuchi, K., Hazama, M., Johnson, P.R. V., Rorsman, P., 2012. The Effects of TAK-875, a Selective G Protein-Coupled Receptor 40/Free Fatty Acid 1 Agonist, on Insulin and Glucagon Secretion in Isolated Rat and Human Islets. Journal of Pharmacology and Experimental Therapeutics 340(2): 483–9, Doi: 10.1124/jpet.111.187708.

[181] Itoh, Y., Kawamata, Y., Harada, M., Kobayashi, M., Fujii, R., Fukusumi, S., et al., 2003. Free fatty acids regulate insulin secretion from pancreatic β cells through GPR40. Nature 422(6928): 173–6, Doi: 10.1038/nature01478.

[182] Tunaru, S., Bonnavion, R., Brandenburger, I., Preussner, J., Thomas, D., Scholich, K., et al., 2018. 20-HETE promotes glucose-stimulated insulin secretion in an autocrine manner through FFAR1. Nature Communications 9(1): 177, Doi: 10.1038/s41467-017-02539-4.

[183] Kalis, M., Levéen, P., Lyssenko, V., Almgren, P., Groop, L., Cilio, C.M., 2007. Variants in the FFAR1 gene are associated with beta cell function. PloS One 2(11): e1090, Doi: 10.1371/journal.pone.0001090.

[184] Kristinsson, H., Sargsyan, E., Manell, H., Smith, D.M., Göpel, S.O., Bergsten, P., 2017. Basal hypersecretion of glucagon and insulin from palmitate-exposed human islets depends on FFAR1 but not decreased somatostatin secretion. Scientific Reports 7(1): 4657, Doi: 10.1038/s41598-017-04730-5.

[185] Ho, J.D., Chau, B., Rodgers, L., Lu, F., Wilbur, K.L., Otto, K.A., et al., 2018. Structural basis for GPR40 allosteric agonism and incretin stimulation. Nature Communications 9(1): 1645, Doi: 10.1038/s41467-017-01240-w.

[186] Otieno, M.A., Snoeys, J., Lam, W., Ghosh, A., Player, M.R., Pocai, A., et al., 2018. Fasiglifam (TAK-875): Mechanistic Investigation and Retrospective Identification of Hazards for Drug Induced Liver Injury. Toxicological Sciences 163(2): 374–84, Doi: 10.1093/toxsci/kfx040.

[187] Zhou, J., Cai, X., Huang, X., Dai, Y., Sun, L., Zhang, B., et al., 2017. A novel glucagon-like peptide-1/glucagon receptor dual agonist exhibits weight-lowering and diabetes-protective effects. European Journal of Medicinal Chemistry 138: 1158–69, Doi: 10.1016/j.ejmech.2017.07.046.

[188] Seino, S., Shibasaki, T., 2005. PKA-Dependent and PKA-Independent Pathways for cAMP-Regulated Exocytosis. Physiological Reviews 85(4): 1303–42, Doi: 10.1152/physrev.00001.2005.

[189] Shibasaki, T., Takahashi, H., Miki, T., Sunaga, Y., Matsumura, K., Yamanaka, M., et al., 2007. Essential role of Epac2/Rap1 signaling in regulation of insulin granule dynamics by cAMP. Proceedings of the National Academy of Sciences of the United States of America 104(49): 19333–8, Doi: 10.1073/pnas.0707054104.

[190] Cheng, X., Ji, Z., Tsalkova, T., Mei, F., 2008. Epac and PKA: a tale of two intracellular cAMP receptors. Acta Biochimica et Biophysica Sinica 40(7): 651–62.

[191] Venkatachalam, K., Zheng, F., Gill, D.L., 2003. Regulation of canonical transient receptor potential (TRPC) channel function by diacylglycerol and protein kinase C. The Journal of Biological Chemistry 278(31): 29031–40, Doi: 10.1074/jbc.M302751200.

[192] Iakoubov, R., Izzo, A., Yeung, A., Whiteside, C.I., Brubaker, P.L., 2007. Protein Kinase Cζ Is Required for Oleic Acid-Induced Secretion of Glucagon-Like Peptide-1 by Intestinal Endocrine L Cells. Endocrinology 148(3): 1089–98, Doi: 10.1210/en.2006-1403.

[193] Meszaros, J.G., Gonzalez, A.M., Endo-Mochizuki, Y., Villegas, S., Villarreal, F., Brunton, L.L., 2000. Identification of G protein-coupled signaling pathways in cardiac fibroblasts: cross talk between G_q and G_s. American Journal of Physiology-Cell Physiology 278(1): C154–62, Doi: 10.1152/ajpcell.2000.278.1.C154.

[194] Ryzhov, S., Goldstein, A.E., Biaggioni, I., Feoktistov, I., 2006. Cross-Talk between Gs- and Gq-Coupled Pathways in Regulation of Interleukin-4 by A2B Adenosine Receptors in Human Mast Cells. Molecular Pharmacology 70(2): 727–35, Doi: 10.1124/mol.106.022780.

[195] Petersen, N., Reimann, F., Bartfeld, S., Farin, H.F., Ringnalda, F.C., Vries, R.G.J., et al., 2014. Generation of L cells in mouse and human small intestine organoids. Diabetes 63(2): 410–20, Doi: 10.2337/db13-0991.

[196] Zietek, T., Rath, E., Haller, D., Daniel, H., Janssen, S., Depoortere, I., et al., 2015. Intestinal organoids for assessing nutrient transport, sensing and incretin secretion. Scientific Reports 5: 16831, Doi: 10.1038/srep16831.

[197] Sakuma, K., Yabuki, C., Maruyama, M., Abiru, A., Komatsu, H., Negoro, N., et al., 2016. Fasiglifam (TAK-875) has dual potentiating mechanisms via Gaq-GPR40/FFAR1 signaling branches on glucose-dependent insulin secretion. Pharma Res Per 4(3): 237, Doi: 10.1002/prp2.237.

[198] Luo, J., Swaminath, G., Brown, S.P., Zhang, J., Guo, Q., Chen, M., et al., 2012. A Potent Class of GPR40 Full Agonists Engages the EnteroInsular Axis to Promote Glucose Control in Rodents. PLoS ONE 7(10): e46300, Doi: 10.1371/journal.pone.0046300.

[199] Hauge, M., Ekberg, J.P., Engelstoft, M.S., Timshel, P., Madsen, A.N., Schwartz, T.W., 2016. Gq and Gs signaling acting in synergy to control GLP-1 secretion. Molecular and Cellular Endocrinology, Doi: 10.1016/j.mce.2016.11.024.

[200] Briere, D.A., Bueno, A.B., Gunn, E.J., Michael, M.D., Sloop, K.W., 2018. Mechanisms to Elevate Endogenous GLP-1 Beyond Injectable GLP-1 Analogs and Metabolic Surgery. Diabetes 67(2): 309–20, Doi: 10.2337/db17-0607.

[201] Goldspink, D.A., Lu, V.B., Billing, L.J., Larraufie, P., Tolhurst, G., Gribble, F.M., et al., 2018. Mechanistic insights into the detection of free fatty and bile acids by ileal glucagon-like peptide-1 secreting cells. Molecular Metabolism 7: 90–101, Doi: 10.1016/j.molmet.2017.11.005.

[202] Sang, L., Dick, I.E., Yue, D.T., 2016. Protein kinase A modulation of CaV1.4 calcium channels. Nature Communications 7: 12239, Doi: 10.1038/ncomms12239.

[203] Zhang, X.-L., Gold, M.S., 2009. Dihydropyridine block of voltage-dependent K+ currents in rat dorsal root ganglion neurons. Neuroscience 161(1): 184–94, Doi: 10.1016/j.neuroscience.2009.03.012.

[204] Chheda, M.G., Ashery, U., Thakur, P., Rettig, J., Sheng, Z.-H., 2001. Phosphorylation of Snapin by PKA modulates its interaction with the SNARE complex. Nature Cell Biology 3(4): 331–8, Doi: 10.1038/35070000.

[205] Mendez, M., Gaisano, H.Y., 2013. Role of the SNARE protein SNAP23 on cAMP-stimulated renin release in mouse juxtaglomerular cells. American Journal of Physiology. Renal Physiology 304(5): F498-504, Doi: 10.1152/ajprenal.00556.2012.

[206] Simpson, A.K., Ward, P.S., Wong, K.Y., Collord, G.J., Habib, A.M., Reimann, F., et al., 2007. Cyclic AMP triggers glucagon-like peptide-1 secretion from the GLUTag enteroendocrine cell line. Diabetologia 50(10): 2181–9, Doi: 10.1007/s00125-007-0750-9.

[207] Kashima, Y., Miki, T., Shibasaki, T., Ozaki, N., Miyazaki, M., Yano, H., et al., 2001. Critical role of cAMP-GEFII--Rim2 complex in incretin-potentiated insulin secretion. The Journal of Biological Chemistry 276(49): 46046–53, Doi: 10.1074/jbc.M108378200.

[208] Islam, D., Zhang, N., Wang, P., Li, H., Brubaker, P.L., Gaisano, H.Y., et al., 2009. Epac is involved in cAMP-stimulated proglucagon expression and hormone production but not hormone secretion in pancreatic α- and intestinal L-cell lines. American Journal of Physiology-Endocrinology and Metabolism 296(1): E174–81, Doi: 10.1152/ajpendo.90419.2008.

[209] Drost, J., van Boxtel, R., Blokzijl, F., Mizutani, T., Sasaki, N., Sasselli, V., et al., 2017. Use of CRISPR-modified human stem cell organoids to study the origin of mutational signatures in cancer. Science (New York, N.Y.) 358(6360): 234–8, Doi: 10.1126/science.aao3130.

[210] Merenda, A., Andersson-Rolf, A., Mustata, R.C., Li, T., Kim, H., Koo, B.-K., 2017. A Protocol for Multiple Gene Knockout in Mouse Small Intestinal Organoids Using a CRISPR-concatemer. Journal of Visualized Experiments : JoVE (125), Doi: 10.3791/55916.

[211] Turton, M.D., O'Shea, D., Gunn, I., Beak, S.A., Edwards, C.M.B., Meeran, K., et al., 1996. A role for glucagon-like peptide-1 in the central regulation of feeding. Nature 379(6560): 69–72, Doi: 10.1038/379069a0.

[212] Batterham, R.L., Cowley, M.A., Small, C.J., Herzog, H., Cohen, M.A., Dakin, C.L., et al., 2002. Gut hormone PYY3-36 physiologically inhibits food intake. Nature 418(6898): 650–4, Doi: 10.1038/nature00887.

[213] Morris, D.L., Ward, I., 2018. Angiotensin II. StatPearls. http://www.ncbi.nlm.nih.gov/pubmed/29763087. [accessed July 9, 2018].

[214] Lavoie, J.L., Sigmund, C.D., 2003. Minireview: Overview of the Renin-Angiotensin System—An Endocrine and Paracrine System. Endocrinology 144(6): 2179–83, Doi: 10.1210/en.2003-0150.

[215] Koshimizu, T., Nakamura, K., Egashira, N., Hiroyama, M., Nonoguchi, H., Tanoue, A., 2012. Vasopressin V1a and V1b Receptors: From Molecules to Physiological Systems. Physiological Reviews 92(4): 1813–64, Doi: 10.1152/physrev.00035.2011.

[216] Morrison, D.J., Preston, T., 2016. Formation of short chain fatty acids by the gut microbiota and their impact on human metabolism. Gut Microbes 7(3): 189–200, Doi: 10.1080/19490976.2015.1134082.

[217] Nøhr, M.K., Pedersen, M.H., Gille, A., Egerod, K.L., Engelstoft, M.S., Husted, A.S., et al., 2013. GPR41/FFAR3 and GPR43/FFAR2 as Cosensors for Short-Chain Fatty Acids in Enteroendocrine Cells vs FFAR3 in Enteric Neurons and FFAR2 in Enteric Leukocytes. Endocrinology 154(10): 3552–64, Doi: 10.1210/en.2013-1142.

[218] Martinez-Augustin, O., Sanchez de Medina, F., 2008. Intestinal bile acid physiology and pathophysiology. World Journal of Gastroenterology 14(37): 5630–40, Doi: 10.3748/WJG.14.5630.

[219] Kawamata, Y., Fujii, R., Hosoya, M., Harada, M., Yoshida, H., Miwa, M., et al., 2003. A G protein-coupled receptor responsive to bile acids. The Journal of Biological Chemistry 278(11): 9435–40, Doi: 10.1074/jbc.M209706200.

[220] Gonzalez, N., Moody, T.W., Igarashi, H., Ito, T., Jensen, R.T., 2008. Bombesin-related peptides and their receptors: recent advances in their role in physiology and disease states. Current Opinion in Endocrinology, Diabetes, and Obesity 15(1): 58–64, Doi: 10.1097/MED.0b013e3282f3709b.

[221] Svendsen, B., Pais, R., Engelstoft, M.S., Milev, N.B., Richards, P., Christiansen, C.B., et al., 2016. GLP1- and GIP-producing cells rarely overlap and differ by bombesin receptor-2 expression and responsiveness. The Journal of Endocrinology 228(1): 39–48, Doi: 10.1530/JOE-15-0247.

[222] Flynn, F.W., 1997. Bombesin Receptor Antagonists Block the Effects of Exogenous Bombesin but Not of Nutrients on Food Intake. Physiology & Behavior 62(4): 791–8, Doi: 10.1016/S0031-9384(97)00237-0.

[223] Kirkham, T.C., Walsh, C.A., Gibbs, J., Smith, G.P., Leban, J., McDermed, J., 1994. A novel bombesin receptor antagonist selectively blocks the satiety action of peripherally administered bombesin. Pharmacology Biochemistry and Behavior 48(3): 809–11, Doi: 10.1016/0091-3057(94)90351-4.

[224] NILSSON, O., BILCHIK, A.J., GOLDENRING, J.R., BALLANTYNE, G.H., ADRIAN, T.E., MODLIN, I.M., 1991. Distribution and Immunocytochemical Colocalization of Peptide YY and Enteroglucagon in Endocrine Cells of the Rabbit Colon*. Endocrinology 129(1): 139–48, Doi: 10.1210/endo-129-1-139.

[225] Gustafsson, M.G.L., 2000. Surpassing the lateral resolution limit by a factor of two using structured illumination microscopy. SHORT COMMUNICATION. Journal of Microscopy 198(2): 82–7, Doi: 10.1046/j.1365-2818.2000.00710.x.

[226] Vangindertael, J., Camacho, R., Sempels, W., Mizuno, H., Dedecker, P., Janssen, K.P.F., 2018. Methods and Applications in Fluorescence An introduction to optical super-resolution microscopy for the adventurous biologist An introduction to optical super-resolution microscopy for the adventurous biologist. Methods Appl. Fluoresc 6: 22003, Doi: 10.1088/2050-6120/aaae0c.

[227] Fothergill, L.J., Callaghan, B., Hunne, B., Bravo, D.M., Furness, J.B., 2017. Costorage of Enteroendocrine Hormones Evaluated at the Cell and Subcellular Levels in Male Mice. Endocrinology 158(7): 2113–23, Doi: 10.1210/en.2017-00243.

[228] Das, A.T., Tenenbaum, L., Berkhout, B., 2016. Tet-On Systems For Doxycycline-inducible Gene Expression. Current Gene Therapy 16(3): 156–67, Doi: 10.2174/1566523216666160524144041.

[229] de Kloet, A.D., Krause, E.G., Kim, D.-H., Sakai, R.R., Seeley, R.J., Woods, S.C., 2009. The effect of angiotensin-converting enzyme inhibition using captopril on energy balance and glucose homeostasis. Endocrinology 150(9): 4114–23, Doi: 10.1210/en.2009-0065.

[230] Cho, H.-J., Robinson, E.S., Rivera, L.R., McMillan, P.J., Testro, A., Nikfarjam, M., et al., 2014. Glucagon-like peptide 1 and peptide YY are in separate storage organelles in enteroendocrine cells. Cell and Tissue Research 357(1): 63–9, Doi: 10.1007/s00441-014-1886-9.

[231] Reimann, F., Gribble, F.M., Gribble, F., 2016. Mechanisms underlying glucose-dependent insulinotropic polypeptide and glucagon-like peptide-1 secretion. J Diabetes Investig 7: 13–9, Doi: 10.1111/jdi.12478.

[232] Ang, S.Y., Evans, B.A., Poole, D.P., Bron, R., DiCello, J.J., Bathgate, R.A.D., et al., 2018. INSL5 activates multiple signalling pathways and regulates GLP-1 secretion in NCI-H716 cells. Journal of Molecular Endocrinology 60(3): 213–24, Doi: 10.1530/JME-17-0152.

[233] Quigley, E.M.M., 2011. Microflora modulation of motility. Journal of Neurogastroenterology and Motility 17(2): 140–7, Doi: 10.5056/jnm.2011.17.2.140.

[234] Lewis, S.J., Heaton, K.W., 1997. Increasing butyrate concentration in the distal colon by accelerating intestinal transit. Gut 41(2): 245–51.

[235] El Oufir, L., Flourié, B., Bruley des Varannes, S., Barry, J.L., Cloarec, D., Bornet, F., et al., 1996. Relations between transit time, fermentation products, and hydrogen consuming flora in healthy humans. Gut 38(6): 870–7.

[236] Aron-Wisnewsky, J., Doré, J., Clement, K., 2012. The importance of the gut microbiota after bariatric surgery. Nature Reviews Gastroenterology & Hepatology 9(10): 590–8, Doi: 10.1038/nrgastro.2012.161.

[237] Cummings, D.E., Shannon, M.H., 2003. Ghrelin and Gastric Bypass: Is There a Hormonal Contribution to Surgical Weight Loss? The Journal of Clinical Endocrinology & Metabolism 88(7): 2999–3002, Doi: 10.1210/jc.2003-030705.

[238] Gunawardene, A.R., Corfe, B.M., Staton, C.A., 2011. Classification and functions of enteroendocrine cells of the lower gastrointestinal tract. International Journal of Experimental Pathology 92(4): 219–31, Doi: 10.1111/j.1365-2613.2011.00767.x.

[239] Roth, K.A., Kim, S., Gordon, J.I., 1992. Immunocytochemical studies suggest two pathways for enteroendocrine cell differentiation in the colon. The American Journal of Physiology 263(2 Pt 1): G174-80, Doi: 10.1152/ajpgi.1992.263.2.G174.

[240] Lund, M.L., Egerod, K.L., Engelstoft, M.S., Dmytriyeva, O., Theodorsson, E., Patel, B.A., et al., 2018. Enterochromaffin 5-HT cells - A major target for GLP-1 and gut microbial metabolites. Molecular Metabolism 11: 70–83, Doi: 10.1016/j.molmet.2018.03.004.

[241] Terry, N., Margolis, K.G., 2017. Serotonergic Mechanisms Regulating the GI Tract: Experimental Evidence and Therapeutic Relevance. Handbook of Experimental Pharmacology 239: 319, Doi: 10.1007/164_2016_103.

[242] Manocha, M., Khan, W.I., 2012. Serotonin and GI Disorders: An Update on Clinical and Experimental Studies. Clinical and Translational Gastroenterology 3(4): e13, Doi: 10.1038/ctg.2012.8.

[243] Mashima, H., Ohno, H., Yamada, Y., Sakai, T., Ohnishi, H., 2013. INSL5 may be a unique marker of colorectal endocrine cells and neuroendocrine tumors. Biochemical and Biophysical Research Communications 432(4): 586–92, Doi: 10.1016/J.BBRC.2013.02.042.

[244] Moriya, R., Shirakura, T., Ito, J., Mashiko, S., Seo, T., 2009. Activation of sodium-glucose cotransporter 1 ameliorates hyperglycemia by mediating incretin secretion in mice. American Journal of Physiology-Endocrinology and Metabolism 297(6): E1358–65, Doi: 10.1152/ajpendo.00412.2009.

[245] Sun, E.W., de Fontgalland, D., Rabbitt, P., Hollington, P., Sposato, L., Due, S.L., et al., 2017. Mechanisms Controlling Glucose-Induced GLP-1 Secretion in Human Small Intestine. Diabetes 66(8): 2144–9, Doi: 10.2337/db17-0058.

[246] Egerod, K.L., Engelstoft, M.S., Grunddal, K. V., Nøhr, M.K., Secher, A., Sakata, I., et al., 2012. A Major Lineage of Enteroendocrine Cells Coexpress CCK, Secretin, GIP, GLP-1, PYY, and Neurotensin but Not Somatostatin. Endocrinology 153(12): 5782–95, Doi: 10.1210/en.2012-1595.

[247] Rai, U., Thrimawithana, T.R., Valery, C., Young, S.A., 2015. Therapeutic uses of somatostatin and its analogues: Current view and potential applications. Pharmacology & Therapeutics 152: 98–110, Doi: 10.1016/J.PHARMTHERA.2015.05.007.

[248] Corleto, V. d., Severi, C., Romano, G., Tattoli, I., Weber, h. c., Stridsberg, M., et al., 2006. Somatostatin receptor subtypes mediate contractility on human colonic smooth muscle cells. Neurogastroenterology and Motility 18(3): 217–25, Doi: 10.1111/j.1365-2982.2005.00752.x.

[249] Abdu, F., Hicks, G.A., Hennig, G., Allen, J.P., Grundy, D., Allen, J., et al., 2002. Somatostatin sst(2) receptors inhibit peristalsis in the rat and mouse jejunum. American Journal of Physiology. Gastrointestinal and Liver Physiology 282(4): G624-33, Doi: 10.1152/ajpgi.00354.2001.

[250] Low, M.J., 2004. The somatostatin neuroendocrine system: physiology and clinical relevance in gastrointestinal and pancreatic disorders. Best Practice & Research Clinical Endocrinology & Metabolism 18(4): 607–22, Doi: 10.1016/J.BEEM.2004.08.005.

[251] Watanabe, T., Kubota, Y., Sawada, T., Muto, T., 1992. Distribution and quantification of somatostatin in inflammatory disease. Diseases of the Colon & Rectum 35(5): 488–94, Doi: 10.1007/BF02049408.

[252] Murphy, K.G., Bloom, S.R., 2006. Gut hormones and the regulation of energy homeostasis. Nature 444(7121): 854–9, Doi: 10.1038/nature05484.

[253] Fouquet, G., Coman, T., Hermine, O., Côté, F., 2018. Serotonin, hematopoiesis and stem cells. Pharmacological Research, Doi: 10.1016/J.PHRS.2018.08.005.

[254] Roth, K.A., Gordonh, J.I., 1990. Spatial differentiation of the intestinal epithelium: Analysis of enteroendocrine cells containing immunoreactive serotonin, secretin, and substance P in normal and transgenic mice (pattern formation/epithelial differentiation/lineage relationships). Proc. Natl. Acad. Sci. USA 87: 6408–12.

[255] Wang, F., Knutson, K., Alcaino, C., Linden, D.R., Gibbons, S.J., Kashyap, P., et al., 2017. Mechanosensitive ion channel Piezo2 is important for enterochromaffin cell response to mechanical forces. The Journal of Physiology 595(1): 79–91, Doi: 10.1113/JP272718.

[256] Das, P., May, C.L., 2011. Expression analysis of the Islet-1 gene in the developing and adult gastrointestinal tract. Gene Expression Patterns : GEP 11(3–4): 244–54, Doi: 10.1016/j.gep.2010.12.007.

[257] Zhang, J., McKenna, L.B., Bogue, C.W., Kaestner, K.H., 2014. The diabetes gene Hhex maintains δ-cell differentiation and islet function. Genes & Development 28(8): 829–34, Doi: 10.1101/gad.235499.113.

[258] Ermund, A., Gustafsson, J.K., Hansson, G.C., Keita, Å. V., 2013. Mucus Properties and Goblet Cell Quantification in Mouse, Rat and Human Ileal Peyer's Patches. PLoS ONE 8(12): e83688, Doi: 10.1371/journal.pone.0083688.

[259] Park, S.-W., Zhen, G., Verhaeghe, C., Nakagami, Y., Nguyenvu, L.T., Barczak, A.J., et al., 2009. The protein disulfide isomerase AGR2 is essential for production of intestinal mucus. Proceedings of the National Academy of Sciences of the United States of America 106(17): 6950–5, Doi: 10.1073/pnas.0808722106.

[260] Sasaki, N., Sachs, N., Wiebrands, K., Ellenbroek, S.I.J., Fumagalli, A., Lyubimova, A., et al., 2016. Reg4+ deep crypt secretory cells function as epithelial niche for Lgr5+ stem cells in colon. Proceedings of the National Academy of Sciences of the United States of America 113(37): E5399-407, Doi: 10.1073/pnas.1607327113.

[261] Brenna, Ø., Furnes, M.W., Munkvold, B., Kidd, M., Sandvik, A.K., Gustafsson, B.I., 2016. Cellular localization of guanylin and uroguanylin mRNAs in human and rat duodenal and colonic mucosa. Cell and Tissue Research 365(2): 331–41, Doi: 10.1007/s00441-016-2393-y.

[262] Fleischer, J., Bumbalo, R., Bautze, V., Strotmann, J., Breer, H., 2015. Expression of odorant receptor Olfr78 in enteroendocrine cells of the colon. Cell and Tissue Research 361(3): 697–710, Doi: 10.1007/s00441-015-2165-0.

[263] Pluznick, J.L., Protzko, R.J., Gevorgyan, H., Peterlin, Z., Sipos, A., Han, J., et al., 2013. Olfactory receptor responding to gut microbiota-derived signals plays a role in renin secretion and blood pressure regulation. Proceedings of the National Academy of Sciences of the United States of America 110(11): 4410–5, Doi: 10.1073/pnas.1215927110.

[264] Psichas, A., Glass, L.L., Sharp, S.J., Reimann, F., Gribble, F.M., 2016. Galanin inhibits GLP-1 and GIP secretion via the GAL1 receptor in enteroendocrine L and K cells. British Journal of Pharmacology 173(5): 888–98, Doi: 10.1111/bph.13407.

[265] Lauffer, L.M., Iakoubov, R., Brubaker, P.L., 2009. GPR119 is essential for oleoylethanolamide-induced glucagon-like peptide-1 secretion from the intestinal enteroendocrine L-cell. Diabetes 58(5): 1058–66, Doi: 10.2337/db08-1237.

[266] Ku, G.M., Pappalardo, Z., Luo, C.C., German, M.S., McManus, M.T., 2012. An siRNA Screen in Pancreatic Beta Cells Reveals a Role for Gpr27 in Insulin Production. PLoS Genetics 8(1): e1002449, Doi: 10.1371/journal.pgen.1002449.

[267] Gilissen, J., Geubelle, P., Dupuis, N., Laschet, C., Pirotte, B., Hanson, J., 2015. Forskolin-free cAMP assay for Gi-coupled receptors. Biochemical Pharmacology 98(3): 381–91, Doi: 10.1016/J.BCP.2015.09.010.

[268] Mccreath, K.J., Espada, S., Gálvez, B.G., Benito, M., De Molina, A., Sepúlveda, P., et al., 2015. Targeted Disruption of the SUCNR1 Metabolic Receptor Leads to Dichotomous Effects on Obesity. Diabetes 64(4): 1154–67, Doi: 10.2337/db14-0346.

[269] Krause, J., Eva, C., Seeburg, P.H., Sprengel, R., 1992. Neuropeptide Y1 subtype pharmacology of a recombinantly expressed neuropeptide receptor. Molecular Pharmacology 41(5): 817–21.

[270] Olah, M.E., 1997. Identification of A2a adenosine receptor domains involved in selective coupling to Gs. Analysis of chimeric A1/A2a adenosine receptors. The Journal of Biological Chemistry 272(1): 337–44.

[271] Chin, A., Svejda, B., Gustafsson, B.I., Granlund, A.B., Sandvik, A.K., Timberlake, A., et al., 2012. The role of mechanical forces and adenosine in the regulation of intestinal enterochromaffin cell serotonin secretion. American Journal of Physiology. Gastrointestinal and Liver Physiology 302(3): G397-405, Doi: 10.1152/ajpgi.00087.2011.

[272] Barton, M., Filardo, E.J., Lolait, S.J., Thomas, P., Maggiolini, M., Prossnitz, E.R., 2018. Twenty years of the G protein-coupled estrogen receptor GPER: Historical and personal perspectives. The Journal of Steroid Biochemistry and Molecular Biology 176: 4–15, Doi: 10.1016/J.JSBMB.2017.03.021.

[273] Qin, B., Dong, L., Guo, X., Jiang, J., He, Y., Wang, X., et al., 2014. Expression of G protein-coupled estrogen receptor in irritable bowel syndrome and its clinical significance. International Journal of Clinical and Experimental Pathology 7(5): 2238–46.

[274] Ledesma de Paolo, M.I., Celener Gravelle, F.P., Celener, D., Gonzalez, E., Rosembeck, G., Bandi, J.C., et al., 1992. Influence of VIP on the number of enterochromaffin and mucosal mast cells in the colon of the rat. Regulatory Peptides 39(2–3): 191–200.

[275] Racké, K., Schwörer, H., Agoston, D. V., Kilbinger, H., 1991. Evidence that neuronally released vasoactive intestinal polypeptide inhibits the release of serotonin from enterochromaffin cells of the guinea pig small intestine. Acta Endocrinologica 124(2): 203–7.

[276] Sheth, S., Brito, R., Mukherjea, D., Rybak, L.P., Ramkumar, V., 2014. Adenosine receptors: expression, function and regulation. International Journal of Molecular Sciences 15(2): 2024–52, Doi: 10.3390/ijms15022024.

[277] Barwell, J., Gingell, J.J., Watkins, H.A., Archbold, J.K., Poyner, D.R., Hay, D.L., 2012. Calcitonin and calcitonin receptor-like receptors: common themes with family B GPCRs? British Journal of Pharmacology 166(1): 51–65, Doi: 10.1111/j.1476-5381.2011.01525.x.

[278] Thangaraju, M., Cresci, G.A., Liu, K., Ananth, S., Gnanaprakasam, J.P., Browning, D.D., et al., 2009. GPR109A is a G-protein-coupled receptor for the bacterial fermentation product butyrate and functions as a tumor suppressor in colon. Cancer Research 69(7): 2826–32, Doi: 10.1158/0008-5472.CAN-08-4466.

[279] Larsen, C.K., Leipziger, J., 2013. P2Y receptors in the gastrointestinal epithelium GENERAL PERSPECTIVE. WIREs Membr Transp Signal 2: 27–36, Doi: 10.1002/wmts.74.

[280] Ishikawa, T., 2001. Mouse Fzd5 and angiogenesis. Development 128(1): 25–33.

[281] Bakirtzi, K., Law, I.K.M., Xue, X., Iliopoulos, D., Shah, Y.M., Pothoulakis, C., 2016. Neurotensin Promotes the Development of Colitis and Intestinal Angiogenesis via Hif-1α-miR-210 Signaling. Journal of Immunology (Baltimore, Md. : 1950) 196(10): 4311–21, Doi: 10.4049/jimmunol.1501443.

[282] Symonds, E.L., Peiris, M., Page, A.J., Chia, B., Dogra, H., Masding, A., et al., 2015. Mechanisms of activation of mouse and human enteroendocrine cells by nutrients. Gut 64(4): 618–26, Doi: 10.1136/gutjnl-2014-306834.

[283] Fakhry, J., Wang, J., Martins, P., Fothergill, L.J., Hunne, B., Prieur, P., et al., 2017. Distribution and characterisation of CCK containing enteroendocrine cells of the mouse small and large intestine. Cell and Tissue Research 369(2): 245–53, Doi: 10.1007/s00441-017-2612-1.

[284] Lahtvee, P.-J., Sá Nchez, B.J., Smialowska, A., Kasvandik, S., Elsemman, I.E., Gatto, F., et al., 2017. Absolute Quantification of Protein and mRNA Abundances Demonstrate Variability in Gene-Specific Translation Efficiency in Yeast. Cell Systems 4: 495–504.e5, Doi: 10.1016/j.cels.2017.03.003.

[285] Genshaft, A.S., Li, S., Gallant, C.J., Darmanis, S., Prakadan, S.M., Ziegler, C.G.K., et al., 2016. Multiplexed, targeted profiling of single-cell proteomes and transcriptomes in a single reaction. Genome Biology 17(1): 188, Doi: 10.1186/s13059-016-1045-6.

[286] Troger, J., Theurl, M., Kirchmair, R., Pasqua, T., Tota, B., Angelone, T., et al., 2017. Granin-derived peptides. Progress in Neurobiology 154: 37–61, Doi: 10.1016/j.pneurobio.2017.04.003.

[287] Leitner, B., Fischer-Colbrie, R., Scherzer, G., Winkler, H., 2002. Secretogranin II: Relative Amounts and Processing to Secretoneurin in Various Rat Tissues. Journal of Neurochemistry 66(3): 1312–7, Doi: 10.1046/j.1471-4159.1996.66031312.x.

[288] Hotta, K., Hosaka, M., Tanabe, A., Takeuchi, T., 2009. Secretogranin II binds to secretogranin III and forms secretory granules with orexin, neuropeptide Y, and POMC. The Journal of Endocrinology 202(1): 111–21, Doi: 10.1677/JOE-08-0531.

[289] El-Salhy, M., Grimelius, L., Wilander, E., Ryberg, B., Terenius, L., Lundberg, J.M., et al., 1983. Immunocytochemical identification of polypeptide YY (PYY) cells in the human gastrointestinal tract. Histochemistry 77(1): 15–23, Doi: 10.1007/BF00496632.

[290] Schwartz, T.W., 1983. Pancreatic polypeptide: a unique model for vagal control of endocrine systems. Journal of the Autonomic Nervous System 9: 99–111.

[291] WILSON, R.M., BODEN, G., OWEN, O.E., 1978. Pancreatic Polypeptide Responses to a Meal and to Intraduodenal Amino Acids and Sodium Oleate*. Endocrinology 102(3): 859–63, Doi: 10.1210/endo-102-3-859.

[292] Lonovics, J., Guzman, S., Devitt, P., Hejtmancik, K.E., Suddith, R.L., Rayford, P.L., et al., 1980. Release of pancreatic polypeptide in humans by infusion of cholecystokinin. Gastroenterology 79(5 Pt 1): 817–22.

[293] GUZMAN, S., LONOVICS, J., CHAYVIALLE, J.-A., HEJTMANCIK, K.E., RAYFORD, P.L., THOMPSON, J.C., 1980. Effects of Gastrin on Circulating Levels of Somatostatin, Pancreatic Polypeptide, and Vasoactive Intestinal Peptide in Dogs*. Endocrinology 107(1): 231–6, Doi: 10.1210/endo-107-1-231.

[294] Fredriksson, R., Lagerström, M.C., Lundin, L.-G., Schiöth, H.B., 2003. The G-protein-coupled receptors in the human genome form five main families. Phylogenetic analysis, paralogon groups, and fingerprints. Molecular Pharmacology 63(6): 1256–72, Doi: 10.1124/mol.63.6.1256.

[295] Regard, J.B., Sato, I.T., Coughlin, S.R., 2008. Anatomical profiling of G protein-coupled receptor expression. Cell 135(3): 561–71, Doi: 10.1016/j.cell.2008.08.040.

[296] Roberts, G.P., Larraufie, P., Richards, P., Kay, R.G., Galvin, S.G., Miedzybrodzka, E.L., et al., 2018. Comparison of human and murine enteroendocrine cells by transcriptomic and peptidomic profiling. BioRxiv: 374579, Doi: 10.1101/374579.

[297] Ziegenhain, C., Vieth, B., Parekh, S., Reinius, B., Guillaumet-Adkins, A., Smets, M., et al., 2017. Comparative Analysis of Single-Cell RNA Sequencing Methods. Molecular Cell 65(4): 631–643.e4, Doi: 10.1016/j.molcel.2017.01.023.

[298] Lopez, M.J., Upchurch, B.H., Rindi, G., Leiter, A.B., 1995. Studies in transgenic mice reveal potential relationships between secretin-producing cells and other endocrine cell types. The Journal of Biological Chemistry 270(2): 885–91, Doi: 10.1074/JBC.270.2.885.

[299] Suvas, S., 2017. Role of Substance P Neuropeptide in Inflammation, Wound Healing, and Tissue Homeostasis. Journal of Immunology (Baltimore, Md. : 1950) 199(5): 1543–52, Doi: 10.4049/jimmunol.1601751.

[300] Sideri, A., Bakirtzi, K., Shih, D.Q., Koon, H.W., Fleshner, P., Arsenescu, R., et al., 2015. Substance P mediates pro-inflammatory cytokine release form mesenteric adipocytes in Inflammatory Bowel Disease patients. Cellular and Molecular Gastroenterology and Hepatology 1(4): 420–32, Doi: 10.1016/j.jcmgh.2015.03.003.

[301] Lisowska, B., Lisowski, A., Siewruk, K., 2015. Substance P and Chronic Pain in Patients with Chronic Inflammation of Connective Tissue. PloS One 10(10): e0139206, Doi: 10.1371/journal.pone.0139206.

[302] Kowalska, K., Carr, D.B., Lipkowski, A.W., 2002. Direct antimicrobial properties of substance P. Life Sciences 71(7): 747–50, Doi: 10.1016/S0024-3205(02)01740-X.

[303] Karagiannides, I., Pothoulakis, C., 2009. Substance P, obesity, and gut inflammation. Current Opinion in Endocrinology, Diabetes, and Obesity 16(1): 47–52, Doi: 10.1097/MED.0b013e328321306c.

[304] Liu, L., Shang, F., Markus, I., Burcher, E., 2002. Roles of Substance P Receptors in Human Colon Circular Muscle: Alterations in Diverticular Disease. Journal of Pharmacology and Experimental Therapeutics 302(2): 627–35, Doi: 10.1124/jpet.102.034702.

[305] Li, C., Micci, M.-A., Murthy, K.S., Pasricha, P.J., 2014. Substance P is essential for maintaining gut muscle contractility: a novel role for coneurotransmission revealed by botulinum toxin. American Journal of Physiology. Gastrointestinal and Liver Physiology 306(10): G839-48, Doi: 10.1152/ajpgi.00436.2012.

[306] Tóth, B., Ben-Moshe, S., Gavish, A., Barkai, N., Itzkovitz, S., 2017. Early commitment and robust differentiation in colonic crypts. Molecular Systems Biology 13(1): 902, Doi: 10.15252/msb.20167283.

[307] Alcaino, C., Farrugia, G., Beyder, A., 2017. Mechanosensitive Piezo Channels in the Gastrointestinal Tract. Current Topics in Membranes 79: 219–44, Doi: 10.1016/bs.ctm.2016.11.003.

[308] Ariyachet, C., Tovaglieri, A., Xiang, G., Lu, J., Shah, M.S., Richmond, C.A., et al., 2016. Reprogrammed Stomach Tissue as a Renewable Source of Functional β Cells for Blood Glucose Regulation. Cell Stem Cell 18(3): 410–21, Doi: 10.1016/J.STEM.2016.01.003.

[309] Parnell, E., Palmer, T.M., Yarwood, S.J., 2015. The future of EPAC-targeted therapies: agonism versus antagonism. Trends in Pharmacological Sciences 36(4): 203–14, Doi: 10.1016/j.tips.2015.02.003.

[310] Hannun, Y.A., Loomis, C.R., Merrill, A.H., Bell, R.M., 1986. Sphingosine inhibition of protein kinase C activity and of phorbol dibutyrate binding in vitro and in human platelets. The Journal of Biological Chemistry 261(27): 12604–9.

[311] Kay, R.G., Galvin, S., Larraufie, P., Reimann, F., Gribble, F.M., 2017. LC/MS based detection and semi-quantitative analysis of INSL5 in human and murine tissues. Rapid Communications in Mass Spectrometry, Doi: 10.1002/rcm.7978.

[312] Ono, T., Nagao, M., Imoto, H., Watanabe, K., Tanaka, N., Motoi, F., et al., 2018. Effects of Calcitonin Gene-Related Peptide on Colonic Motility and Defecation in Conscious Dogs. Journal of Gastrointestinal Surgery: 1–7, Doi: 10.1007/s11605-018-3858-y.

[313] Zhu, H., Aryal, D.K., Olsen, R.H.J., Urban, D.J., Swearingen, A., Forbes, S., et al., 2016. Cre-dependent DREADD (Designer Receptors Exclusively Activated by Designer Drugs) mice. Genesis 54(8): 439–46, Doi: 10.1002/dvg.22949.

[314] Fujii, M., Matano, M., Nanki, K., Sato, T., 2015. Efficient genetic engineering of human intestinal organoids using electroporation. Nature Protocols 10(10): 1474–85, Doi: 10.1038/nprot.2015.088.

Appendices

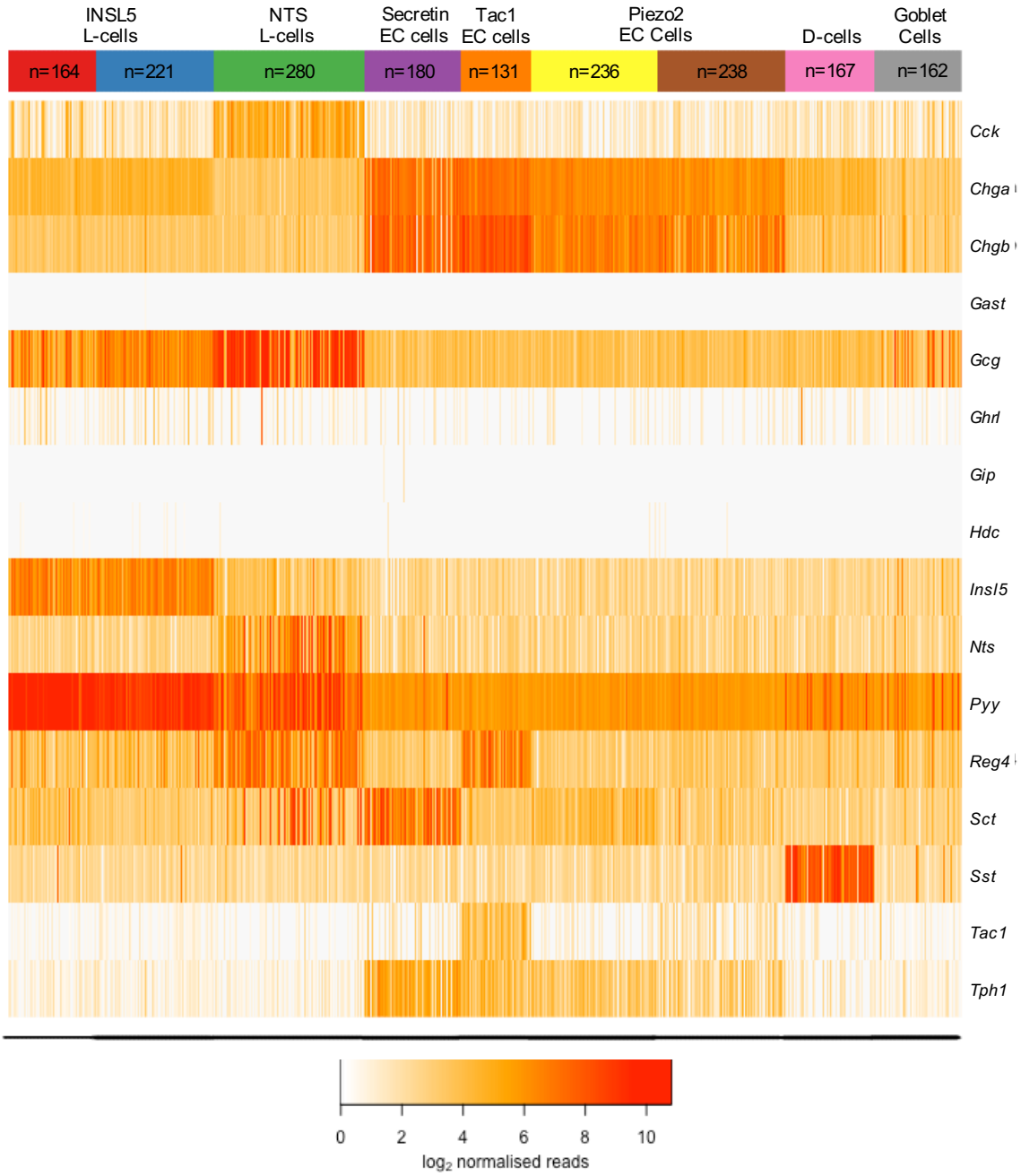

Appendix 1: *Heat-map of log_2 normalised reads from each cell for the scRNA-seq analysis of colonic EECs for a selection of known EEC markers.*

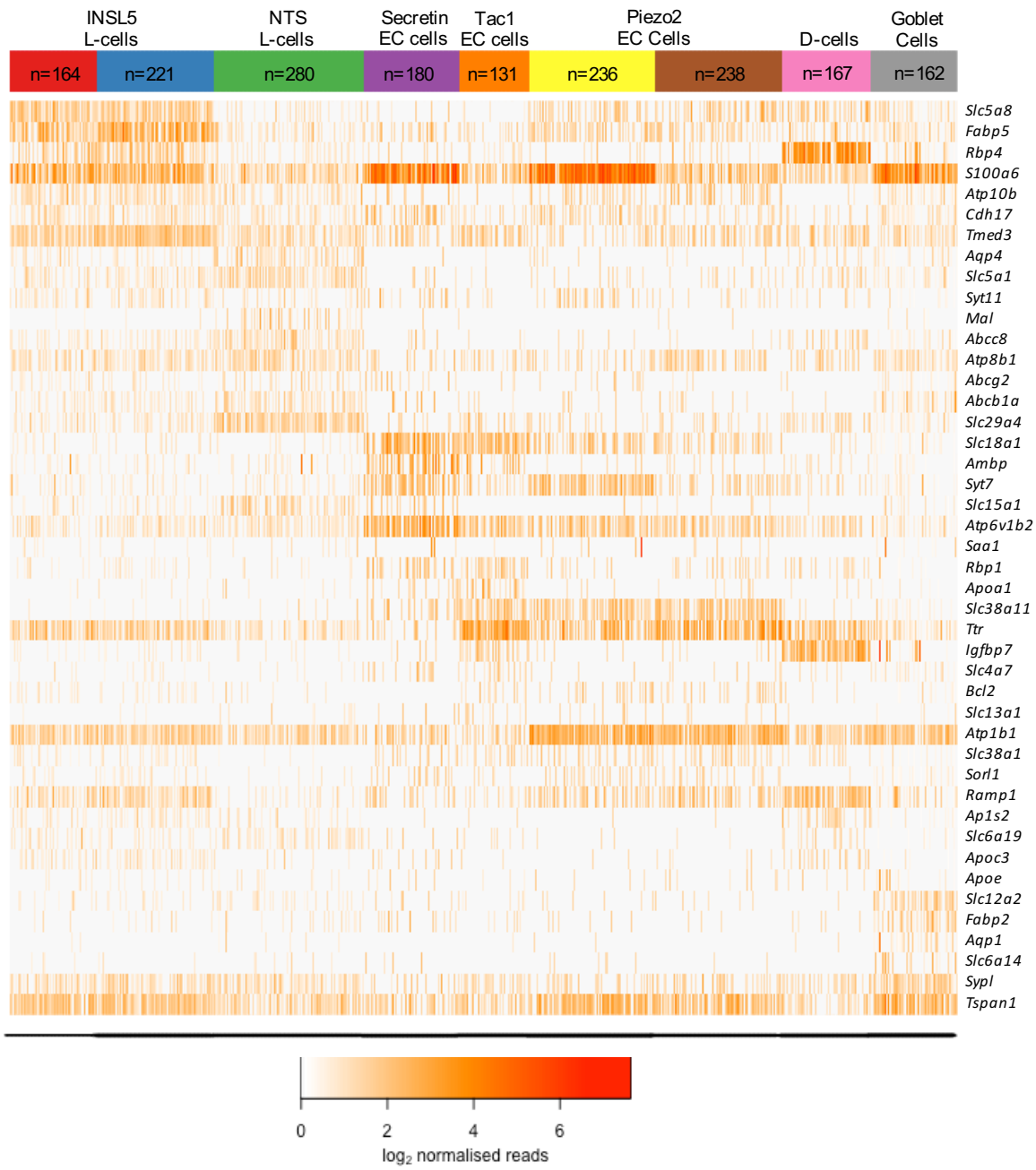

Appendix 2: *Heat-map of log_2 normalised reads across all scRNA-seq analysed cells for the top differentially expressed transporter genes from each colonic EEC subgroup as identified using edgeR.*

Ensembl ID	Gene	Protein Product
ENSMUSG00000000194	*Gpr107*	G Protein-Coupled Receptor 107
ENSMUSG00000000562	*Adora3*	Adenosine A3 Receptor
ENSMUSG00000001761	*Smo*	Smoothened, Frizzled Class Receptor
ENSMUSG00000002871	*Tpra1*	Transmembrane Protein, Adipocyte Asscociated 1
ENSMUSG00000002885	*Adgre5*	Adhesion G Protein-Coupled Receptor E5
ENSMUSG00000004730	*Adgre1*	Adhesion G Protein-Coupled Receptor E1
ENSMUSG00000005823	*Gpr108*	G Protein-Coupled Receptor 108
ENSMUSG00000007989	*Fzd3*	Frizzled Class Receptor 3
ENSMUSG00000008734	*Gprc5b*	G Protein-Coupled Receptor, Class C, Group 5, Member B
ENSMUSG00000011171	*Vipr2*	Vasoactive Intestinal Peptide Receptor 2
ENSMUSG00000013033	*Adgrl1*	Adhesion G Protein-Coupled Receptor L1
ENSMUSG00000016028	*Celsr1*	Cadherin, Egf Lag Seven-Pass G-Type Receptor 1
ENSMUSG00000018500	*Adora2b*	Adenosine A2B Receptor
ENSMUSG00000019429	*Ffar3*	Free Fatty Acid Receptor 3
ENSMUSG00000019464	*Ptger1*	Prostaglandin E Receptor 1 (Subtype Ep1), 42Kda
ENSMUSG00000019828	*Grm1*	Glutamate Receptor, Metabotropic 1
ENSMUSG00000019905	*Gprc6a*	G Protein-Coupled Receptor, Class C, Group 6, Member A
ENSMUSG00000020090	*Npffr1*	Neuropeptide Ff Receptor 1
ENSMUSG00000020123	*Avpr1a*	Arginine Vasopressin Receptor 1A
ENSMUSG00000020178	*Adora2a*	Adenosine A2A Receptor
ENSMUSG00000020793	*Galr2*	Galanin Receptor 2
ENSMUSG00000020963	*Tshr*	Thyroid Stimulating Hormone Receptor
ENSMUSG00000021298	*Gpr132*	G Protein-Coupled Receptor 132
ENSMUSG00000021678	*F2rl1*	Coagulation Factor Ii (Thrombin) Receptor-Like 1
ENSMUSG00000021886	*Gpr65*	G Protein-Coupled Receptor 65
ENSMUSG00000022122	*Ednrb*	Endothelin Receptor Type B
ENSMUSG00000022297	*Fzd6*	Frizzled Class Receptor 6
ENSMUSG00000022755	*Adgrg7*	Adhesion G Protein-Coupled Receptor G7
ENSMUSG00000023473	*Celsr3*	Cadherin, Egf Lag Seven-Pass G-Type Receptor 3
ENSMUSG00000024027	*Glp1r*	Glucagon-Like Peptide 1 Receptor
ENSMUSG00000024462	*Gabbr1*	Gamma-Aminobutyric Acid (Gaba) B Receptor, 1
ENSMUSG00000024553	*Galr1*	Galanin Receptor 1
ENSMUSG00000025127	*Gcgr*	Glucagon Receptor
ENSMUSG00000025496	*Drd4*	Dopamine Receptor D4
ENSMUSG00000025804	*Ccr1*	Chemokine (C-C Motif) Receptor 1
ENSMUSG00000025905	*Oprk1*	Opioid Receptor, Kappa 1
ENSMUSG00000026180	*Cxcr2*	Chemokine (C-X-C Motif) Receptor 2
ENSMUSG00000026237	*Nmur1*	Neuromedin U Receptor 1
ENSMUSG00000026271	*Gpr35*	G Protein-Coupled Receptor 35
ENSMUSG00000026322	*Htr4*	5-Hydroxytryptamine (Serotonin) Receptor 4, G Protein-Coupled
ENSMUSG00000026343	*Gpr39*	G Protein-Coupled Receptor 39
ENSMUSG00000026424	*Gpr37l1*	G Protein-Coupled Receptor 37 Like 1
ENSMUSG00000026432	*Avpr1b*	Arginine Vasopressin Receptor 1B

ENSMUSG00000026469	*Xpr1*	Xenotropic And Polytropic Retrovirus Receptor 1
ENSMUSG00000026525	*Opn3*	Opsin 3
ENSMUSG00000027584	*Oprl1*	Opiate Receptor-Like 1
ENSMUSG00000027762	*Sucnr1*	Succinate Receptor 1
ENSMUSG00000027765	*P2ry1*	Purinergic Receptor P2Y, G-Protein Coupled, 1
ENSMUSG00000028004	*Npy2r*	Neuropeptide Y Receptor Y2
ENSMUSG00000028012	*Rrh*	Retinal Pigment Epithelium-Derived Rhodopsin Homolog
ENSMUSG00000028172	*Tacr3*	Tachykinin Receptor 3
ENSMUSG00000028184	*Adgrl2*	Adhesion G Protein-Coupled Receptor L2
ENSMUSG00000028738	*Tas1r2*	Taste Receptor, Type 1, Member 2
ENSMUSG00000028950	*Tas1r1*	Taste Receptor, Type 1, Member 1
ENSMUSG00000029072	*Tas1r3*	Taste Receptor, Type 1, Member 3
ENSMUSG00000029090	*Adgra3*	Adhesion G Protein-Coupled Receptor A3
ENSMUSG00000029193	*Cckar*	Cholecystokinin A Receptor
ENSMUSG00000029530	*Ccr9*	Chemokine (C-C Motif) Receptor 9
ENSMUSG00000029778	*Adcyap1r1*	Adenylate Cyclase Activating Polypeptide 1 (Pituitary) Receptor Type I
ENSMUSG00000030324	*Rho*	Rhodopsin
ENSMUSG00000030406	*Gipr*	Gastric Inhibitory Polypeptide Receptor
ENSMUSG00000031070	*Mrgprf*	Mas-Related Gpr, Member F
ENSMUSG00000031210	*Gpr165*	G Protein-Coupled Receptor 165
ENSMUSG00000031298	*Adgrg2*	Adhesion G Protein-Coupled Receptor G2
ENSMUSG00000031364	*Grpr*	Gastrin-Releasing Peptide Receptor
ENSMUSG00000031390	*Avpr2*	Arginine Vasopressin Receptor 2
ENSMUSG00000031486	*Adgra2*	Adhesion G Protein-Coupled Receptor A2
ENSMUSG00000031785	*Adgrg1*	Adhesion G Protein-Coupled Receptor G1
ENSMUSG00000031861	*Lpar2*	Lysophosphatidic Acid Receptor 2
ENSMUSG00000031932	*Gpr83*	G Protein-Coupled Receptor 83
ENSMUSG00000032259	*Drd2*	Dopamine Receptor D2
ENSMUSG00000032492	*Pth1r*	Parathyroid Hormone 1 Receptor
ENSMUSG00000032528	*Vipr1*	Vasoactive Intestinal Peptide Receptor 1
ENSMUSG00000032641	*Gpr19*	G Protein-Coupled Receptor 19
ENSMUSG00000032773	*Chrm1*	Cholinergic Receptor, Muscarinic 1
ENSMUSG00000032860	*P2ry2*	Purinergic Receptor P2Y, G-Protein Coupled, 2
ENSMUSG00000033446	*Lpar6*	Lysophosphatidic Acid Receptor 6
ENSMUSG00000033470	*Cysltr2*	Cysteinyl Leukotriene Receptor 2
ENSMUSG00000033569	*Adgrb3*	Adhesion G Protein-Coupled Receptor B3
ENSMUSG00000033717	*Adra2a*	Adrenoceptor Alpha 2A
ENSMUSG00000034677	*Gpr142*	G Protein-Coupled Receptor 142
ENSMUSG00000034881	*Tbxa2r*	Thromboxane A2 Receptor
ENSMUSG00000034987	*Hrh2*	Histamine Receptor H2
ENSMUSG00000035431	*Sstr1*	Somatostatin Receptor 1
ENSMUSG00000035773	*Kiss1r*	Kiss1 Receptor
ENSMUSG00000036362	*P2ry13*	Purinergic Receptor P2Y, G-Protein Coupled, 13
ENSMUSG00000036381	*P2ry14*	Purinergic Receptor P2Y, G-Protein Coupled, 14

ENSMUSG00000036437	*Npy1r*	Neuropeptide Y Receptor Y1
ENSMUSG00000036904	*Fzd8*	Frizzled Class Receptor 8
ENSMUSG00000037605	*Adgrl3*	Adhesion G Protein-Coupled Receptor L3
ENSMUSG00000037661	*Gpr160*	G Protein-Coupled Receptor 160
ENSMUSG00000037759	*Ptger2*	Prostaglandin E Receptor 2 (Subtype Ep2), 53Kda
ENSMUSG00000038390	*Gpr162*	G Protein-Coupled Receptor 162
ENSMUSG00000038668	*Lpar1*	Lysophosphatidic Acid Receptor 1
ENSMUSG00000039059	*Hrh3*	Histamine Receptor H3
ENSMUSG00000039167	*Adgrl4*	Adhesion G Protein-Coupled Receptor L4
ENSMUSG00000039809	*Gabbr2*	Gamma-Aminobutyric Acid (Gaba) B Receptor, 2
ENSMUSG00000039904	*Gpr37*	G Protein-Coupled Receptor 37 (Endothelin Receptor Type B-Like)
ENSMUSG00000039942	*Ptger4*	Prostaglandin E Receptor 4 (Subtype Ep4)
ENSMUSG00000040016	*Ptger3*	Prostaglandin E Receptor 3 (Subtype Ep3)
ENSMUSG00000040229	*Gpr34*	G Protein-Coupled Receptor 34
ENSMUSG00000040432	*Ltb4r2*	Leukotriene B4 Receptor 2
ENSMUSG00000040495	*Chrm4*	Cholinergic Receptor, Muscarinic 4
ENSMUSG00000040836	*Gpr161*	G Protein-Coupled Receptor 161
ENSMUSG00000041075	*Fzd7*	Frizzled Class Receptor 7
ENSMUSG00000041293	*Adgrf1*	Adhesion G Protein-Coupled Receptor F1
ENSMUSG00000041347	*Bdkrb1*	Bradykinin Receptor B1
ENSMUSG00000041468	*Gpr12*	G Protein-Coupled Receptor 12
ENSMUSG00000041762	*Gpr155*	G Protein-Coupled Receptor 155
ENSMUSG00000041907	*Gpr45*	G Protein-Coupled Receptor 45
ENSMUSG00000042262	*Ccr8*	Chemokine (C-C Motif) Receptor 8
ENSMUSG00000042429	*Adora1*	Adenosine A1 Receptor
ENSMUSG00000042804	*Gpr153*	G Protein-Coupled Receptor 153
ENSMUSG00000043366	*Olfr78*	Olfactory Receptor, Family 51, Subfamily E, Member 2
ENSMUSG00000043398	*Gpr135*	G Protein-Coupled Receptor 135
ENSMUSG00000043880	*Olfr323*	Olfactory Receptor, Family 11, Subfamily L, Member 1
ENSMUSG00000043895	*S1pr2*	Sphingosine-1-Phosphate Receptor 2
ENSMUSG00000043953	*Ccrl2*	Chemokine (C-C Motif) Receptor-Like 2
ENSMUSG00000043999	*Gpr75*	G Protein-Coupled Receptor 75
ENSMUSG00000044017	*Adgrd1*	Adhesion G Protein-Coupled Receptor D1
ENSMUSG00000044052	*Ccr10*	Chemokine (C-C Motif) Receptor 10
ENSMUSG00000044067	*Gpr22*	G Protein-Coupled Receptor 22
ENSMUSG00000044199	*S1pr4*	Sphingosine-1-Phosphate Receptor 4
ENSMUSG00000044288	*Cnr1*	Cannabinoid Receptor 1 (Brain)
ENSMUSG00000044337	*Ackr3*	Atypical Chemokine Receptor 3
ENSMUSG00000044338	*Aplnr*	Apelin Receptor
ENSMUSG00000044359	*P2ry4*	Pyrimidinergic Receptor P2Y, G-Protein Coupled, 4
ENSMUSG00000044453	*Ffar1*	Free Fatty Acid Receptor 1
ENSMUSG00000044674	*Fzd1*	Frizzled Class Receptor 1
ENSMUSG00000044819	*Oxgr1*	Oxoglutarate (Alpha-Ketoglutarate) Receptor 1
ENSMUSG00000044933	*Sstr3*	Somatostatin Receptor 3

ENSMUSG00000045005	*Fzd5*	Frizzled Class Receptor 5
ENSMUSG00000045092	*S1pr1*	Sphingosine-1-Phosphate Receptor 1
ENSMUSG00000045267	*Tas2r119*	Taste Receptor, Type 2, Member 1
ENSMUSG00000045281	*Gpr20*	G Protein-Coupled Receptor 20
ENSMUSG00000045382	*Cxcr4*	Chemokine (C-X-C Motif) Receptor 4
ENSMUSG00000045502	*Hcar2*	Hydroxycarboxylic Acid Receptor 2
ENSMUSG00000045509	*Gpr150*	G Protein-Coupled Receptor 150
ENSMUSG00000045730	*Adrb2*	Adrenoceptor Beta 2, Surface
ENSMUSG00000045824	*Olfr574*	Olfactory Receptor, Family 51, Subfamily T, Member 1
ENSMUSG00000045967	*Gpr158*	G Protein-Coupled Receptor 158
ENSMUSG00000046159	*Chrm3*	Cholinergic Receptor, Muscarinic 3
ENSMUSG00000046733	*Gprc5a*	G Protein-Coupled Receptor, Class C, Group 5, Member A
ENSMUSG00000046856	*Gpr1*	G Protein-Coupled Receptor 1
ENSMUSG00000046908	*Ltb4r1*	Leukotriene B4 Receptor
ENSMUSG00000046922	*Gpr6*	G Protein-Coupled Receptor 6
ENSMUSG00000046985	*Tapt1*	Transmembrane Anterior Posterior Transformation 1
ENSMUSG00000047259	*Mc4r*	Melanocortin 4 Receptor
ENSMUSG00000047415	*Gpr68*	G Protein-Coupled Receptor 68
ENSMUSG00000047875	*Gpr157*	G Protein-Coupled Receptor 157
ENSMUSG00000047904	*Sstr2*	Somatostatin Receptor 2
ENSMUSG00000048216	*Gpr85*	G Protein-Coupled Receptor 85
ENSMUSG00000048337	*Npy4r*	Neuropeptide Y Receptor Y4
ENSMUSG00000048376	*F2r*	Coagulation Factor Ii (Thrombin) Receptor
ENSMUSG00000048521	*Cxcr6*	Chemokine (C-X-C Motif) Receptor 6
ENSMUSG00000048779	*P2ry6*	Pyrimidinergic Receptor P2Y, G-Protein Coupled, 6
ENSMUSG00000048965	*Mrgpre*	Mas-Related Gpr, Member E
ENSMUSG00000049103	*Ccr2*	Chemokine (C-C Motif) Receptor 2
ENSMUSG00000049112	*Oxtr*	Oxytocin Receptor
ENSMUSG00000049115	*Agtr1a*	Angiotensin Ii Receptor, Type 1
ENSMUSG00000049130	*C5ar1*	Complement Component 5A Receptor 1
ENSMUSG00000049241	*Hcar1*	Hydroxycarboxylic Acid Receptor 1
ENSMUSG00000049511	*Htr1b*	5-Hydroxytryptamine (Serotonin) Receptor 1B, G Protein-Coupled
ENSMUSG00000049551	*Fzd9*	Frizzled Class Receptor 9
ENSMUSG00000049608	*Gpr55*	G Protein-Coupled Receptor 55
ENSMUSG00000049649	*Gpr3*	G Protein-Coupled Receptor 3
ENSMUSG00000049741	*Rxfp4*	Relaxin/Insulin-Like Family Peptide Receptor 4
ENSMUSG00000049791	*Fzd4*	Frizzled Class Receptor 4
ENSMUSG00000050075	*Gpr171*	G Protein-Coupled Receptor 171
ENSMUSG00000050147	*F2rl3*	Coagulation Factor Ii (Thrombin) Receptor-Like 3
ENSMUSG00000050158	*Olfr165*	Olfactory Receptor, Family 2, Subfamily M, Member 5
ENSMUSG00000050164	*Mchr1*	Melanin-Concentrating Hormone Receptor 1
ENSMUSG00000050232	*Cxcr3*	Chemokine (C-X-C Motif) Receptor 3
ENSMUSG00000050288	*Fzd2*	Frizzled Class Receptor 2
ENSMUSG00000050350	*Gpr18*	G Protein-Coupled Receptor 18

ENSMUSG00000050511	*Oprd1*	Opioid Receptor, Delta 1
ENSMUSG00000050534	*Htr5b*	5-Hydroxytryptamine (Serotonin) Receptor 5B
ENSMUSG00000050541	*Adra1b*	Adrenoceptor Alpha 1B
ENSMUSG00000050824	*Sstr5*	Somatostatin Receptor 5
ENSMUSG00000050921	*P2ry10*	Purinergic Receptor P2Y, G-Protein Coupled, 10
ENSMUSG00000051043	*Gprc5c*	G Protein-Coupled Receptor, Class C, Group 5, Member C
ENSMUSG00000051182	*Olfr655*	Olfactory Receptor 655
ENSMUSG00000051209	*Gpr119*	G Protein-Coupled Receptor 119
ENSMUSG00000051314	*Ffar2*	Free Fatty Acid Receptor 2
ENSMUSG00000051980	*Casr*	Calcium-Sensing Receptor
ENSMUSG00000052336	*Cx3cr1*	Chemokine (C-X3-C Motif) Receptor 1
ENSMUSG00000052821	*Cysltr1*	Cysteinyl Leukotriene Receptor 1
ENSMUSG00000053004	*Hrh1*	Histamine Receptor H1
ENSMUSG00000053164	*Gpr21*	G Protein-Coupled Receptor 21
ENSMUSG00000053251	*Olfr212*	Olfactory Receptor 212
ENSMUSG00000053368	*Rxfp2*	Relaxin/Insulin-Like Family Peptide Receptor 2
ENSMUSG00000053647	*Gper1*	G Protein-Coupled Estrogen Receptor 1
ENSMUSG00000054200	*Ffar4*	Free Fatty Acid Receptor 4
ENSMUSG00000054764	*Mtnr1a*	Melatonin Receptor 1A
ENSMUSG00000054988	*Agtr1b*	Angiotensin Ii Receptor, Type 1B
ENSMUSG00000056492	*Adgrf5*	Adhesion G Protein-Coupled Receptor F5
ENSMUSG00000056529	*Ptafr*	Platelet-Activating Factor Receptor
ENSMUSG00000056679	*Gpr173*	G Protein-Coupled Receptor 173
ENSMUSG00000058396	*Gpr182*	G Protein-Coupled Receptor 182
ENSMUSG00000059588	*Calcrl*	Calcitonin Receptor-Like
ENSMUSG00000059867	*Olfr960*	Olfactory Receptor 960
ENSMUSG00000060470	*Adgrg3*	Adhesion G Protein-Coupled Receptor G3
ENSMUSG00000060509	*Xcr1*	Chemokine (C Motif) Receptor 1
ENSMUSG00000061039	*Olfr920*	Olfactory Receptor 920
ENSMUSG00000061577	*Adgrg5*	Adhesion G Protein-Coupled Receptor G5
ENSMUSG00000061972	*Olfr99*	Olfactory Receptor 99
ENSMUSG00000062585	*Cnr2*	Cannabinoid Receptor 2 (Macrophage)
ENSMUSG00000062905	*Vmn1r32*	Vomeronasal 1 Receptor 32
ENSMUSG00000063239	*Grm4*	Glutamate Receptor, Metabotropic 4
ENSMUSG00000064272	*Gpbar1*	G Protein-Coupled Bile Acid Receptor 1
ENSMUSG00000067586	*S1pr3*	Sphingosine-1-Phosphate Receptor 3
ENSMUSG00000067714	*Lpar5*	Lysophosphatidic Acid Receptor 5
ENSMUSG00000068740	*Celsr2*	Cadherin, Egf Lag Seven-Pass G-Type Receptor 2
ENSMUSG00000069170	*Adgrv1*	Adhesion G Protein-Coupled Receptor V1
ENSMUSG00000070337	*Gpr179*	G Protein-Coupled Receptor 179
ENSMUSG00000070423	*Olfr558*	Olfactory Receptor, Family 51, Subfamily E, Member 1
ENSMUSG00000070687	*Htr1d*	5-Hydroxytryptamine (Serotonin) Receptor 1D, G Protein-Coupled
ENSMUSG00000071489	*Ptgdr*	Prostaglandin D2 Receptor (Dp)
ENSMUSG00000071893	*Vmn1r4*	Vomeronasal 1 Receptor 4

ENSMUSG00000072875	*Gpr27*	G Protein-Coupled Receptor 27
ENSMUSG00000073964	*Olfr570*	Olfactory Receptor 570
ENSMUSG00000073966	*Olfr561*	Olfactory Receptor 561
ENSMUSG00000074037	*Mc1r*	Melanocortin 1 Receptor (α-MSH Receptor)
ENSMUSG00000074361	*C5ar2*	Complement Component 5A Receptor 2
ENSMUSG00000078698	*Mrgpra3*	Mas-Related Gpr, Member A3
ENSMUSG00000079227	*Ccr5*	Chemokine (C-C Motif) Receptor 5 (Gene/Pseudogene)
ENSMUSG00000079355	*Ackr4*	Atypical Chemokine Receptor 4
ENSMUSG00000081683	*Fzd10*	Frizzled Class Receptor 10
ENSMUSG00000091735	*Gpr62*	G Protein-Coupled Receptor 62
ENSMUSG00000094295	*Olfr819*	Olfactory Receptor 247
ENSMUSG00000095730	*Vmn2r29*	Vomeronasal 2, Receptor 32

Appendix 3: *Table of annotated GPCR genes examined in the differential expression analysis.*